IWLHS 2013

International Workshop on Hydraulic Design of Low-Head Structures

Daniel B. Bung · Stefano Pagliara
Editors

IWLHS 2013

Proceedings of the International Workshop on Hydraulic Design of Low-Head Structures

Aachen, Germany
February 20-22, 2013

IWLHS 2013

Editors

Daniel B. BUNG
FH Aachen University of Applied Sciences, Germany

Stefano PAGLIARA
University of Pisa, Italy

Published by: Bundesanstalt für Wasserbau
Federal Waterways Engineering and Research Institute
e-mail:info@baw.de
www.baw.de

BAWProceedings
ISBN 978-3-939230-04-5
ISSN 2700-8444 (online)

Printed in Germany

This book has been printed on FSC (Forest Stewardship Council) certified paper from well managed forests.

Table of Contents

5 Sewer Structures

6 Experimental Studies

7 Small Hydropower

Preface

For thousands of years, the construction and operation of hydraulic structures has helped people manage natural river flow in order to control and divert water for flood protection, irrigation, navigation, supply and sanitation purposes. Several existing ancient structures demonstrate our ancestors' tremendous grasp of hydraulic problems and their solutions.

Nowadays, hydraulic engineers face different challenges, resulting mainly from the benefits of the rapid development of new materials and construction techniques, and from the added requirements of ecological and economic considerations, resulting in the adaptation of hydraulic structures. For instance, the European Water Framework Directive, claiming habitat continuity as a main feature for favorable ecological conditions of our rivers, led to intensive studies on fishways and ramps, even resulting in a new field of hydraulic research: eco-hydraulics. These desirable ecological conditions must coincide with new technological needs, such as those evoked by the demand for expansion of renewable energy sources and a higher capacity of inland waterways and related structures, such as weirs and locks. Economic considerations often induce new sophisticated designs on single elements or even on whole structures requiring more hydraulic and structural investigations, e.g. on gate vibrations. On the other hand, climate change becomes apparent in many regions of the world. More variable rainfall and resulting runoff challenge hydraulic engineers to review discharge capacity, refurbish and upgrade existing structures, such as flood protection measures and sewer systems.

The investigation of water-structure interaction thus still demands our attention to fulfill future needs. Particularly, multiphase flow problems, such as air-water flows and sediment-water flows, are still not fully understood. Even many phenomena that have been in research focus for a long time, such as the hydraulic jump, still need further investigation to improve insight and knowledge. These investigations can be based on different approaches, experimental and numerical modeling as well as field studies. Each of these approaches may provide useful results, but most notably the combination of all approaches may still be the most appropriate means.

The International Workshop on Hydraulic-Design of Low-Head Structures, held on 20 - 22 February 2013 in Aachen / Germany, aimed to contribute to the advance and spread of knowledge by bringing together experts working in the specialized field of low-head structure design from both research and practice communities. It was yet another event in a series of successful workshops and symposia organized by the IAHR Hydraulic Structures Technical Committee during the last decade. In total, 19 papers from 10 countries were presented in the fields of

- Weirs and gates,
- Stepped spillways,
- Ramps and fishways,
- Sewer structures,
- Experimental studies and
- Small hydropower

contributing to a successful workshop and indicating the strong interest in, and need for, hydraulic structures research worldwide.

Prof. Dr. Daniel B. Bung
Chair of Local Organizing Committee,
Vice-Chair of International Scientific Committee

Prof. Dr. Stefano Pagliara
Chair of IAHR Hydraulic Structures Technical Committee,
Chair of International Scientific Committee

Acknowledgements

The Local Organizing Committee is grateful for the confidence provided by the IAHR Hydraulic Structures Technical Committee. It was a challenging task as well as a great pleasure to organize and host the IWLHS 2013 workshop at FH Aachen University of Applied Sciences. The members of the Technical Committee Leadership Team gave valuable advices based on their long experience in conference organization.

Moreover, the LOC thanks the members of the International Scientific Committee for their excellent job in reviewing the contributions and guaranteeing a high scientific quality of the presented papers and these proceedings.

Special thanks go to BAW and arxio GmbH for the support in regard to the publication of these proceedings.

Prof. Dr. Daniel B. Bung
Chair of Local Organizing Committee

Organization

IAHR Technical Committe on Hydraulic Structures - Leadership Team

Stefano Pagliara (Chairman),	University of Pisa
Robert Janssen (Vice-Chairman),	Bechtel Corporation
Blake Tullis,	Utah State University
Daniel B. Bung,	FH Aachen University of Applied Sciences
Hubert Chanson,	The University of Queensland
Jorge Matos,	Technical University of Lisbon - IST
Michael Pfister,	EPF Lausanne

Local Organizing Committee

Daniel B. Bung (Chairman),	FH Aachen University of Applied Sciences
Mario Oertel,	FH Lübeck University of Applied Sciences
Peter Weinmann,	Federal Waterways Engineering and Research Institute (BAW)
Sébastien Erpicum,	University of Liège
Walter Kleiker,	FH Aachen University of Applied Sciences

International Scientific Committee

Stefano Pagliara (Chair),	University of Pisa
Daniel B. Bung (Vice-Chair),	FH Aachen University of Applied Sciences
Blake Tullis,	Utah State University
Brian Crookston,	Schnabel Engineering
Christoph Heinzelmann,	Federal Waterways Engineering and Research Institute (BAW)
Fabián Bombardelli,	University of California
Holger Schüttrumpf,	RWTH Aachen University
Hubert Chanson,	The University of Queensland
Jorge Matos,	Technical University of Lisbon - IST
Michael Pfister,	EPF Lausanne
Rita de Carvalho,	University of Coimbra
Robert Boes,	ETH Zurich
Robert Janssen,	Bechtel Corporation
Youichi Yasuda,	Nihon University

Organizing Institutions

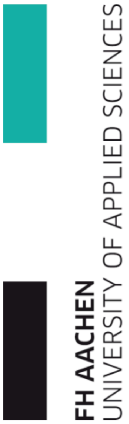

FH Aachen
University of Applied Sciences

International Association for
Hydro-Environment Engineering and Research

Bundesanstalt für Wasserbau
(Federal Waterways Engineering and Research Institute)

1 Keynote Lectures

IWLHS, 20-22/02/2013, Aachen - Bung & Pagliara (eds) - © 2013 Bundesanstalt für Wasserbau ISBN 978-3-939230-04-5

Current and Future Hydraulic Structure Research and Training Needs

B. P. Tullis
Utah State University, Logan, UT, USA

ABSTRACT: There are many relevant current and future hydraulic research needs. This paper discusses the challenges associated with maintaining the hydraulic structure knowledge base. This can be done in part by professional engineers at all levels engaging in training activities (as trainers and trainees) at conferences, workshops, webinars, and in the workplace. Engineers also need to develop life-long learning skills and habits in order to better transfer applied hydraulic structure research from the literature to engineering practice. On the research side, the use of nonlinear weirs to increase the discharge capacity at existing spillways is discussed, along with recent research developments and future needs.

Keywords: hydraulic structure research, life-long learning, labyrinth weir, piano key weir, nonlinear weir

1 INTRODUCTION

From a big-picture perspective, many of the global water issues have remained unchanged, some of which include adequate quality and quantities of safe drinking water; the development of hydropower resources at both the large and small scale; and the storage and distribution of agricultural, industrial, and municipal water supplies. Over the years, decades, and centuries, hydraulic structure research has played a key role in identifying and solving many of the challenges associated with meeting those goals. In recent years, hydraulic structure research has been influenced by improvements in technological tools and instrumentation (e.g., computational fluid dynamic simulation tools, particle image velocimetry and other multi-dimensional velocity acquisition techniques, etc.) that have allowed researchers to more accurately and fully understand flow field behaviors and fluid-structure interactions. Hydraulic structure research has also been influenced by a greater emphasis and concern for minimizing and/or mitigating the negative environmental impacts of hydraulic structures without losing the societal benefits of water storage and distribution. The way in which water is collected, stored, distributed, and bypassed in some regions of the world has changed and will likely continue to change as a result of changes in climate (e.g., Queensland Australia has experienced both extreme drought and extreme flooding in the last decade), which will likely impact hydraulic structure research, as well.

The goal of this paper is to discuss some current and future hydraulic structure design research and training needs relevant to the United State and perhaps elsewhere. Hydraulic structure research is a relatively mature field that has relied heavily on empirical relationships derived from experimental data typically obtained from laboratory-scale models. Unlike the race to extend space travel to the moon in the 1960's or to find a cure for cancer; a singular, common hydraulic structure research goal or objective really doesn't exist. Researchers are busy filling in widespread gaps in the hydraulic structure knowledge base in areas such as head-discharge relationships, cavitation, air-water flow, sediment transport, flow resistance, energy dissipation, and environmental impacts and interactions to name a few. In the absence of a singular or small set of universally accepted future hydraulic structure research objectives, this paper discusses two fundamental hydraulic structure issues that are of common concern in the United State and likely other place as well: (1) a decline in the level of experience and expertise in the workplace related to hydraulic structure design, and (2) the need to increase the capacity of existing spillways.

2 MAINTAINING THE KNOWLEDGE BASE

In the United States, the Army Corps of Engineers (USACE) and the United States Bureau of Reclamation (USBR) were responsible for many of the "large" dam construction projects, including such dams as Hoover, Grand Coulee, Glen Canyon, and Folsom, that have been constructed in the last century. Jordanelle Dam (1992) and Seven Oaks (2000) were the last large dams built by the USBR and USACE, respectively. Due primarily to changes in federal policies and public opinion related to environmental protection, large-dam construction in the US essentially came to an end. Maintenance, repair, and modernization of the aging large-dam infrastructure, along with smaller dam construction, have subsequently become the primary charge of the dam engineering profession. Declines in dam construction activity have resulted in a diminished opportunity for entry-level and middle-career civil engineers to learn the craft and problem-solving tricks-of-the-trade from the seasoned experts. Many of the engineers with large-dam design experience in the US have either retired and/or passed away, leaving a void in the dam engineering knowledge base.

There are still many talented and qualified dam engineering firms in the US who are active and successful in the profession, but the lack of large-dam engineering experience will likely become problematic eventually. For example, Hoover dam's spillways (two side-channel, drum-gated weirs that transition into 15-m diameter spillway tunnels) have only operated twice since construction, once in 1941 and again in 1983. Both times, the spillway tunnels experienced significant cavitation damage and repairs were required. The spillway tunnels at Glen Canyon dam, located on the Colorado River several 100 kilometers upstream of Hoover, also experienced cavitation damage during the spring floods of 1983. As a result these and similar events, the USBR studied spillway cavitation and developed some guidance for reducing cavitation risks, which were published in Engineering Monograph No. 41 (*Air-Water Flow in Hydraulic Structures*). While research results, such as those presented in Monograph No. 41, are available in the literature, much of the collective expertise and experience behind that information retired with the researchers.

Despite the change in dam construction emphasis and the declining practicality and probability of maintaining all of the experience-based expertise developed during the large-dam construction era, it is still important for the junior and senior members of the dam construction profession actively engage in training and information exchange. Technical conferences, workshops, and webinars are good forums for such exchanges. Senior and junior dam engineers, as well as hydraulic structure researchers, should actively pursue opportunities to share lessons learned and case-study experiences as presenter, moderators, listeners, and workshop participants in an effort to transfer knowledge and continually reinforce dam engineering fundamentals.

The primary goals in engineering education at the university level include helping students develop an understanding of fundamental engineering principles (e.g., conservation of energy, momentum, and mass), develop good problem-solving skills, and become effective life-long learners. One way in which professional engineers remain effective life-long learner is to spend time in the literature. Though much of the work in the professional engineering journals is theoretical in nature and of limited use to practitioners, the literature also contains applied hydraulic structure research (e.g, data, and design guidelines) intended to aid in solving many practical engineering problems.

In a hydraulic structure design course I teach, one of the course objectives is to have students develop original spreadsheet-based hydraulic structure design programs using published design procedures and data found in the literature. Several years ago, a former student who had completed his schooling and was working as a professional engineer requested via email a spreadsheet program that would calculate the head-discharge relationship for a particular control structure that hadn't been addressed specifically in the class. I was surprised and disappointed that, rather than doing a quick literature review on the topic and subsequently creating his own spreadsheet program, my former student was hoping to find a solution based on someone else's work. Consequently, students in the class are now required to independently research a specific hydraulic structure (e.g., morning glory spillway, siphon spillway, long-throated flume, stair-stepped spillway, energy dissipation basin, etc.) and produce a short, concise, well-written technical report on the topic. The students are required to read, understand, and cite a minimum of three credible references (government design manuals, peer-reviewed journal articles, published books). They must synthesize the relevant information (e.g., design equations, accuracy limitations, assumptions, maintenance and operational challenges, etc.) and include a summary list of 7-10 bulleted key informational items on the subject. Beyond the specific research topic and writing exercise, the goal is to reinforce life-long learning skills through implementing engineering solutions available in the literature. The independent learning skills of hydraulic structure engineers and the degree to which seasoned

professionals can provide training to junior engineers are both key points in helping to maintain the hydraulic structure knowledge base and our ability to solve problems.

3 INCREASING EXISTING SPILLWAY DISCHARGE CAPACITY

A common theme with many reservoirs in the US is the need to increase spillway capacity to improve dam safety. This can be driven by a number of factors, including land use-induced changes on watershed outflows, increased design storm magnitudes predictions resulting from improved statistical data records, and design increases due to climate change. To maintain dam safety as the magnitudes of transient flood events entering existing reservoirs increase, the base-flow reservoir water level must be lowered to provide more flood storage volume and/or the discharge efficiency of the outflow control structures must be increased. The downside of the former option is that during non-flood periods, less stored water is available for use. If the discharge efficiency of the spillway can be increased, base-flow water storage volumes can be increased while maintaining proper freeboard requirements for dam safety.

Replacing linear weirs (e.g., ogee crest weirs) with nonlinear weirs (labyrinth or piano key weirs) is becoming a relatively common approach to increasing existing spillway discharge capacity. Comparing weir walls of common height, wall thickness, crest shape, and channel width; Crookston and Tullis (2012A) found that the linear weir (weir oriented perpendicular to the approach flow) had the highest unit discharge and discharge coefficient (Cd) (see Eq. 1), relative to labyrinth weirs with sidewall angles ranging from 6° to 35°. The increase in weir length produced by the labyrinth weirs over the linear weirs, which ranged from 760% to 160%, was sufficient to increase the net total discharge by as much as 3 to 6 times. Brazos Dam (TX, USA) is an example of a project where the spillway discharge capacity was increased by replacing linear weirs with labyrinth weirs (see Figure 1).

$$Q = \frac{2}{3} C_d L \sqrt{2g} H^{3/2} \qquad (1)$$

(a) (b)

Figure 1. Brazos Dam (a) before the spillway upgrade [crest-gated spillway (left) and emergency embankment spillway just after demolition started (right)] and (b) after the spillway upgrade project (two-segment labyrinth weir) (photos courtesy of the City of Waco, TX, USA).

Piano Key (PK) weirs, which are rectangular labyrinth weirs (in plan view) with cantilevered apexes, represent another effective method for increasing the total weir length and discharge capacity within a channel of fixed width, relative to a linear weir. Figure 2 shows photographic overviews of the PK weirs at St. Marc and l'Etroit dams (France), which were some of the earliest prototype PK weirs constructed. Most PK weirs applications are located on top of concrete dams where there the footprint restrictions typically wouldn't accommodate a labyrinth weir. PK weirs can also be used for in-channel applications with weir footprint restrictions. An in-channel PK weir has been proposed for Dartmouth dam (Australia) and one is currently under construction at Von Phong dam (Vietnam) (see Figure 3).

While passive (non-gated weirs) flow control structures, like labyrinth and PK weirs, are effective at increasing discharge capacity, they have limited effectiveness at passing sediment bedload materials (sands and gravels), which could result in reservoir sediment management issue, and their head-discharge characteristics are not adjustable. Active (gated weirs) control structures installed in parallel with passive

flow control structures should be considered for some applications. Sediment transport impediment may not be a significant problem at some run-of-the-river structures where the upstream flow velocities are sufficiently large during flood events to entrain and transport sediment over the weir, but a gated structure may be more successful generally at discharging sediments. If gated spillways are installed along side a labyrinth or PK weir [St. Marc dam, see Figure 2(a)], the required passive control structure weir length needed to pass the design flood can be reduced. The 'composite' spillway structures (active and passive control) are particularly beneficial for dams in remote areas where a dam tender is not always present. The labyrinth or PK weir will accommodate the smaller return-period storm events. For larger storm events, the passive control structure will accommodate the leading edge of the flood-flow hydrograph, giving operators time to reach the dam and open the spillway gates as flood flows increase.

(a) (b)

Figure 2. Piano Key Weirs at St. Marc (a) and L'Etroit (b) dams (France).

Figure 3. Von Phong dam (Vietnam) in-channel PK weir under construction (photo courtesy of Quat Dinh Sy).

Though not a complete list by any means, some recent labyrinth weir research studies include: head-discharge relationships (Crookston and Tullis 2012a, Tullis et al. 1995), design methods (Crookston and Tullis 2012a, Falvey 2003, Tullis et al. 1995); nappe interference, instability, and vibration (Crookston and Tullis 2012b, 2012e); in-channel vs. reservoir labyrinth weir applications (Crookston and Tullis 2012c, arced labyrinth weirs hydraulics (Crookston and Tullis 2012d); submergence (Tullis et al. 2007); and energy dissipation (Lopes et al. 2008).

Some recent PK weir research topics include the following: optimizing head-discharge relationship based on PK weir geometry variations (Anderson and Tullis 2012a, Machiels et al. 2011a, 2011b, Ribeiro et al. 2011), hydraulic comparisons of PK and labyrinth weirs (Anderson and Tullis 2012b), PK weir submergence (Dabling and Tullis 2012, Belaabed and Ouamane 2011), in-channel vs. reservoir PK weir applications (Anderson and Tullis 2012c), PK weir 1D computational flow dynamics simulation (Erpicum et al. 2011), and various model studies of specific prototype structures.

4 FUTURE NONLINERAR WEIR RESEARCH

Some of the general goals associated with on-going and future nonlinear weir research can be categorized as the following: hydraulic performance optimization, unintended consequence mitigation, incorporate nonlinear weir head-discharge characteristic into basin-wide hydraulic management schemes.

4.1 *Hydraulic Performance Optimization*

Labyrinth weir design in practice became much more efficient and practical with the Tullis et al. (1995) design procedure, which featured an easy-to-program spreadsheet-based design method for sizing a quarter-round crested labyrinth weir based on a design head-discharge requirement. Falvey (2003) presented a modified design method based on the Tullis et al. (1995) data. Crookston and Tullis (2012a) improved the accuracy and extent of the labyrinth weir design data (quarter- and half-round crest shapes) and provided an alternative spreadsheet-based design method that could be used to either size a new labyrinth weir or analyze the hydraulics of a predetermined or existing labyrinth weir geometry.

The least hydraulically efficient portion of a labyrinth weir is the upstream apex, which features a relatively long crest length discharging into a relatively small volume immediately downstream of the apex. The restricted flow volume, coupled with colliding nappes from adjacent labyrinth weir sidewalls, causes local submergence to develop (the local tailwater exceeds the crest elevation but downstream weir sections are not submerged), causing a reduction in local discharge efficiency (Crookston and Tullis 2012e). The upstream apex discharge efficiency can make a difference on a labyrinth weir design but at present, we don't have a method to account for that influence. As an example, all of the labyrinth weirs illustrated in Figure 4 have the same sidewall angle, weir height, and total weir length. Without a way to account for apex influences on discharge efficiency in current labyrinth weir design methods, the predicted head-discharge relationships for all three weirs would be identical, although in reality the discharge efficiency likely decreases with increasing upstream apexes. This may represent a relatively small uncertainty in the overall design process, but for applications were additional labyrinth weir length may be cost prohibitive due to footprint restrictions, small optimizations such as the upstream apex discharge efficiency may become important with respect to meeting design performance objectives.

4.2 *Unintended Consequences*

Hydraulic structure hydrodynamic behaviors can be complicated and because engineers can't always fully describe, document, or understand these complexities, hydraulic designs sometimes result in unintended consequences. As our understanding of the hydraulic behavior of these structures improves, the probability of unintended consequences diminishes. The following are examples of research topics that may merit additional studies. Labyrinth and PK weir are effective flow energy dissipation structures due to the turbulent mixing that takes place on the downstream apron. Some work has been published on residual energy downstream of labyrinth weirs (Lopes et al. 2011); additional studies should look at the interaction between energy dissipation and air entrainment (the goal may be to either increase or limit air concentrations in the flow depending on the application and environmental needs). Half-round crest shapes are hydraulically more efficient than quarter-round crest shapes at low upstream heads because the nappe remains attached to the downstream crest profile (nonaerated nappe), which supports a negative pressure development downstream of the crest, increasing the driving head differential. The extent to which non-aerated nappes at the model scale can be reproduced at prototype scales has not been determined. Any adverse structural issues associated with negative pressure and on the downstream weir wall face have not been determined. Nappe vibrations, not observed at the model scale, have been reported at prototype structures at low-head flow conditions. The actual cause has not been determined and the options for mitigating are not fully understood either. Other unknown, unintended consequences will likely be identified with additional applications.

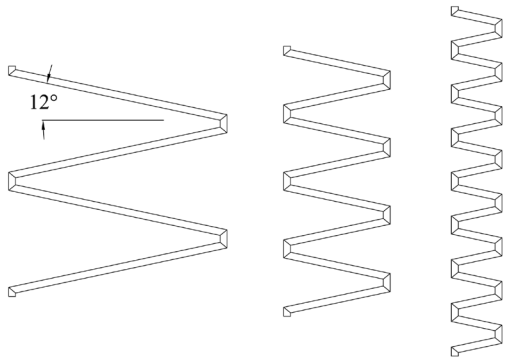

Figure 4. Labyrinth weir configurations (12° sidewall angle) of equal weir length but different cycle numbers.

4.3 *Basin-wide hydraulic management schemes with nonlinear weirs*

The improved hydraulic efficiency of nonlinear weirs means that flood-flow hydrographs will be routed through the reservoir more efficient, resulting in a decreased lag time (time difference between reservoir inflow and outflow hydrograph peek discharges) and less floodwater going into storage. The more efficient weir will would make it possible to increase base-flow reservoir storage level and still meet the necessary dam safety requirements. A consequence of the increased reservoir flood routing efficiency is an outflow hydrograph with a shorter duration and a higher discharge peek. If flood-flow restrictions exist downstream of the dam, the increased discharge efficiency of the spillway may cause flooding problems. It is important to match the head-discharge characteristics of the spillway control structure with both the upstream and downstream flood routing requirements. The head-discharge characteristics of labyrinth and piano key weirs can be modified to some extent by staging partial, whole, or multiple cycles at different crest elevations. More design information regarding staged nonlinear weirs is needed to support the design of such structures.

5 CONCLUSION

Many relevant, interesting, and important hydraulic structure research areas are currently being studied by engineering from around the world. Though it may not be practical to identify a single or subset of "most important" current and/or future research topics, the broad-spectrum goal of improving the effectiveness with which hydraulic structures can help meet civilizations need for water (i.e., safe drinking water, hydropower, agriculture, industrial, etc.) remains universal. The focus of this paper was limit to two general hydraulic structure-related issues: maintaining the hydraulic structure knowledge base and increasing discharge capacity of existing spillways. To help maintaining the hydraulic structure knowledge base, professional engineers must develop life-long learning skills and junior and senior engineers must be willing to participate in professional training activities (e.g., conferences, workshops, webinars, etc.). Replacing existing linear weirs with nonlinear weirs represents an effective way of increasing the discharge capacity of an existing spillway without a spillway replacement. A significant amount of research has been done in recent years on labyrinth and piano key weirs but, as with most hydraulic structures there is more research is required to more fully understand the appropriate design techniques, the hydraulic benefits, and the unintended consequences.

NOTATION

C_d	weir discharge coefficient
g	gravity acceleration
H	upstream total head on the weir measured relative to the weir crest elevation
L	weir crest length
Q	discharge

REFERENCES

Anderson, R.M., B.P. Tullis (2012a). Piano Key Hydraulics and Labyrinth Weir Comparisons. J. of Irrigation and Drainage Eng., 138(4), 358-361.

Anderson, R.M. and B.P. Tullis (2012b). "Comparison of Piano Key and Rectangular Labyrinth Weir Hydraulics." J. Irrig. Drain. Eng., 138(6), 358-361.

Anderson, R.M. and B.P. Tullis (2012c). "Piano Key Weirs: Reservoir versus Channel Applications." J. of Irrigation and Drainage Eng., 138(8), 773-776.

Belaabed, F., Ouamane, A. (2011). Contributions to the study of the piano key weirs submerged by the downstream level. Labyrinth and Piano Key Weirs- PKW2011, Francis and Taylor, London, 89-96.

Crookston, B.M. and Tullis, B.P. (2012a). Hydraulic design and analysis of labyrinth weirs. Part 1: Discharge relationships. J. of Irrigation and Drainage, ASCE, Posted ahead of print (Oct. 29, 2012).

Crookston, B.M. and Tullis, B.P. (2012b). Hydraulic design and analysis of labyrinth weirs. Part 2: Nappe aeration, instability and vibration. J. of Irrigation and Drainage, ASCE, Posted ahead of print (Oct. 11, 2012).

Crookston, B.M. and Tullis, B.P. (2012c). Discharge efficiency of reservoir-application-specific labyrinth weirs. J. of Irrigation and Drainage, ASCE, 138(6), 773-776.

Crookston, B.M. and Tullis, B.P. (2012d). Arced labyrinth weirs. J. of Hydraulic Eng., ASCE, 138(6), 555-562.

Crookston, B.M. and Tullis, B.P. (2012e). Labyrinth weirs: Nappe interference and local submergence. J. of Irrigation and Drainage, ASCE, 138(8), 757-765.

Dabling, M.R., Tullis, B.P. (2012). Piano key weir submergence in channel applications. J of Hydraulic Eng., ASCE, 138(7), 661-666.

Erpicum, S., Machiels, O.,Archambeau, P., Dewals, J., Pirotton, M. (2011). 1D numerical modeling of the flow over a piano key weir. Labyrinth and Piano Key Weirs- PKW2011, Francis and Taylor, London, 151-158.

Falvey, H. (2003). Hydraulic design of labyrinth weirs. ASCE, Reston, VA, USA, 162 pages.

Lopes, R., Matos, J., Melo, J. (2011). Flow properties and residual energy downstream of labyrinth weirs. Labyrinth and Piano Key Weirs- PKW2011, Francis and Taylor, London, 97-104.

Machiels, O., Erpicum, S., Dewals, J., Archambeau, P. (2011a). Experimental observations of flow characteristics over a piano key weir. J. of Hydraulic Res., IAHR, 49(3), 359-366.

Machiels, O., Erpicum, S., Archambeau, P., Dewals, J., Pirotton, M. (2011b). Influence of the piano key weir height on its discharge capacity. Labyrinth and Piano Key Weirs – PKW2011, Francis and Taylor, London, 59-66.

Ribiero, M., Boillat, J.-L., Schleiss, A.J., Le Doucen, O., Langier, F. (2011). Experimental parametric study for hydraulic design of piano key weirs. Labyrinth and Piano Key Weirs- PKW2011, Francis and Taylor, London, 183-190.

Tullis, B.P, Young, J. Chandler, M. (2007). Head-discharge relationships for submerged labyrinth weirs. J. of Hydraulic Eng., ASCE, 133(3), 248-254.

Tullis, J.P., Amanian, H., Waldron, D. (1995). Design of labyrinth spillways. J. of Hydraulic Eng., ASCE, 121(3), 247-255.

USBR (1980). "Air-Water Flow in Hydraulic Structures," Engineering Monograph No. 41. USBR, Denver, Co., USA.

IWLHS, 20-22/02/2013, Aachen - Bung & Pagliara (eds) - © 2013 Bundesanstalt für Wasserbau ISBN 978-3-939230-04-5

Physical and Numerical Modelling in Low-Head Structures Design

B. Dewals, P. Archambeau, F. Rulot, M. Pirotton & S. Erpicum
University of Liege, HECE Research group, ArGEnCo Department, Belgium

ABSTRACT: Physical and numerical modelling may be combined within so-called composite or hybrid modelling. This enables to optimally take benefit of the respective strengths of each modelling approach, while compensating for their specific drawbacks. Different types of composite modelling may be identified, such as embedding a detailed physical model within a broader scale numerical model, interconnecting different physical and numerical models focusing each on specific processes, or validating a numerical model from experimental data before exploiting the numerical model to generate more results than available from the experimental facility. Besides, specifically in more basic research, composite modelling may also be used to improve in-depth understanding of the relative importance of different processes which act simultaneously in the experimental test and may be artificially separated in numerical simulations.

Keywords: composite modelling, physical modelling, numerical modelling, scale effects

1 INTRODUCTION

Physical models have been used for decades in hydraulic engineering, both for project design and for research. They offer as main advantage the ability to reproduce the whole complexity of the prototype flows and transport processes, provided suitable scale factors and similarity rules are applied (Sutherland 2011). However, challenging issues remain regarding accurate and minimally intrusive measurements of complex turbulent flow, processing of raw data, best estimations of measurement uncertainties. As a side benefit, physical models act as powerful communication tools in the promotion of projects and engineering solutions (ASCE 2000).

The widespread use of numerical modelling by the hydraulic engineering community has developed for about 25 years. It has been built upon significant developments in the underlying mathematical models, increasingly robust numerical solution techniques, as well as the striking breakthroughs in computational power. Once a numerical model has reached a satisfactory level of development and validation, the costs of application of the model may be extremely low compared to undertaking physical modelling. Numerical models may apply for very large areas and enable a high flexibility in terms of geometric changes or sensitivity analysis with respect to a number of input parameters and numerical characteristics of the model. Last but not least, numerical models enable to retrieve the evolution of flow variables everywhere in an intrinsically non-intrusive way. Nonetheless, the significance of the results of numerical simulations crucially depends on a number of modelling characteristics, including (Dewals et al. 2012; Sutherland 2011; Van Os 2004):

- the processes actually included in the model (e.g. air entrainment, surface tensions, feedback of sediment transport on flow turbulence …);
- the exact mathematical formulation of the set of governing equations (e.g., conservative vs. non-conservative formulation of transport equations);
- validity and simplifying assumptions in the closure relations for bed shear stress, sediment transport capacity, turbulence parameterization …;

- accuracy and resolution of boundary conditions and input data, such as bathymetry and topographic data, as well as initial conditions;
- resolution time step, size of the grid cells and numerical scheme, which strongly influence the possible occurrence of artefacts (numerical oscillations, overshoots, …) and the degree of smearing of variations in flow parameters as a results of numerical diffusion …

Today, the combined application of physical and numerical modelling, referred to as *composite* or *hybrid* modelling (Frostick et al. 2011; Novak 2010), is widely recognized as the most effective strategy for the in-depth analysis of complex flow and transport processes, both in basic research and for the design of real-world projects. This is implicitly supported by the very standard procedure of validating numerical models against high quality experimental data considered as a reference (e.g., Erpicum et al. 2009b). A composite modelling approach aims at capitalizing on the benefits of a synergetic implementation of physical and numerical modelling as two highly complementary components (Erpicum Accepted; Sutherland 2011).

In this paper we identify three main strategies to combine physical and numerical modelling for saving costs while enhancing the quality of the study, as sketched in Figure 1:
- *physical modelling embedded within a numerical model*: physical modelling may be focused on a restricted area of high complexity (e.g., near-field of a structure) and, therefore, based on a setup characterized by a high scale factor enabling to minimize scale effects. Suitable boundary conditions are provided by a numerical model conducted at a larger scale, i.e. covering a wide area such as a whole reservoir as well as the reaches upstream and downstream of the structure of interest (Erpicum Accepted; Erpicum 2012)
- *interconnection of focused numerical and physical models*: when multiple processes are involved, possibly at multiple scales, they may be addressed by using interconnected physical and numerical models which focus each on a specific part of the flow for which they turn out to represent the most suitable approach (Erpicum Accepted);
- *validation and extrapolation process*: numerical modelling may be validated against experimental and subsequently used to extend the analysis beyond the range of parameters (e.g. flow conditions, geometry, time horizon …) which may be considered in the available experimental facility (e.g., Dufresne et al. 2011; Roger et al. 2009; Stilmant et al. 2012).

Moreover, the numerical model may also be used to isolate the specific influence of individual processes, which could hardly be separated in the field or in experimental conditions. For instance, sediment transport is governed by the flow characteristics but it may also lead to significant feedbacks on the mean flow through a number of different processes (Figure 2) such as morphodynamic changes, roughness changes due to deposits and/or bedforms, as well as turbulence damping or enhancement by suspended load (Cao and Carling 2002). Whereas the respective effects of each of these processes may hardly be distinguished in an experimental test, numerical models may be used to quantify their relative importance by artificially separating them in the simulations.

The different types of composite modelling are often combined within a single study. For instance, a micro-scale physical model, with a large scale factor, may be embedded within a broader scale numerical model, which is in turn just one component of a set of interconnected focused numerical and physical models, while other components are used within a "validation - extrapolation" procedure.

In the following sections, we detail demonstrative examples of the three main strategies in hybrid modelling of low head hydraulic structures (sections 2 to 4), as well as one example of basic research supported by hybrid modelling (section 5).

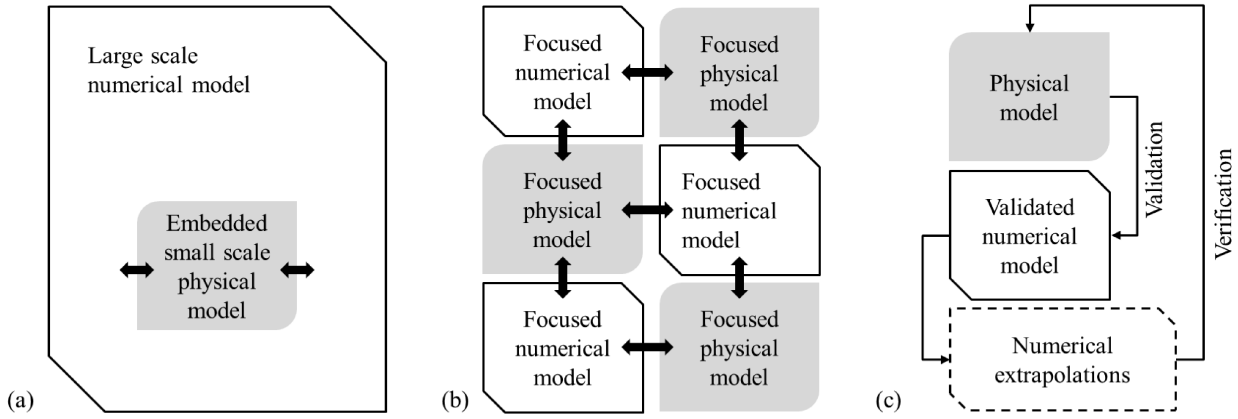

Figure 1. Conceptual approaches in composite modelling, including (a) refined scale by physical modelling embedded within a broader scale numerical model; (b) combining focused numerical and physical models; and (c) validation, extrapolation and verification process. Black arrows represent exchanges of data such as boundary conditions.

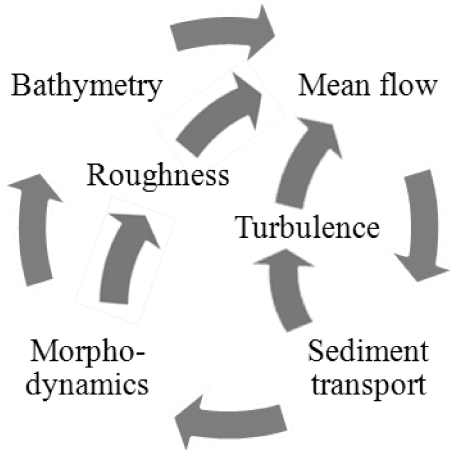

Figure 2. Multiple feedback processes between mean flow, turbulent characteristics, sediment transport and morphodynamic changes.

2 MICRO-SCALE PHYSICAL MODELS COMBINED TO MACRO-SCALE NUMERICAL MODELS

The ability of the numerical models to consider large simulation areas is generally used to perform large scale hydraulic analysis of the projects and, as a result, to precisely define the flow conditions close to a specific area or a structure for which a scale model study is necessary (due to the complexity of the local flow and sediment transport processes for instance). The detailed knowledge of the approach flow conditions in the near-field of a structure enables to reduce the layout of the scale model while setting up adequate boundary conditions to keep the physical model representative. For a given available spatial extent in a laboratory, the scale factor of the model may thus be increased, maximizing the accuracy of the measurements on the experimental setup while reducing the scale effects. For instance, such an approach has been successfully applied in the study of the design of a hydropower plant water intake as detailed below.

A small hydropower plant is to be built between a wide navigation channel and a neighbour river. The power plant head is some meters for a discharge around 100 m^3/s, while the discharge in the upstream 150 m wide channel can be ten times the one through the turbines (Figure 3). Because of site considerations, the distance between the free surface water intake and the turbines is very short, so that an accurate design of the structures is needed to ensure satisfactory operating conditions of the turbines (uniform upstream velocity field). Moreover, several additional water intakes with discharges as small as 2 m^3/s have to be placed close to the trash racks to enable the fishes to go safely through the chute.

All these considerations with free surface to under pressure flow transition and complex geometry suggest designing the water intake by a scale model study. The power plant structures dimensions and discharges require a large scale factor to reach satisfactory representativeness and accuracy while the upstream channel characteristics limit the scale factor because of surface availability in the laboratory and water supply capacity.

The hydraulic studies of the project have been carried out successively by two complementary approaches: a first step realized on the basis of numerical modelling to study the flows at the scale of the upstream channel, and a second one using a physical scale model to study in details the flow conditions at the scale of the power plant water intake. The layout and boundary conditions of the physical scale model have been defined using the numerical results in order to increase as much as possible the scale factor while limiting the model area to the available space in the laboratory and preserving its representativeness.

The limits of the reduced layout of the physical model have been defined first by comparison of the flow fields computed in the full upstream channel with the ones computed considering the scale model limited extend (Figure 3). Such an approach provides objective validation of the representativeness of the scale model regarding for instance approach flow conditions to the water intake. In a second time, the geometry and the characteristics of the boundary conditions of the physical model have been optimized by comparison of the numerical flow fields from the full upstream channel modelling with the flow fields measured in the physical model (Figure 4). The suitability of the reduced layout of the physical model has thus been objectively verified. A scale factor of 1:25 has been made possible, with only two fifths of the upstream channel width represented on a length of 150 m (only once the full channel width!).

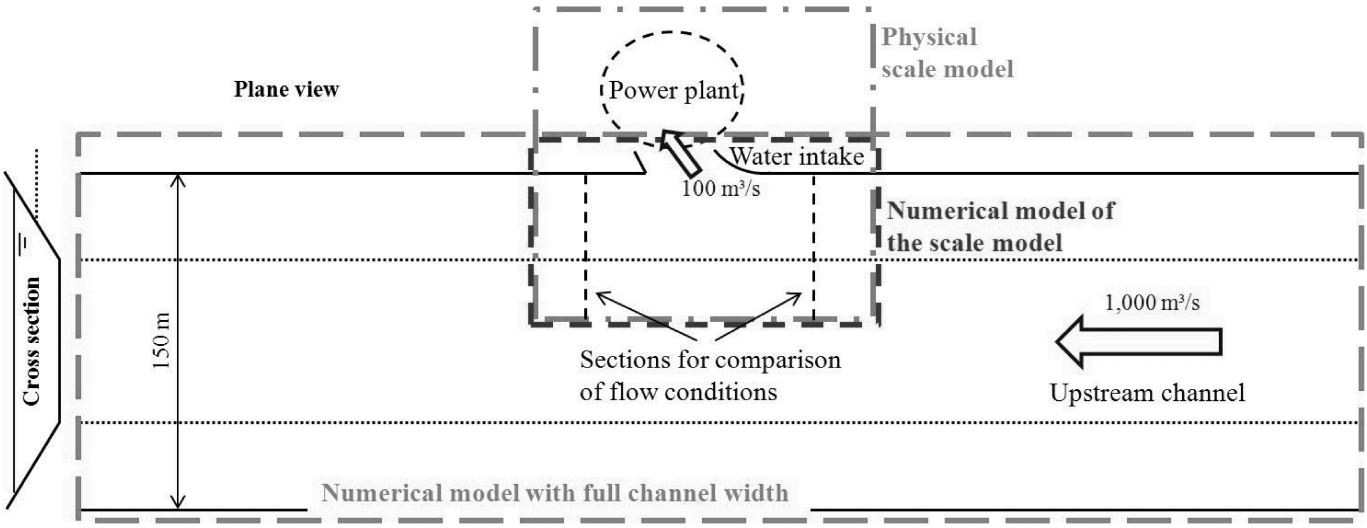

Figure 3. Main characteristics of the system to be studied and extent of the numerical and physical models.

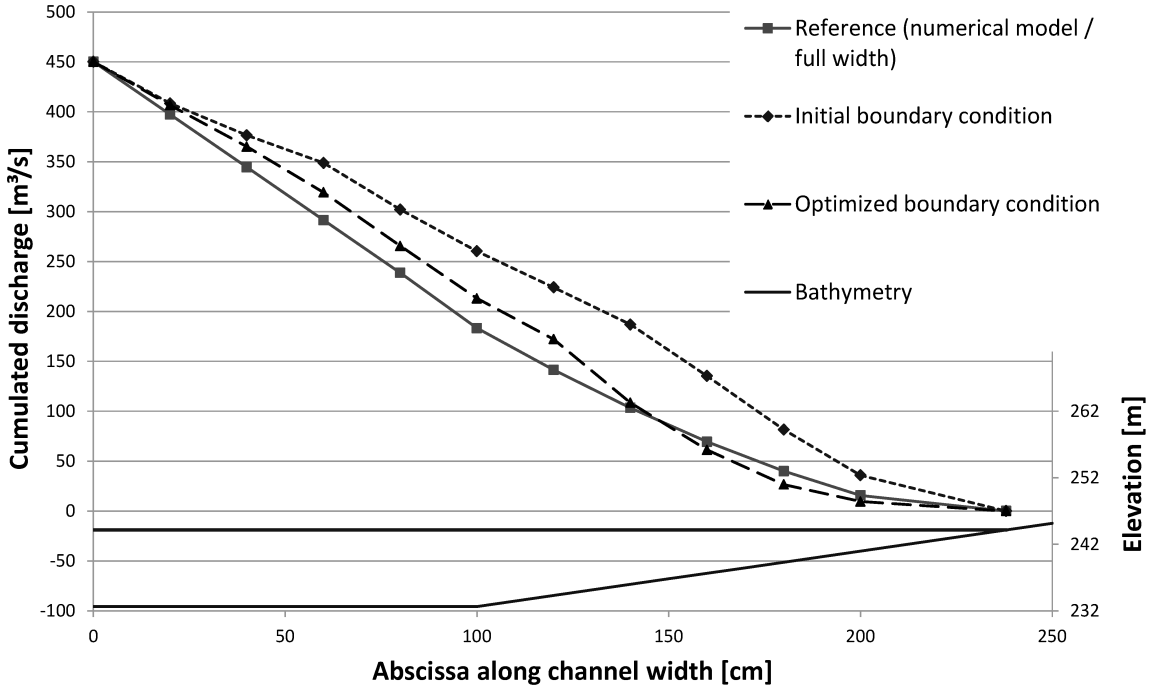

Figure 4. Comparison of numerical and experimental flow fields upstream of the water intake depending on the physical model boundary geometry.

3 CAPITALIZE ON THE RESPECTIVE STRENGTHS OF PHYSICAL AND NUMERICAL MODELS

A composite modelling strategy may involve several numerical and physical models, each applied to study the range of processes, space- and time-scales for which they are best suited. Those models are interconnected in the sense that they exchange data, mainly boundary conditions and offer thus a synergetic implementation of multiple and complementary focused models.

Such an approach has been followed in the analysis of a project located in an Alpine valley, in which low-head hydropower schemes have been in operation for over a century. It consists in the replacement of five old hydropower schemes by a single one, which will produce almost 50 % more power than the total of the existing ones. Project implementation is scheduled to last about 10 years and involves the following hydraulic engineering works:

- building of a new dam (4.5 m high, 40 m wide) and water intake in the upstream part of the river section,
- construction of a tunnel through the mountain to reach the new underground hydropower plant located downstream of the existing schemes,
- restoration of the river section where the existing schemes are located and which will be bypassed as a result of the construction of the new scheme.

Consequently, a number of hydraulic engineering issues need to be addressed to guide the implementation of the project, including:

- estimation of the trapping efficiency of the reservoir upstream of the new dam (storage capacity: approximately 200,000 m³),
- computation of the sedimentation rate in the reservoir and prediction of the location of the deposits,
- evaluation of the performance of sediment management options, such as hydraulic flushing,
- overall hydraulic optimization of the shape of the new water intake and specific optimization of the transition from a free surface flow in the water intake to an under pressure flow in the penstock,
- analysis of the hydraulic impact and the efficiency of a partially submerged wall in front of the trash rack to divert small fishes from passing through the grille,
- simulation of flood levels upstream of the new dam, both in the planned situation and at different stages of construction,
- design of the restoration plan to ensure stability of the riverbed after decommissioning of the five existing low-head dams.

Neither a single numerical model nor a single physical model would be suited to cover all those seven items in order to inform properly the project engineers. In contrast a combination of focused numerical *and* physical models have succeeded in delivering reliable, accurate and effective results to illuminate designers concerning the most crucial hydraulic issues of the project. Table 1 summarizes the developed strategy, strongly based on composite modelling. The most significant parts of the analysis are further detailed in the following paragraphs.

3.1 *Reservoir sedimentation and measures for sustainable sediment management*

The catchment is characterized by very steep slopes and the tributaries include several mountain streams. Therefore, significant amounts of sediment deposits are expected in the reservoir during flood periods. Complementary numerical models have been applied to evaluate the cut-off diameter of the new reservoir, the equilibrium bed profile in the reservoir as well as to assess the feasibility and effectiveness of flushing operations.

3.1.1 *Cut-off diameter of the reservoir*

First, a numerical model has been used to evaluate the grain size of sediment particles likely to reach the water intake at the beginning of the operation of the new reservoir. To this end, a two-step procedure has been followed:

- the reservoir hydrodynamics was first simulated by a flow model for normal operation conditions. A grid spacing of 1 m by 1 m has been used as well as a two-length-scale depth-averaged k-e turbulence model (Erpicum et al. 2009b).
- next, the flow field was analysed in terms of sediment transport capacity in the reservoir, by means of particle tracking algorithm (Figure 5), to predict the maximum size of grains able to reach the water intake and, therefore, to cause to accelerated degradation of the turbines blades.

3.1.2 *Profile of the balance retained in the absence of specific management*

Second, the long-term equilibrium profile of the bathymetry of the reservoir was computed using a sequential resolution of a flow model and of a model for sediment transport and morphodynamics (Figure 6). The sensitivity of the final result was analysed and was found reasonably small with respect to the main sediment characteristics such as grain size, whereas the amount of sediment supply from upstream has a much greater influence on the equilibrium profile.

3.1.3 *Efficiency of flushing operations*

Finally, the rapid and highly transient flow and morphodynamics changes during flushing operations were simulated using a synchronous resolution of a flow, a sediment transport and a morphodynamic model (Figure 7). These simulations confirmed the efficiency of flushing operations conducted based on discharges of return periods of the order of 1 year. The volume of sediments scoured in the reservoir was compared to the amount of water released during the whole flushing operations, which enabled to define an optimal duration for the flushing, corresponding to the time during which the efficiency of the operation remains high.

Table 1. Interconnection of focused numerical and physical models in the study of a hydropower project.

Issue	**Type of analysis**	**Objective**	**Spatial extent**	**Space scale of the analysis/ Scale factor**	**Time scale of the analysis**	**Relevant processes**
Trapping efficiency of the new reservoir	Numerical model for flow and sediment transport	Estimate the cut-off diameter of the reservoir	5 km (upstream reservoir)	1 m (= grid spacing)	< 1 hour (travelling time through the reservoir)	Turbulent flow and sediment transport
Sedimentation in the new reservoir	Numerical model for flow, sediment transport and *morphodynamics*	Compute the equilibrium bathymetry in the reservoir and estimate the time	5 km (upstream reservoir)	1 m (= grid spacing)	2 to 5 years (sequential resolution of the numerical model)	Turbulent flow, sediment transport and morphodynamic changes
Sediment management options	Numerical model for flow, sediment transport and *morphodynamics*	Compare the efficiency of different scenarios of flushing operations	5 km (upstream reservoir)	1 m (= grid spacing)	24 to 48 hours (synchronous resolution of the numerical model)	High velocity flow, sediment erosion and rapid morphodynamic changes
Overall shape optimization of the water intake	Numerical model for flow	Find the optimal geometry of the water intake	190x275 m	0.25 m (= grid spacing)	None (constant discharges)	Turbulent flow
Specific optimization of the outlet from the reservoir	Scale physical model	Effect of a submerged wall in front of the trash rack to divert fishes	60x110 m	1:20	None (constant discharges)	Turbulent flow, current patterns
Specific optimization of the inlet into the penstock	Scale physical model	Study the risk of vortex formation	40x4.2m	1:14.58	None (constant discharges)	Turbulent flow, vortex formation
Simulation of flood levels upstream of the new dam	Numerical model for flow	Estimate design levels for flood protections	5 km (upstream reservoir)	1 m (= grid spacing)	None (constant discharges)	Turbulent flow
River restoration	Numerical model for flow	Plan the decommissioning of the existing dams	10 km (bypassed river section)	1 m (= grid spacing)	Flood duration (Q_1, Q_{10}, Q_{100}, Q_{500})	Turbulent flow, bed shear stress, stability of armour layer

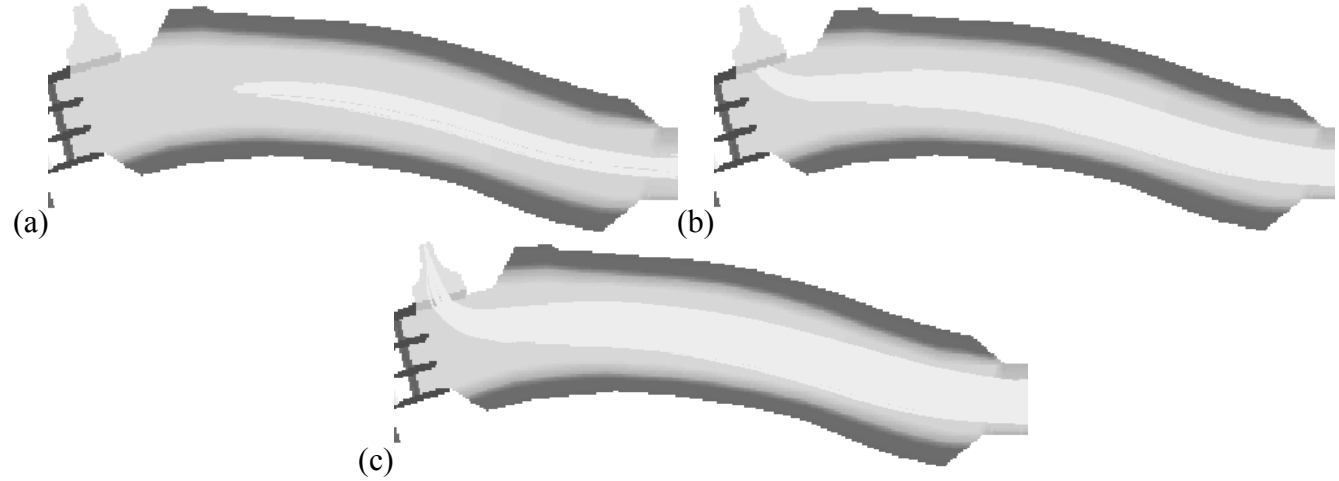

Figure 5. Tracking of sediment particles in the downstream part of the reservoir. The region in light color defines the envelope of the trajectories of the particles for grain sizes of (a) 0.425 mm, (b) 0.300 mm, (c) 0.250 mm.

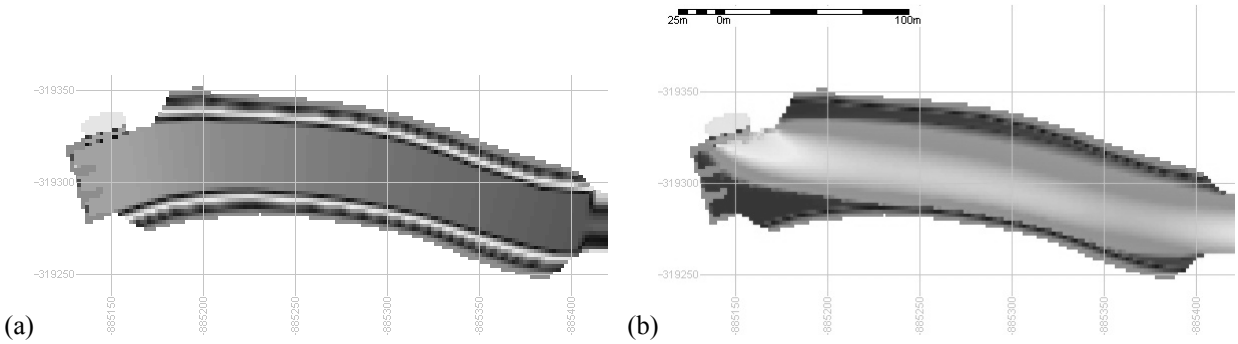

Figure 6. Initial reservoir bathymetry (a) and simulated equilibrium profile (b).

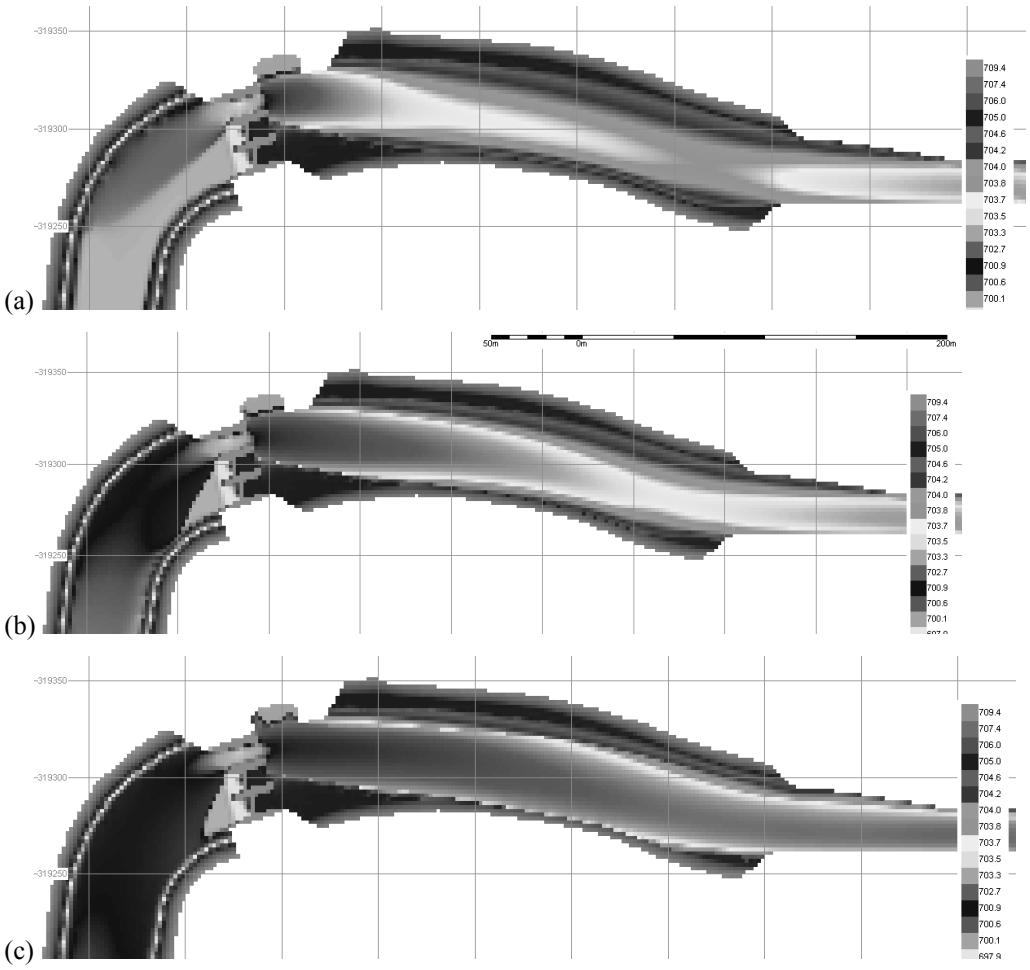

Figure 7. Evolution of the reservoir bathymetry during a flushing operation.

3.2 *Optimization of the water intake based on combined numerical and physical modelling*

The water intake structures, located close to the dam on the right bank of the river, have to divert from the main stream the discharge to the power plant, whatever the upstream level and the discharge in the reservoir. In addition, they have to prevent sediments, floating debris, air and fishes to enter the penstock, while minimizing head losses affecting the power plant efficiency.

The design of the water intake structures has been defined by successive and complementary application of both numerical and physical modelling approaches. A first numerical model has been used to define the overall geometry of the water intake structures, from the reservoir to the penstock inlet. The flexibility and the rapidity of numerical modelling enabled to test quickly a large range of geometry modifications to objectively suggest an optimized solution. In a second time, two large scale factor physical models have been built to analyse in details specific flow features which were not satisfactorily represented in the numerical model. The boundary conditions of these scale models have been defined from the numerical model results. The first scale model, with a 1:14.6 scale factor, has been used to analyse the risk of vortex formation at the transition from the free surface flow in the water intake to an under pressure flow in the penstock. A specific anti-vortex structure has also been designed and validated by using this dedicated physical model. The second scale model, with a 1:20 scale factor, enabled to analyse the effect on the free surface currents in the reservoir close to the dam of a partially submerged wall in front of the trash rack, with as main purpose to create a surface current diverting the small fishes from the water intake and guiding them to the mobile dam right bay, where the minimum discharge in the downstream river is continuously released.

3.3 *Stability of the riverbed after decommissioning of the existing dams*

More and more efforts are undertaken to restore rivers in a state close to their natural conditions, with the particular motivation of fulfilling the requirements of the Water Framework Directive 2000/60/EC (e.g., Borja et al. 2006). Like in many other on-going projects, river restoration was also part of the present one.

Besides restoration measures such as fish passages, bank restoration, bars or meanders, decommissioning of man-made structures is another important component of river restoration schemes (Raven et al. 2002). It enables to restore the longitudinal connectivity (migration of species for reproduction, food provisioning, etc.) and, in some instances, also the lateral connectivity (exchanges between rivers and riparian ecosystems). However, such interventions can have significant impacts on river, hydraulics and morphology, including bed degradation or aggradation and bank failures.

Although small scale river restoration projects, such as local rip rap or fish ladders, may be assessed based on relatively simple analyses and some degrees of trial and error approach, large scale river restoration projects, such as decommissioning of dams, require far more comprehensive and detailed analyses (Parasiewicz 2001). In particular, due to the high investment costs of these projects and the possible large scale impacts, trial and error approach must be avoided. For this kind of large projects, multidimensional flow and morphodynamic modelling constitute a very valuable support. Detailed flow modelling enables to detect erosion-prone areas where caution should be taken regarding bed and banks stability, as well as to evaluate the variability of flow parameters (for fish reproduction, spawning, etc.). To achieve this goal in the project discussed here, we have implemented a methodology which relies on 2D flow modelling to evaluate scenarios of river restoration based on several criteria related to flow, sediment transport and ecological objectives.

Figure 8 shows the general methodology developed to identify optimal restoration projects. First, both the topographic model and the boundary conditions for flow modelling are set up. The former constitutes a key input data, mainly in the riverbed, because it directly governs flow velocity and sediment transport. The accuracy of the dataset is therefore crucial. As the riverbed stability is one of the most important constraints of the restoration project, upstream discharge is taken close to the effective discharge, which transports the largest fraction of the bed-material load. The downstream boundary condition is prescribed as a free surface elevation of a location where this value is known from a rating curve (e.g., weir) or a gauging station. The mesh size is then determined from a trade-off between the expected result accuracy and the computational time. The second step consists in the calibration of parameters, such as a friction coefficient, using reference data (e.g., field survey, flood levels). Next, using a flow model, the present situation is modelled as a comparison basis. Restoration scenarios, which consist in local topography changes of the present situation, are implemented to create modified topographic models. If computed results, such as flow velocity, bottom shear stress and water depth on the new configuration comply with riverbed stability criteria and satisfy restoration objectives, then a satisfactory project is reached.

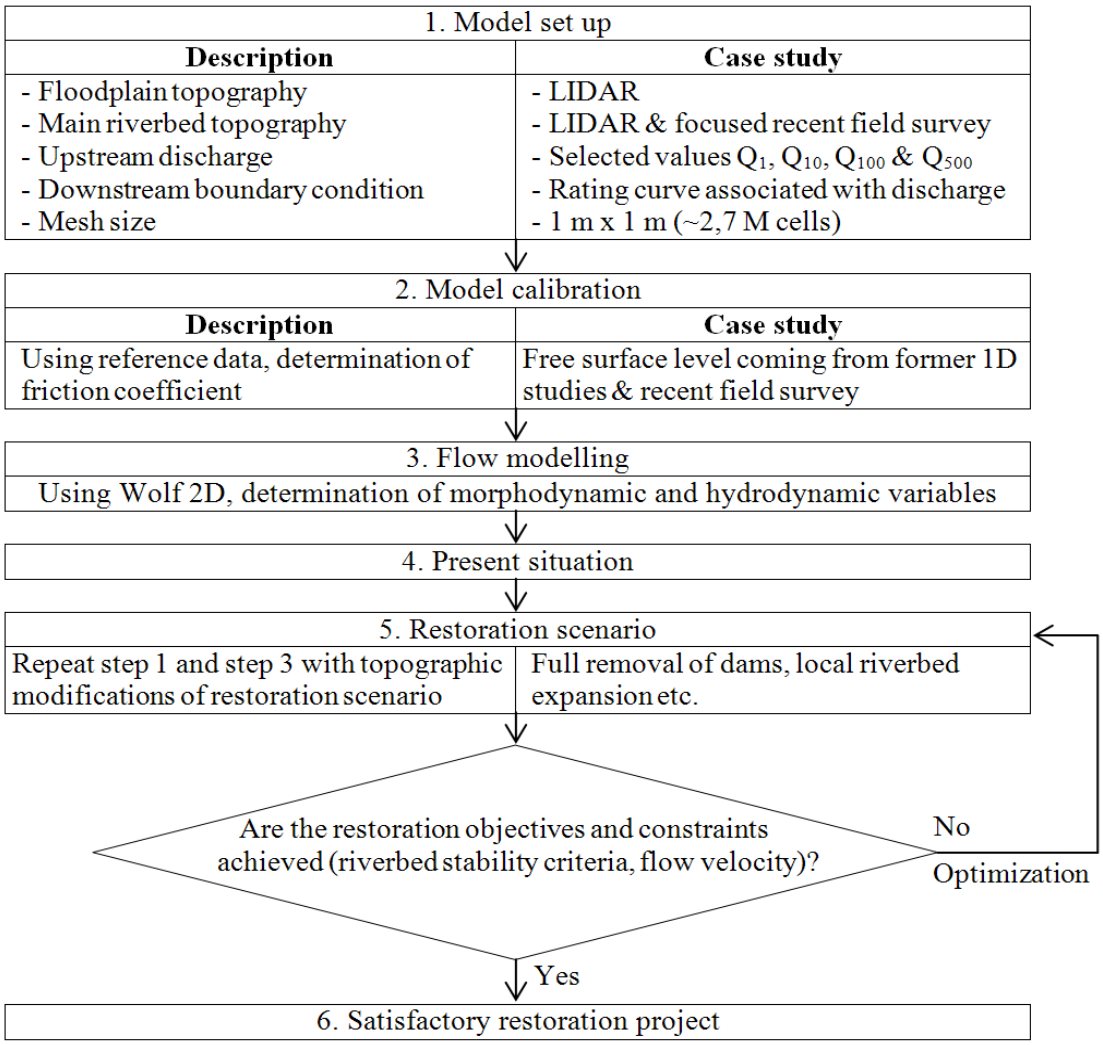

Figure 8. Developed methodology to evaluation river restoration scenarios (Rulot et al. 2012).

Several scenarios have been defined differing by the topography modifications at water intakes. The configuration in which all dams are removed and replaced by a more natural river section referred to as "scenario 1". Other restoration scenarios involve widening of the river to create valuable wetlands. The comparison between restoration scenarios and the present situation is mainly based on:

- Differences in water depths;
- Difference in flow velocity;
- Shields parameter (i.e. non-dimensional shear stress, governing inception of sediment transport).

As an example, comparing Shields parameter values between the present situation and "scenario 1" reveals that typical boulders (d ~ 20 cm) are not set into motion in the present situation, while they are very likely to be moved by the flow in this restoration scenario. This is just one example of outputs of the flow simulations, which provide valuable information to support the selection of the optimal restoration scenario. Several additional scenarios have also been tested.

4 VALIDATION AND EXTRAPOLATION PROCESS

Numerical models may be validated against experimental results, and subsequently used to extend the analysis beyond the range of parameters which may be considered in the available experimental facility or to speed up the analysis of geometry modifications before a final validation on the scale model. In addition, a physical model has often to be destroyed after testing and analysis (Sutherland 2011) while a numerical model can last. The latter, if well calibrated and documented, is thus extremely useful if it is needed to return to a study…

4.1 *Influence of the aeration rate on the mixed flow pattern in a gallery*

Experimental investigations have been carried out on a physical model of a gallery to determine expected flow discharge and the influence of the aeration rate on the flow discharge (Erpicum et al. 2009a). In parallel, numerical simulations have been performed with a 1D model for mixed flows, calibrated against the experimental results (Kerger et al. 2009). Stationary numerical results gave new insight into the mechanisms regulating flows in the gallery and the numerical model has been enabled a posteriori test of additional flow configurations in the system as well as small change in the structures geometry.

The physical model (Figure 9) included a Plexiglas circular pipe linking two tanks. Topography of the upstream and downstream tanks has been built regarding realistic in-situ natural conditions. The gallery inlet and outlet structures were also represented. Three air vents have been added upstream of the gallery, on the top of the circular cross section, with the purpose to feed the gallery with air to prevent the formation of low pressures within the flowing water.

The model has been equipped with an electromagnetic flowmeter on the pumping system, a limnimeter and a Pitot tube in the reservoir, 9 Pitot tubes and 14 graduated scales regularly distributed along the gallery.

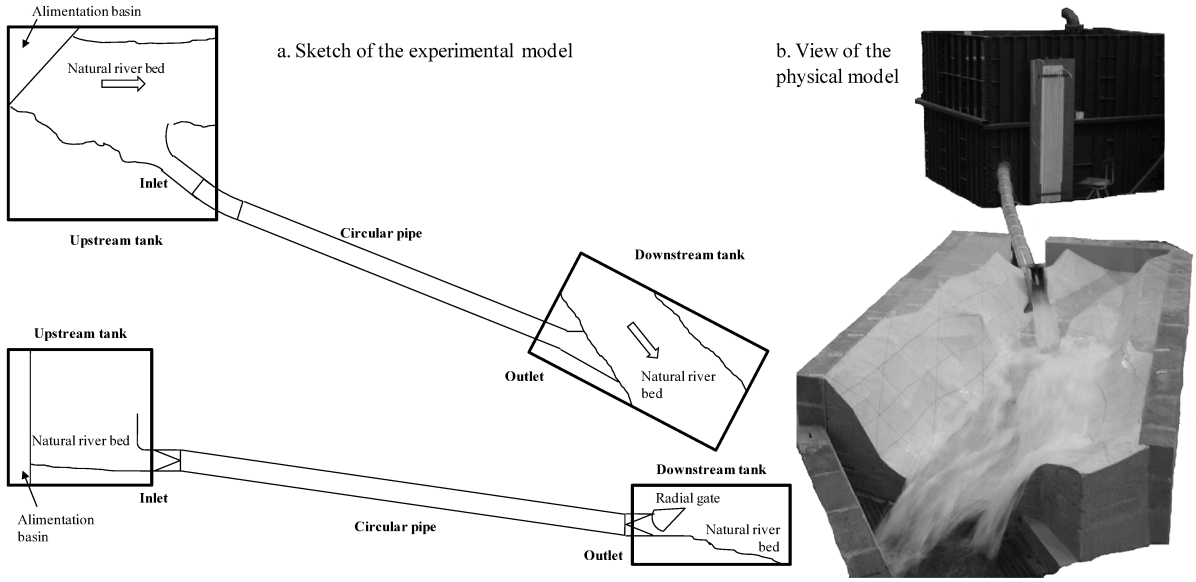

Figure 9. Description of the experimental setup

Investigations focused mainly on stationary flows and aimed at determining the flow discharge as a function of the upstream pressure head and downstream gate opening. In this case, strong air/water interactions alter the flow behaviour. In particular, the flow discharge through the gallery is strongly influenced by air/water interaction and depends of the aeration rate.

Various two-phase flow patterns have been observed according to the flow discharge through the gallery. Figure 10 shows the experimental relation between the flow discharge and the upstream pressure head. The curve defines 5 areas corresponding to the 5 flow patterns traditionally mentioned in literature.

In a first step, numerical simulations have been performed under the assumption of a pure water flow. A first head/discharge relation (dotted line in Figure 10) has been computed, assuming a free surface in each mesh if the water height is below the pipe crown (air phase above the free surface is at atmospheric pressure / high aeration rate). A second head/discharge relation (continuous line) has been computed by activating a negative Preissmann slot, i.e. considering sub-atmospheric pressurized flow (low aeration).

Numerical results are in good accordance with experimental data for smooth stratified flows and fully pressurized flows. Bubbly and intermittent flows show a similar behaviour two the sub-atmospheric pressurized flows. A periodic instability between two unstable steady flow regimes occurs in the area of wavy stratified flows. The instability induces large period (10s to 60s) oscillation of the water level in the upstream reservoir of the physical model.

Experimental and numerical data for the distribution of the total head and the pressure head (water level for free surface flow) along the gallery are given in Figure 11 for an intermittent flow. When pressure distribution along the gallery is computed under the assumption of a free surface flow, large discrepancies of the results are observed. The upstream pressure head is overestimated. Activation of a negative Preissmann slot gives the curve corresponding to a pressurized flow. A large area of sub-atmospheric pressure in the upstream part of the pipe is consequently identified. Results are in better accordance and it

has been concluded that the aeration rate of the pipe is not sufficient to induce the apparition of a free surface flow.

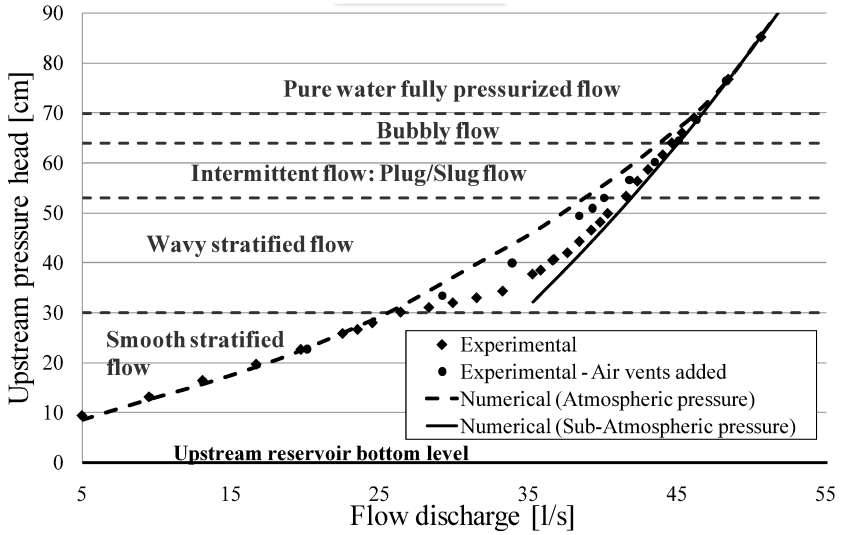

Figure 10. Experimental head/discharge relation and observed flow pattern

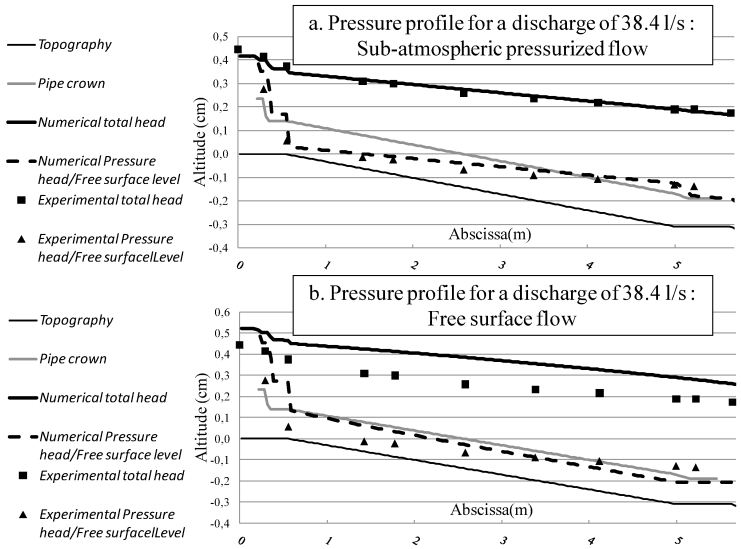

Figure 11. Computed total head and pressure head distribution for an intermittent sub-atmospheric pressurized flow and free-surface flow computation

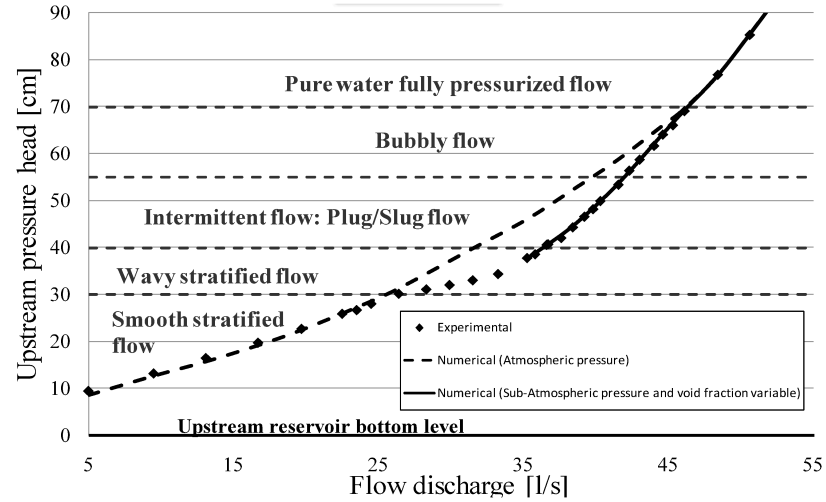

Figure 12. Head – discharge relation computed with variable void fraction

Application of a Homogeneous Equilibrium Model (Kerger et al. 2012) enables to overcome the results discrepancy observed for bubbly and intermittent flows. The effect of the entrained air on the water flow is indeed accurately computed, the model parameters having been calibrated considering the experimental results.

Figure 12 shows a comparison between experimental and numerical data for the relation between the flow discharge through the gallery and the upstream pressure head. Taking into account air/water interaction in the computation obviously gives more accurate results for bubbly and intermittent flows.

4.2 *Rehabilitation studies of a gated weir*

An old dam is equipped with a spillway made of three automatic gates on a broad crested weir and a two slopes channel downstream. Following a revision of the hydrology of the upstream river, the spillway capacity has to be increased at constant reservoir level. One of the rehabilitation solutions is to modify the profile of the broad crested weir, the discharge coefficient of which is around 0.365, to tend toward an ogee crested profile.

Because of the reservoir shape, complex sill profile and downstream channel geometry, physical modelling appears as the most confident approach to represent the whole flow characteristics. However, it is not the most efficient way to test several weir and downstream channel profiles to define objectively the optimal solution.

A composite modelling approach enabled to propose a confident and objectively optimized rehabilitation solution while drastically decreasing the number of spillway geometries tested on the scale model.

In a first step, a 1:35 scale model of the existing geometry has been build (Figure 13 - left). It enabled to define the discharge capacity of the existing structures and to document the flow characteristics along the spillway for a wide range of operating conditions. In particular, it showed that for higher discharge, when the gates are fully opened, the control section is partially located in the first section of the downstream channel, whose plane geometry, small slope and limited width restrict the discharge capacity. The physical model also provided calibration and validation data for a numerical model of the spillway, representing only the weir and the downstream channel (Figure 13 - right).

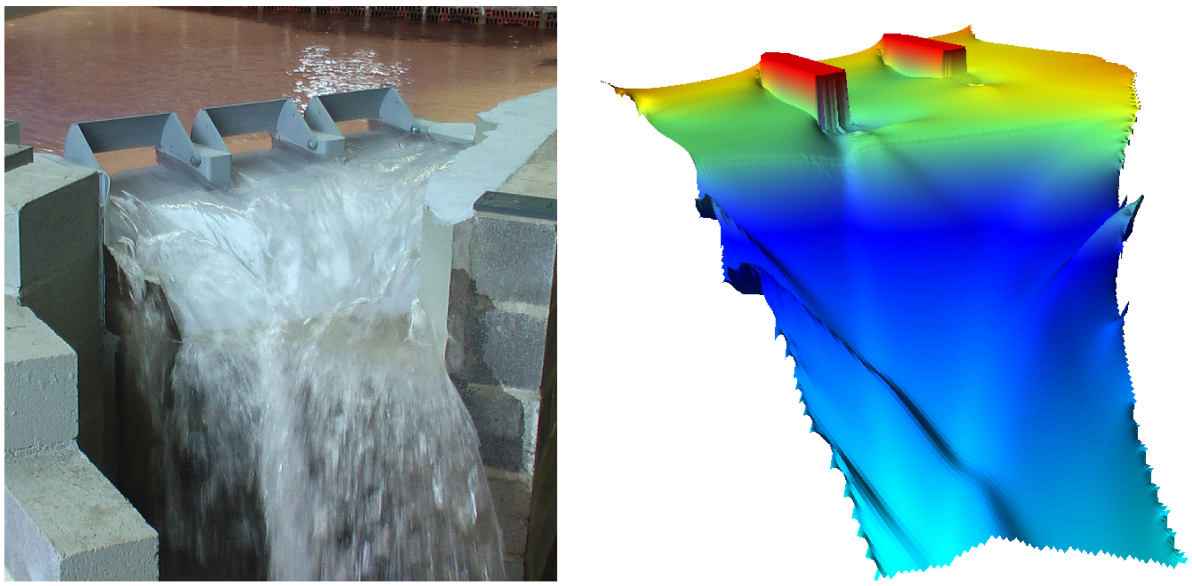

Figure 13. Scale model of the spillway (left) and corresponding numerical model (right)

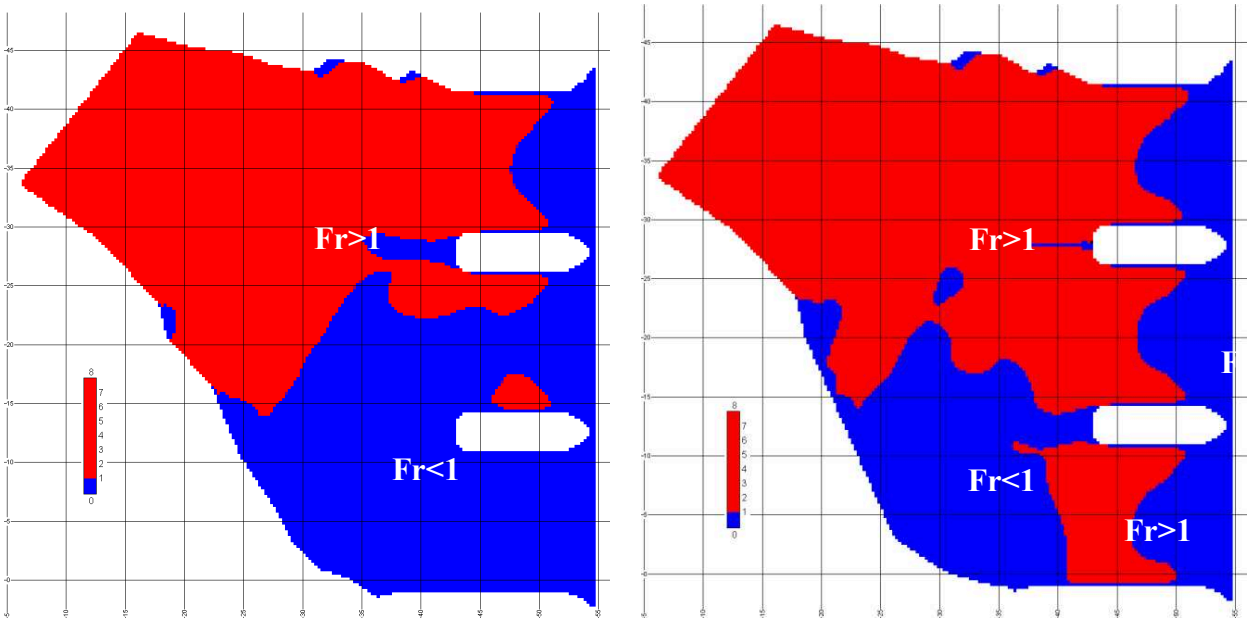

Figure 14. Numerical model - Froude number distribution on the spillway – Existing geometry (left) and proposed rehabilitated design (right)

The numerical model has been used in a second step to rapidly test several sill and channel profile modifications, in order to find the solution which minimizes the excavation but ensures high enough discharge capacities. In particular, it has been verified that the control section is always located on the top of the weir, with thus a Froude number higher than one through all of the three bays (Figure 14).

Finally, the optimized geometry defined using the numerical model has been validated on the scale model (Figure 15), to demonstrate definitively its performances.

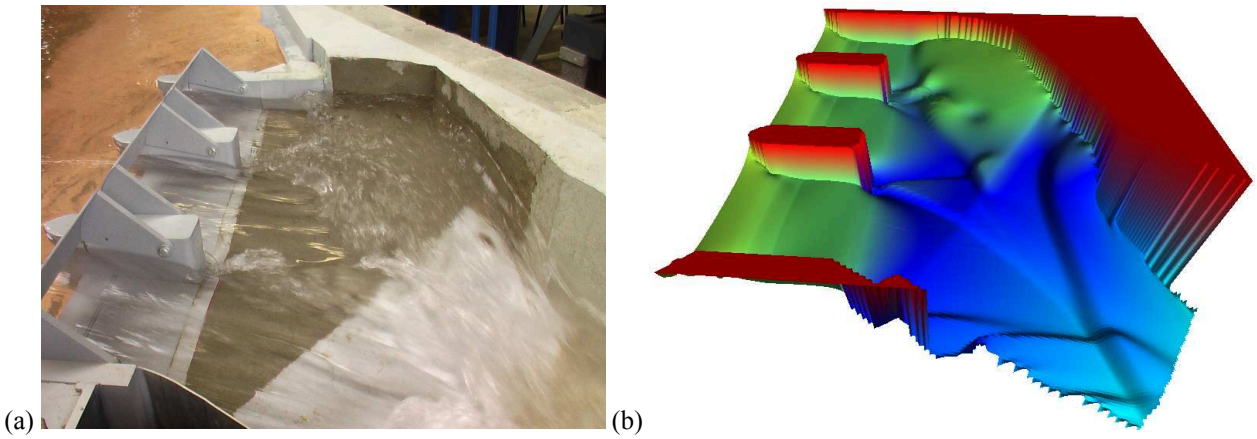

Figure 15. Final design - Physical (a) and numerical (b) modelling

5 QUANTIFYING THE RELATIVE INFLUENCE OF DIFFERENT PROCESSES

Field observations provide without doubt the most realistic figure of the complex interconnected processes governing flow and sediment transport in real-world conditions. However, interpretation and basic understanding of the underlying physics may be complicated in the case of field measurements due to the high degree of complexity of interconnected processes which influence the observations. Therefore, experimental conditions are often preferred and offer a complementary view by enabling to replicate the main features of a flow situation of interest in a controlled environment. Nonetheless, even in an experimental setup, such a flume, not all influences may be controlled separately. In contrast, the somehow virtual environment created by numerical simulations enables to distinguish between individual effects, such as those sketched in Figure 2. This type of investigation may contribute to a better identification of the relative importance of several factors influencing flow and sediment transport.

In this section, we present a recent basic research on hydrodynamics and sedimentation in shallow rectangular reservoirs, which may be common appurtenant structures of low head hydraulic projects and are

widespread in urban hydraulics. In this research, composite modelling has been applied to appreciate the relative importance of the geometric effect of morphodynamic changes and the increased roughness induced by sediment deposits.

5.1 *Recent research on flow and sedimentation in shallow rectangular reservoirs*

Two main types of shallow reservoirs may be distinguished: *(i) retention basins*, which contribute to flood protection by temporarily storing large volumes of water (river floods, rains in sewage), and *(ii) sedimentation basins*, which store polluted water before it is sent to a treatment plant. The size of these reservoirs varies from a few hundred cubic meters for the smallest (e.g., in sewage networks) to millions of cubic meters for large hydraulic engineering structures.

Depending on the operation goal of the structure, sediment deposits must be either maximized (to trap polluted sediments) or minimized (to maintain storage capacity with minimum maintenance cost). The prediction of deposition areas, which is a prerequisite for the optimal operation of these reservoirs, depends on the detailed knowledge of the flow characteristics. Despite the simple geometry of rectangular reservoirs, the flow patterns may show complex recirculations and large-scale turbulent structures both in 2D (horizontal recirculations) and in 3D (vertical recirculations, spiral flow).

Based on the results of a systematic study of flow and sediment transport in shallow rectangular tanks (Kantoush et al. 2008), Dewals et al. (2008) demonstrated the complexity of the flows that develop in such reservoirs, despite their particularly simple geometry (Figure 16). Besides a symmetric jet flow (flow pattern S1), several asymmetric flow patterns have been identified, in spite of the hydraulic and geometric symmetry of the setup. Characterized by large-scale turbulent structures, the main flow patterns may be classified based on the presence of one or two reattachment points (flow patterns A1 and A2, respectively).

The hydrodynamic instabilities which take place in such reservoirs and the underlying physics were also described, using an approach combining the results of the experiments with 2D numerical modelling and theoretical stability analysis (Dewals et al. 2008).

While the aforementioned experiments focused mainly on the influence of the reservoir geometry on the flow pattern for constant hydraulic conditions, an experimental campaign undertaken at the University of Liege (ULg) has led to new contributions regarding the influence of hydraulic parameters on the flow pattern, as well as a previously unreported quantification of the variability of the flow (Dufresne et al. 2010a). These test also enabled to develop a first prediction formula to forecast the type of flow pattern based on the geometry of the reservoir (Dufresne et al. 2010a). The validity of this formula has been confirmed by all experimental results published so far (e.g., Camnasio et al. 2011).

Several series of experiments have been conducted to study the sedimentation in rectangular shallow reservoir. Among others, Dufresne et al. (2010b) considered bed load sediment inflows lower than the transport capacity of the flow at the inlet. This is an extreme situation, which to date provides only a partial knowledge of the role played by sediment characteristics and concentration on the location and thickness of deposits.

Based on state-of-the-art depth-averaged turbulence models (Erpicum et al. 2009b), a numerical model successfully predicted the observed flow patterns (Dewals et al. 2008; Dufresne et al. 2011). However, the limits of current models has been demonstrated when it comes to predicting the detailed turbulent characteristics (Reynolds stresses), especially in the recirculation zones.

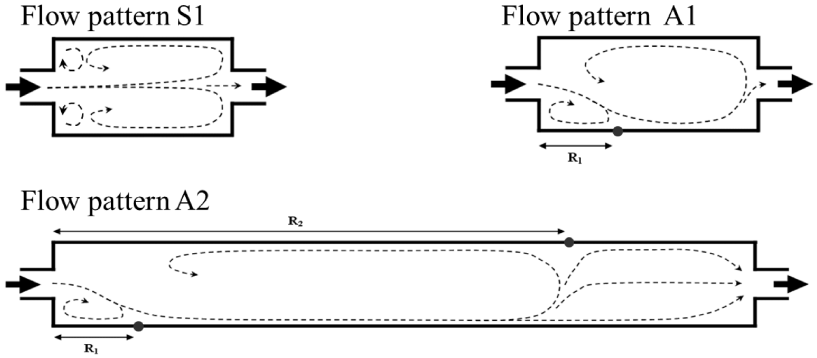

Figure 16. Typology of the main flow patterns observed in rectangular shallow reservoirs (Dufresne et al. 2010a): depending on the shape of the reservoir, the flow has zero, one or two reattachment points (•).

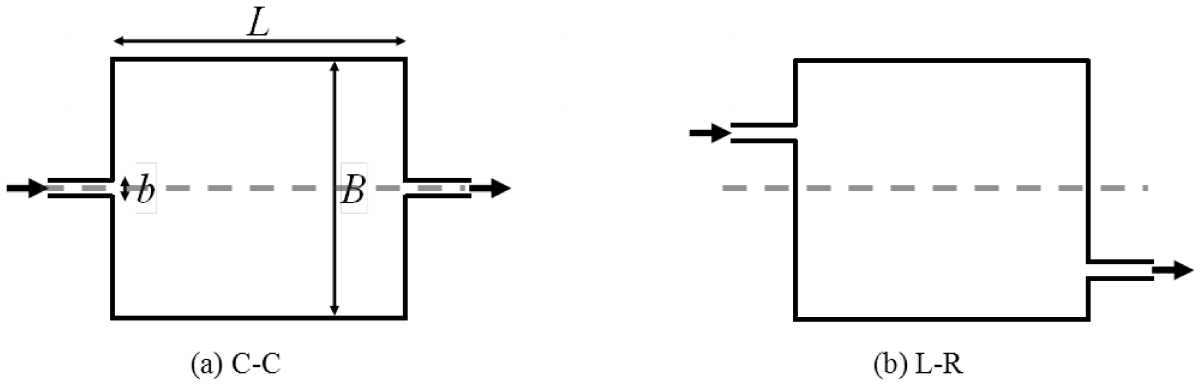

Figure 17. Standard reservoir configuration with inlet and outlet channels located along the centreline of the reservoir (a) vs. reservoir with inlet and outlet channel located on the left side on the reservoir centreline (b).

5.2 *Physical modelling*

To investigate the specific influence of the location of the inlet and outlet channels on flow and sedimentation in rectangular shallow reservoirs, Camnasio et al. (2012) conducted experimental tests in a rectangular shallow PVC reservoir with a smooth flat bottom (maximum depth 0.3 m, maximum length L = 6 m and maximum width B = 4 m) endowed with inlet and outlet free surface channels (width b = 0.25 m, length 1 m each). The channels can be moved respectively along the upstream and the downstream side of the reservoir in order to obtain reservoir configurations with asymmetric locations of the inlet and of the outlet channel. Two out of the four configurations chosen for the tests are shown in Figure 17.

Movable PVC walls allow adjustment of the length L and the width B of the reservoir in order to test different length-to-width ratios L/B and expansion ratios B/b. However, for the tests here presented, reservoir width was set to B = 4 m and reservoir length to L = 4.5 m (L/B = 1.125, B/b = 16). This geometric configuration is characterized, when the channels are placed at the centre of both reservoir sides, by a stable symmetric flow field S1 (Camnasio et al. 2011): this flow field is formed by a main jet that goes straight from the inlet to the outlet and by two recirculation zones which develop on each side of the main jet, and which are characterized by lower velocities.

The reservoir is fed with a constant discharge Q and the water depth h of the reservoir is regulated by a flap gate placed at the end of the downstream channel. The entering discharge is measured by an electromagnetic flow meter placed on the pressurized pipe leading to the experimental facility. A second discharge check is obtained by water level measurement above the flap gate placed at the end of the outlet channel, since it behaves like a sharp inclined weir. After the pressurized pipe leading to the inlet channel, a honeycomb is placed in order to have an approximately uniform velocity distribution on the entire channel cross section. During tests with suspended load, the sediments are continuously fed from a container into a mixing tank, where they are mixed to the inflowing discharge by a rotating propeller. Then, the water-sediments mixture is lead to the experimental reservoir by the pressurized conduit. The sediments quantity from the container could be adjusted to the desired value by regulating a purpose-made opening.

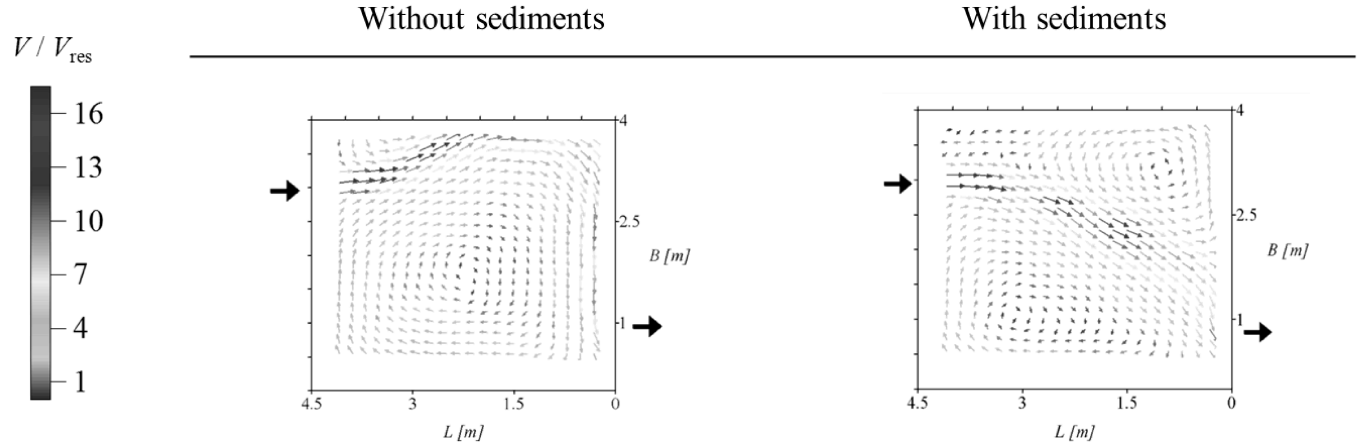

Figure 18. Influence of suspended load on the experimentally measured velocity field in a shallow rectangular reservoir. Velocity V has been normalized with respect to a hypothetical plug flow velocity V_{res} throughout the whole reservoir cross-section. Adapted from Camnasio et al. (2012).

During the experiments presented here, the water depth was fixed at $h = 0.2$ m for a constant discharge of $Q = 7$ l/s. The resulting Froude number and Reynolds number are $Fr_{in} = Q/(bh)/(gh)^{1/2} = 0.1$, $\mathrm{Re}_{in} = 4\rho Qh/(bh\mu) = 112{,}000$ (turbulent flow), both referring to the inlet channel.

Velocities were measured at 8 cm from the reservoir bottom by UVP, first during clear water tests, then during tests with sediment supply, in order to investigate the possible influence of suspended load and/or of sediments deposits on the flow patterns. Vector velocity maps were produced for all the tested reservoir configurations. The time-averaged local horizontal velocity V at every measurement point was normalized to the average theoretical plug flow velocity $V_{res} = Q/(B \cdot h) = 8.75$ mm/s assuming the basic hypothesis of a one-dimensional motion of the whole discharge Q through the cross section $B\,h$. Figure 18 shows the distribution of the normalized average horizontal velocities $V_{nd} = V/V_{res}$ in the entire reservoir for the so-called L-R configuration, i.e. with inlet and outlet channels located respectively on the left and right sides of the reservoir centreline. The velocities along the main jet have a minimum in the order of 100 mm/s, while in the centre of the recirculation zones, velocity reaches a minimum of about 10 – 20 mm/s. The right hand side of Figure 18 corresponds to the flow patterns measured after 4 hours of sediments supply. The flow pattern which developed during tests with suspended sediments is different from the one developing during clear water tests (Camnasio et al. 2012).

Sediment deposits thickness on the entire reservoir bottom was measured by a laser method after 2 hours and after 4 hours of sediment supplying. The laser was placed in a water-proof box attached to the movable metal bar, at a known height from reservoir bottom. The voltage given by the laser is linked to the distance of the laser light source from the top of the sediments deposits, through a calibration line calculated for the instrument under real operating conditions. The current intensity signal coming from the laser was first converted into a voltage signal. Then it was sent to the PC by a USB high-speed data acquisition module.

5.3 *Numerical modelling*

Figure 19 shows profiles of the longitudinal velocity in different cross-sections of the reservoirs, as simulated with a k-ε turbulence model for the initial situation with a flat bottom and for the bathymetry obtained after 4 hours of sediment deposition. The results follow closely the experimental observations, both in the recirculations and in the main the jet. Changing the bottom roughness would lead to hardly noticeable changes in the velocity profiles, which is in agreement with Babarutsi et al. (1989) and Chu (2004) for unilateral expansions: since the bed friction number remains here very low, the flow is classified as “non-frictional” and is thus not influenced by the roughness. When the topography corresponding to sediment deposits is considered, the velocity increases by up to 10% in the centre of the jet and the change of flow pattern is visible in the cross-sectional profiles.

To analyse the feedback effect of morphodynamic evolution on the flow pattern, the time evolution of the measured thickness of sediment deposits has been implemented in the flow simulation as a time-varying topography. Four hours of flow have been simulated, corresponding to the total duration of the experiments with sediments. Since only three maps of measured sediments deposits were available (initial condition, deposits after 2 h and deposits after 4 h), linear interpolation in time has been used for the intermediary time step.

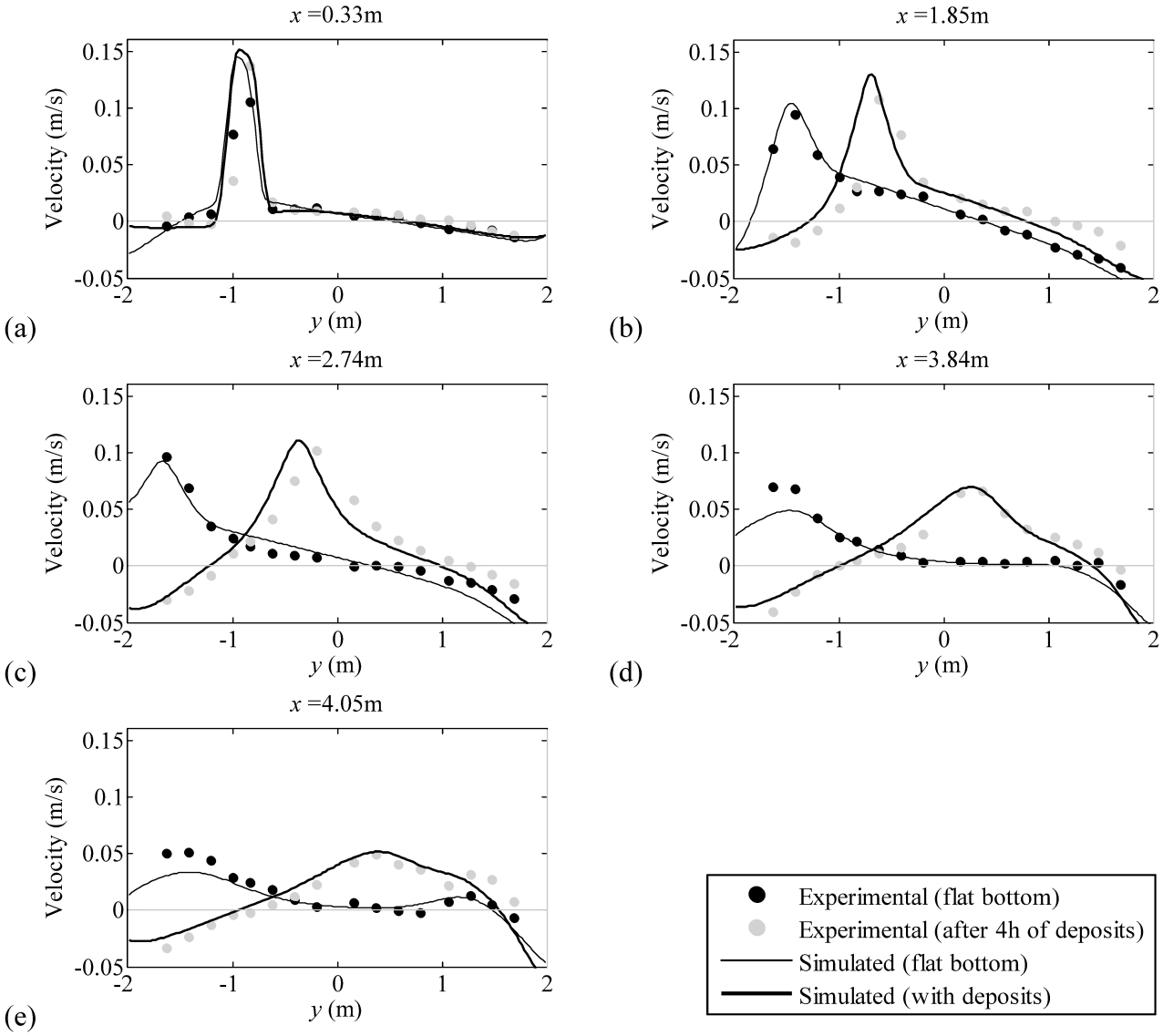

Figure 19. Comparison between measured and simulated velocity profiles along different cross-sections of the reservoir in both configurations: without suspended load (initial flat topography) and after 4h of sediment deposits. Adapted from Camnasio et al. (2012).

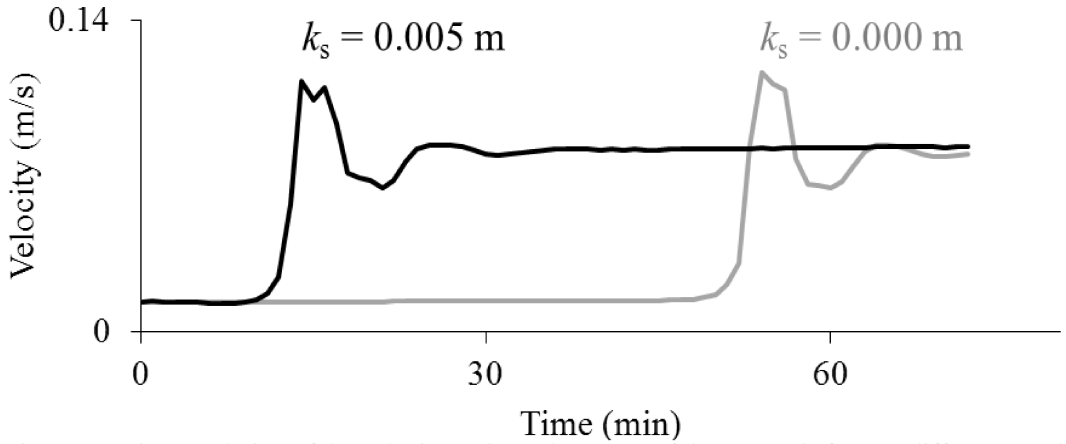

Figure 20. Time evolution of the velocity (m/s) at the centre of the reservoir for two different roughness coefficients.

At the end of the simulation, the mean thickness of deposits remains below 10% of the water depth. Simulation results have shown that the numerical model succeeds in reproducing the change in flow pattern as a result of the change in bathymetry. This is consistent with the experimental results (Figure 21).

In Figure 20, the velocity magnitude in the middle of the reservoir is used as an indicator to appreciate the dynamics of the flow pattern modification. This variable confirms that a sudden shift takes place after some sedimentation time. Figure 20 reveals a strong influence of the bottom roughness on the timing of

the change in flow pattern. Interestingly, those two parameters did not influence significantly the velocity profiles. Consequently, the numerical model not only succeeds in reproducing the process of flow pattern change but also enables to quantify the relative importance of the geometric effect (bathymetry change) and increased roughness due to deposits. In contrast, those two processes could not be distinguished from experimental tests only.

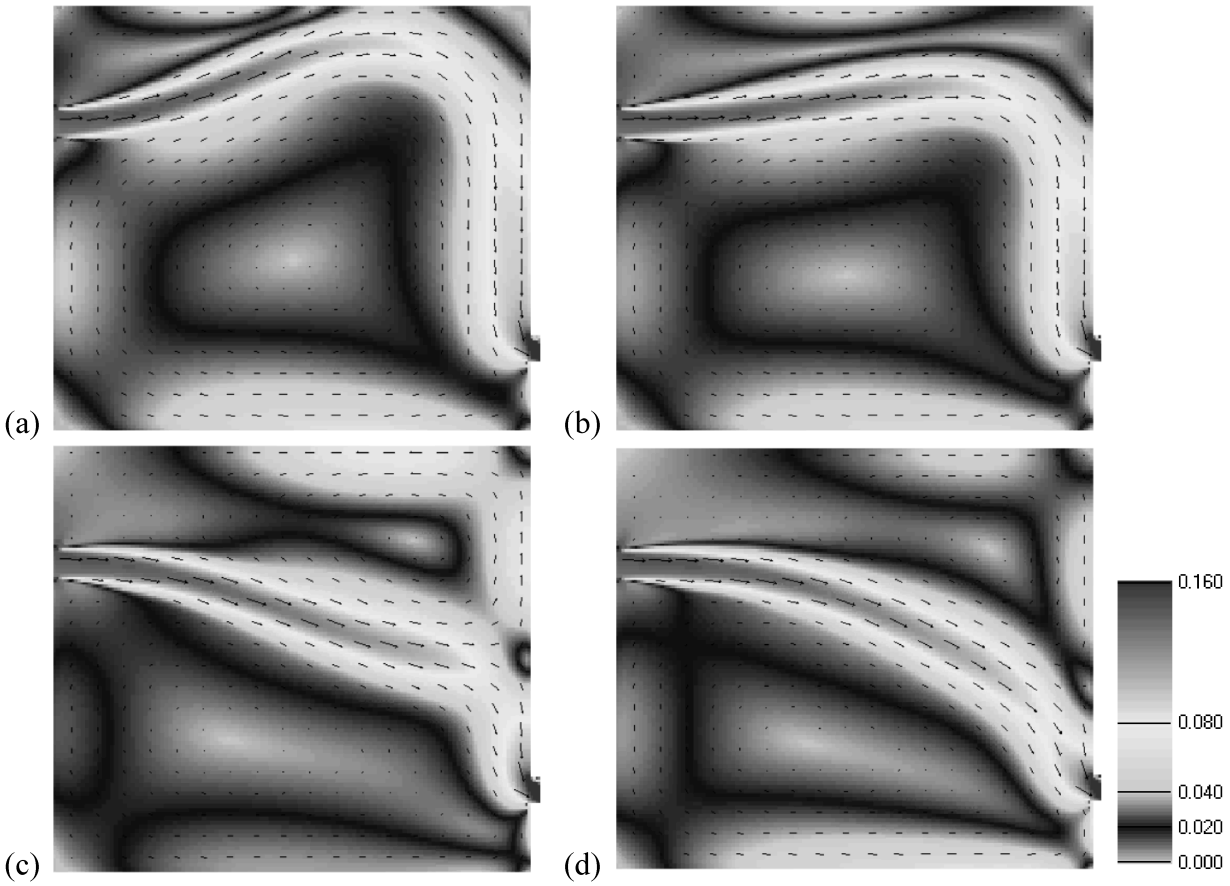

Figure 21. Time evolution of the velocity field (m/s) in the reservoir as sediment deposits develop on the bottom.

6 CONCLUSIONS

In this paper, we reviewed four types of composite modelling approaches, from which valuable benefits can be taken both for real-world projects design and for more basic research.

Embedding a physical model within a broader scale numerical model enables to increase the scale factor and, therefore build more representative experimental models less affected by scale effects.

Besides this increasingly standard approach in composite modelling, different numerical and physical models may be interconnected to address specific aspects of a single real-world project or research question, as could be demonstrated here in the case of an on-going hydropower project involving reservoir sedimentation and sediment management issues, shape optimization of the water intake under environmental constraints, flood levels computation as well as renaturation of a river section where old low-head hydropower plants will be decommissioned. In such a strategy, each type of model (physical vs. numerical, hydraulic vs. morphodynamic, small vs. large scale) is applied to conduct part of the studies for which it is best suited and may interactively exchange data with the other components of the overall composite modelling strategy deployed. This generally enables to take maximum benefit from each type of model and this approach is often combined with the first one, namely a refined physical model embedded within a broader scale numerical model.

Physical models may also be used to validate numerical modelling, which is in turn applied to investigate more combinations of hydraulic and geometric parameters thanks to the high flexibility of numerical models compared to experimental ones. Their relatively low cost to conduct multiple runs makes numerical models particularly efficient to perform comprehensive sensitivity analyses.

Finally, we have detailed a fundamental analysis of the feedback of reservoir sedimentation on the mean flow in a shallow reservoir. In this case, composite modelling enabled to appreciate the relative in-

fluence on the flow characteristics of changes in the reservoir bathymetry and in the bottom roughness as a result of sediment deposits. These two influences could hardly be separated if the research relies solely on physical modelling and not on composite modelling.

REFERENCES

ASCE. (2000). "Hydraulic modeling - Concepts and practice." Reston, Virginia.

Babarutsi, S., Cho, V. H., and Ganoulis, J. (1989). "Experimental investigation of shallow recirculating flows." J. HYDRAUL. ENGNG. (ASCE), 115(7 , Jul. 1989), 906-924.

Borja, Á., Galparsoro, I., Solaun, O., Muxika, I., Tello, E. M., Uriarte, A., and Valencia, V. (2006). "The European Water Framework Directive and the DPSIR, a methodological approach to assess the risk of failing to achieve good ecological status." Estuarine, Coastal and Shelf Science, 66(1–2), 84-96.

Camnasio, E., Orsi, E., and Schleiss, A. J. (2011). "Experimental study of velocity fields in rectangular shallow reservoirs." Journal of Hydraulic Research, 49, 352-358.

Camnasio, E., Erpicum, S., Orsi, E., Pirotton, M., Schleiss, A., and Dewals, B. (2012). "Effects of inlet and outlet location on flow and sedimentation in rectangular reservoirs." Journal of Hydraulic Research (submitted).

Cao, Z., and Carling, P. A. (2002). "Mathematical modelling of alluvial rivers: reality and myth. Part 2: Special issues." Water & Maritime Engineering, 154, 297-307.

Chu, V. H., Liu, F., and Altai, W. (2004). "Friction and confinement effects on a shallow recirculating flow." Journal of Environmental Engineering and Science, 3(5), 463-475.

Dewals, B., Erpicum, S., Archambeau, P., and Pirotton, M. (2012). "Experimental study of velocity fields in rectangular shallow reservoirs." Journal of Hydraulic Research, 50(4), 435-436.

Dewals, B. J., Kantoush, S. A., Erpicum, S., Pirotton, M., and Schleiss, A. J. (2008). "Experimental and numerical analysis of flow instabilities in rectangular shallow basins." Environmental Fluid Mechanics, 8, 31-54.

Dufresne, M., Dewals, B. J., Erpicum, S., Archambeau, P., and Pirotton, M. (2010a). "Classification of flow patterns in rectangular shallow reservoirs." Journal of Hydraulic Research, 48(2), 197-204.

Dufresne, M., Dewals, B. J., Erpicum, S., Archambeau, P., and Pirotton, M. (2010b). "Experimental investigation of flow pattern and sediment deposition in rectangular shallow reservoirs." International Journal of Sediment Research, 25(3), 258-270.

Dufresne, M., Dewals, B. J., Erpicum, S., Archambeau, P., and Pirotton, M. (2011). "Numerical investigation of flow patterns in rectangular shallow reservoirs." Engineering Applications of Computational Fluid Mechanics, 5(2), 247-258.

Erpicum, S., Kerger, F., Archambeau, P., Dewals, B. J., and Pirotton, M. (2009a). "Experimental and Numerical Investigation of Mixed Flow in a Gallery." Multiphase Flow, New Forest.

Erpicum, S., Meile, T., Dewals, B. J., Pirotton, M., and Schleiss, A. J. (2009b). "2D numerical flow modeling in a macro-rough channel." International Journal for Numerical Methods in Fluids, 61(11), 1227-1246.

Erpicum, S., Dewals, B.J., Archambeau, P., Pirotton, M. (Accepted). "Composite modeling to enhance hydraulic structures studies." La Houille Blanche.

Erpicum, S., Dewals, B.J., Vuillot, J.-M., Archambeau, P., Pirotton, M. . (2012). "The Taoussa Project (Mali): an example of effective composite modeling." Proc. of the 4th IAHR Int. Symp. On Hydraulic structures, Porto, Portugal.

Frostick, L. E., McLelland, S. J., and Mercer, T. G. (2011). "Users guide to physical modelling and experimentation – IAHR design manual." CRC Press Taylor & Francis group, Leiden.

Kantoush, S. A., Cesare, G. D., Boillat, J. L., and Schleiss, A. J. (2008). "Flow field investigation in a rectangular shallow reservoir using UVP, LSPIV and numerical modelling." Flow Measurement and Instrumentation, 19, 139-144.

Kerger, F., Erpicum, S., Archambeau, P., Dewals, B. J., and Pirotton, M. (2009). "Numerical Simulation of 1D Mixed Flow with Air/Water Interaction." Multiphase Flow, New Forest.

Kerger, F., Archambeau, P., Dewals, B. J., Erpicum, S., and Pirotton, M. (2012). "Three-phase bi-layer model for simulating mixed flows." Journal of Hydraulic Research, 50(3), 312-319.

Novak, P., Guinot, V., Jeffrey, A., Reeve, D.E. . (2010). Hydraulic modelling – An introduction., Spon Press, London, UK.

Parasiewicz, P. (2001). "MesoHABSIM: A concept for application of instream flow models in river restoration planning." Fisheries, 26(9), 6-13.

Raven, P. J., Holmes, N. T. H., Charrier, P., Dawson, F. H., Naura, M., and Boon, P. J. (2002). "Towards a harmonized approach for hydromorphological assessment of rivers in Europe: a qualitative comparison of three survey methods." Aquatic Conservation: Marine and Freshwater Ecosystems, 12(4), 405-424.

Roger, S., Dewals, B. J., Erpicum, S., Schwanenberg, D., Schuttrumpf, H., Kongeter, J., and Pirotton, M. (2009). "Experimental and numerical investigations of dike-break induced flows." Journal of Hydraulic Research, 47(3), 349-359.

Rulot, F., Detrembleur, S., Archambeau, P., Erpicum, S., Pirotton, M., and Dewals, B. (2012). "Multidimensional Flow Modelling to guide Hydromorphological Restoration of an Alpine River." 9th International Symposium on Ecohydraulics, Vienna, Austria.

Stilmant, F., Pirotton, M., Archambeau, P., Roger, S., Erpicum, S., and Dewals, B. (2012). "Dike-break induced flows: a simplified model." Environmental Fluid Mechanics, 1-12.

Sutherland, J., Barfuss, S.L. . (2011). "Composite modelling: combining physical and numerical models." Proc. of the 34th IAHR World Congress, Brisbane, Australia, 4505-4512.

Van Os, A., Soulsby, R., Kirkegaard, J. (2004). "The future role of experimental methods in European hydraulic research: towards a balanced methodology." Journal of Hydraulic Research, 42(4), 341-356.

2 Weirs and Gates

IWLHS, 20-22/02/2013, Aachen - Bung & Pagliara (eds) - © 2013 Bundesanstalt für Wasserbau ISBN 978-3-939230-04-5

Experimental Study of Stage-Discharge Relationships for Flows over Radial Gates and Flap Gates

L. Delattre & Y. Zech
Université catholique de Louvain (UCL), Institute of Mechanics, Materials and Civil Engineering, Hydraulics Laboratory, Place du Levant 1, B-1348 Louvain-La-Neuve, Belgium

P. Dierickx
Waterways Administration of the Walloon Region (SPW-SETHY), Boulevard du Nord 8, B-5000 Namur, Belgium

S. Soares-Frazão
Université catholique de Louvain (UCL), Institute of Mechanics, Materials and Civil Engineering, Hydraulics Laboratory,, Place du Levant 1, B-1348 Louvain-La-Neuve, Belgium

ABSTRACT: Floods forecasting and management of large regulated rivers require the ability to properly combine classical flow routing with the regulation dams that act as internal boundaries. Therefore a good knowledge of the stage-discharge relationships of these dams is mandatory. The Meuse River in Belgium is such a regulated river, for which the HYDROAXE software was developed jointly by the Belgian Ministry of Public Works (SPW-SETHY) and the Hydraulics Laboratory of the Université catholique de Louvain (Belgium). Working for a constant improvement of this software, this paper presents an experimental study of flow over a typical dam of the River Meuse, i.e. a dam controlled by radial gates equipped with flap gates. Measurements of the upstream water level and of the discharge are presented for different positions of the flap gate. According to earlier works on gates featuring a variable inclination, mainly drum gates, it is observed that the stage-discharge relationship depends on the inclination of the flap. However, the theoretical discharge coefficient obtained by means of formulae of the literature always exceeds the measured discharge coefficient. This suggests that further work is required to obtain a stage-discharge relationship adapted to the particular case of radial gates equipped with flap gates.

Keywords: Dam discharge modelling, Flood forecasting software, Physical model of gate, flow over gate, flow below gate

1 INTRODUCTION

The Meuse River in Belgium (Figure 4) is regulated through 15 dams (e.g. the La Plante dam illustrated in Figure 5) consisting of radial gates and flap gates (Figure 6). For low discharges water flows over the flap gate. This mobile part being progressively lowered when the discharge increases in order to maintain the prescribed water level in the regulated reaches. For higher discharges, the radial gate is raised incrementally and the water flows both over and under the gate. For further increasing discharges, the gates are completely raised and the water level is unregulated.

To predict the water levels along the Meuse River, the HYDROAXE software was developed at the Université catholique de Louvain, Belgium (e.g. Scherer and al. 1998, Dal Cin and al. 2005). HYDROAXE is a real-time flood forecasting tool based on the numerical resolution of the 1D Saint-Venant equations, including the Exchange Discharge Model (Bousmar and Zech 1999) to account for momentum exchanges between the minor bed and the floodplains. In its current state, HYDROAXE covers the Meuse River from the dam of Hastière close to the French border until the dam of Monsin close to the city of Liege. Based on 18-hours discharge prediction, the model provides in a few seconds the hourly evolution of the water level along this reach of about 150 km. The considered reach is equipped with 15 dams as indicated in Figure 4. The model takes into account the operation of the dam gates and their influence on the flow. In this context, the accuracy of the stage-discharge relationships used in the numerical model for the gates is crucial.

In this paper, we present an experimental study of flow over a scale model of the radial and flap gate of the La Plante dam (Figure 5). Among the wide range of stage-discharge relationships that can be found in literature for flows over weirs and gates, the formulae by Bradley (1954) and Sinniger and Hager (1989) appeared as the most appropriated for our case. These formulae are used to predict the discharge

in our experiments, and the results are compared to the measurements. Finally, conclusions are drawn regarding their applicability to the Meuse River dams.

2 FLOW OVER THE GATE

2.1 *Some existing theoretical models and experimental studies concerning flows over weirs*

Among the theoretical and experimental studies about flows over weirs that can be found in the literature, only very few consider a variable flap angle (Bradley 1954, Sinniger and Hager 1989). Other models developed for sharp crested weirs may also be considered, such as those developed by Chow (1959), Naudasher (1991) or Novak (1996).

In the models proposed by Chow (1959) and by Naudascher (1991), the discharge coefficient is calculated from the known discharge and a water depth h, defined as the difference between the elevations of the water surface upstream the gate and the highest point of the gate (Figure 8). For a gate of width L, the equation proposed by Chow (1959) is

$$Q = C\,L\,h^{3/2} \tag{1a}$$

$$\text{with } C = \sqrt{0.3048}\left(3.27 + 0.40\frac{h}{w}\right) \tag{1b}$$

where the discharge coefficient C is given in ($m^{1/2}s^{-1}$). Naudascher (1991) proposed

$$Q = \frac{2}{3}\mu\sqrt{2g}L\,h^{3/2} \tag{2a}$$

$$\text{with } \mu = 0.61 + 0.08\frac{h}{w} \tag{2b}$$

In these two models, the discharge coefficient depends linearly on the value of h / w, where w is the distance between the toe and the highest point of the gate (Figure 8). It must be noted that only the upstream water level is taken into account in h, and not the total head. In the model by Novak (1996), the discharge coefficient also depends linearly on the value h / w but the total head above the highest point of the gate, denoted by H (Figure 1), is used, instead of h, to calculate the discharge:

$$Q = \mu\sqrt{2g}\,L\,H^{3/2} \tag{3a}$$

$$\text{with } \mu = 0.602 + 0.075\frac{h}{w} \tag{3b}$$

2.2 *The theoretical model based on Bradley (1954) and Sinniger & Hager (1989)*

The theoretical model is based on the work of Bradley for flows over drum gates for which the upstream face is quite similar to a flap gate. Bradley proposed the following relationship between the discharge and the total head.

$$Q = C\,L\,H^{3/2} \tag{4}$$

Where C is the discharge coefficient and L is the width of the channel.

The evolution of C [$ft^{1/2}.s^{-1}$] as a function of the angle θ between the horizontal and the tangent to the downstream lip of the gate is shown in Figure 1 following Bradley (1954), for different values of the ratio H / r, r being the radius of the gate. It must be noted that if θ is positive, the highest point of the gate is the lip of the gate; otherwise, it is the crest of the gate.

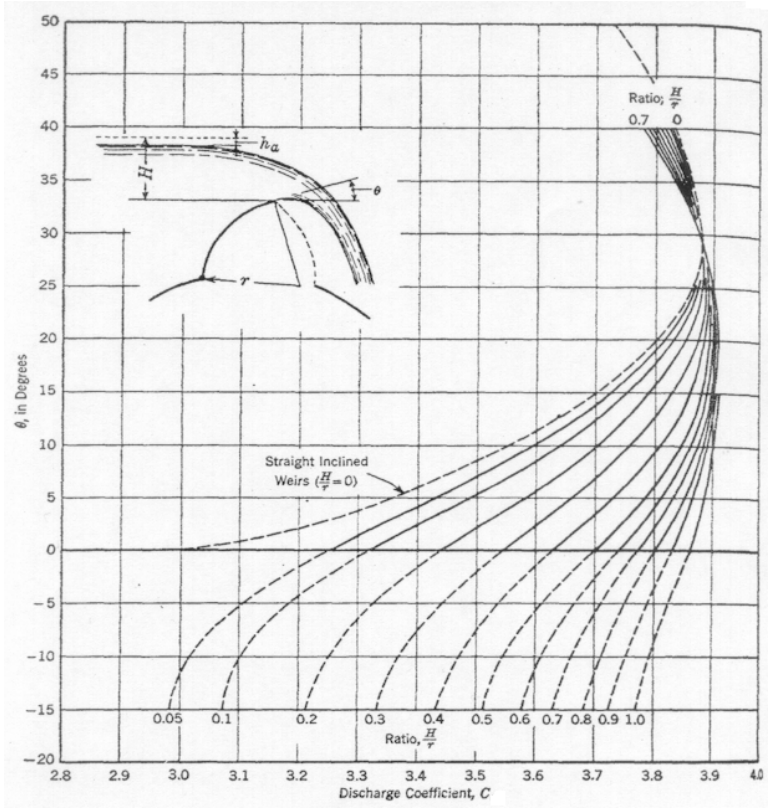

Figure 1. Discharge coefficient C [$ft^{1/2}.s^{-1}$] (Bradley 1954)

Sinniger and Hager (1989) proposed an analytical expression for the curves observed by Bradley (1954) where the discharge coefficient C is a function of θ, H / r and g, the gravity acceleration.

$$C = \sqrt{2g}\ \mu\left(\theta, \frac{H}{r}\right) \tag{5}$$

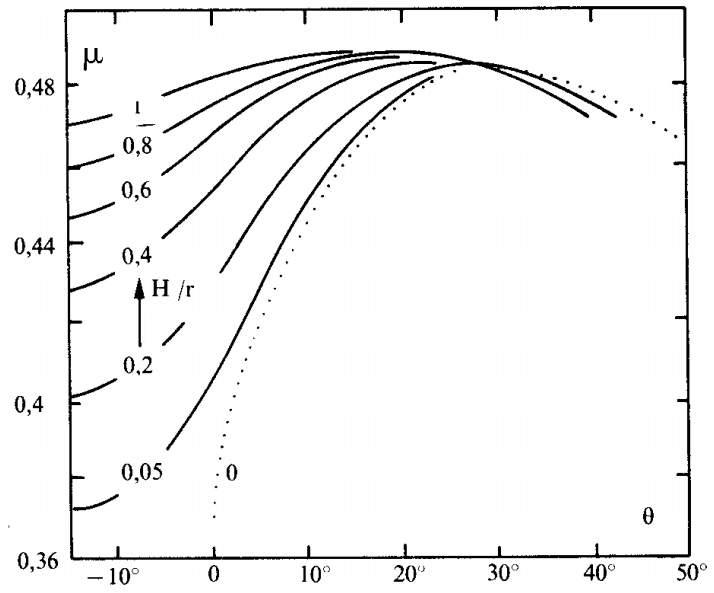

Figure 2. Discharge coefficient $\mu = C / (2g)^{1/2}$ (Sinniger and Hager, 1989)

The dimensionless discharge coefficient μ (Figure 2) is defined according to the following equations:

$$\mu_{\min} = 0.313\left[1 + \frac{1}{2}\left(\frac{H}{r}\right)^{1/3}\right], \text{ for } \theta_{\min} = -20^{\circ} \tag{6a}$$

$$\mu_{max} = 0.483\left[1+\frac{1}{69}\left(\frac{H}{r}\right)^{1/3}\right], \text{ for } \theta_{max} = 20^{\circ}\left[1+\frac{1}{2}\left(1-\frac{H}{r}\right)^{2}\right] \tag{6b}$$

$$\overline{\mu} = \frac{\mu_{min}}{\mu_{max}} \tag{6c}$$

$$\Delta = \frac{\theta - \theta_{min}}{\theta_{max} - \theta_{min}} \tag{6d}$$

$$\frac{\mu}{\mu_{max}} = \overline{\mu} + (1-\overline{\mu})\left[\Delta\, e^{1-\Delta}\right]^{4} \tag{6e}$$

One characteristic in the behaviour of this model is that it reproduces the observed two-limb curve of the discharge coefficient with H / r for a fixed θ: both in the descriptions by Bradley (1954) and Sinniger and Hager (1989) illustrated in Figures 1 and 2, for angles $\theta < \theta_{max}$ the discharge coefficient increases for increasing H / r while for angles $\theta > \theta_{max}$, the discharge coefficient decreases for increasing H / r. It can be shown by studying the partial derivative of function μ (6e) with respect to H / r that this trend is reproduced by the empirical model (6), but only for a limited range of values, i.e. $H / r \in [0.10;0.50]$ and $\theta \in [27°, 43°]$ (Figure 3).

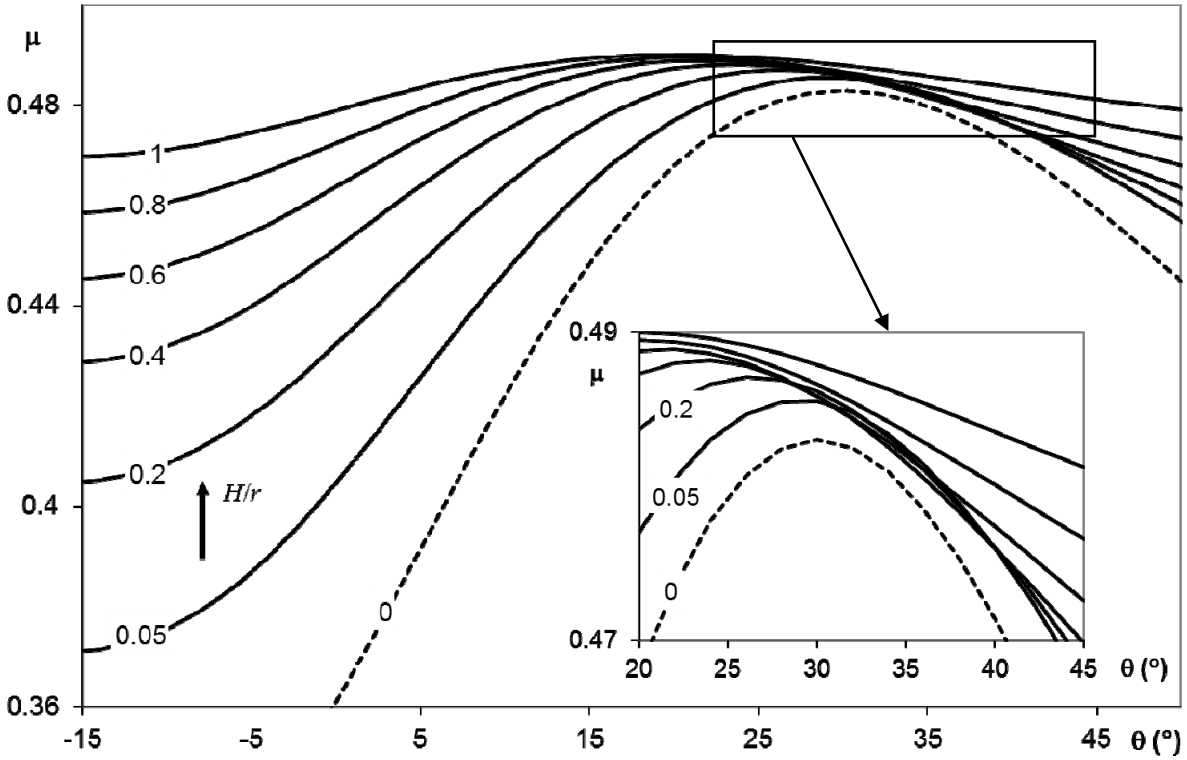

Figure 3. Discharge coefficient following Sinniger and Hager (1989)

In our study, we will focus on the model by Sinniger and Hager (1989). This model is based on the initial observations by Bradley (1954), as it considers a variable flap angle and thus appears more adapted to the actual gates of the River Meuse. However, the models by Chow (1959), Novak (1996) and Naudasher (1991) will also be considered in the comparisons with the experiments, to illustrate and highlight the strengths and weaknesses of each approach.

3 EXPERIMENTAL SET-UP

The La Plante dam is located near the city of Namur on the Meuse River (Figure 4). It is composed of four radial and flap gates (Figures 5 and 6). The physical model replicates a one-meter wide section of a gate of the La Plane dam at the scale $\lambda = 1/25$, including the design of the approach channel upstream and the stilling basin downstream the gate (Figures 6 and 7). The radial gate in the scale model is 0.141 m high, and the flap angle can vary between -33.36° and 65.24° (Figure 7) in order to reproduce the range of discharges considered in the River Meuse for flow over the gate.

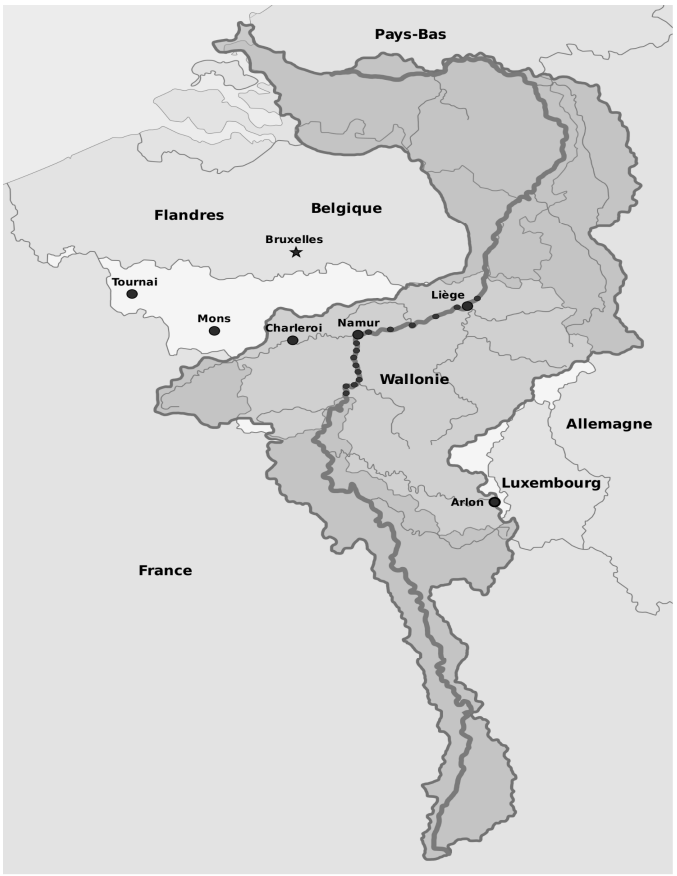

Figure 4. Overview of Meuse basin and river (fr.wikipedia.org)

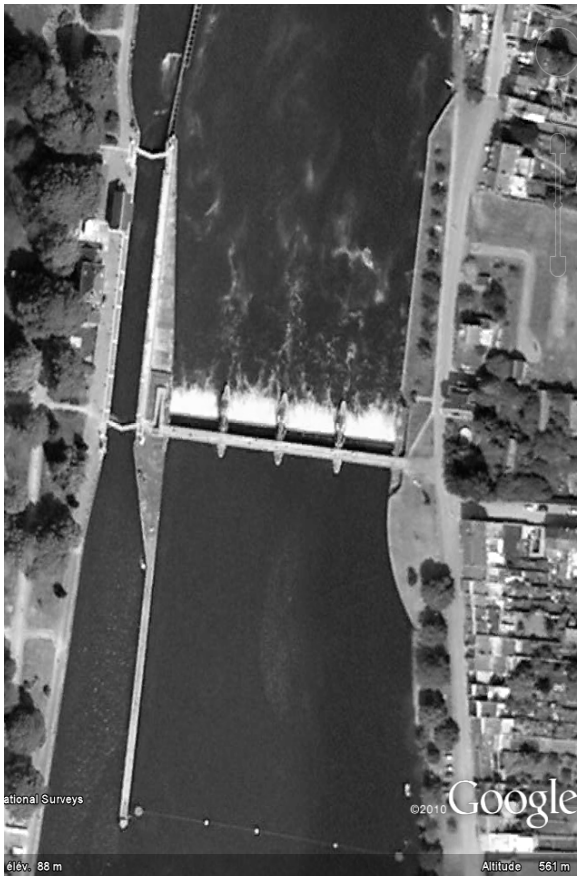

Figure 5. View of the La Plante dam (GoogleEarth)

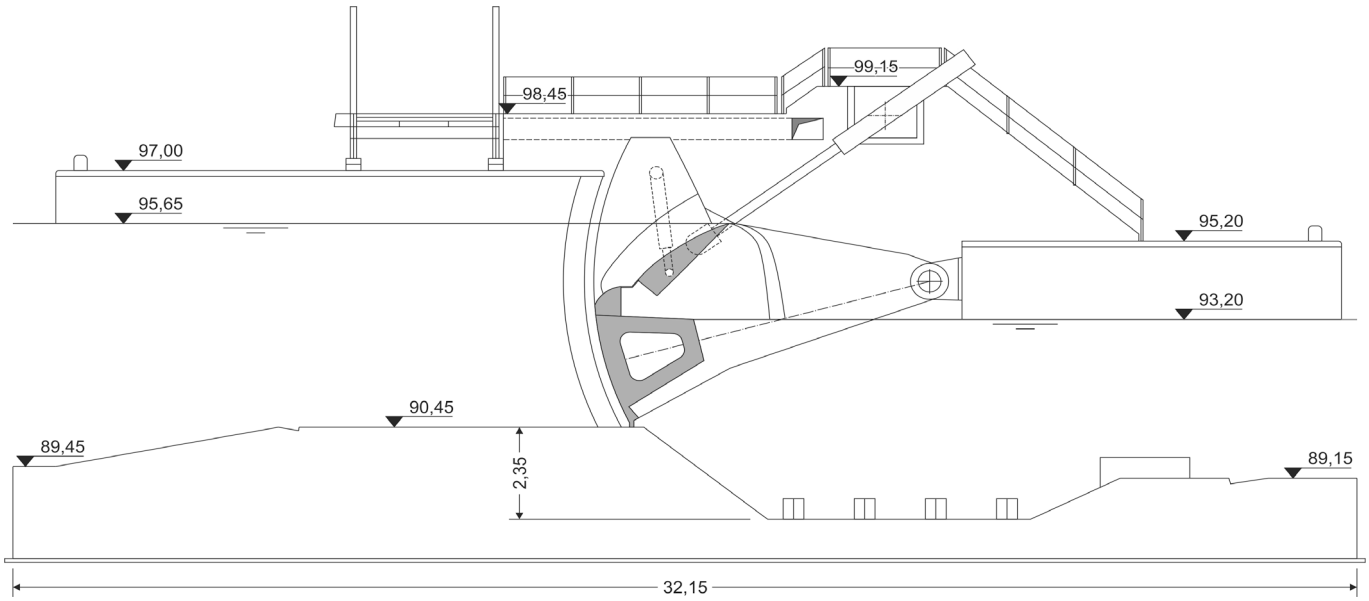

Figure 6. Transversal view of the gates in place on the Meuse River with upstream and downstream channel

Analysis of historical discharges and gate openings at the dam of La Plante showed that the maximum discharge occurring for a flow over the flap gate is about 300 m³/s. Above this value and to control the upstream level at a threshold of navigability, the radial gate starts opening and the water flows both over the flap gate and below the radial gate. When the discharge reaches 500 m³/s, there is no more flow over the flap gate, and the whole discharge flows below the radial gate only. For discharges higher than 800 m³/s, the radial gate is completely open resulting in an uncontrolled flow through the dam.

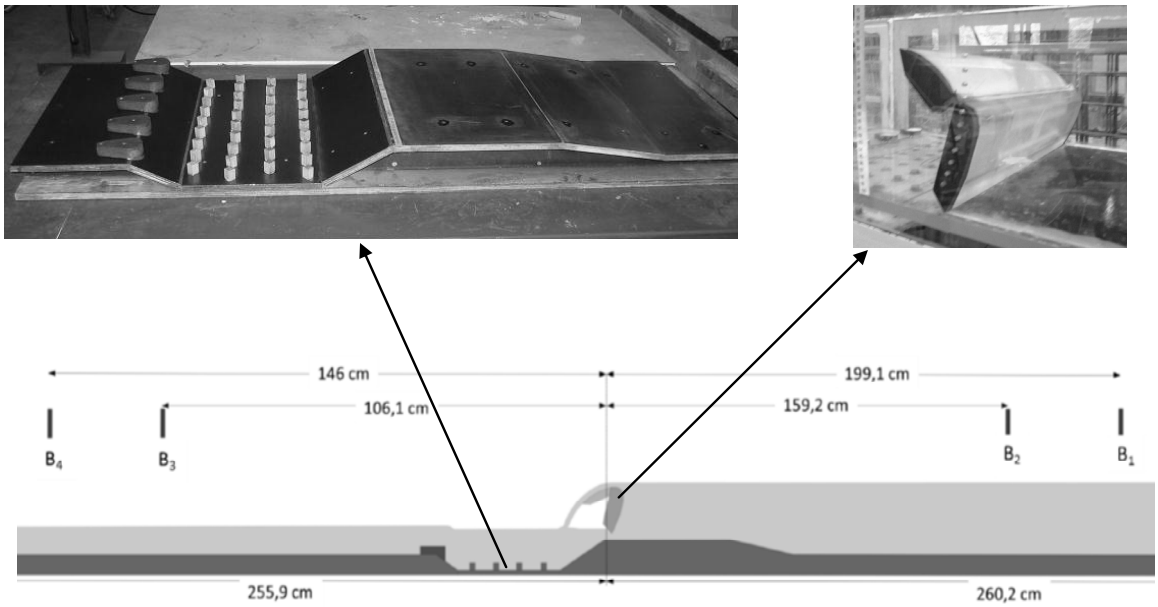

Figure 7. Experimental set-up

Using the Froude similitude to design the scale model, the scale factor for the discharge is $\lambda_Q = \lambda^{2.5}$. As the width of the prototype gate is 22.5 m, our physical model that is 0.495 m wide only represents a 12.375 m wide portion of the real gate. Accounting for the fact that the actual dam is composed of 4 gates, the scaled discharges are provided in Table 1. In the present study, we will focus on flow over the flap gate only, i.e. discharges up to 13.2 l/s in the scale model (300 m³/s in prototype).

The flume is equipped with 4 ultrasonic probes to measure the water level. The probes are located as indicated in Figure 7 at distances upstream and downstream from the gate equal to at least 3 times the maximum water depth in the channel. The discharge is obtained by an electromagnetic flow meter (ABB).

Table 1. Discharge ranges in the prototype and in the scale model

Type of flow	$Q_{prototype}$ (m³/s)	Q_{model} (l/s)
Flow over the gate only	0 – 300	0 – 13.2
Flow over and under the gate	300 – 500	13.2 - 22
Flow under the gate only	500 – 800	22 – 32.5
Uncontrolled flow	800 and higher	32.5 and higher

4 EXPERIMENTAL RESULTS

The experiments were conducted for 6 positions of the gate. The geometrical parameters are summarized in Table 2.

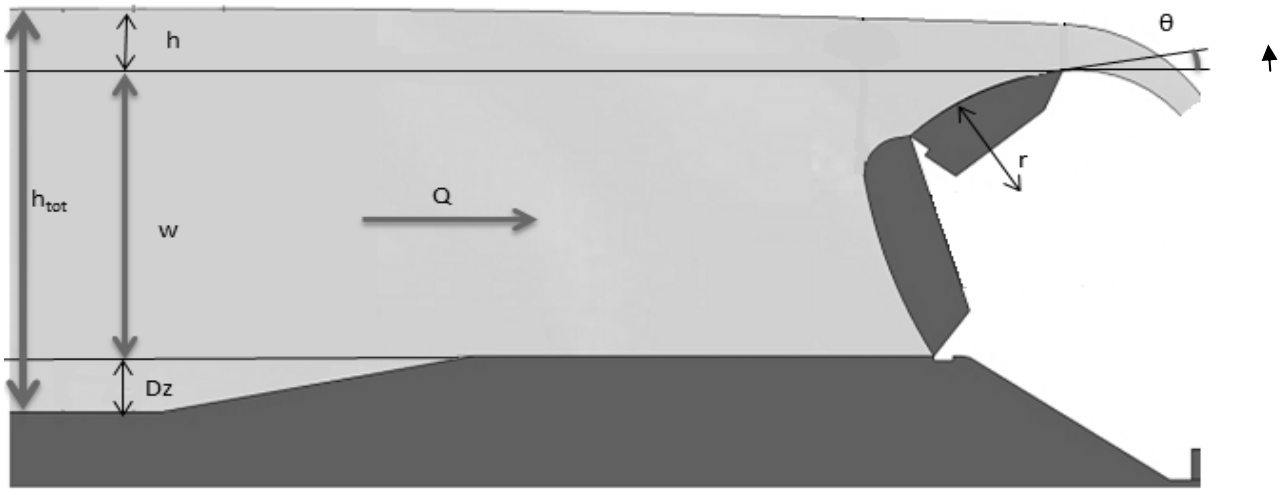

Figure 8. Sketch of the experimental set-up with geometrical parameters

Table 2. Geometrical parameters of the experimentation as shown in Figure 8.

Position	θ (°)	$w^{\dagger}$ (m)	r (m)	Dz (m)	L (m)
A*	-33.36	0.142	0.180	0.0231	0.495
B	-19.89	0.148	0.180	0.0231	0.495
C	-5.97	0.164	0.180	0.0231	0.495
D	13.64	0.198	0.180	0.0231	0.495
E	35.57	0.228	0.180	0.0231	0.495
F	65.24	0.248	0.180	0.0231	0.495

* Lower position of the gate, $w^{\dagger}$ is the position of the highest point above the gate toe level (lip of the gate in case of a positive θ, crest otherwise)

For each position of the flap gate, experiments were conducted by varying the inflow discharge and the upstream water level. The resulting measured discharges and water level were averaged over about 2000 values, acquired at a rate of 25 Hz. In order to compare the measured discharge coefficient with the prediction by the formula by Sinniger and Hager (1989), the measurements were grouped by ranges of H / r, as illustrated in Figure 9. For each range of considered values of H / r, the curves by equations (6) are indicated, together with the measured discharge coefficients (equations 4-5).

It can be observed that the general trend is well reproduced in the experiments; however the theoretical model overestimates the discharge coefficient. It should be noted that equations (6) are only valid for flap angles larger than -20°, while in our experiments the lowest angle was -33.36°.

The general trend given by both the empirical model (6) and the experimental results is an increase of μ with increasing H / r. For angles of the flap gate below θ_{max} (θ_{max} is between 25° and 28° depending on H / r), the difference between measured and predicted discharge coefficient is larger than for value of the angle above θ_{max}. For angles above θ_{max}, this difference significantly reduces. For instance for $H / r < 0.15$, the theoretical value of μ overestimates on average for the 2 results above θ_{max} the experimental value of μ by 5% while for the 4 results below θ_{max} we have an average overestimation of 25%. It must be noted that this difference of overestimation of μ, between value of the angle above and below θ_{max} is reducing for increasing H / r. For instance for H / r between 0.28 and 0.33, the average overestimation of μ for angles above θ_{max} is about 2 % while it is now 11% for angles below θ_{max}.

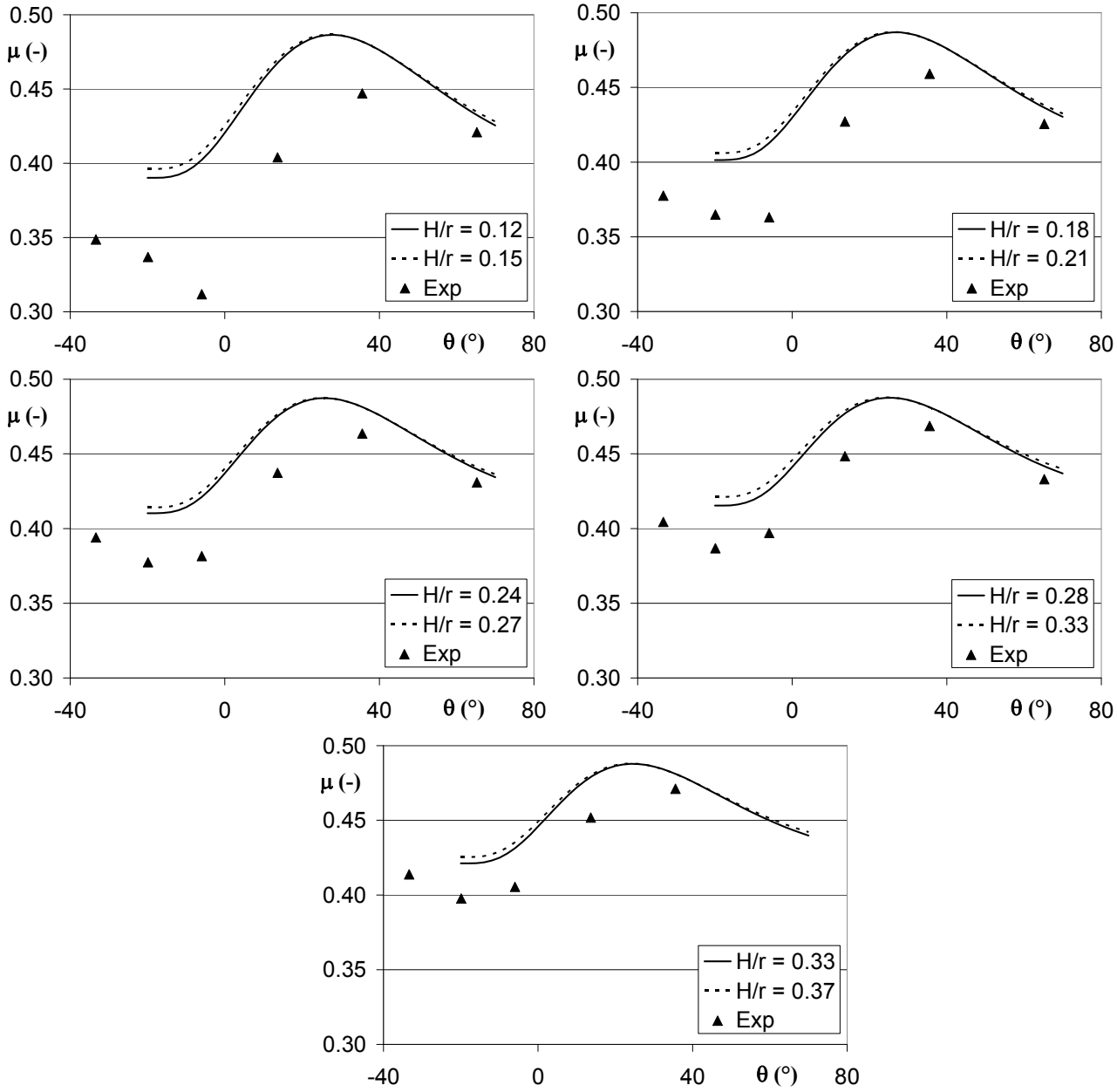

Figure 9. Discharge coefficient vs. θ (angle between the horizontal and the tangent to the downstream lip of the gate).
For $H/r > 0.33$ the measurement was not possible at $\theta = 65.24°$ due to too high upstream level compared to the channel design.

In order to analyze in greater detail the influence of gate flat position, the computed discharge coefficients from experimental results are compared to the models by Sinniger and Hager (1989), i.e. equations (6), Novak (1996) and Naudasher (1991). Figure 10 presents these comparisons for each position θ of the flap gate. The results obtained with the model proposed by Chow (1959) are very similar to those obtained with the model of Naudasher (1991) and were thus not included herein (i.e. the maximum differences on μ between both models is about 0.25 %).

The discharge coefficient in the formulae by Chow (1959), Novak (1996) and Naudasher (1991) do not depend on the flap angle. However, the experimental measurements clearly show a dependence on this angle, as already outlined before. This trend is well reproduced by the model of Sinniger and Hager (1989) that overestimates the discharge coefficient. For negative angles, the increase of μ with the upstream head represented by the ratio H / r is more influential than for higher angles of the flap gate. For high angles (above θ_{max}), the flap gate is closer to vertical. In this configuration, the radial gate and the flap are nearly aligned and the geometry of the entire gate is closer to that of a classical radial gate without a flap. This may explain why for the highest angle ($\theta = 65.24°$), the experimental results are in better agreement with the models by Novak (1996) and Naudasher (1991) than for lower position of the flap.

It should be noted that the best agreement is obtained with the formula by Sinniger and Hager (1989). For lower angles of the flap (below θ_{max}), the measurements tend to follow the formula by Sinniger and Hager (1989), but less closely. Also it can be noted that for higher values of H / r, the agreement between

the experimental measurements and the predictions by means of the Sinniger and Hager (1989) formula improves.

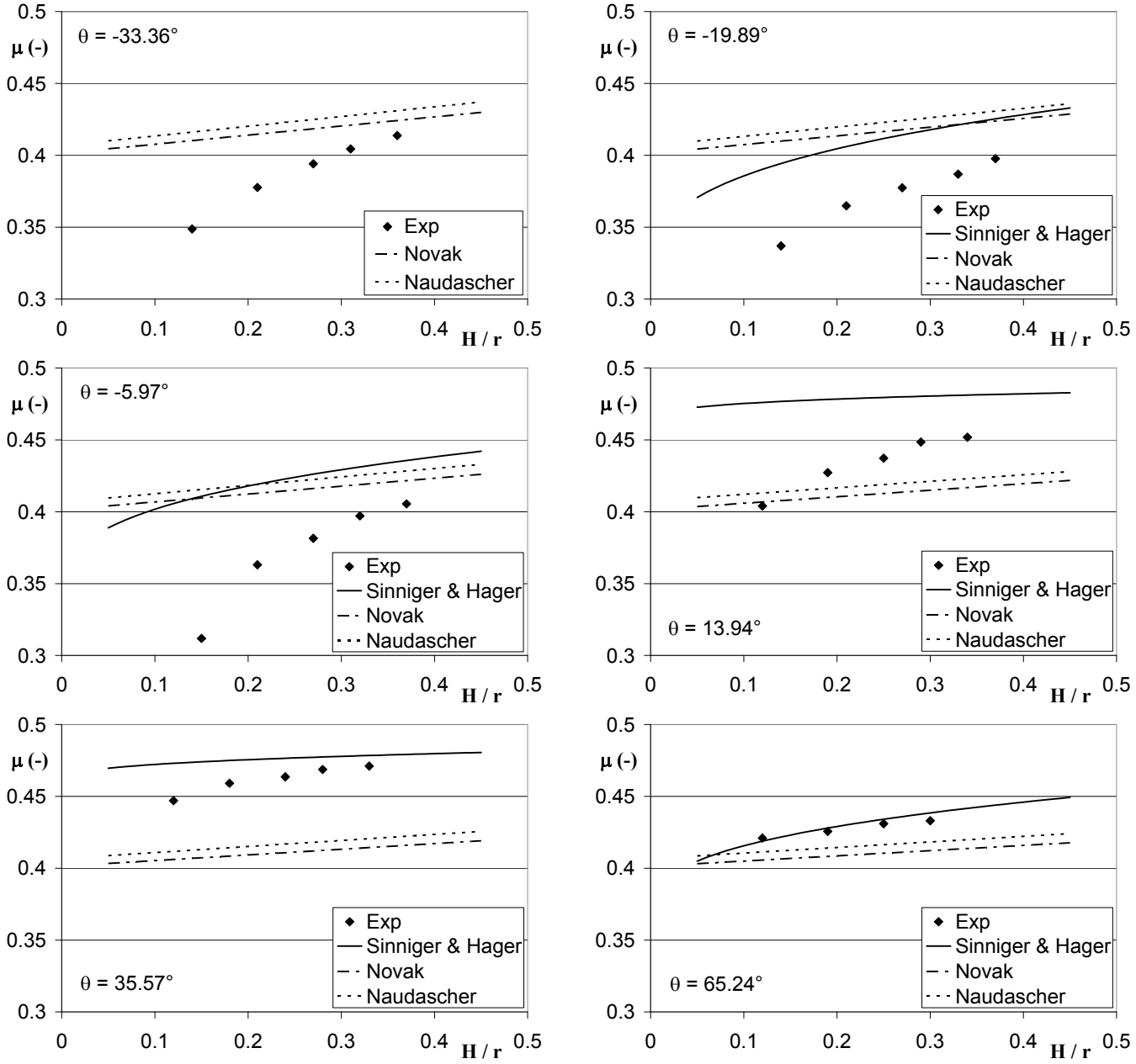

Figure 10. Discharge coefficient vs. upstream head

5 CONCLUSIONS

Experiments of flow over a radial gate equipped with a flap gate were presented. These experiments were conducted with the following objectives: (i) reproduce at a smaller scale a real gate at dams on the River Meuse in Belgium, and (ii) check the applicability of published empirical models to predict the discharge over such a gate. In the experiments, six positions of the flap gate were considered, and for each position, measurements were obtained for about five values of the discharges.

Among the existing formulae in the literature, the one proposed by Sinniger and Hager (1989) for drum gates appeared as the best suited, as it is the only one to the knowledge of the authors to account for a variable inclination of the flap gate. However, the comparisons between this model and the experiments showed that it is not completely adapted to our gate. Indeed, the formula always over-predicted the discharge coefficient. The reasons for these observed discrepancies could be the following. First, this formula was initially developed for drum gates that also present a variable angle. In the present case, we consider a radial gate with a flap gate. The approach flow might contribute to discrepencies, especially

for low values of the flap angle. Another possible reason could be some local head losses arising from the scaled model.

Future work will be conducted by first carefully checking the scale model, then carrying out more experiments to complete the set of experimental points. Especially, it will be checked if for low angles, close to the θ_{min} value of Sinniger and Hager (1989), a minimum of the discharge coefficient exists. Then, from this more complete set of experimental data, a new model for radial gates with flap gates could be developed.

ACKNOWLEDGEMENTS

The authors acknowledge the contributions by Olivier Ghijs and Xavier Briot, undergraduate students at the Université catholique de Louvain, Belgium, in the design of the scale model and in the experimental work.

NOTATION

λ	scaling factor for distance
λ_Q	scaling factor for discharge
Q	Discharge
C	Coefficient of discharge in $ft^{1/2}.s^{-1}$
L	Width of the channel
H	Total head over the maximum point of the gate
θ	Angle of the tangent to the downstream lip of the gate with the horizontal
r	Radius of the gate (top mobile part)
g	Gravity acceleration
μ	Discharge coefficient (dimensionless)
μ_e	Experimental discharge coefficient (dimensionless)
μ_t	Theoretical discharge coefficient (dimensionless)

REFERENCES

Adriansen (2001). Modèle de prevision d'axes hydrauliques de crues sur la Meuse Wallonne et la Haute Sambre.

Bousmar et al. (1998). One-dimensional unsteady flow computation in channels with floodplains, Hydraulic Engineering Software VII, Computational Mechanics Publications, Proceedings of the Hydrosoft'98 Conference, Como, Italy, Sept. 1998, pp. 205-214.

Bousmar and Zech (1999). Momentum transfer for practical flow computation in compound channels. Journal of Hydraulic Engineering. 125, n°7, 696-706.

Bradley (1954). Rating curves for flow over drum gates. Transactions ASCE. 119, 403-420.

Briot and Ghys (2012). Etude des écoulements en surverse, sousverse et mixte au droit d'une vanne de barrage en Haute-Meuse.

Chow (1959). Open channel hydraulics. International student edition. Tokyo : McGraw-Hill Kogakusha.

Dal Cin (2002). Marché de services pour l'étude de l'implantation d'un système de visualisation des prévisions de zones inondables de la Meuse en cas de crue.

Dal Cin (2004). Marché de services de echerché et de développement pour l'amélioration et l'extension du modèle de prévision d'axes hydrauliques de crues de la Meuse.

Dal Cin et al. (2005). "An integrated approach for real-time flood-map forecasting on the Belgian Meuse River", Natural Hazards, Volume 36, Issue 1-2, 2005, pp. 237-256.

Dal Cin (2006). Marché de services pour la mise à jour du modèle de prévision de crues de la Meuse.

Dal Cin (2008). Marché de services pour l'amélioration du modèle de prévision d'axes hydrauliques de la Meuse dans le but d'une exploitation opérationnelle.

Devaux et al. (2006). Etude sur modèle réduit de la relation hauteur-débit des vannes équipant les barrages de la Haute-Meuse.

Dubois (2011). Ecoulements contrôlés par vannes au droit des barrages de la Haute Meuse : étude théorique et expérimentale.

Naudascher (1991). IAHR Hydraulic structures design manual. Vol.3. Hydrodynamic forces. Rotterdam: Balkema.

Novak et al. (1996). Hydraulic structures. Second Edition. London: E&FN SPON.

Scherer et al. (1998). "Object-oriented building of a river network model for transient flow", Hydraulic Engineering Software VII, Computational Mechanics Publications, Proceedings of the Hydrosoft'98 Conference, Como, Italy, Sept. 1998, pp. 341-350.

Sinniger and Hager (1989). Traité de Génie Civil de l'Ecole Polytechnique de Lausanne, Volume 15: Constructions hydrauliques – écoulements stationnaires. Lausanne : Presse Polytechniques Romandes.

IWLHS, 20-22/02/2013, Aachen - Bung & Pagliara (eds) - © 2013 Bundesanstalt für Wasserbau ISBN 978-3-939230-04-5

Inlet Sluices for Flood Control Areas with Controlled Reduced Tide in the Scheldt Estuary: an Overview

T. De Mulder[1,2], J. Vercruysse[1], K. Verelst[1] & P. Peeters[1]
1 Flanders Hydraulics Research, Antwerp, Belgium
2 Hydraulics Laboratory, Civil Engineering Dept., Ghent University, Ghent, Belgium
T. Maris[3] & P. Meire[3]
3 Ecosystem Management Research Group, Biology Dept., University of Antwerp, Antwerp, Belgium

ABSTRACT: Flood Control Areas (FCAs) are one of the measures to protect the Flemish part of the Scheldt estuary against storm surges. Recently, in some of these FCAs a Controlled Reduced Tide (CRT) was introduced by means of simple sluice constructions, aiming at a combination of flood control with nature development and the ecological functions of intertidal areas. This paper gives an overview of the different types of inlet sluices and energy dissipation measures that have been designed, built and/or are under construction: an inlet sluice with an inclined drop, an inlet sluice with a pooled step cascade and a combined inlet-outlet sluice with an internal drop structure.

Keywords: flood control area, controlled reduced tide, inlet sluice, inclined drop, pooled step cascade, vertical drop

1 INTRODUCTION

After a major flooding event in 1976 in the Scheldt estuary, the so-called Sigmaplan was conceived in 1977 to better protect the north of Belgium (Flanders) against flooding (Figure 1).

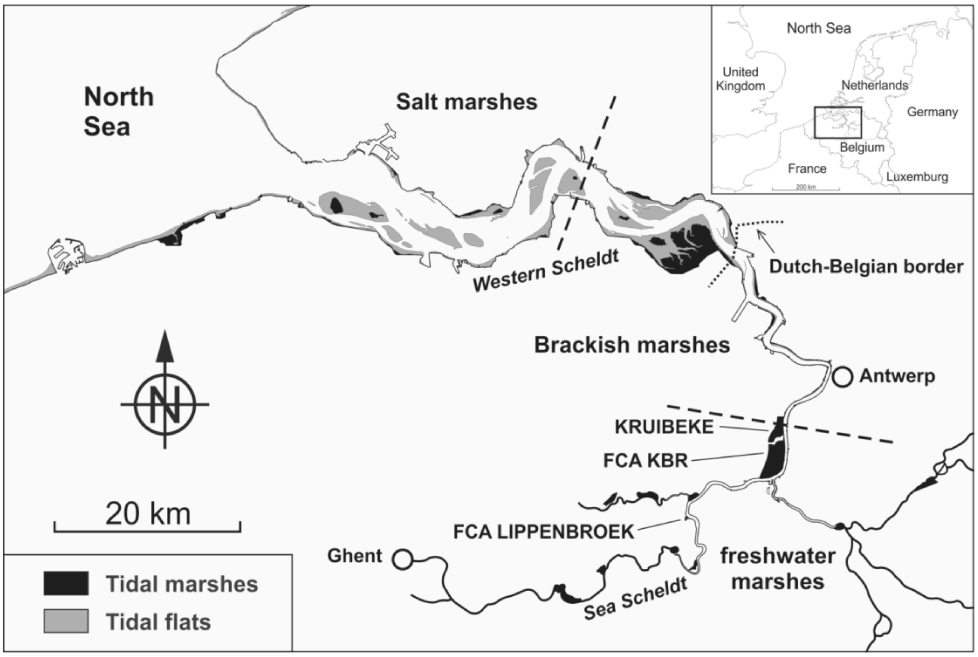

Figure 1. Location of Scheldt estuary and Flood Control Areas.

One of the measures in the Sigmaplan is to build a set of Flood Control Areas (FCAs). To this end, specific polders along the tidal river Scheldt are selected which have an elevation below mean high tide level. As a first construction step, a sufficiently high ring dike surrounding the polder needs to be built. Secondly, the existing levee between the polder and the river needs to be lowered, in order to create an

overflow dike. During storm surges, water can overtop the overflow dike and be stored in the FCA, thus damping the tidal wave in the river and mitigating the flooding of nearby valuable areas. To drain the water from the FCA when the water level in the river is sufficiently low again, outlet sluices are included within the overflow dike (Figure 2, left). The corresponding culverts are equipped with flap gates on the river side. On average, such a FCA is flooded once or twice a year. A dozen of FCAs are currently operational, and many more are under design and/or construction.

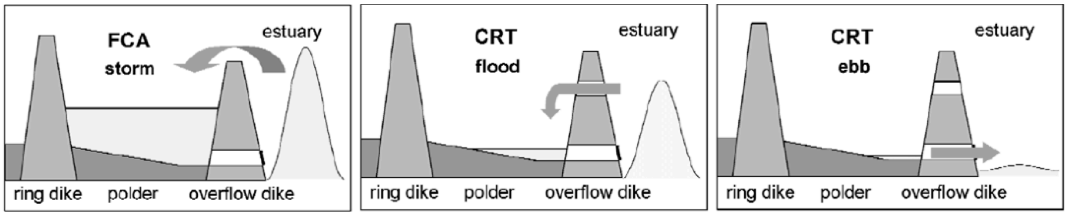

Figure 2. Operation principles of a Flood Control Area (FCA) without (left panel) and with (middle and right panels) a Controlled Reduced Tide (CRT)

Due to changing physical circumstances and new insights in water management, an actualization of the Sigmaplan was elaborated in 2005, aiming at satisfying both safety and ecological needs along the river Scheldt in a sustainable way.

Among other measures, some FCAs are now being designed and constructed with a so-called Controlled Reduced Tide (CRT) (Maris et al., 2007). Such type of FCAs (further abbreviated as: FCA-CRTs) does not only flood during storm surges, but also in normal tidal conditions. To this end, inlet sluices are built high in the river dike. During a (semi-diurnal) tidal cycle, a limited amount of river water flows into the FCA (Figure 2, middle), as long as the water level in the river exceeds the invert level of the inlet sluices. When inflow ceases, the water level in the FCA stagnates. As soon as the water level in the river becomes sufficiently low again, water is drained from the FCA through the outlet sluices in the overflow dike (Figure 2, right). When the water level in the river becomes sufficiently high again, the flap gates of the outlet sluices close and outflow from the FCA ceases, yielding again a stagnating water level.

The tidal regime aimed at within the FCA, should be comparable to tides in the estuary, but adapted to the scale of the FCA. For the development of functional intertidal habitat (i.e. tidal marshes and tidal flats) the low elevated FCA area has to face similar inundation frequencies as the natural outer dike habitats. Natural marshes only flood during spring tide, tidal flats can be flooded every tide. To achieve similar inundation patterns in the FCA, the high water levels have to be reduced without damping the spring tide – neap tide variation. This can be achieved by well-designed high positioned inlet sluices that take in large volumes of water during spring tide but, thanks to the high position, nearly no water during neap tide. A low elevated outlet sluice evacuates the water during ebb.

In this way, FCA-CRTs intend to contribute to the restoration of estuarine habitats, many of which have disappeared or degraded over the course of time because of agricultural, urban or industrial developments in a densely populated and land-scarce Scheldt estuary region (Cox et al., 2006). Intertidal areas have important ecological functions with effects on aeration, cycling and recycling of nutrients, water quality, sedimentation and primary production (Maris et al., 2007).

Because of the safety function – i.e. providing storage capacity to mitigate storm surges – that a FCA-CRT still needs to fulfill, only simple, reliable and easy to maintain technology should be relied upon for the introduction of a reduced tide. Therefore, robust inlet sluice systems have been selected, based upon culverts, possible equipped with valves. Also safeguarding the storage capacity needed for storm events is essential. With a reduced tide, the exchanged water volumes and hence suspended matter, can be controlled. Sluice dimensions determine flooding frequencies that influence sedimentation rates.

The sill level and the cross-section of the inlet sluices have been determined by means of mathematical models, simulating the tidal water levels in the polder for given water levels in the river.

Instead of constructing the floor slab of the culverts at the sill level predicted by the mathematical models (in order to get the requested tidal regime in the polder), it was decided to put the floor slab about 0.5 m lower and add some overflow weirs (e.g. at the downstream end of the inlet sluice culverts). Those weirs can be made easily by piling up stop logs in the available recesses in the vertical culvert walls. Hence, by choosing the appropriate weir height, the intake level(s) of the inlet sluice can be set to the requested value(s). Moreover, once the FCA-CRT is operational, the heights of the stop log weirs can be easily adapted, if needed to optimize the inundated areas and/or to respond to evolutions in the FCA-CRT or in the river.

Since FCAs are constructed in polders with a relatively low mean elevation (in order to maximize the storage capacity for flood mitigation), the water flowing in through the inlet culverts needs to drop significantly. If no special measures were taken, high flow velocities would result in important erosion. This is inacceptable for reasons of stability of the inlet sluice construction itself, as well as for the stability of the overflow dike in which the sluice is constructed. Therefore, some energy dissipating (and erosion protection) measures have to be included in the design of the inlet sluice for a FCA-CRT. This paper gives an overview of some structures that have been designed and/or built in the Scheldt estuary.

2 INLET SLUICE WITH INCLINED DROP – PILOT PROJECT "LIPPENBROEK"

A fairly small polder of about 10 ha, called "Lippenbroek" (municipality: Hamme), was selected to become a pilot project. The FCA-CRT Lippenbroek became operational in March 2006. The polder is situated in the freshwater part of the estuary (Figure 1).

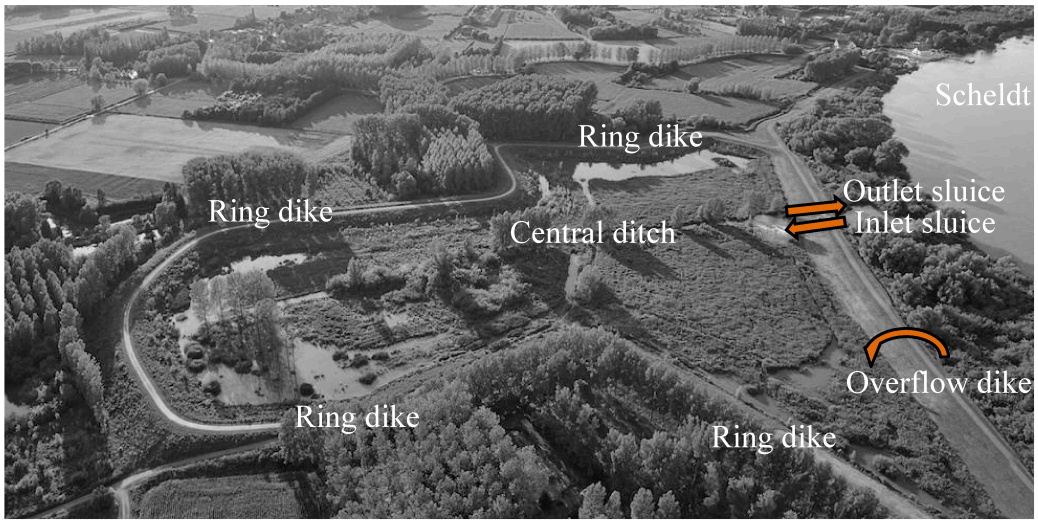

Figure 3. Aerial view of FCA-CRT Lippenbroek (source: www.sigmaplan.be).

The FCA is surrounded by a ring dike. The levee between river and polder is 450 m long, 40 m of which have been lowered to function as an overflow dike (Figure 3).

The (new) inlet sluice has been constructed at a distance of about 50 m from the (existing) outlet sluice. At the riverside, a creek connects both sluices to the river. At the polder side, an inlet basin connects both sluices to a central ditch or creek within the polder (Figure 4).

Some characteristic levels and sluice dimensions for FCA-CRT Lippenbroek are given in Table 1 and Table 2 respectively. The levels are expressed with respect to TAW, i.e. the Belgian reference level (which is approximately the mean low tide level along the Belgian North Sea coast).

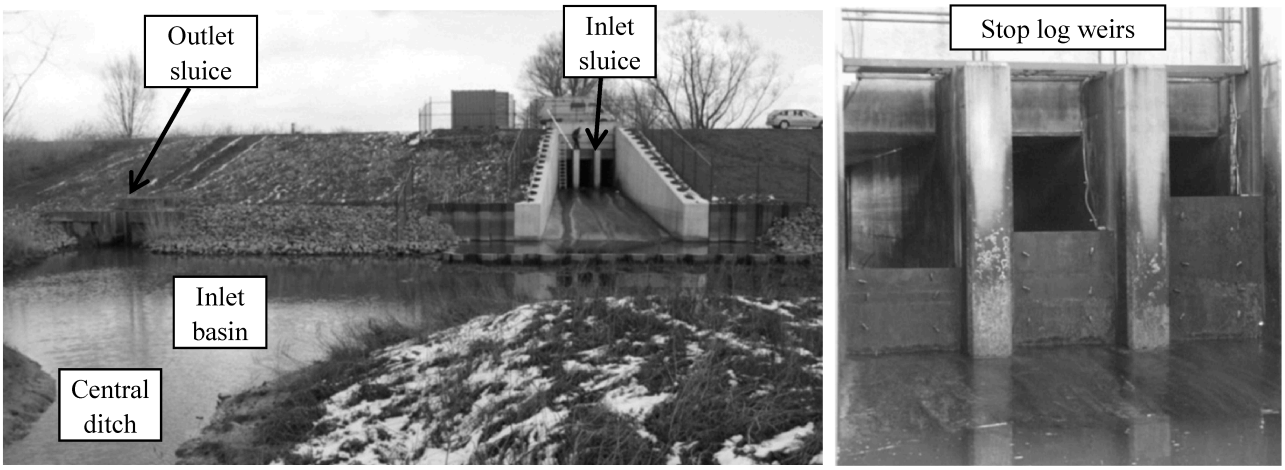

Figure 4. View from polder upon inlet sluice and outlet sluice of FCA-CRT Lippenbroek (left) and upon stop log weirs at downstream end of inlet sluice culverts (right)

Table 1. Characteristic levels for FCA-CRT Lippenbroek.

FCA-CRT Lippenbroek			Tidal river characteristics	
Ring dike	Crest level	+8.35 m TAW	mean high tide	+6.0 m TAW (spring tide)
Levee	Crest level	+8.00 m TAW		+5.6 m TAW (mean tide)
Overflow dike	Crest level	+6.80 m TAW		+5.1 m TAW (neap tide)
Inlet sluice	Level of culvert ceiling	+5.90 m TAW	mean low tide	+0.1 m TAW (spring tide)
	Crest level of stop log weirs	+5.30/+5.00/+4.70 m TAW		+0.3m TAW (mean tide)
	Level of culvert floor	+4.00 m TAW		+0.5 m TAW (neap tide)
Outlet sluice	Level of culvert ceiling	+3.00 m TAW		
	Level of culvert floor	+1.50 m TAW		
Polder	Mean elevation	+2.6 m TAW		

Table 2. Characteristic culvert dimensions for sluices of FCA-CRT Lippenbroek.

Inlet sluice		Outlet sluice	
Number of culverts	3	Number of culverts	1
Culvert width	1.00 m	Culvert width	1.50 m
Culvert height	1.90 m	Culvert height	1.50 m
Culvert length	ca. 13 m	Culvert length	ca. 40 m

The geometry of the inlet sluice is depicted in Figure 5. An inclined drop has been chosen to direct the water inflow through the culverts into the Lippenbroek polder. Besides some orientating hydraulic calculations, no explicit reference was made to specific recommendations in (hydraulic) literature to select and size this type of construction. Given the limited vertical drop height and inlet sluice dimensions in this pilot project, a (gently) sloping concrete slab of moderate size (without chute blocks and baffle blocks) was just believed to be simple to construct and elegant to integrate in the landward slope of the dike (since sidewalls protruding above the dike slope could be avoided).

The inclined slab has a slope of 13.5%, corresponding to a drop in height of 2.25 m over a horizontal distance of 16.57 m. Due to diverging sidewalls (each having an angle of about 5° with respect to the longitudinal axis of the slab), the slab width varies from 4 m at the top to 7 m at the toe. The total area of the slab is about 92 m².

At the toe of the drop, a stilling basin has been constructed. It consists of a horizontal concrete slab (with a small end sill), surrounded by gabions. The sizing of the slab has been based on calculations of the hydraulic jump during various tidal cycles in the river, taking into account the time evolution of the tail water depths in the polder. The maximum Scheldt level considered during these design calculations was at mean spring tide (+6.0 m TAW, Table 1), corresponding to an estimated total discharge of 6.5 m³/s, i.e. a specific discharge at the top of the inclined drop of 1.6 m³/s/m. The latter value has been confirmed by discharge measurements on site in Lippenbroek (Peeters et al., 2009). The resulting length of the concrete slab is about 7 m. Combined with a width of 15 m, yields a slab surface of about 100 m².

Note that the construction occasionally also operates under much higher water levels in the river, hence much higher specific discharges. For a Scheldt level of +6.8 m TAW– i.e. the crest level of the FCA overflow dike, which is exceeded on average once or twice a year – the specific discharge is estimated (based on a culvert formula, validated by scale model tests) to be 3.1 m³/s/m. No stability issues regarding possible erosion downstream of the stilling basin were raised:

(i) Given the limited surface of the polder and its specific topography, high inflow discharges result in rapidly increasing tail water depths, hence limited duration of exposure to non-protected parts of the inlet basin and shifting of the hydraulic jump in the direction of the inclined drop.

(ii) Because the inlet sluice construction was completely surrounded by sheet pile walls, the structural engineers did not consider the potential erosion to be harmful for the stability of the construction.

(iii) The location of the potential erosion was considered to be sufficiently far from the landward slope of the neighboring dike sections.

(iv) Regular monitoring in the FCA-CRT was planned and, if needed, the authorities in charge of the FCA-CRT were ready to restore and/or increase additional erosion measures such as gabions.

(v) The ecological engineers are in favor of hydraulic conditions that stimulate the morphodynamic evolution (creek formation) of the polder (as long as the constructional stability of sluice and dike are not at stake, of course).

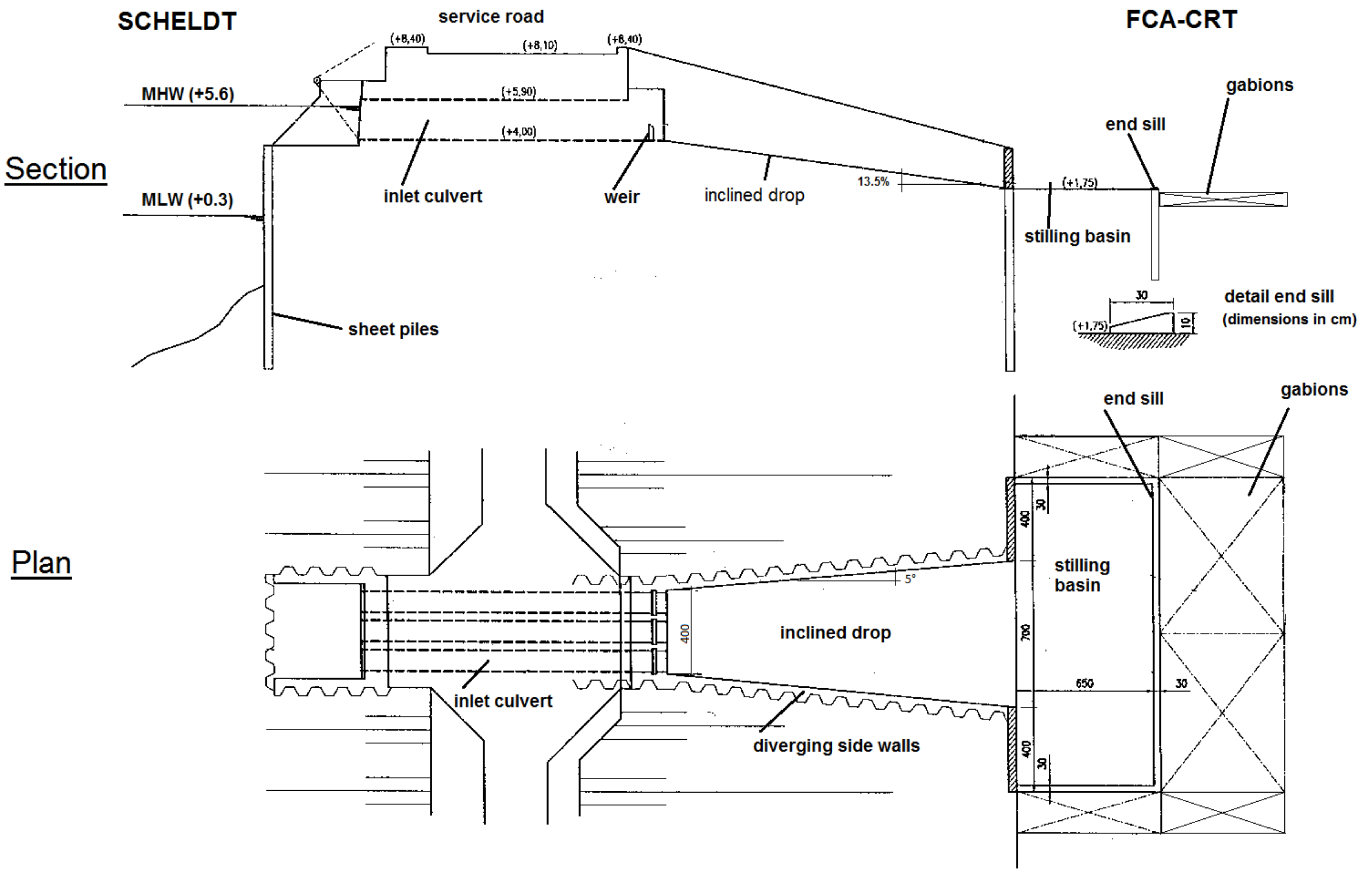

Figure 5. Sketch of inlet sluice for FCA-CRT Lippenbroek

Since the FCA-CRT is operational (March 2006), neither constructional problems have been observed, nor excessive erosion in the immediate neighborhood of the inlet sluice construction.

Note that in March 2006, the crest levels of the stop log weirs in the three inlet culverts have been adapted somewhat, in order to create sufficiently different inundated areas in the polder during spring and neap tide conditions. The uniform crest level of +4.8 m TAW (i.e. the value that was assumed for all inlet culverts during the design calculations) was modified into varying crest levels of +4.7/+5.0/+5.3 m TAW (i.e. the values that are specified in Table 1 and are illustrated in Figure 4). Since then, no further changes have been made to the crest levels of the stop log weirs.

Figure 6. Energy dissipation and aeration of water flowing into FCA-CRT Lippenbroek
(left: view from polder towards inlet sluice ; right: view from inlet sluice towards polder).

The inlet and outlet sluice systems described above, allow the tidal amplitude in the polder to be reduced on average from 5 m (in the river) to 1 m (in the polder), but the natural spring-neap tidal cycle is maintained. The tidal range in the polder varies from a few decimeters at neap tide to over 1.5 m at spring tide (Beauchard et al., 2011). The form of the tidal curve in the polder differs from the one in the estuary, as a stagnant phase is present both at high and low water in the polder, but the crucial characteristics of the tide for ecological purposes are still present.

Figure 6 illustrates the energy dissipation and aeration that accompanies the inflow of water into FCA-CRT Lippenbroek. Based on intensive ecological monitoring since the FCA-CRT is operational, the amount of aeration provided by the inlet construction is considered to be satisfactory.

3 INLET SLUICE WITH POOLED STEP CASCADE – CASE "KBR"

The largest FCA set up in Flanders so far, has a total area of about 600 ha and is referred to as "Kruibeke-Bazel-Rupelmonde" (abbreviated: KBR). A Controlled Reduced Tide will be introduced in several parts of KBR. The one in the polder called "Kruibeke" will be referred to as FCA-CRT Kruibeke (Figure 7). It has an area of about 200 ha and is situated at the limit of the brackish zone of the Scheldt estuary (Figure 1). FCA-CRT Kruibeke is to date (November 2012) not yet operational.

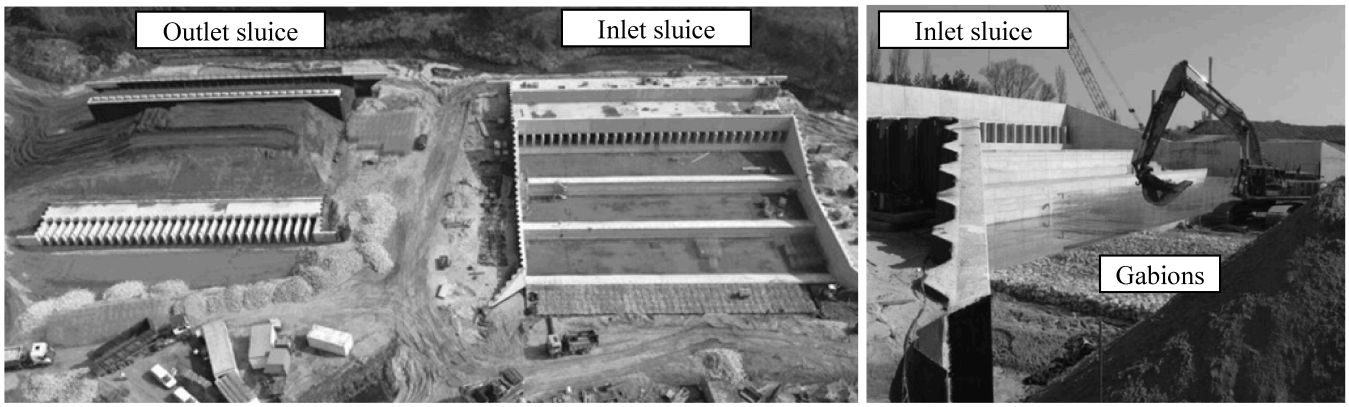

Figure 7. View upon outlet and inlet sluices (left) and bottom protection downstream of end sill inlet sluice (right) constructed at FCA-CRT Kruibeke

The levee between river and polder for FCA-CRT Kruibeke is about 1900 m long, 1650 m of which will function as an overflow dike.

The inlet and outlet sluices are built adjacent to each other in the north of the polder (Figure 7), in order to concentrate the tidal energy in one place. Some characteristic levels and sluice dimensions for FCA-CRT Kruibeke are given in Table 3 and Table 4 respectively.

Table 3. Characteristic levels for FCA-CRT Kruibeke.

FCA-CRT Kruibeke			Tidal river characteristics	
Ring dike	Crest level	+8.35 m TAW	mean high tide	+5.8 m TAW (spring tide)
Levee	Crest level at sluices	+8.35 m TAW		+5.4 m TAW (mean tide)
Overflow dike	Crest level	+6.80 m TAW		+4.9 m TAW (neap tide)
Inlet sluice	Level of culvert ceiling	+6.40 m TAW	mean low tide	-0.2 m TAW (spring tide)
	Crest level of stop log weirs	+4.70 to +5.50 m TAW*		+0.0m TAW (mean tide)
	Level of culvert floor	+4.20 m TAW		+0.4 m TAW (neap tide)
Outlet sluice	Level of culvert ceiling	+2.70 m TAW		
	Level of culvert floor	+0.50 m TAW		
Polder	Mean elevation	+1.3 m TAW		

* Range of crest level stop log weirs considered during design. Levels to be tuned when FCA-CRT is in operation.

Table 4. Characteristic culvert dimensions for sluices of FCA-CRT Kruibeke.

Inlet sluice		Outlet sluice	
Number of culverts	15	Number of culverts	15
Culvert width	3.00 m	Culvert width	3.00 m
Culvert height	2.20 m	Culvert height	2.20 m
Culvert length	ca. 25 m	Culvert length	ca. 55 m

The geometry of the inlet sluice is sketched in Figure 8. Note that instead of an inclined drop (like the FCA-CRT Lippenbroek), a stepped cascade was chosen to direct the water inflow through the culverts into the Kruibeke polder. Several considerations motivated this choice:

(i) The drop height between the floor level of the inlet culverts and the mean elevation of the polder is much higher at Kruibeke (2.9 m) as compared to Lippenbroek (1.4 m).

(ii) The total width of the inlet sluice is much larger in Kruibeke (ca. 51 m) as compared to Lippenbroek (4 to 7 m). The construction of an inclined slab of such a size is more difficult.

(iii) The water board in charge of the FCA-CRT decided to change the design conditions. Before, it was assumed that the inlet culverts would be closed manually (e.g. by closing a slide gate in each inlet culvert) prior to early flood warnings that predicted overtopping of the overflow dike. This measure was intended to maximize the storage capacity available in the FCA for storm surge mitigation. After the decision of the water board, it could no longer be assumed that the inlet culverts would be closed in such circumstances. Hence, the design Scheldt level could be higher than the crest level of the FCA overflow dike (+ 6.8 m TAW).

(iv) The surface of the FCA-CRT Kruibeke (200 ha) is much larger than FCA-CRT Lippenbroek (10 ha) and additionally, the topography at Kruibeke gives rise to a slow increase of the tail water depths in the polder in response to water inflow.

(v) During the design of the inlet sluice at Kruibeke fish migration was of much more concern than during the (earlier) design at Lippenbroek. Therefore, a pooled step cascade was selected, since this type of construction was considered to be less harmful for fish migrating towards the polder through the inlet sluice culverts.

(vi) The extra aeration that a cascade was likely to produce (as compared to an inclined drop) was considered to be an ecological asset.

The cascade consists of three steps, the dimensions of which are presented in Table 5 and Figure 8. Every step has an end sill, turning the construction into a pooled step cascade. To protect fish migrating from the river into the polder via the inlet sluice, the ecological engineers required the height of the end sill, i.e. the pool depth, to be at least one third of the drop height between consecutive steps.

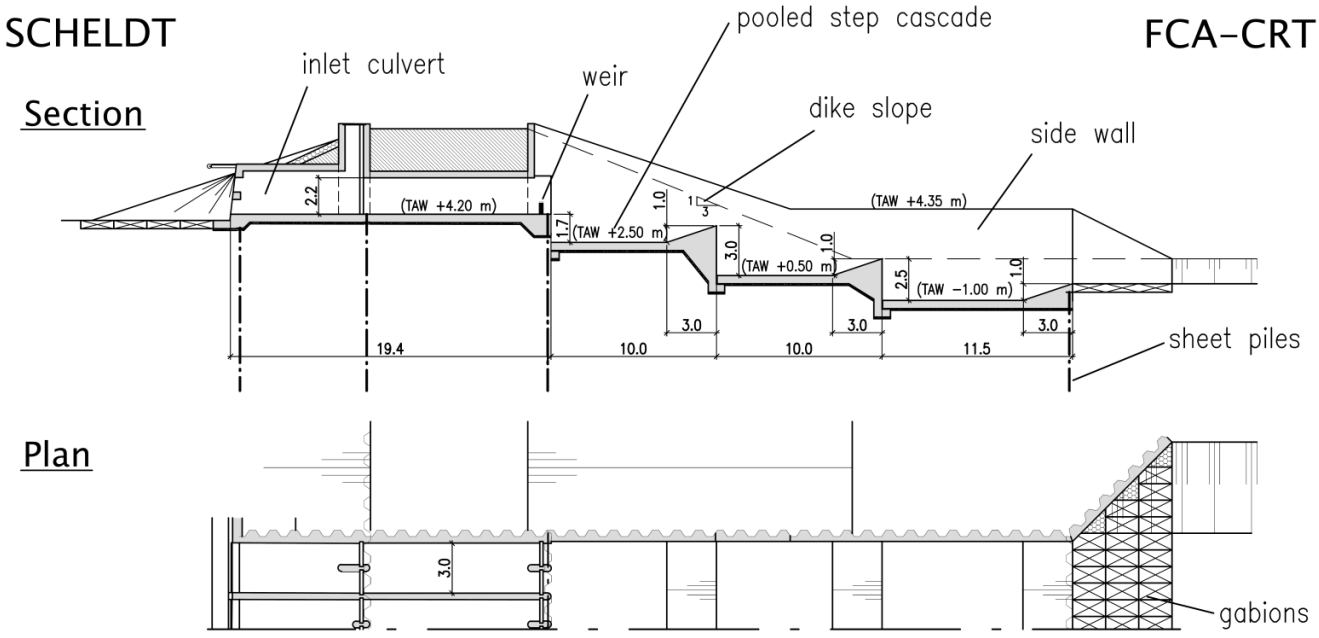

Figure 8. Sketch of inlet sluice for FCA-CRT Kruibeke.

During the design, Scheldt levels up to +8.0 m TAW have been considered, i.e. levels that are significantly above the crest level of the FCA overflow dike (+6.8 m TAW). Such high levels – though accompanied by relatively high tail water depths due to the preceding filling of the polder – still might give rise to supercritical flow above parts of the inlet sluice construction. The specific discharge (estimated with culvert formulas, validated by scale model tests) and critical flow depth corresponding to various high tide levels and crest levels of the stop log weirs are presented in Table 6.

The cascade has been dimensioned for nappe flow, based upon the guidelines in Chanson (2002 & 2004). These guidelines, however, are not valid for pooled step cascades, of which the hydrodynamics was still poorly known at the time. Therefore, it was decided to test the design afterwards in a scale model (scale 1:12) at Flanders Hydraulics Research (De Mulder et al., 2011).

Table 5. Characteristic dimensions of pooled step cascade for FCA-CRT Kruibeke.

		Upper step	Intermediate step	Lower step
brink level of falling jet	[m TAW]	+4.7 to +5.5*	+3.5	+1.5
floor level upstream	[m TAW]	+4.2	+2.5	+0.5
floor level downstream	[m TAW]	+2.5	+0.5	-1.0
step height (s)	[m]	1.7	2.0	1.5
step length (L)	[m]	10.0	10.0	11.5
slope (s/L)	[-]	0.17	0.20	0.13
weir or end sill height (w)	[m]	0.5 to 1.3*	1.0	1.0
drop height of falling jet (w+s)	[m]	2.2 to 3.0*	3.0	2.5

* Depending on crest level of stop log weirs.

Table 6. Specific discharge and critical flow depth for FCA-CRT Kruibeke.

Scheldt level [m TAW]	Crest level stop log weirs [m TAW]	Specific discharge q [m³/s/m]	Critical flow depth h_c [m]
+8.0	+4.7	8.6	1.96
	+5.5	5.8	1.50
+6.8	+4.7	4.5	1.27
	+5.5	2.1	0.78
+5.8	+4.7	1.7	0.67
	+5.5	0.3	0.21

In the physical model, (steady) flows at Scheldt levels up to +7.1 m TAW have been tested, with various tail water depths. It was confirmed that nappe flow is present over the stepped cascade, as was intended during the design calculations. A photo of the flow pattern corresponding to a Scheldt level +6.8 m TAW (and a very low tail water depth) is shown in Figure 9. In presence of stop log weirs, the specific discharge measured in the physical model showed a good agreement to the values estimated during the design for Scheldt levels up to +6.8 m TAW. For higher Scheldt levels, the values adopted during design seem to be somewhat overestimated.

The flow characteristics and residual head immediately downstream of the lowest step have been investigated in the model. For a Scheldt level of +6.8 m TAW, the energy dissipation was found to be 70 to 80% of the head available in the river (depending on the crest level of the stop log weirs).

In the meantime, the inlet sluice design has been constructed on site. As shown in the right part of Figure 7, gabions are used to protect the bottom immediately downstream of the end sill of the lower step. The water board has preferred this supplementary erosion mitigation measure, though no serious stability concerns are raised (since the inlet sluice construction is totally surrounded by deep sheet pile walls).

As mentioned above, FCA-CRT Kruibeke is to date (November 2012) not yet operational.

Figure 9. Nappe flow conditions in the pooled step cascade scale model (scale 1:12) for FCA-CRT Kruibeke, corresponding to a water level of +6.8 m TAW in the river Scheldt

4 COMBINED INLET-OUTLET SLUICE WITH INTERNAL DROP STRUCTURE

Currently, several FCA-CRTs are under design, in which the inlet and outlet sluices are combined in one single structure. A schematic view of such a construction is given in Figure 10. Note that the inlet culverts are situated on top of the outlet culverts.

During inflow, water enters through the inlet culverts. The intake level can be adjusted by means of a stop log weir. If needed, the amount of inflow can be further reduced by (partially) closing a slide gate in some culverts.

During outflow, water is drained through the outlet culverts. The latter are equipped with flap gates at the river side.

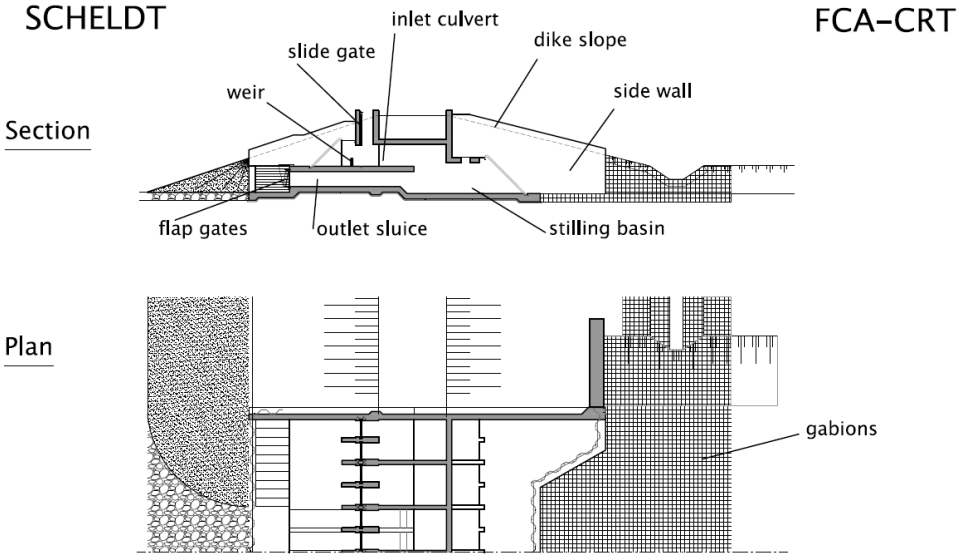

Figure 10. Schematic view of a combined inlet-outlet sluice (source: IMDC, 2008).

To dissipate the energy of the inflowing water, use is made of a vertical drop and a stilling basin. The stilling basin is formed by lowering part of the floor slab of the outlet culvert. Typically, dimensions of the stilling basin are based upon formulas in Chow (1982), French (1986), Sinniger & Hagen (1989) and Ritzema (1994).

The combined inlet-outlet sluice is believed to offer some important advantages both from the structural and the ecological point of view:

(i) reduction of construction and maintenance costs (only one foundation is needed; less concrete),
(ii) the inflow and outflow hydro- and morphodynamics are concentrated in one place, which is favorable for:
    - "natural" creek formation in the polder,
    - the constructed creek at the riverside of the combined inlet-outlet sluices to remain at depth,
(iii) reduced losses of tidal marshes along the river,
(iv) reduced losses of available length for overflow dike.

The combined inlet-outlet structures which are currently under design, are meant for FCA-CRTs situated at different locations in the estuary, involving different characteristics of polders and river tide. Moreover, the desktop designs are made by distinct design teams. Hence, it is not surprising that a diversity of geometries are being proposed.

In order to identify possible flaws in the design and to support the optimization of the different combined inlet-outlet structures from the hydraulic point of view, an intensive physical model study (scale 1:8) has been initiated at Flanders Hydraulics Research. To allow different geometries to be tested consecutively in an efficient way, a flexible model set-up has been designed and built (Figure 11). Among other things, the dimensions of the space available for the vertical drop and those of the stilling basin can be easily modified.

Some results of the optimization of a first combined inlet-outlet sluice design are discussed in a companion paper by Vercruysse et al. (2013).

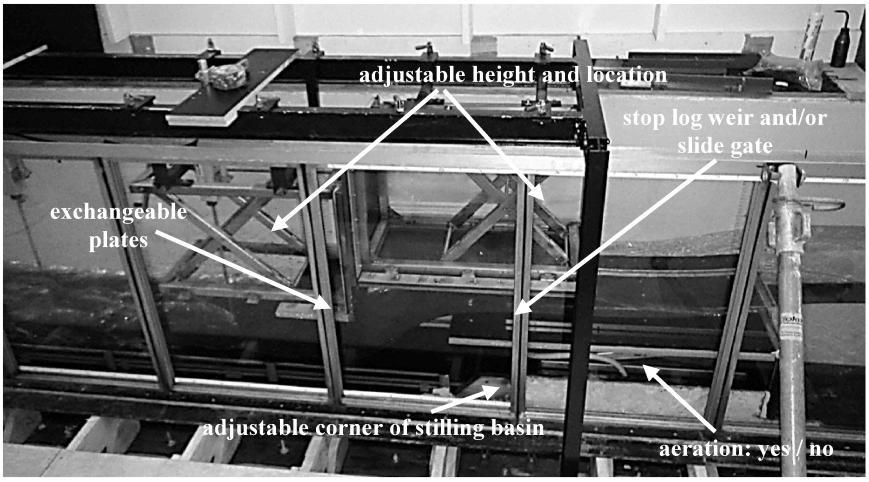

Figure 11. Flexible model set-up (scale 1:8) to test combined inlet-outlet structure geometries.

5 CONCLUSIONS

Flood Control Areas (FCAs) with a Controlled Reduced Tide (CRT) are being developed in the Flemish part of the Scheldt estuary, in order to combine flood control with nature development and the ecological functions of intertidal areas.

This paper has given an overview of the different types of inlet sluices and energy dissipation structures that have been designed, built and/or are under construction.

In a first pilot project (FCA-CRT Lippenbroek, 10 ha, in operation), the inlet sluice was built separated from the (existing) outlet sluice. To dissipate energy during inflow, use was made of an inclined drop and a stilling basin. No scale model tests were carried out prior to construction. Yet, FCA-CRT Lippenbroek operates quite satisfactorily, both from the constructional and the ecological point of view.

For a much larger project (FCA-CRT Kruibeke, 200 ha, built but not yet in operation as of November 2012) the inlet and outlet sluice have been built adjacent to each other. To dissipate energy during inflow, a cascade with three steps is relied upon. To protect fish migrating into the polder through the inlet sluice, pooled steps have been chosen. Due to lack of specific guidelines at the time, the design was based upon literature for non-pooled cascades. Scale model tests have confirmed afterwards that the design performs more or less as expected.

For a set of FCA-CRTs which are currently under design, combined inlet-outlet sluices are proposed. In this type of structure, the inlet culverts are on top of the outlet culverts. Energy is dissipated during inflow by means of a vertical drop and a stilling basin. At present, an intensive physical model study is carried out to evaluate and optimize the geometry from the hydraulic point of view. Some first results are reported in a companion paper (Vercruysse et al., 2013).

It has been attempted in this paper to provide some insight into the selection and design process of the aforementioned constructions.

From the hydraulic point of view, each of those constructions needs to be designed to withstand the most critical combinations of upstream and downstream conditions (i.e. Scheldt levels and tail water depths in the polder, respectively), which are site-specific (i.e. a function of local tidal conditions, available storage capacity, topography, length and crest level of the overflow dike etc.).

One should be aware, however, that many constraints are imposed to the (multi-disciplinary) design team (such as constructability, operational procedures and maintenance issues, sustainability, adaptability, ecological concerns, etc.), which are equally (or sometimes even more) important for the final lay-out as compared to purely hydraulic considerations.

With respect to ecology, research is still on-going, based on intensive monitoring of FCA-CRT Lippenbroek and the Scheldt estuary (see e.g. Peeters et al., 2009; Beauchard et al., 2011). Therefore, the constraints imposed on the hydraulic design by ecological issues such as fish migration, aeration, sediment influx and morphodynamic evolutions, might change over the course of time. The results of the first (six) years of monitoring, however, clearly show that the ecological development is very positive. The biological characteristics of the new marshes in FCA-CRT Lippenbroek (Jacobs et al., 2009), as well as the ecological structure (Jacobs et al., 2009; Beauchard, 2012) and ecological functions such as retention of nitrogen and delivery of silica (Jacobs et al. 2008), turn out to be already very similar to the ones of the natural marshes along the estuary.

Finally, it should be emphasized that the often tight time frame for design and construction, rarely allows a complete and in-depth hydraulic optimization study to be carried out.

ACKNOWLEDGEMENTS

Waterwegen & Zeekanaal nv, and in particular ir. S. Nollet, is gratefully acknowledged for stimulating discussions during the design and construction of FCA-CRT's Lippenbroek and Kruibeke. Thanks are also extended to ir. P. De Vleeschauwer of IMDC nv for his contributions to the design of FCA-CRT Kruibeke.

REFERENCES

Beauchard, O., Jacobs, S., Cox, T.J.S., Maris, T., Vrebos, D., Van Braeckel, A., Meire, P. (2011). A new technique for tidal habitat restoration: Evaluation of its hydrological potentials. Ecological Engineering, Vol. 37, Issue 11, pp. 1849-1858.

Beauchard, O. (2012) Tidal freshwater habitat restoration through controlled reduced tide system: a multi-level assessment. PhD Thesis, University of Antwerp.

Bos, M.G. (1989). Discharge measurement structures. International Institute for Land Reclamation and Improvement/ILRI publication 20. Wageningen, The Netherlands.

Chanson, H. (2002). The hydraulics of stepped chutes and spillways. A.A. Balkema Publishers.

Chanson, H. (2004). The hydraulics of open channel flows: An introduction. 2nd edition. Elsevier Butterworth Heinemann.

Chow, V.T. (1982). Open-Channel Hydraulics. McGraw-Hill Book Company.

Cox, T., Maris, T., De Vleeschauwer, P., De Mulder, T., Soetaert, K., Meire, P. (2006). Flood control areas as an opportunity to restore estuarine habitat. Ecological Engineering, Vol. 28, Issue 1, pp. 55-63.

De Mulder, T., Vercruysse, J., Peeters, P., Mostaert, F. (2011). Flood Control Area Kruibeke-Bazel-Rupelmonde: Report of scale model tests inlet sluices FCA-CRT Kruibeke. [in Dutch]. Report no. 604-09, version 2-0, Flanders Hydraulics Research, Antwerp, Belgium.

French, R.H. (1986).Open-Channel Hydraulics. McGraw-Hill Book Company.

IMDC (2008). Structural types of inlet/outlet constructions for FCA-CRTs [in Dutch]. Report no. I/RA/11296/08.036/PRA, Commissioned by Waterwegen & Zeekanaal nv, 23 pp.

Jacobs, S., Struyf, E., Maris, T., Meire, P. (2008). Spatiotemporal aspects of silica buffering in restored tidal marshes. Estuarine, Coastal and Shelf Science, Vol. 80, pp. 42-52.

Jacobs, S., Beauchard, O., Struyf, E., Cox, T., Maris, T., Meire, P. (2009). Restoration of tidal freshwater vegetation using controlled reduced tide (CRT) along the Schelde Estuary (Belgium). Estuarine, coastal and shelf science, Vol. 85, pp. 368-376.

Maris, T.,. Cox, T., Temmerman, S., De Vleeschauwer, P., Vandamme, S., De Mulder, T., Van den Bergh, E., Meire, P. (2007). Tuning the tide: creating ecological conditions for tidal marsh development in a flood control area. Hydrobiologia, Vol. 588, pp.31-43.

Peeters, P., Claeys, S., Michielsen, S., De Schutter, J., Temmerman, S., Meire, P., Vandenbruwaene, W., Maris, T., Chen, M., Wartel, S. (2009). Sediment behaviour within a flood control area with a controlled reduced tide – Pilot project Lippenbroek. In: Proceedings Congrès SHF-31ième Journées de l'hydraulique: "Morphodynamiques et débits solides dans les estuaires, les baies et les deltas", Paris, 22-23 septembre 2009. Société Hydrotechnique de France: Paris. ISBN 2-906831-79-4.

Ritzema H.P. (1994). Drainage principles and applications. International Institute for Land Reclamation and Improvement/ILRI publication 16, second edition. Wageningen, The Netherlands.

Sinniger, R.O., Hager, W.H. (1989). Constructions hydrauliques – Ecoulement stationnaires. Presses polytechniques romandes, Lausanne.

Vercruysse, J., De Mulder, T., Verelst, K., Peeters, P. (2013). Stilling basin optimization for a combined inlet-outlet sluice in the framework of the Sigmaplan. In: Proceedings of International Workshop on Hydraulic Design of Low-Head Structures, 20 - 22 February 2013, Aachen/Germany.

IWLHS, 20-22/02/2013, Aachen - Bung & Pagliara (eds) - © 2013 Bundesanstalt für Wasserbau ISBN 978-3-939230-04-5

Stilling Basin Optimization for a Combined Inlet-Outlet Sluice in the Framework of the Sigmaplan

J. Vercruysse[1], T. De Mulder[1,2], K. Verelst[1] & P. Peeters[1]
1 Flanders Hydraulics Research, Antwerp, Belgium
2 Hydraulics Laboratory, Civil Engineering Department, Ghent University, Ghent, Belgium

ABSTRACT: Within the framework of the so-called Actualised Sigmaplan, i.e. the masterplan to create a sustainable Schelde estuary, flood control areas (FCA) are setup in well-chosen polders along the tidal part of the river Scheldeand its tributaries. In some of these FCAs a semi-diurnal, controlled reduced tide (CRT) is introduced, by means of simple inlet and outlet sluices. Nowadays, it is preferred to combine inlet and outlet sluices in one single structure, in which the inlet culverts are situated on top of the outlet culverts. At inflow, energy is dissipated by means of a vertical drop and a stilling basin. In this paper, results are presented of a physical model study (scale 1:8) aiming at the optimization of the inlet configuration, i.e. the stilling basin, starting from the desktop design of the in- and outlet construction for FCA-CRT Bergenmeersen.

Keywords: Actualised Sigmaplan, inlet sluice, vertical drop, stilling basin, hydraulic jump, physical model

1 FLOOD CONTROL AREA – REDUCED TIDE AREA (FCA-CRT)

After a major flooding in the north of Belgium (Flanders) in 1976, a masterplan – the so-called Sigmaplan – was elaborated in 1977 to mitigate storm surges in the Schelde estuary as to increase the level of safety. Due to changing physical circumstances and new insights in water management, the Sigmaplan was profoundly updated in 2005 – i.e. the so-called Actualised Sigmaplan. The Actualised Sigmaplan aims at satisfying both safety and ecological needs along the tidal part of the river Schelde and its tributaries in a sustainable way. Therefore, different restoration techniques are elaborated which combine safety with estuarine restoration, e.g. dike strengthening together with more space for the river, flood control areas (FCAs) with or without a controlled reduced tide (CRT), non-tidal wetlands, etc. In this paper, only flood control areas with a controlled reduced tide (abbreviated: FCA-CRTs) are considered.

During storm surges, FCA-CRTs are filled via a lowered levee (referred to as "overflow dike" in Figure 1). On average, this takes place once or twice a year depending on the level of the overflow dike. In addition, a well-designed system with inlet and outlet sluices allows limited semi-diurnal water exchange between the estuary and the FCA-CRT. The goal is to obtain inundation characteristics in the polder which are similar to natural tidal marshes along the estuary, in order to restore estuarine habitats which have disappeared over the past two centuries or degraded (elsewhere) in the estuary (Cox et al., 2006 ; Maris et al., 2007).

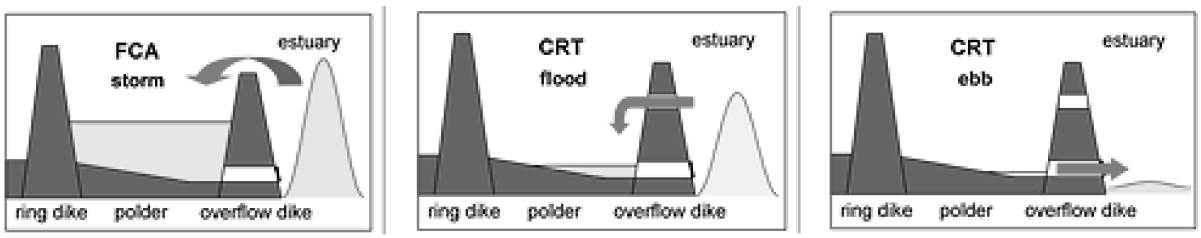

Figure 1. Working principles of a flood control area with controlled reduced tide (FCA-CRT): during storm surge (left) and in normal tidal conditions (middle and right).

2 COMBINED INLET-OUTLET SLUICE FOR FCA-CRT FUNCTIONING

An overview of the different types of sluice systems that have been designed, built and/or are under construction for FCA-CRTs in Flanders, is given in a companion paper (De Mulder et al., 2013). At first, the sluice system was setup with adjacent inlet and outlet sluice constructions. Nowadays it is preferred to combine inlet and outlet sluices in one single construction. Combining the inlet and outlet in one structure is believed to offer some important advantages, both from the structural and ecological point of view (IMDC, 2008).

Figure 2 provides a sketch of a combined inlet-outlet sluice. The inlet culverts are placed on top of the outlet culverts. The inflow can be adjusted by placing a stop log wall on the floor slab of the inlet culvert. The outlet culverts are equipped with flap gates in order to drain the FCA-CRT when the Schelde level is lower than the FCA-CRT level. After passing the stop log wall the incoming water drops vertically and plunges into the stilling basin underneath. The latter is formed by a concrete slab lowered with respect to the floor slab of the outlet culverts in order to assure that a certain water level is provided in the stilling basin.

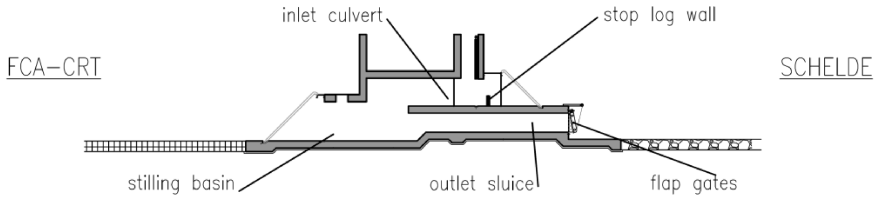

Figure 2. Schematic view of a combined inlet-outlet construction.

3 DESIGN OF FCA-CRT BERGENMEERSEN

The future FCA-CRT Bergenmeersen has an area of about 38 ha and is situated in the freshwater part of the Schelde estuary (Figure 3). The agency in charge of the design and construction of the FCA-CRT is Waterwegen & Zeekanaal nv. Different parties were involved in the design of the FCA-CRT Bergenmeersen. Only the parties involved in the design of the combined inlet and outlet structure are mentioned explicitly below.

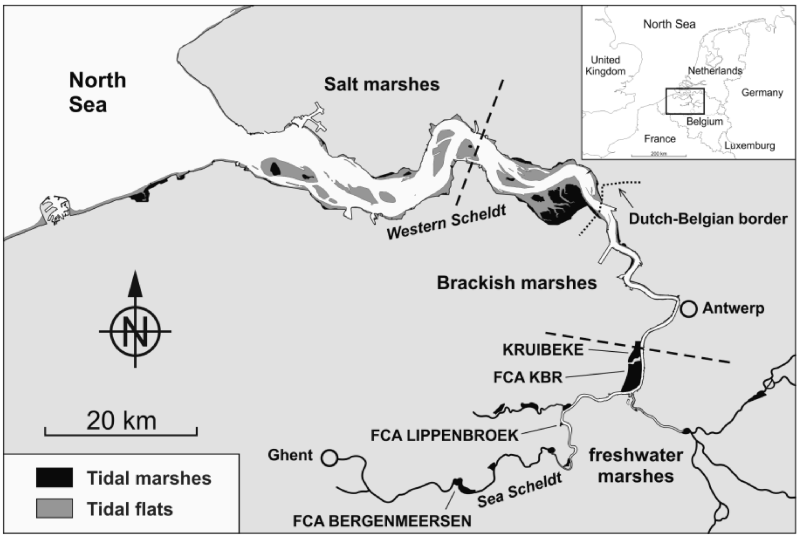

Figure 3. Location of FCA-CRT Bergenmeersen in the Schelde estuary.

By means of a numerical model study at Flanders Hydraulics Research (Coen et al., 2010), the required sill levels and (total) cross-sectional areas of the inlet and outlet culverts have been determined, in order to obtain a suitable reduced tide, i.e. aiming for a profound springtide/neap tide cycle, in the polder. The numerical model study was carried out using Mike 11, a 1-D unsteady river flow model from the DHI group. Within Mike 11, a FCA-CRT is modeled using a combination of branches. The sluices are modeled using the built-in culvert unit of MIKE 11. Culvert model parameters are calibrated following in situ discharge measurements at pilot project Lippenbroek (Peeters et al., 2009).

Given the optimal configuration of inlet and outlet culverts , a 5 month period of “normal” tidal conditions has been simulated numerically, supplemented with some shorter simulation periods of storm surges. Figure 4 contains all times series of predicted water levels in the FCA-CRT (abbreviated as: CRT level) as a function of the water level in the Schelde near Bergenmeersen. Both water levels are expressed (in m AD) with respect to the Belgian datum level (i.e. the so-called reference level TAW, which is approximately the mean level of low water along the Belgian North Sea coast).

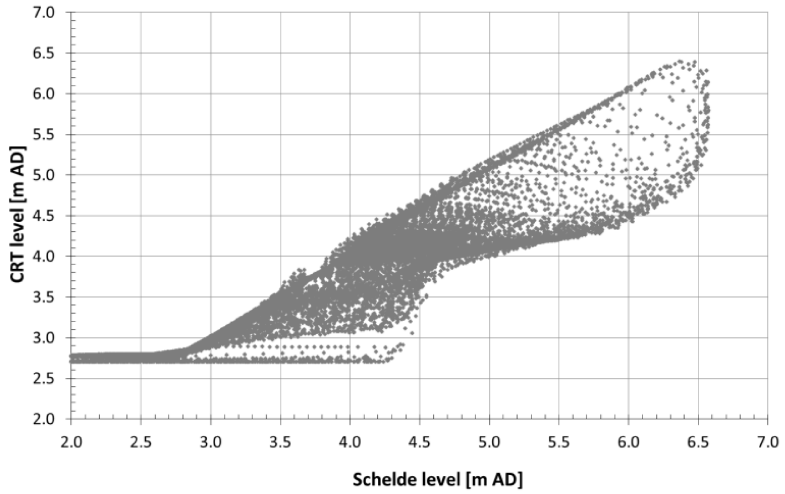

Figure 4. Numerical simulations predicted CRT levels in function of Schelde level.

The detailed structural design of the combined inlet-outlet sluice has been subcontracted by the agency (Waterwegen en Zeekanaal nv) to the consulting engineering company IMDC nv. The dimensions of the stilling basin have been determined based upon formulae in literature (IMDC, 2010). The dimensioning of the length and the depth of the stilling basin is based on a comparison of formulas mentioned in Chow (1982), French (1986), Sinniger and Hager (1989) and Ritzema (1994).The outcome of the desktop design is shown in Figure 5.

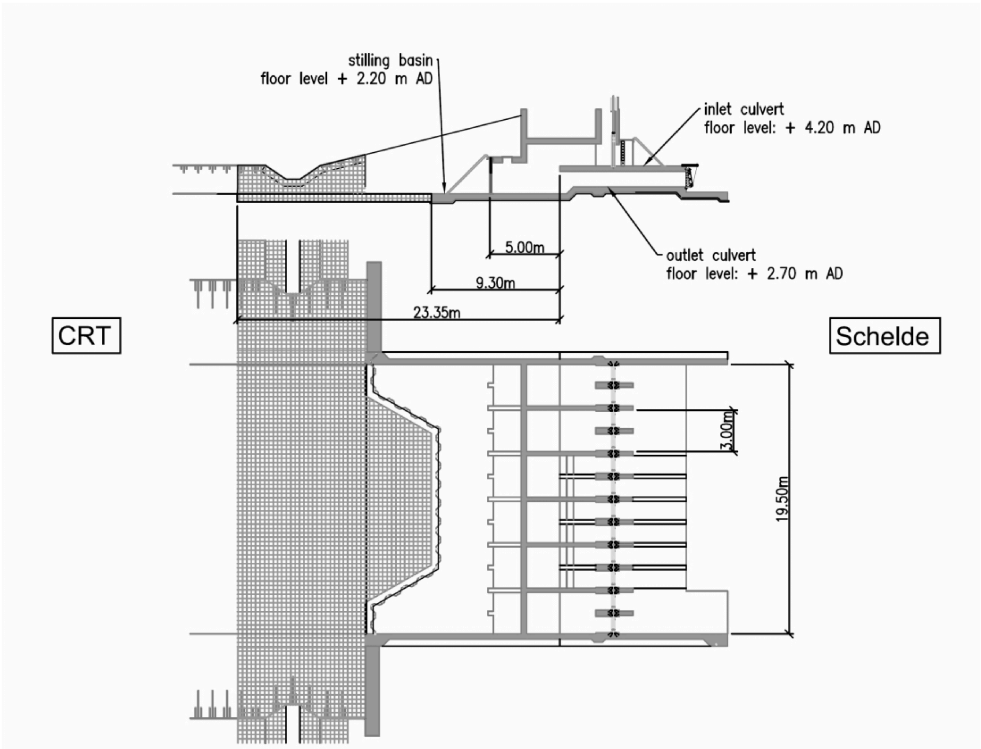

Figure 5 . Combined inlet-outlet sluice for FCA-CRT Bergenmeersen designed by IMDC nv.

The characteristic culvert dimensions corresponding to the desktop design in Figure 5 are summarized in Table 1.

Table 1. Characteristic culvert dimensions for FCA-CRT Bergenmeersen.

FCA-CRT Bergenmeersen					
Inlet culverts	Number of culverts	6	Outlet culverts	Number of culverts	3
	Culvert width	3.0 m		Culvert width	3.0 m
	Culvert height	1.6 m		Culvert height	1.1 m

Note in Figure 5 that:
- The drop height from the floor level of the inlet culvert to the floor level of the stilling basin is 2.0 m.
- The brink of the inlet culvert floor slab where the water starts dropping vertically (further abbreviated as: the brink), is used underneath (and in Figure 4) as a reference point to measure (horizontal) distances.
- The floor level of the stilling basin is proposed to be 0.50 m below the floor level of the outlet culvert. At 5.0 m downstream of the brink, the 6 inlet culverts are combined into one stilling basin. The combined stilling basin has parallel (i.e. non-diverging) sidewalls, which end at 19.0 m downstream of the brink (where they are attached to a wing wall).
- In the center of the construction, the concrete floor slab of the stilling basin ends at 9.3 m downstream of the brink (though the slab is extended somewhat further downstream at the edges of the construction). Between 9.3 m and 23.4 m downstream of the brink bottom protection is provided by gabions.

To be able to relate some characteristic levels in the design of the FCA-CRT to the tidal characteristics of the river Schelde near Bergenmeersen, Table 2 is provided.

Table 2. Characteristic levels for FCA-CRT Bergenmeersen.

FCA-CRT Bergenmeersen			**Tidal river characteristics**	
Ring dike	Crest level	+8.00 m AD	MHW	+6.2 m AD (extreme spring) +5.3 m AD (spring) +5.0 m AD (mean) +4.7 m AD (neap)
Levee	Crest level	+8.00 m AD		
Overflow dike	Crest level	+6.40 m AD		
Inlet culverts	Level of culvert ceiling	+5.80 m AD	MLW	+2.2 m AD (spring) +2.1 m AD (mean) +2.0 m AD (neap)
	Crest level of stop log walls	+4.4 to +5.7 m AD*		
	Level of culvert floor	+4.20 m AD		
Outlet culverts	Level of culvert ceiling	+3.80 m AD		
	Level of culvert floor	+2.70 m AD		
Polder	Mean elevation	+3.7 m AD		

* Range of stop log crest levels considered during design. Levels to be tuned when FCA-CRT is in operation.

The extreme spring tide referred to in Table 2, is defined as the level which is exceeded on average three times per year. Knowing that the corresponding water level is +6.2 m AD, this means that in such conditions the water level in the Schelde is 2.0 m above the floor of the inlet culvert. Similarly, from Table 2 and Figure 5 can be found that the water level in the Schelde is 1.1 m above the floor of the inlet culvert at mean spring tide. The corresponding specific discharges are equal to be 4.4 $m^3/s/m$ (extreme spring tide) and 1.8 $m^3/s/m$ (mean spring tide).

4 PHYSICAL SCALE MODEL

Both the agency and the consulting engineers preferred the desktop design (Figure 5) to be tested in a scale model, before the design would be approved for construction. Therefore, a physical model study was initiated at Flanders Hydraulics Research.

Because several designs of combined inlet-outlet sluices for other FCA-CRTs than Bergenmeersen are coming up in near future, the idea was to setup a flexible scale model in order to test different designs consecutively without major intermediate model (re)construction efforts. Moreover, the scale model setup should also allow the identification of possible flaws with and an optimization of a design.

To this end, the geometry of the design is somewhat simplified. Basically, a so-called 2DV model is aimed at, with a geometrical scale 1:8 for the vertical and longitudinal dimensions. The lateral direction is not relevant in a 2DV model. The model is built in a narrowed section of the large flow flume at Flanders Hydraulics Research. This flow flume has a length of 57.0 m, a width of 2.40 m, a height of 1.40 m and a maximum discharge of approximately 0.4 m^3/s. The dimensions of the narrowed section are: a length of 15.0 m, a width of 0.56 m and a height of 1.0 m. In order to allow an optimal visualisation of the flow patterns, one side of the narrowed channel is transparent. By means of exchangeable plates fixed on movable mechanical lifts, a wide range of geometrical arrangements can be addressed (Figure 6). Aeration of the falling jet is provided by two tubes mounted under the ceiling of the outlet culvert in the model. These tubes are in connection with the atmospheric pressure. The aeration method to be applied in the prototype has not been decided yet.

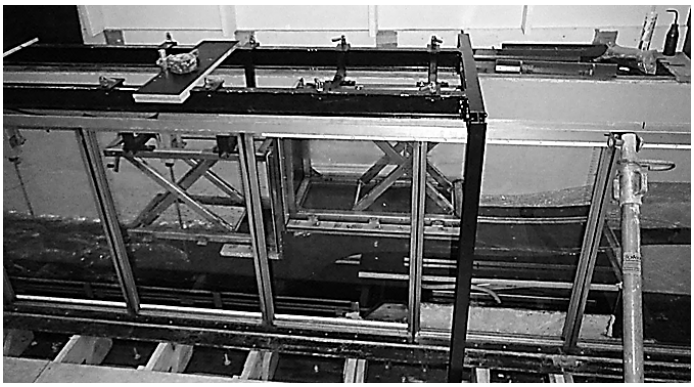

Figure 6. Possible adjustments scale model geometry.

The following measurement equipment is used in the physical model study:
- 2 electronic floaters to measure the water level upstream and downstream of the narrowed model section,
- 4 wave height meters to measure the water level on 4 locations in the model section,
- 3 electromagnetic discharge meters on the supply conduits,
- 2 electromagnetic velocimeters to measure a point velocity in the stilling basin.

Besides the electronic registrations, also visual registrations are carried out:
- drop length,
- end of the hydraulic jump,
- water level in the outlet culvert.

5 EXPERIMENTS

This section of the paper presents scale model results for the combined inlet-outlet sluice which has been designed for FCA-CRT Bergenmeersen The main focus was on inflows into the FCA-CRT, since these require most energy to be dissipated. Moreover, fixing the location of the hydraulic jump (downstream of the vertical drop) in the stilling basin for the combinations of water levels in the FCA-CRT (further abbreviated to: CRT level) and given water levels in the river Schelde (further abbreviated to: Schelde level) is looked at. When the hydraulic jump can be located above the concrete slab of the stilling basin, the velocity above the bottom protection (gabions) downstream of the slab will be limited and erosion downstream of the construction will be limited.

First the results of the desktop design will be presented. Then the results of some optimization efforts will be presented. Most of these experiments have been carried out with aeration of the falling jet in the vertical drop, though some comparative measurements without aeration did not show noticeable differences as far as the hydraulic jump is concerned.

5.1 *Desktop design*

The first geometry tested was the (original) desktop design. Figure 7 presents the flow pattern in the stilling basin with a Schelde level of + 6.20 m AD (this is an extreme spring tide with an occurrence of approximately three times a year) and three different levels in the CRT.

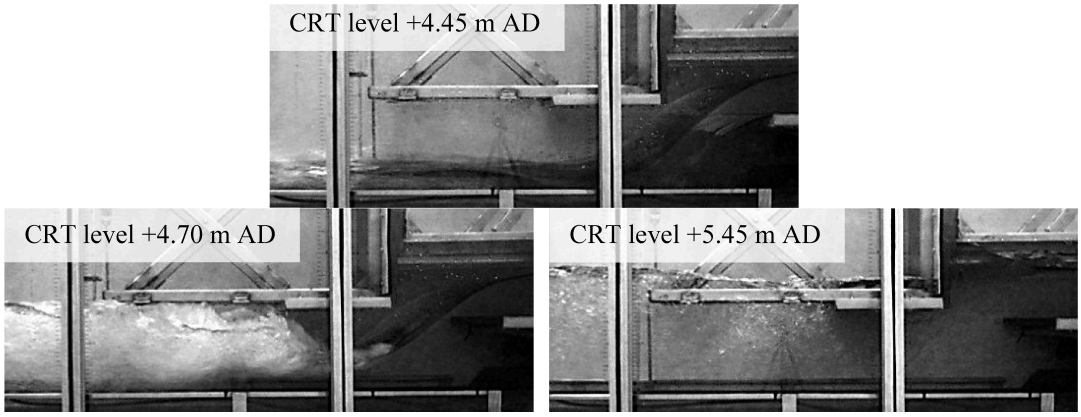

Figure 7. Illustration of flow pattern for a Schelde level of + 6.20 m AD and three different CRT levels:
top: CRT level + 4.45 m AD ➔ supercritical flow downstream of drop
bottom left: CRT level + 4.70 m AD ➔ hydraulic jump fixed
bottom right: CRT level + 5.45 m AD ➔ culvert drowned.

For a Schelde level of + 6.20 m AD, Figure 8 shows the near bottom velocity at 10 m downstream of the drop as a function of the CRT level. The near bottom velocity at 10 m is used as the design velocity for the gabions downstream of the structure. (Notice indeed in Figure 5, that the bottom protection starts at a distance of 9.3 m downstream of the drop in the center of the construction.)

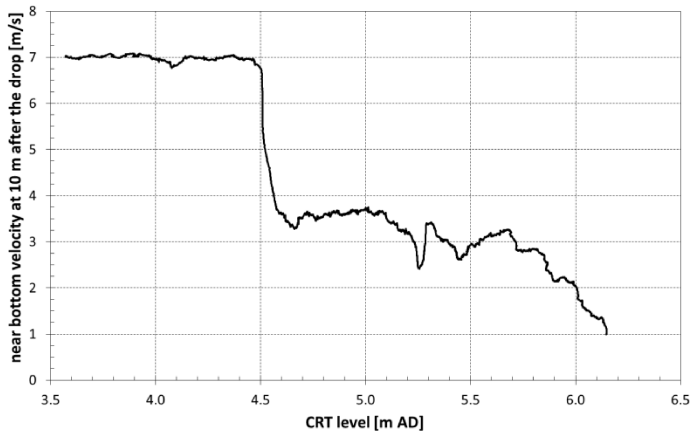

Figure 8. Near bottom velocity in function of the CRT level with a Schelde level + 6.20 m AD at 10 m downstream of the drop (note that the velocimeter is limited to 7 m/s).

Figure 8 shows a sudden drop of the near bottom velocity at a CRT level of + 4.50 m AD. This is caused by the transformation of supercritical to subcritical flow by means of a hydraulic jump. After this transition, the velocity remains at an almost constant level until the inlet sluice is drowned (Figure 7 below) and the discharge decreases. The CRT level at which the jump starts directly downstream of the drop is further referred to in this paper as the conjugate CRT level.

Figure 9 presents the measured conjugate CRT level as a function of the Schelde level. For comparison purposes, the conjugate CRT level calculated with the Bélanger equation (Bélanger, 1949) is also shown in Figure 9.

Bélanger equation:

$$Y_2 = Y_1 \cdot \frac{1}{2} \cdot \left(\sqrt{1 + 8 \cdot {Fr_1}^2} - 1\right) \qquad (1)$$

where Fr_1 = Froude number upstream of the jump, Y_1 and Y_2 = water levels upstream and downstream of the jump respectivelyY_1 can be calculated with the formula by Rand (1955):

$$Y_1 = \Delta z \cdot 0.54 \cdot \left(\frac{q^{2/3}}{g^{1/3} \cdot \Delta z}\right)^{1.275} \qquad (2)$$

where Δz = drop height, q = discharge per unit width , g =gravity acceleration.

Also the equation of the water depth upstream and downstream of the jump by Chanson (2002) and the equation of the water depth downstream of the jump by Rand (1955) were evaluated. The difference between the three analytical formulae is a maximum of 0.1 m. The numerical results by Coen et al. (2010), presented earlier in Figure 4, are used to verify that during operation the CRT level is continuously above the conjugate CRT level.

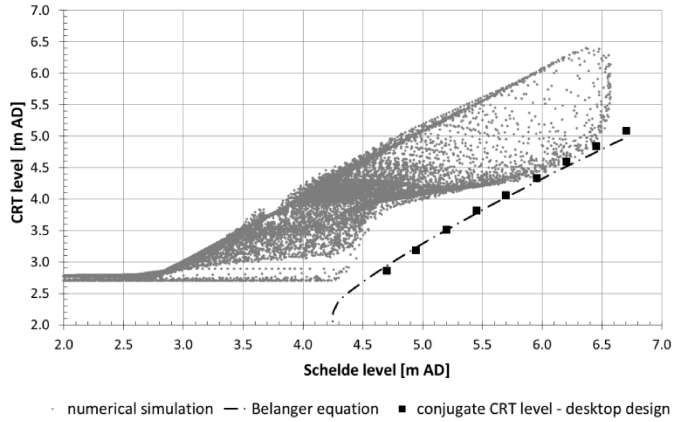

Figure 9. Comparison of predicted CRT levels during operation with the conjugate CRT level.

Figure 9 shows that the CRT levels during operation (predicted with the numerical model) are continuously above the conjugate CRT level. This means that the supercritical flow is transformed into subcritical flow in the area before the gabions (i.e. above the concrete floor slab of the stilling basin). At a Schelde level around + 6.20 m AD, however, there is no margin between the minimum predicted CRT level and the measured conjugate CRT level. Therefore, several optimization efforts have been made to increase that margin. Changes to the stilling basin geometry are made, some of which are classical in the hydraulic literature.

5.2 *Gabion sill*

Tests are carried out with a gabion sill with height 0.25 m and 0.50 m at a distance of 14 m and 19 m downstream of the drop. Because the floor level of the outlet culvert is situated 0.50 m above the floor level of the stilling basin, the maximum height of the gabion sill is limited to 0.50 m. Figure 10 left shows the near bottom velocity in function of the CRT level at a Schelde level + 6.20 m AD. Figure 10 right presents the measured conjugate CRT level in function of the Schelde level and compares this level with the predicted CRT levels.

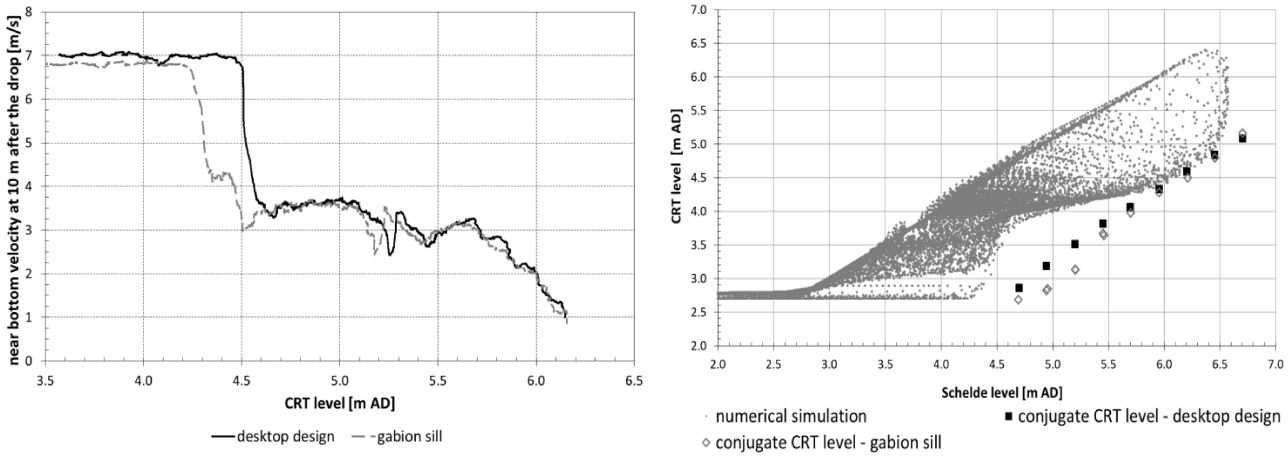

Figure 10. Left: Near bottom velocity in function of the CRT level with a Schelde level + 6.20 m AD at x=10 m at x=10 m when using a gabion sill with height 0.50 m at 14 m downstream of the drop (notice that the velocity meter is limited to 7 m/s); Right: Comparison of predicted CRT levels during operation with the conjugate CRT level.

Notice in Figure 10 left that a gabion sill has only a limited effect on advancing the transformation from supercritical to subcritical flow. Figure 10 right shows that a gabion sill only has a considerable effect on advancing the hydraulic jump for Schelde levels below + 5.50 m AD.

5.3 *Deepening the stilling basin*

Figure 11 left shows the near bottom velocity at a distance of 10.0 m downstream of the drop in function of the CRT level with a Schelde level of +6.20 m AD when increasing the stilling basin depth from 0.50 m to 1.00 m below the outlet culvert invert level. Figure 11 right presents the measured conjugate CRT level as a function of the Schelde level when the stilling basin is deepened and compares this level

with the predicted CRT levels. For comparison purposes, the conjugate CRT level (re)calculated with the Bélanger equation for the deepened stilling basin, is also shown in Figure 11.

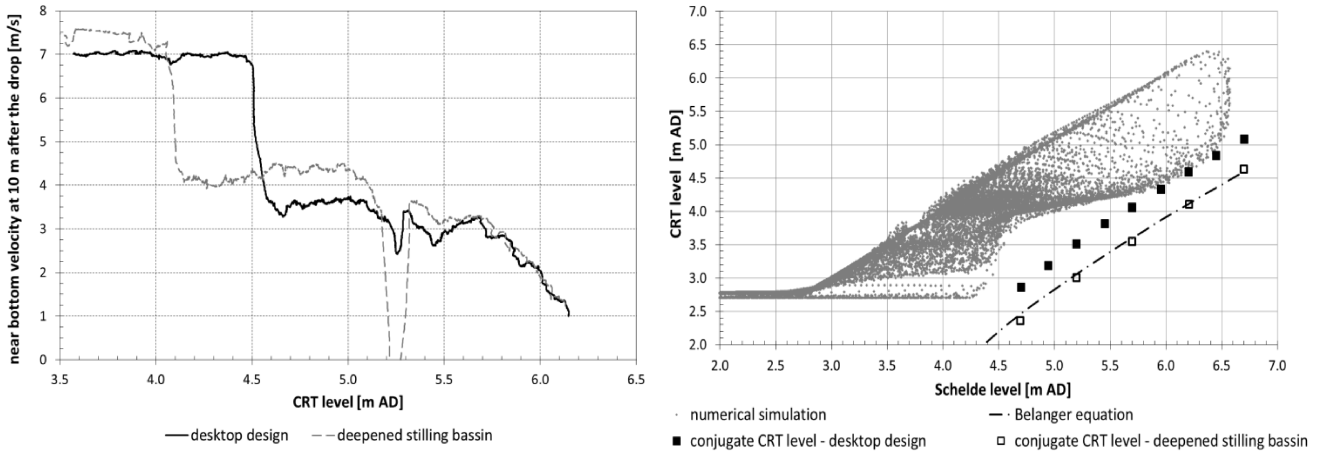

Figure 11. Left: Near bottom velocity in function of the CRT level with a Schelde level of + 6.20 m AD at x=10 m downstream of the drop when deepening the stilling basin to 1.0 m (notice that the velocity meter is limited to 7 m/s) ; Right: Comparison of predicted CRT levels during operation.

Figure 11 left shows that deepening the stilling basin to 1.0 m reduces the conjugate water level by about 0.45 m. Figure 11 right shows that deepening the stilling basin reduces the conjugate CRT level by 0.4 m to 0.5 m for the entire range of Schelde levels, and provides a margin with the predicted CRT levels.

5.4 *Baffle beam*

The effect of adding a beam at a distance of 5.0 m downstream of the drop was studied. The beam will be further referred to as a "baffle beam", since it can be interpreted as a set of baffle blocks with zero spacing in the spanwise direction. The baffle beam dissipates part of the drop energy and due to this, the conjugate CRT level decreases. The maximum height of the baffle beam must be below the floor level of the outlet culvert and thus is limited to 0.5 m. In the scale model, baffle beams with height 0.25 m and 0.50 m were tested. Figure 12 shows the flow pattern downstream of the drop with a CRT level of + 4.45 m AD and a Schelde level of + 6.20 m AD when using a baffle beam with a height of 0.50 m.

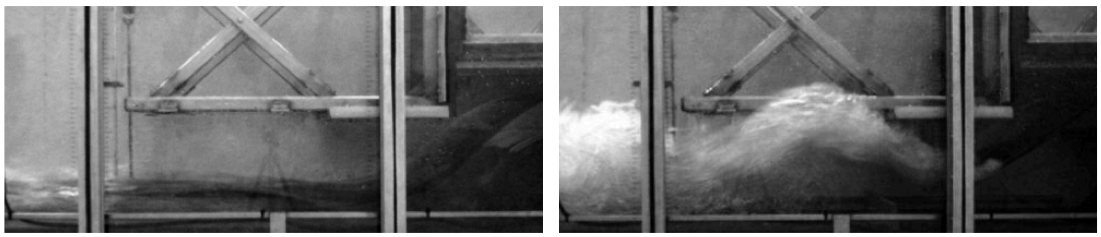

Figure 12. Flow pattern in the stilling basin (CRT level + 4.45 m AD / Schelde level + 6.20 m AD)
Left : desktop design ; Right : baffle beam with height 0.50 m at 5.0 m downstream of the drop.

Notice in Figure 12 that the baffle beam deviates the supercritical flow in the upward direction. Through the dissipation of energy with the baffle beam, the water downstream of the baffle beam is transformed to subcritical flow with a lower conjugate CRT level.

Figure 13 left presents the near bottom velocity downstream of the drop in function of the CRT level with a Schelde level of + 6.20 m AD, when a baffle beam with a height of 0.50 m is placed at 5.0 m downstream of the drop. Because the transformation to subcritical flow is not a clear hydraulic jump, the near bottom velocity is also given at 7.5 m and 12 m downstream of the drop. Figure 13 right shows the measured conjugate CRT level as a function of the Schelde level when a baffle beam with height 0.25 m and 0.50 m is used and compares this level with the predicted CRT levels.

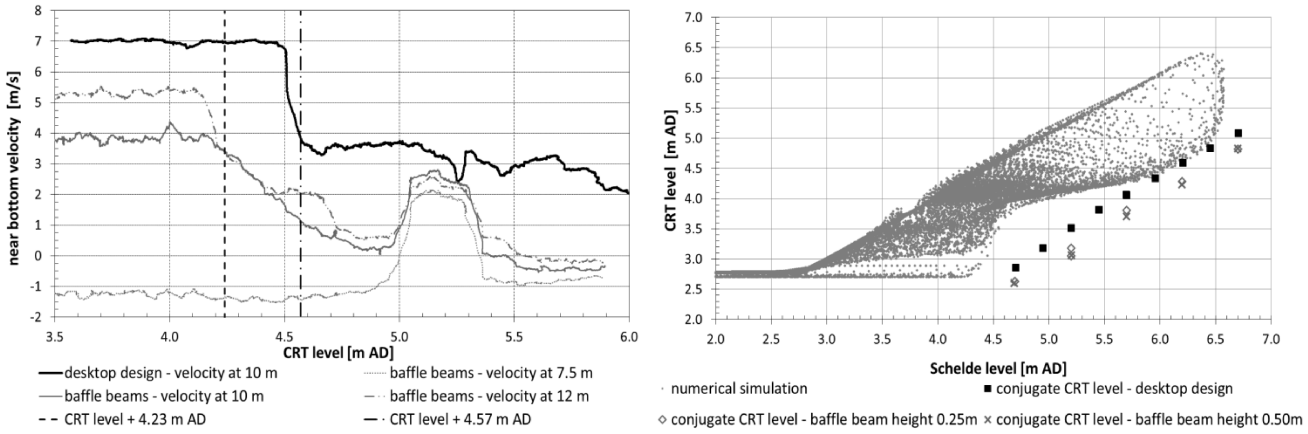

Figure 13. Left Near bottom velocity in function of the CRT level with a Schelde level of + 6.20 m AD at x=7.5 m, 10.0 m and 12.0 m downstream of the drop when using a baffle beam with height 0.50 m at 5.0 m downstream of the drop (notice that the velocity meter is limited to 7 m/s) ; Right Comparison of predicted CRT levels during operation with the conjugate CRT level.

Notice in Figure 13 left that a baffle beam advances the transformation from supercritical to subcritical flow. Because the energy is partly dissipated, the velocity is lower for the full range of Schelde levels. When the CRT level rises, the drop length increases, see Figure 14. At a CRT level of + 5.10 m AD the drop goes beyond the baffle beam. Consequently, the velocity rises to a value almost equal to the velocity for the desktop design. For a CRT level equal to + 5.30 m AD the ceiling of the stilling basin is drowned (Figure 7). The falling jet now bumps into the vertical wall downstream of the inlet culvert and is redirected towards the baffle beam. The interaction between the jet and the baffle beam positively influences the near bottom velocity downstream of the baffle beam.

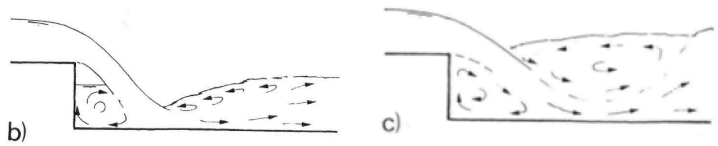

Figure 14. Flow pattern downstream of a sudden drop in a rectangular channel (Vischer & Hager, 1995).

The use of a baffle beam decreases the conjugate CRT level for the full range of Schelde levels. The baffle beams with a height of 0.25 m and 0.50 m result in an almost similar decrease of the conjugate CRT level.

During the tests, an unstable flow pattern was noticed using the baffle beams. For a Schelde level of + 6.20 m AD this unstable flow pattern occurs between CRT levels + 4.50 m AD and + 4.90 m AD. Between these two levels the flow pattern changes constantly between the distinct patterns shown in Figure 15.

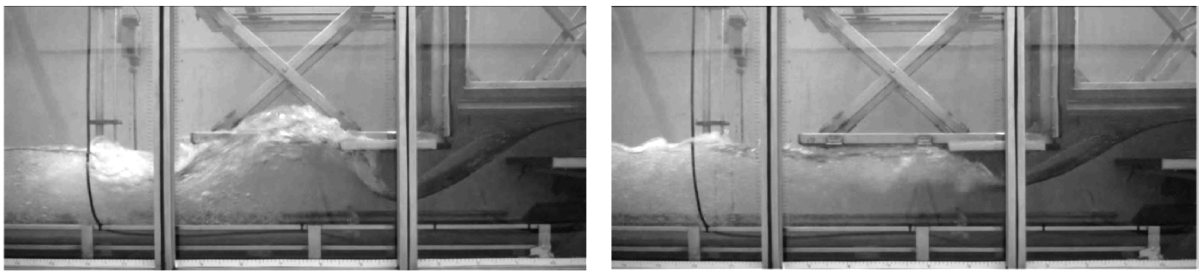

Figure 15. Unstable flow patterns when using a baffle beam with height 0.50 m (CRT level + 4.60 m AD / Schelde level + 6.20 m AD).

5.5 *Baffle blocks*

Peterka (1984) and Thompson & Kilgore (2006) advice to use baffle blocks instead of one baffle beam for energy dissipation. Baffle blocks reduce the length of the jump and the conjugate water level. Based on the literature formula for dimensioning the baffle blocks, blocks with a height of 0.66 m, a width of 0.56 m and a distance between the blocks of 0.56 m are recommended for a Schelde level of + 6.20 m AD. In the scale model, blocks with a height of 0.50 m and 0.75 m were tested. The width and the distance between the blocks for both type of baffle blocks was 0.50 m. The baffle blocks do not obstruct the

whole area, therefore it is permitted that the height is above the floor level of the outlet culvert. Figure 16 presents the flow pattern for baffle blocks with a height of 0.50 m, a CRT level of + 4.45 m AD and a Schelde level of + 6.20 m AD.

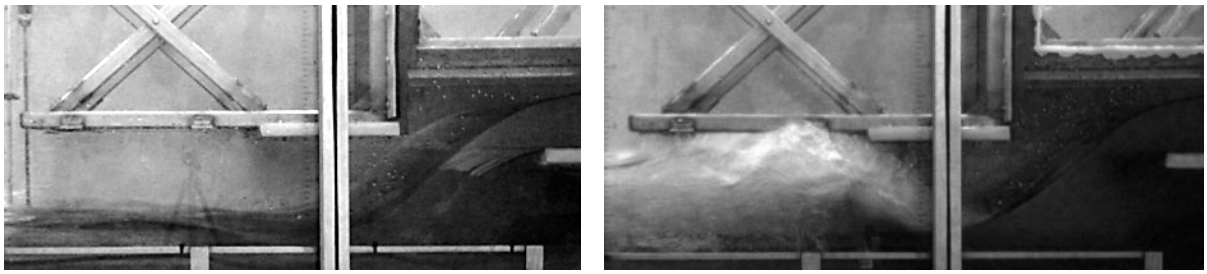

Figure 16. Flow pattern in stilling basin (CRT level + 4.45 m AD / Schelde level + 6.20 m AD)
Left : desktop design ; Right : baffle blocks with height 0.50 m at 5.0 m downstream of the drop.

When using baffle blocks, the hydraulic energy is partly dissipated. For this configuration the jump starts at a lower conjugate CRT level. It is also noticed that baffle blocks result in a greater energy dissipation when compared to a baffle beam. The aforementioned unstable flow pattern with the baffle beam was not noticed. Figure 17 left presents the near bottom velocity after the drop in function of the CRT level with a Schelde level of + 6.20 m AD when baffle blocks with height 0.50 m are placed at 5.0 m downstream of the drop. Because the transformation is not a clear hydraulic jump, the near bottom velocity is also given at 7.5 m and 12.0 m downstream of the drop. Figure 17 right presents the influence of baffle blocks with height 0.50 m and 0.75 m on the conjugate CRT level as a function of the Schelde level. According to Thompson & Kilgore (2006) the conjugate CRT level can be reduced to 85 % when using baffle blocks. In Figure 17 right a line is plotted indicating 85% of the conjugate CRT level calculated with the Bélanger equation.

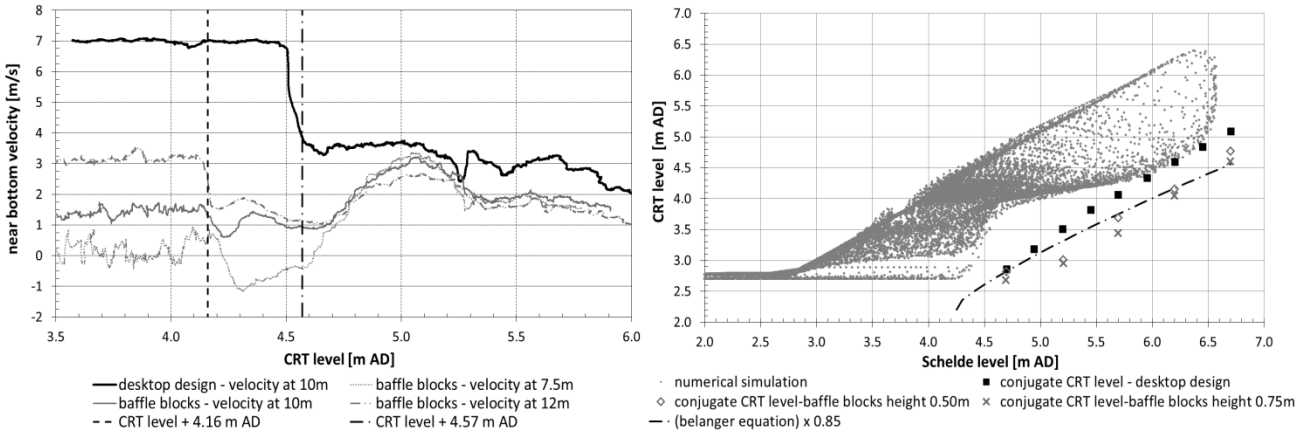

Figure 17. Left: Near bottom velocity in function of the CRT level with a Schelde level + 6.20 m AD at x=7.5 m, 10.0 m and 12.0 m downstream of the drop when using baffle blocks with height 0.50 m at 5.0 m after the drop (notice that the velocimeter is limited to 7 m/s) ; Right: Comparison of predicted CRT levels during operation with the conjugate CRT level when using baffle blocks.

In Figure 17 left it should be noticed that the near bottom velocity decreases for the full range of Schelde levels when using baffle blocks. If the representative velocity for the desktop design is used to determine the effectiveness, it can be stated that baffle blocks reduce the conjugate CRT level by 0.4 m. Similarly to the case of one baffle beam, a rise in near bottom velocity is noticed for CRT levels from + 5.0 m AD. Figure 17 right shows that baffle blocks reduce the conjugate CRT level over the full range of Schelde levels. The effect of baffle blocks with height 0.50 m and 0.75 m on the conjugate CRT level is similar. The conjugate CRT level at the design discharge of the baffle blocks (corresponding to a Schelde level of + 6.20 m AD) is approximately 15 % lower than the value for a normal hydraulic jump without baffle blocks.

6 CONCLUSION

Within the framework of the Sigmaplan, different flood control areas with controlled reduced tide (FCA-CRTs) are being setup along the Schelde estuary. To introduce the reduced tide in the polder, simple inlet and outlet sluices are relied upon. Most recently, combined inlet-outlet sluices are being advocated. In such structures the inlet culverts are on top of the outlet culverts. During inflow, a falling jet drops from the floor slab of the inlet culvert and plunges into a stilling basin. The energy of the plunging jet is additionally dissipated by means of a hydraulic jump.

In this paper, a physical model study is described to test a desktop design of such a structure for a specific case, i.e. FCA-CRT Bergenmeersen. The desktop design turns out to be satisfactory. Yet, at inflow discharges corresponding to an extreme spring tide (i.e. a Schelde level of +6.20 m AD which is exceeded on average three times per year), there is only a small margin in terms of fixing the location of the hydraulic jump above the concrete slab of the stilling basin. Therefore, some optimization efforts have been carried out to increase that margin, by adding some obstacles in the stilling basin or by modifying the basin geometry: (i) adding a gabion sill, (ii) deepening the stilling basin, (iii) adding a baffle beam and (iv) adding baffle blocks.

It turned out that adding a gabion sill does not increase the margin at extreme spring tide levels. Deepening the stilling basin increases the margin over the full range of Schelde levels (but this design modification is not applicable in practice, since the preparatory work for the construction of the prototype is in a too advanced stage). The same goes for adding a baffle beam, though in some range of CRT levels (i.e. tailwater depths) an unstable flow pattern was observed. The use of baffle blocks gives the best results for fixing the location of the hydraulic jump and no unstable flow patterns are observed.

For the designs with a non-obstructed hydraulic jump (i.e. a design without sill, beams, blocks, …), there was a good correlation between the literature formulae and the scale model results. Peterka (1984) and Thompson & Kilgore (2006) present formulae for dimensioning baffle blocks and state that when using baffle blocks (according to this formulae) the conjugate CRT level may be lowered to 85 %. This was – for the design discharge of the baffle blocks – confirmed by the scale model results.

Notwithstanding the abovementioned optimization efforts, it was decided by the agency to retain the original desktop design. This decision was motivated by the fact that the predicted CRT levels do (though marginally) exceed the conjugate CRT level and the preparation of the construction in the field was already in an advanced stage. In addition, the agency reckoned that - if during operation of the FCA-CRT unacceptable circumstances would be encountered - there are still means to elegantly modify the stilling basin geometry without major constructional efforts. Adding a baffle beam in the stop log recesses seems to be the most likely solution.

Of course, the lessons learned from the abovementioned optimization efforts will be taken into account for the design of the upcoming FCA-CRT projects.

NOTATION

Y_1	Water level upstream of hydraulic jump [m]
Y_2	Conjugate water level downstream of hydraulic jump [m]
Fr_1	Froude number upstream of hydraulic jump [-]
q	Discharge per unit width [m^2/s]
g	Gravity acceleration [m/s^2]
Δz	Drop height [m]

REFERENCES

Bélanger, J.B. (1849) Notes sur le Cours d'Hydraulique. (Hydraulic Course Notes.) *Mém. Ecole Nat. Ponts et Chaussées* (Paris, France) [in French].

Chanson, H. (2002). The hydraulics of stepped chutes and spillways. Swets & Zeitlinger: Lisse. ISBN 90-5809-352-2

Chow, V.T. (1982). Open-Channel Hydraulics. McGraw-Hill Book Company.

Coen, L., Peeters, P., Mostaert, F. (2010). Studies ten behoeve van aanleg van overstromingsgebieden en natuurgebieden in het kader van het Sigmaplan: addendum bij ondersteunende studies: cluster Kalkense meersen.(Study for the implementation of Flood Control Areas and Controlled Reduced Tide areas within the framework of the Sigmaplan: addendum: cluster Kalkense meersen) [in Dutch]. Report no. 713_17, version 2.0, Flanders Hydraulics Research, 9p.

Cox, T., Maris, T., De Vleeschauwer, P., De Mulder, T., Soetaert, K., Meire, P. (2006). Flood control areas as an opportunity to restore estuarine habitat. Ecological Engineering, Vol. 28, Issue 1, pp. 55-63.

De Mulder, T., Vercruysse, J., Verelst, K., Peeters, P., Maris, T., Meire, P. (2013) Inlet sluices for Flood Control Areas with Controlled Reduced Tide in the Scheldt estuary: an overview. IWLSH 2013.

French, R.H. (1986).Open-Channel Hydraulics. McGraw-Hill Book Company.

IMDC (2008). Structural types of inlet/outlet constructions for FCA-CRTs [in Dutch]. Report no. I/RA/11296/08.036/PRA, Commissioned by Waterwegen & Zeekanaal nv, 23 pp.

IMDC (2010). Modelproeven op in- en uitwateringsconstructie en energiedissipatiegracht (Model tests on combined inlet and outlet sluice and dissipation ditch) [in Dutch]. Report no. I/NO/11336/10.212/MOE Commissioned by Waterwegen & Zeekanaal nv, 21 pp.

Maris, T., Cox, T., Temmerman, S., De Vleeschauwer, P., Vandamme, S., De Mulder, T., Van den Bergh, E., Meire, P. (2007). Tuning the tide: creating ecological conditions for tidal marsh development in a flood control area. Hydrobiologia, Vol. 588, pp.31-43.

Peeters, P., Claeys, S., Michielsen, S., De Schutter, J., Temmerman, S., Meire, P., Vandenbruwaene, W., Maris, T., Chen, M., Wartel, S. (2009). Sediment behaviour within a flood control area with a controlled reduced tide – Pilot project Lippenbroek. In: Proceedings Congrès SHF-31ième Journées de l'hydraulique: "Morphodynamiques et débits solides dans les estuaires, les baies et les deltas", Paris, 22-23 septembre 2009. Société Hydrotechnique de France: Paris. ISBN 2-906831-79-4.

Peterka, A.J. (1984). Hydraulic design of stilling basins and energy dissipators. Eight printing. Engineering monograph (Washington), 25. U.S. Dept. of the Interior, Bureau of Reclamation: Washington

Rand, W. (1955). Flow geometry at straight drop spillways. Proceedings of the American Society of Civil Engineers 811-13.

Ritzema H.P. (1994). Drainage principles and applications. International Institute for Land Reclamation and Improvement/ILRI publication 16, second edition. Wageningen, The Netherlands.

Sinniger, R.O., Hager, W.H. (1989). Constructions hydrauliques – Ecoulement stationnaires. Presses polytechniques romandes, Lausanne.

Thompson, P.L., Kilgore, R.T. (2006). Hydraulic design of energy dissipators for culverts and channels. Third edition. Hydraulic Engineering Circular, 14. U.S. Department of Transportation. Federal Highway Administration: Arlington. 287p.

Vischer, D.L., Hager, W.H. (eds.) (1995). Energy dissipators. Hydraulic Structures Design Manual: Hydraulic Design Considerations, 9. A.A. Balkema: Rotterdam. ISBN 90-54109-198-9.

IWLHS, 20-22/02/2013, Aachen - Bung & Pagliara (eds) - © 2013 Bundesanstalt für Wasserbau ISBN 978-3-939230-04-5

A Two Parametric Study of Submerged Sluice Gate Water Outflows within Sloped Open Channels

E. Retsinis
Civil Engineer, National Technical University of Athens, Postgraduate Student, National Technical University of Athens, JD Research Hydrolab – A non Profit Foundation, 12, Polykarpou St., N. Smyrni, Athens 17123, Greece

J. Demetriou
Dr Civil Engineer, Associate Professor (RD), National Technical University of Athens, School of Civil Engineering, JD Research Hydrolab – A non Profit Foundation, 12, Polykarpou St., N. Smyrni, Athens 17123, Greece

ABSTRACT: In this mainly experimental and also computational study, the various water flow characteristics of submerged sluice gate outflows within a sloped (angle φ) open channel are measured, analyzed, presented and discussed-in a suitable two parametric evaluation. A special dimensionless (A) parameter is examined as function both of φ and a suitable Froude number. In a similar way, the discharge coefficient is investigated as a function of φ and a parameter D corresponding to the dimensionless small difference of depths (upstream, downstream). The authors believe that the present results may help the hydraulic engineer when dealing with sluice gate submerged underflows within sloped open channel.

Keywords: Sluice Gates' Submerged Flows, Sloped Channels

1 INTRODUCTION

The steady turbulent water flow under a sharp edged sluice gate and subsequent downstream water flowing formations, belong to some of the most important low head hydraulic phenomena which are appearing in practice within rectangular open channels. Depending on further downstream water flow regulation, the flow beyond the sluice gate may permanently be free or submerged.

Fig.1 schematically shows the general flow case, where the free surface water channel is inclined (angle φ, J_o=sinφ) and includes a discharge measuring hydraulic structure, i.e. a sluice gate perpendicular to the channel floor-which has the same width as the channel-with a lower aperture b and a downstream regulating gate.

The water free surface profile is gradually varied upstream, and horizontal-beyond a depth d_3-downstream. The water discharge per unit channel width is q, the most important cross sections are 1 (water depth d_1) and 3 (depth d_3) with $d_1 \geq d_3$, while a significant role play the free flow depth d_2 (when the regulating gate is fully opened) and depth d_s-when the regulating gate is closed enough. All depths are perpendicular to the floor, while when d_s is larger than d_2 the entire flow is "submerged", a hydraulic phenomenon which may due not only to a regulating gate but even to a downstream obstacle. Furthermore depths d_1 are taken at a sufficient distance from the sluice gate. Then head of the flow is the small difference between water levels upstream and downstream of the sluice gate.

In case of submerged flow an inner water flow region is created, the recirculating roller, within which the local total discharge is zero, while this roller contributes with its weight in increasing the underflow local pressures. In cross sections 1 and 3 the local pressures are generally considered as hydrostatically distributed.

The onedimensional equations (per unit channel width) between sections 1 and 3 along the flow, are

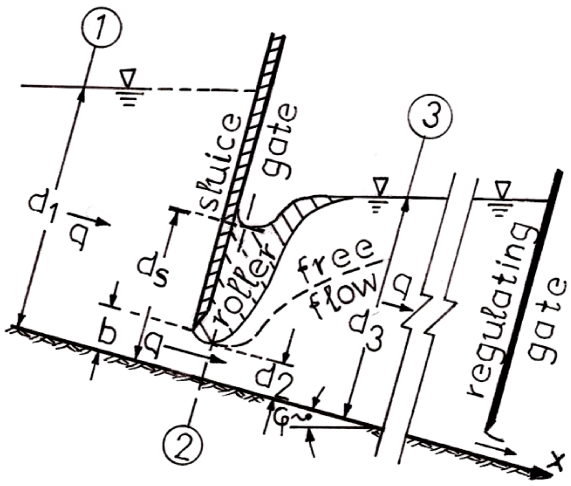

Figure 1. Schematic flow details.

the continuity equation

$$q=d_1\cdot V_1=d_3\cdot V_3, \quad (1)$$

and the momentum equation, with G_x dynamic forces from all boundaries,

$$0.5\cdot\rho\cdot g\cdot(d_1^2-d_3^2)\cdot\cos\varphi+W\cdot J_o-G_x=\rho\cdot q^2\cdot[(1/d_3)-(1/d_1)], \quad (2)$$

where $W\cdot J_o$ is the water weight component between sections 1 and 3 along the flow direction and ρ=water density. An interesting flow parameter is the Froude number at section 3,

$$Fr_3=q\cdot g^{-1/2}\cdot d_3^{-3/2},$$

which is usually less than unity (subcritical flow regime).

Henderson (1966), has considered another approach, with a control volume corresponding to the flow between sections 2 (lower depth d_2 through which the entire discharge $q=V_2\cdot d_2=V_s\cdot d_2$ is passing and which has hydrostatic pressures, and the depth d_s-d_2 also with hydrostatic pressures) and section 3. The complete momentum equation along the flow and between sections 2 and 3 is

$$0.5\cdot\rho\cdot g\cdot(d_s^2-d_3^2)+W'\cdot J_o-G_x'=\rho\cdot q\cdot(V_3-Vs)\approx\rho\cdot q\cdot(V_3-V_2)=\rho\cdot q^2\cdot[(1/d_3)-(1/d_2)], \quad (3)$$

where $W'\cdot J_o$ and G_x' are the water weight component and force between sections 2 and 3 (along the flow direction) and V_s is the velocity in d_s ($V_s=V_2$).

If the channel is horizontal ($\varphi=0^o$, $W'\cdot J_o=0$) and $G_x'=0$, Fr_3 may be introduced in such a way that eq. (3) is re-expressed (Henderson's equation),

$$(d_s/d_3)^2=1+2\cdot Fr_3^2\cdot[1-(d_3/d_2)],$$

or,

$$[(d_s/d_3)^2-1]/[1-(d_3/d_2)]=2\cdot Fr_3^2. \quad (3a)$$

It should be mentioned that eqs. (2, 3) are already simplified, since the momentum correction factors are omitted.

For the present analysis ($\varphi\geq0^o$) a more general dimensionless parameter may be introduced for all angles φ,

$$A=[(d_s/d_3)^2-1]/[1-(d_3/d_2)], \quad (4)$$

considered as a function of angle φ and Fr_3, based on the laboratory measurements and corresponding to a general solution of eq. (3)-including the effects from W', G_x',

$$A=f(\varphi,Fr_3),$$

where b, d_s, d_3, angles φ and q are experimentally determined, while Fr_3 may be calculated. In practical problems with small angles $\varphi(\leq6^o)$, d_2 may be considered as $d_2=c_c\cdot b$, where c_c=contraction coefficient-with a mean value $c_c\approx0.6$, Pajer, (1937), and Demetriou (2007).

In this investigation the discharge is expressed through the well known equation,

$q=c_d \cdot b \cdot [2 \cdot g \cdot (d_1-d_3)]^{1/2}=c_d \cdot b^{3/2} \cdot [2 \cdot g \cdot \{(d_1-d_3)/b\}]^{1/2}$,

where c_d is a function of angle φ and $(d_1-d_3)/b$,

$c_d=f'[\varphi, (d_1-d_3)/b]$.

Since q, b, d_1, d_3, are measured in the laboratory c_d may determined and correlated to angles φ and $(d_1-d_3)/b$.

When $d_3 \rightarrow d_2$ (free flow) then q is larger than in the case $d_3 \neq 0$ (submerged flow) and this is natural because of the smaller water mass over the free flow. This means that for (φ, d_1)=const. and decreasing d_3 (or increasing d_1-d_3) the discharging outflow is expected to increase. Also it should be noted, that at cross section 2 the upper stream line of the free flow coincides with the lower limit of the roller-along a small length from sluice gate aperture.

2 PREVIOUS WORKS

The basic elements of the water flow under a vertical sluice gate within an horizontal open channel may be found in Chow's, (1959), or Henderson's (1966), books, or in the papers by Covinda et. al. (1963), and Pajer (1937). Retsinis (2003), has performed a large number of measurements on sluice gate underflows within a sloped open channel.

Demetriou (2006), Dimitriou et. al. (2010), Retsinis et. al. (2004), and (2005), and Demetriou et. al. (2006), have also presented their investigations on sluice gate underflows within sloped open channels. Finally Demetriou (2007), has measured the contraction coefficient for free flows under sluice gates within inclined open channels.

3 THE EXPERIMENTAL MESUREMENTS

All experimental measurements were performed in a small tilting perspex channel. The discharges were volumetrically measured, the depths were determined with accurate level gauges, while the Reynolds numbers were large enough. Angles φ were 0^o-1^o-2^o-3^o-4^o-5^o-6^o, while the apertures b varied between 3 cm and 5 cm. When measuring various flow properties it is obvious that they are affected by existing quantities which are included in a phenomenon (water weights, exercised forces, e.t.c.).

In the following Tables 1, 3, all final experimental results are presented, after rejecting some erroneous measurements.

4 RESULTS. ANALYSIS AND DISCUSSION

Table 1 presents A measured values-vs angles φ and Fr_3. Based on these values eq. (5) is expressed, from which A predicted values are resulting and put also in Table 1, showing a good agreement to A measured values, i.e. eq.(5) is a correct equation, since both groups of A are practically coinciding.

Table 1. A vs angles φ and Fr_3.

φ^o	Fr_3	A measured	A predicted	φ^o	Fr_3	A measured	A predicted
6	0.063	0.062	0.062	4	0.274	0.348	0.351
6	0.065	0.065	0.065	4	0.407	0.610	0.613
6	0.069	0.071	0.072	4	0.423	0.640	0.645
6	0.084	0.097	0.097	4	0.435	0.670	0.670
6	0.089	0.105	0.106	3	0.082	0.046	0.046
6	0.098	0.123	0.123	3	0.128	0.089	0.088
6	0.106	0.138	0.139	3	0.138	0.099	0.099
6	0.108	0.142	0.143	3	0.148	0.111	0.110

φ^o	Fr_3	A measured	A predicted	φ^o	Fr_3	A measured	A predicted
6	0.109	0.143	0.144	2	0.162	0.095	0.094
6	0.111	0.148	0.147	2	0.182	0.115	0.114
6	0.112	0.149	0.149	2	0.201	0.134	0.135
6	0.113	0.151	0.152	2	0.205	0.138	0.139
6	0.115	0.155	0.156	2	0.213	0.149	0.148
6	0.118	0.160	0.162	2	0.228	0.165	0.166
6	0.366	0.771	0.769	2	0.246	0.185	0.187
5	0.116	0.126	0.127	2	0.260	0.206	0.206
5	0.131	0.152	0.152	2	0.452	0.471	0.473
5	0.136	0.161	0.161	1	0.209	0.108	0.108
5	0.141	0.171	0.169	1	0.216	0.114	0.115
5	0.148	0.179	0.180	1	0.217	0.115	0.115
5	0.149	0.181	0.182	1	0.234	0.131	0.132
5	0.149	0.182	0.183	1	0.238	0.136	0.136
5	0.174	0.229	0.227	1	0.257	0.155	0.156
5	0.183	0.247	0.245	1	0.273	0.173	0.173
5	0.197	0.270	0.272	1	0.306	0.209	0.211
5	0.276	0.432	0.436	1	0.311	0.215	0.217
5	0.319	0.534	0.533	1	0.372	0.293	0.290
5	0.327	0.548	0.551	0	0.175	0.055	0.055
5	0.351	0.607	0.606	0	0.217	0.087	0.086
4	0.095	0.075	0.075	0	0.247	0.113	0.112
4	0.095	0.075	0.075	0	0.428	0.298	0.296
4	0.110	0.093	0.093	0	0.464	0.331	0.333
4	0.122	0.109	0.109	0	0.477	0.343	0.346
4	0.133	0.124	0.123				
4	0.178	0.186	0.188				
4	0.204	0.231	0.229				
4	0.224	0.265	0.263				
4	0.237	0.286	0.286				
4	0.244	0.296	0.298				
4	0.253	0.312	0.313				
4	0.255	0.320	0.317				
4	0.257	0.321	0.321				

The correlation coefficient is r^2=0.9999. The maximum difference between A measured and predicted, is less than ±1%.

Based on the above measured values and a computer program the following accurate equation may be determined (φ in degrees):

$$A=a1+b1\cdot\varphi+c1\cdot Fr3+d1\cdot\varphi2+e1\cdot Fr_3^2+f1\cdot\varphi\cdot Fr3+g1\cdot\varphi3+h1\cdot Fr_3^3+i1\cdot\varphi\cdot Fr_3^2+j1\cdot\varphi2\cdot Fr3, \quad (5)$$

where a_1, b_1, c_1, d_1, e_1, f_1, g_1, h_1, i_1, j_1, arithmetic coefficients given in Table 2. Eq. (5) holds for $0^o \le \varphi \le 6^o$ and $0.06 \le Fr_3 \le 0.46$.

Table 2. Arithmetic Coefficients for eq. (5).

a_1	b_1	c_1	d_1	e_1	f_1	g_1	h_1	i_1	j_1
0.001401	0.004750	-0.179177	-0.001550	3.250996	0.076825	-0.000015	-2.866600	0.075774	0.025879

All predicted A values from eq. (5) and Table 2 are also shown in Table 1.

Based on eq. (5) and Table 2, Fig. 2 presents an iso-A diagram for $0.05 \le A \le 0.75$ with an A step of 0.05. When angle φ=const. A are strongly increasing with Fr_3, while for Fr_3=const. A are smoothly increasing

with angle φ, i.e. A is primarily depending on angle φ. Eq. (5) holds for any intermediate φ and Fr_3 values, while Eq. (5) and Fig. 2 give quite the same results.

For $\varphi=0^o$ and various Fr_3 values, eq. (5) gives A values very close to $2\cdot Fr_3^2$, i.e. eq. (5) is close to the theory (deviations of about ±10%). These deviations are rather normal since all theoretical onedimensional momentum equations (eqs. 3, 3a) are simplified, while-actually-the present solution of A (eq. 5) based on experimental evidence indirectly includes all effects from acting forces on all boundaries.

For $\varphi>0^o$, in eq. (5) are also indirectly included all effects from actual momentum change, weight and exercised forces, since the experiments are always real-based on all acting quantities.

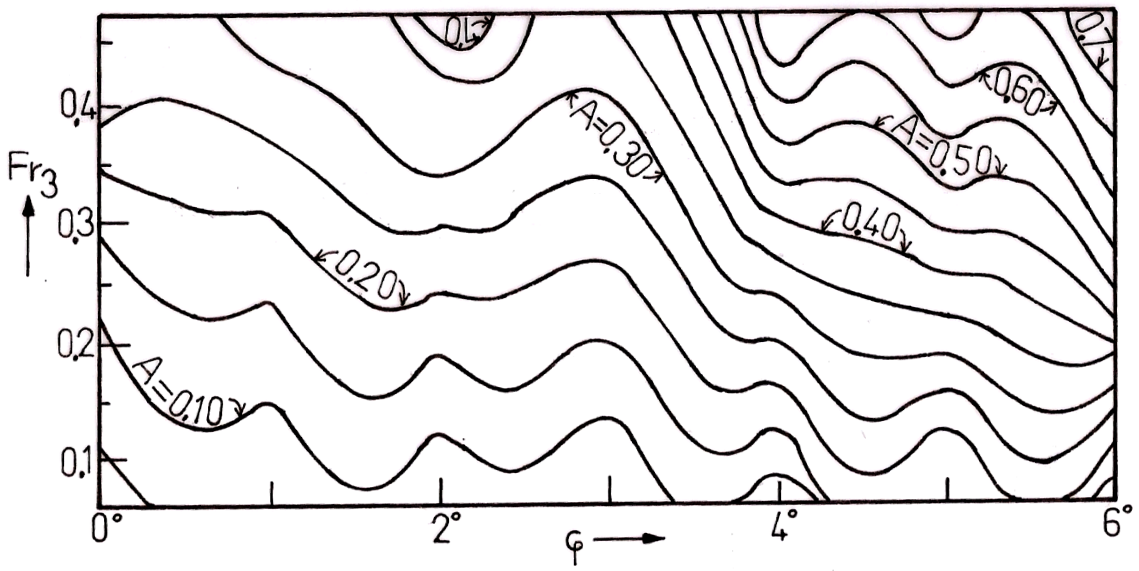

Figure 2. iso-A curves vs angles φ and Fr_3.

Table 3 presents measured and predicted (from the further down eq. 6) c_d values as functions of angle φ and $D=(d_1-d_3)/b$, under the same thoughts concerning Table 1 and eq. (5).

Table 3. c_d vs angles φ and $(d_1-d_3)/b$.

φ^o	D	c_d measured	c_d predicted	φ^o	D	c_d measured	c_d predicted
6	0.138	0.277	0.280	2	0.607	0.422	0.420
6	0.267	0.284	0.286	2	0.700	0.427	0.421
6	0.333	0.289	0.289	2	0.846	0.430	0.423
6	0.345	0.286	0.289	2	0.855	0.416	0.423
6	0.495	0.290	0.293	2	0.926	0.427	0.424
6	0.571	0.300	0.295	2	1.000	0.420	0.424
6	0.600	0.293	0.296	2	1.062	0.432	0.425
6	0.662	0.299	0.297	2	1.168	0.421	0.425
6	0.971	0.300	0.300	2	1.482	0.432	0.428
6	1.354	0.304	0.302	1	0.177	0.418	0.419
5	0.163	0.353	0.358	1	0.308	0.429	0.425
5	0.179	0.357	0.359	1	0.370	0.420	0.427
5	0.200	0.365	0.360	1	0.400	0.431	0.428
5	0.667	0.372	0.374	1	0.467	0.434	0.430
5	0.963	0.379	0.377	1	0.507	0.424	0.431
4	0.073	0.302	0.305	1	0.833	0.429	0.436
4	0.085	0.306	0.306	1	0.889	0.430	0.436
4	0.086	0.300	0.306	1	0.928	0.430	0.437
4	0.093	0.301	0.306	1	1.743	0.448	0.443

φ^o	D	c_d measured	c_d predicted	φ^o	D	c_d measured	c_d predicted
4	0.125	0.309	0.308	1	7.215	0.650	0.649
4	0.197	0.311	0.312	0	1.643	0.454	0.450
4	0.203	0.310	0.312	0	1.787	0.445	0.452
4	0.215	0.319	0.313	0	1.840	0.449	0.453
4	0.226	0.314	0.313	0	3.116	0.482	0.488
4	0.288	0.318	0.316	0	4.964	0.515	0.514
4	0.303	0.315	0.317				
4	0.306	0.316	0.317				
4	0.459	0.321	0.322				
4	0.609	0.331	0.325				
4	0.707	0.329	0.326				
4	1.440	0.327	0.332				
4	1.510	0.331	0.333				
4	1.640	0.337	0.334				
3	1.030	0.355	0.358				
3	1.088	0.358	0.359				
3	1.152	0.357	0.359				
3	1.682	0.357	0.364				
3	1.726	0.364	0.364				
3	2.930	0.389	0.395				
2	0.138	0.400	0.404				
2	0.493	0.413	0.418				
2	0.517	0.418	0.418				

The correlation coefficient is r^2=0.9968.

The maximum difference between c_d, measured and predicted, is ±2%.

Based on the measured c_d values and a computer program the following equation may be determined (φ in degrees),

$$c_d=a_2+b_2\cdot\varphi+c_2\cdot\varphi^2+d_2\cdot\varphi^3+e_2\cdot\varphi^4+f_2\cdot\varphi^5+g_2\cdot D+h_2\cdot D^2+i_2\cdot D^3+j_2\cdot D^4+k_2\cdot D^5, \quad (6)$$

where a_2, b_2, c_2, d_2, e_2, f_2, g_2, h_2, i_2, j_2, k_2, arithmetic coefficients given in Table 4.

Table 4. Arithmetic Coefficients for eq. (6).

a_2	b_2	c_2	d_2	e_2	f_2	g_2	h_2	i_2	j_2	k_2
0.412176	-0.09631	0.168171	-0.09995	0.021977	-0.00160	0.081869	-0.07922	0.035335	-0.00638	0.000399

Eq. (6) holds for $0^o\leq\varphi\leq6^o$ and $0.07\leq D\leq7.07$ and may apply for any intermediate angle φ and D parameter.

Based on eq. (6) and Table 4, Fig. 3 shows an iso-c_d diagram for $0.30\leq c_d\leq0.62$ with a step of 0.02. When angle φ=const., in general c_d are rapidly increasing with D, while when D=const. c_d are strongly decreasing with increasing angle φ, i.e. c_d is really depending on both φ and D. For $\varphi=0^o$ and increasing D values, c_d varies between ~0.42 and ~0.64.

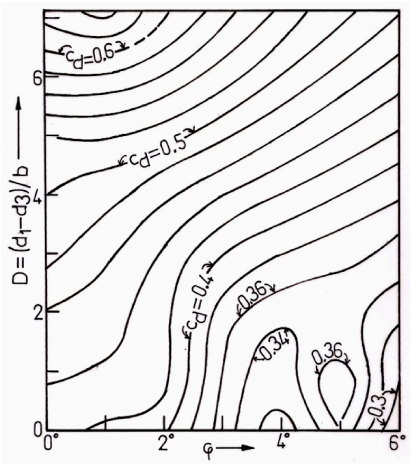

Figure 3. iso-c_d values vs angles φ and $(d_1\text{-}d_3)/b$.

As a short example suppose that: 1) φ=4°=const., b=0.50 m, d_1=1.50 m=const., d_3=1.00 m. Since $(d_1\text{-}d_3)/b$=(1.50-1.00)/0.50=1, c_d≈0.35 (from eq. (6) or Fig. 3) and so q_1=0.35·0.50·[2·9.81·(1.50-1.00)]$^{1/2}$≈0.55 m^2/sec, Fr_3=0.55·9.81$^{-1/2}$·1$^{-3/2}$≈0.175, d_2=0.60·0.50=0.3 m. Then from eq. (5) or Fig. 2, A≈0.187 or [$(d_s/1.00)^2$-1]/[1-(1.00/0.6·0.50)]=0.187, i.e. d_s≈0.75 m and d_3-d_s=0.25 m.

2) If d_3=0.70 m then $(d_1\text{-}d_3)/b$=0.80/0.50=1.6 and from Fig. 3, c_d≈0.34, q_2=0.34·0.50·[2·9.81·(1.50-0.70)]$^{1/2}$≈0.67 m^2/sec>q_1, Fr_3=0.67·9.81$^{-1/2}$·0.70$^{-3/2}$≈0.36, A≈0.49=[$(d_s/0.70)^2$-1]/[1-(0.70/0.30)], d_s≈0.41 m and d_3-d_s=0.29 m. It should be noted that since Fr_3 must be less than one, there is a limit for very small d_3 values, while for the complete free surface profile one can advise Demetriou et. al. (2006).

5 CONCLUSIONS

In this, mainly experimental and also computational study, the various water flow elements of submerged sluice gate (of b aperture) outflows within a sloped (angle φ) open channel are measured, presented and discussed-in a suitable two parametric evaluation. The A parameter (eq. 4), connecting d_s/d_3 and d_3/d_2 (Fig. 1) ratios, is examined as a function of angle φ ($0^o \le \varphi \le 6^o$) and Froude number, Fr_3. In a similar way the discharge coefficient, c_d, is examined as a function of two parameters, angle φ and $(d_1\text{-}d_3)/b$=D ratios. The main conclusions are: (1). A is given by eq. (5) and Table 2, or by Fig. 2 in the form of iso-A curves, as function of φ and Fr_3. (2). When angle φ=const. A are increasing with Fr_3. (3). When Fr_3=const. A are weakly increasing with angle φ. (4). For φ=0° the A predicted value, is very close to A value given by the theory (eq. 3a). (5). c_d is given by eq. (6) and Table 4, or by Fig. 3 in the form of iso-c_d curves, as function of angle φ and D parameter. (6). For φ=const. c_d are increasing with D. (7). When D=const. c_d are decreasing with increasing angles φ. The authors of this study believe that the present results may help the hydraulic engineer when dealing with sluice gate submerged underflows within sloped open channels.

NOTATION

q	discharge per unit channel width
g	gravity acceleration
b	sluice gate aperture
d	water depth
x	longitudinal coordinate
φ	channel slope (degrees)
J_o	channel slope
Fr	Froude number
V	mean water velocity
c_d	discharge coefficient

REFERENCES

Covinda Rao and Rajaratnam N. (1963). The Submerged Hydraulic Jump. J. of the Hydr. Div., ASCE, Vol. 89, No HY1, pp. 139-162.

Chow V. T. (1959). Open Channel hydraulic, Mc-Graw Hill, p. 427.

Demetriou J. (2006). Submerged Inclined Hydraulic Jumps. A Comparison Between Theory and Measurement, 15th Congress of APD-IAHR, IIT Madras, Chennai, INDIA, August 7-10, pp. 3-9.

Demetriou J. (2006). Boundary Shear Force Prediction in Inclined-Submerged Hydraulic Jump. 7th ICCE Int. Congress on Civil Engineering, Tarbiat Modarres Univ., Tehran, IRAN, May 8-10, 8 pages.

Demetriou J. and Retsinis G. (2006). Basic Flow Characteristics of Submerged Jumps Under Sluice Gates. Int. Symp. on Hydraulic Structures, Ciudad Guayana, VENEZUELA, October, 9 pages.

Demetriou J. (2006). The Main Characteristics of the Submerged Hydraulic Jump Within Horizontal Channels, FLOW 2006, Patras, GREECE, 7 pages.

Demetriou J. (2007). Flow Around Sluice Gates in Inclined Channels. 6th National Congress of EEDYP, 14-16 June, Chania, Greece, 7 pages.

Dimitriou D., Demetriou J. and Retsinis E., (2010), An Efficiencies' Comparison Concerning The Energy Losses Between Inclined Submerged And Free Water Outflows Downstream of a Hydropower Plant, IGHEM 2010, The 8th International Conference on Hydraulic Efficiency Measurements, October, Roorkee, INDIA, 8 pages.

Dimitriou D. and Demetriou J. (2010). Energy Loss in Submerged Hydraulic Jump Within Inclined Channel, Int. Conf. on Hydro-Science and Engineering ICHE 2010, IIT Madras, Chennai-INDIA, 2-5 Aug., 9 pages.

Henderson F. M. (1966). Open Channel Flow, McMillan Co., p.208.

Pajer G. (1937). The Flow Characteristics at an Underflow Sluice Gate (in German). Zeitschrift fur Angenwandte Mathematic und Mechanic, Vol. 17, No 5, pp. 259-269.

Retsinis E. (2003). Hydraulic Jumps in Sluice Gates. Dissertation for the partial fulfilment of assessment leading to the title of postgraduate diploma, NTUA, School of Civil Engineering.

Retsinis E. and Demetriou J. (2004). Discharge Coefficient in Inclined and Submerged Sluice Gate Flow, FLOW 2004, Athens, Greece, 8 pages.

Retsinis E. and Demetriou J. (2005). Submerged Hydraulic Jumps in Channels With Small Inclination Angle, 5th Greek Congress on the Integrated Water Management Based on the Runoff Basin, Xanthi, GREECE, April, 4 pages.

3 Stepped Spillways

IWLHS, 20-22/02/2013, Aachen - Bung & Pagliara (eds) - © 2013 Bundesanstalt für Wasserbau ISBN 978-3-939230-04-5

Flat and Pooled Stepped Spillways for Overflow Weirs and Embankments: Cavity Flow Processes, Flow Aeration and Energy Dissipation

P. Guenther, S. Felder & H. Chanson
The University of Queensland, School of Civil Engineering, Brisbane QLD 4072, Australia

ABSTRACT: For overflow weirs and embankments, the stepped chute profile may increase the rate of energy dissipation on the waterway. Herein four different stepped chute configurations were tested with a focus on the cavity flow processes, flow aeration and energy dissipation performances. Detailed flow visualisations and air-water flow measurements were conducted for all configurations. The results highlighted the strong flow aeration. The residual energy was the lowest for the flat stepped weir. The data for the stepped spillway configuration with in-line and staggered configurations of flat and pooled steps showed large differences in terms of residual head in the transverse direction consistent with the three-dimensional flow motion. The in-line and staggered configurations did not provide any advantageous performances in terms of energy dissipation and flow aeration, and they were affected by three-dimensional patterns leading to some flow concentration.

Keywords: Stepped spillways, Weirs, Embankments, Flat steps, Pooled steps, Cavity ejection, Energy dissipation, Flow aeration, Residual head

1 INTRODUCTION

Worldwide the design floods of several reservoirs were re-evaluated and the revised spillway outflow was typically larger than that used in the original design. The occurrence of these larger floods could result in dam overtopping with catastrophic consequences when an insufficient storage or spillway capacity is available. A number of overtopping protection systems were developed for embankments and earthfill dams. These include concrete overtopping protection systems, timber cribs, sheet-piles, riprap and gabions, reinforced earth, minimum energy loss (MEL) weirs, embankment overflow stepped spillways and the precast concrete block protection systems developed by the Russian engineers (ASCE 1994, Chanson 2009a). During the last three decades, a number of embankment dam stepped spillways were built with a range of construction techniques, including gabions, reinforced earth, pre-cast concrete slabs and roller compacted concrete (RCC) (Chanson 1995,2001). The stepped profile is designed to increase the rate of energy dissipation on the chute (Chanson 2001, Ohtsu et al. 2004) and the design engineers must assess accurately the turbulent kinetic energy dissipation above the steps, in particular for large discharges per unit width corresponding to the skimming flow regime. A characteristic feature of skimming flows is the high level of turbulence and free-surface aeration (Rajaratnam 1990, Peyras et al. 1992). The water flows downs the steps as a coherent free-stream skimming over the pseudo-bottom formed by the step edges. In the step cavities, the turbulent recirculation is maintained through the transmission of shear stress from the free-stream. At the free-surface, air is continuously trapped and released, and the resulting two-phase mixture interacts with the flow turbulence yielding some intricate air-water structure associated with complicated energy dissipation mechanisms (Chanson & Toombes 2002, Gonzalez & Chanson 2008).

Although the prediction of the turbulent dissipation constitutes a critical design stage, the present literature is skewed towards steep slopes with flat horizontal steps, typical of modern gravity dams. In the present study, new measurements were conducted in a large facility with a channel slope of 26.6º (2H:1V) and step heights of 0.10 m. Four stepped geometries were tested: flat horizontal steps, pooled

steps, and in-line and staggered configurations of flat and pooled steps. The focus of the present works was on the cavity ejection processes, flow aeration and energy dissipation performances.

2 PHYSICAL MODELLING AND INSTRUMENTATION

2.1 *Presentation*

In free-surface flows, a dimensional analysis gives a series of dimensionless relationships between the two-phase flow properties at a dimensionless location along the chute and the channel characteristics, inflow properties and fluid properties (Chanson & Gonzalez 2005, Felder & Chanson 2009). When the same fluids, air and water, are used in models and prototype, the independent parameters include both Froude and Reynolds numbers, since the Morton number is an invariant (Wood 1991, Chanson 2009b, Pfister & Chanson 2012).

Traditionally, the experiments are conducted based upon an undistorted Froude similitude, but it is nearly impossible to achieve a true dynamic similarity of high-velocity air–water flows in small size laboratory models because of the number of relevant dimensionless parameters. Recent results demonstrated that the physical studies must be conducted in large size facilities operating at large Reynolds numbers to minimise viscous scale effects (Felder & Chanson 2009). Herein the study was performed based upon an undistorted Froude similarity and the experimental flow conditions were selected to achieve large dimensionless discharges corresponding to Reynolds numbers ranging from 1×10^4 to 1×10^6.

2.2 *Experimental flume and instrumentation*

New experiments were performed at the University of Queensland on a large stepped spillway model with a slope of 26.6º (2H:1V). The experimental facility was newly designed. It consisted of a broad-crested weir with upstream rounded corner followed by a 0.52 m wide (W = 0.52 m) stepped chute made of 10 steps (h = 0.10 m, l = 0.2 m). Constant flow rates were supplied by a large upstream intake basin with a size of 2.9 m × 2.2 m and a depth of 1.5 m, and smooth inflows to the test section were delivered through a 4.23:1 smooth convergent.

The air-water flow measurements were conducted with a two-tip phase detection intrusive probe (Ø = 0.25 mm, Δx = 7.2 mm, Δz = 1.5 mm). The probe was excited by an air-bubble detector (Ref. UQ82.518) and sampled at 20 kHz per tip for 45 s. The measurements were performed at all step edges downstream of the inception point of free surface aeration. Herewith the raw data yielded the void fraction C, bubble count rate F, and interfacial velocity V. Further observations were conducted with a HD video camera Sony™ HDR-XR160E (Standard HQ HD quality 25 fps), two dSLR camera Pentax™ K-7 and Canon™ 450D. More details on the experimental facility, instrumentation and experimental data were reported in Felder et al. (2012).

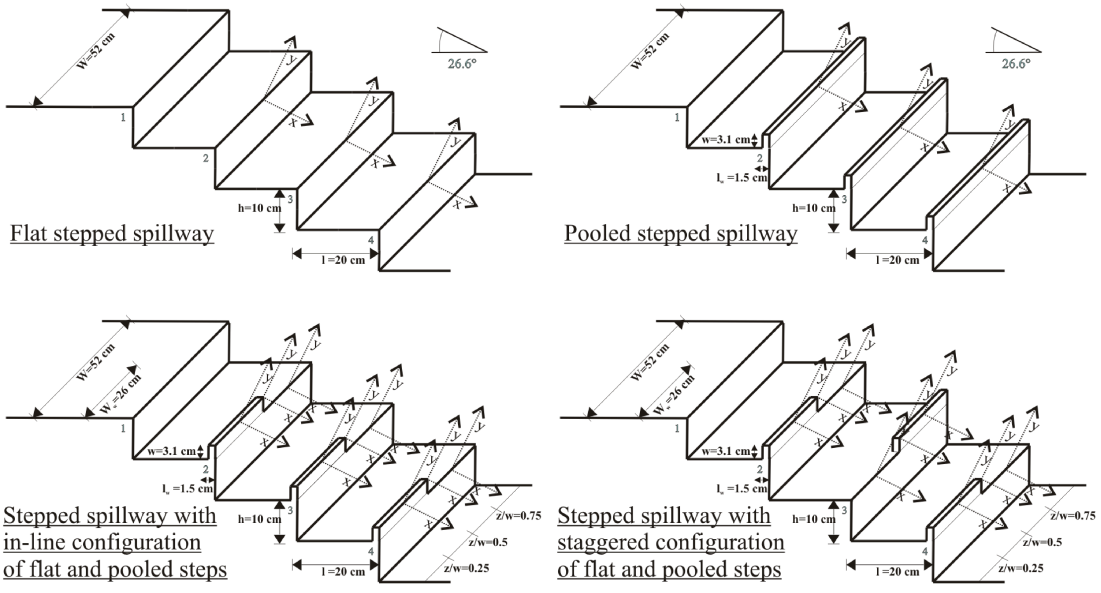

Figure 1. Definition sketch of the stepped configurations

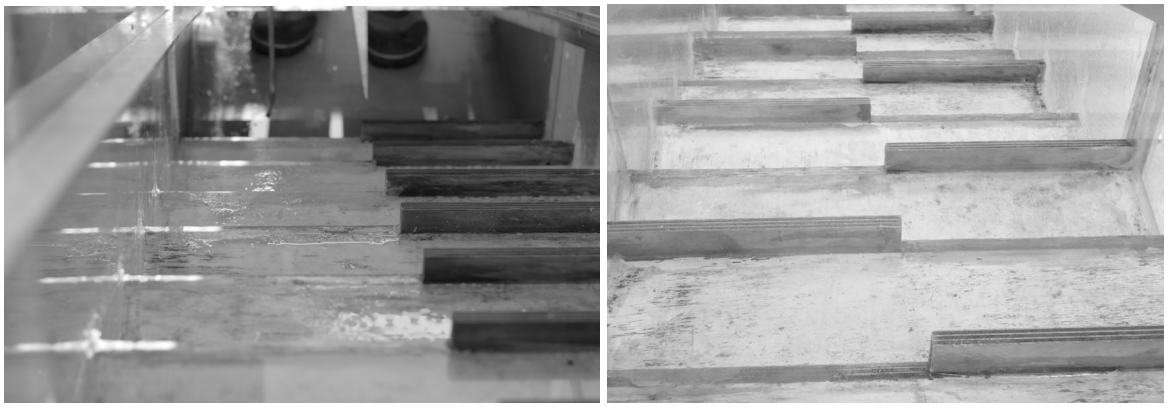

Figure 2. Photographs of the stepped configurations with in-line (Left) and staggered (Right) stepped arrangements - View from upstream looking downstream

2.3 *Experimental investigations*

The experimental study was conducted for four stepped spillway configurations (Fig. 1 & 2). These were a stepped spillway with flat horizontal steps, a pooled stepped spillway with weir height w = 0.031 m, and two stepped spillways with in-line and staggered configurations of flat and pooled steps. The in-line stepped spillway configuration consisted of pooled steps (w = 0.031 m) and flat steps in-line for half the channel width (W_w = W/2 = 0.26 m). The staggered pooled stepped spillway configuration was characterised by alternating flat and pooled steps. On the flat and pooled stepped spillways, the air-water flow measurements were conducted on the channel centreline. For the in-line and staggered configurations, the measurements were performed at three transverse locations: z/W = 0.25, 0.5 (centreline) & 0.75.

The flow patterns were observed for a wide range of discharges $0.002 \leq Q \leq 0.155$ m^3/s. The air-water flow measurements were performed for discharges within $0.013 \leq Q \leq 0.130$ m^3/s corresponding to Reynolds numbers between 1×10^5 to 1×10^6. Most two-phase flow experiments were conducted in the transition and skimming flow regimes.

3 FLOW PATTERNS

The visual investigations of the flow patterns included the observations of the air-water flow patterns for all stepped spillway configurations for a broad range of discharges. For some low discharges, the air-water flows on the pooled stepped spillway exhibited some small instabilities linked with some pulsations for small discharges. The flow processes on the stepped spillways with in-line and staggered configurations of flat and pooled steps showed some three-dimensional air-water flow features including standing sidewall waves and supercritical shockwaves.

The flat stepped spillway showed some typical flow patterns with nappe ($d_c/h < 0.5$), transition ($0.5 < d_c/h < 0.9$) and skimming flow ($d_c/h > 0.9$) regimes depending upon the dimensionless flow rate d_c/h, where d_c is the critical flow depth. Some similar flow regimes were observed on the pooled stepped spillway (Fig. 3), although some pulsating flow was seen for some nappe flow rate. For the smallest flow rates ($d_c/h < 0.45$), a nappe flow regime was observed on the pooled stepped chute and the water discharged in a succession of free falling nappes from one step pool to the following. However, for $0.3 \leq d_c/h \leq 0.45$, a pulsating flow was observed in the first step cavity leading to some small instability of the following free-falling nappes. The pulsations in the first step cavity were periodic and had a frequency of about 1 Hz (1 s period) for $d_c/h = 0.3$. These pulsations were seen about every 5 seconds for $d_c/h = 0.45$. The pulsating mechanism was comparable to the self-induced instabilities on pooled stepped spillways with slopes $\theta = 8.9°$ & 30º (Thorwarth 2008, Felder & Chanson 2012, Takahashi et al. 2008). For intermediate flow rates $0.45 \leq d_c/h \leq 0.97$, a transition flow regime was observed with some strong splashing in the air-water flow region downstream of the inception point of air-entrainment. For larger discharges $d_c/h > 0.97$, a skimming flow regime occurred with some stable recirculation motions in the step cavities (Fig. 3, Right). At the upstream end of the chute, the flow was transparent (clear-waters) and the water surface was parallel to the pseudo-bottom formed by the pool step weirs equivalent to skimming flows on flat stepped spillways. The flow depth however was larger than on flat stepped chutes because of the pool height. Downstream of the inception point of free-surface aeration, the flow was highly aerated.

Figure 3. Skimming flow regime on flat and pooled stepped spillways - Left: flat steps, Q = 0.114 m^3/s, d_c/h = 1.7, Re = 8.8×10^5; Right: pooled steps, Q = 0.100 m^3/s, d_c/h = 1.56, Re = 7.7×10^5

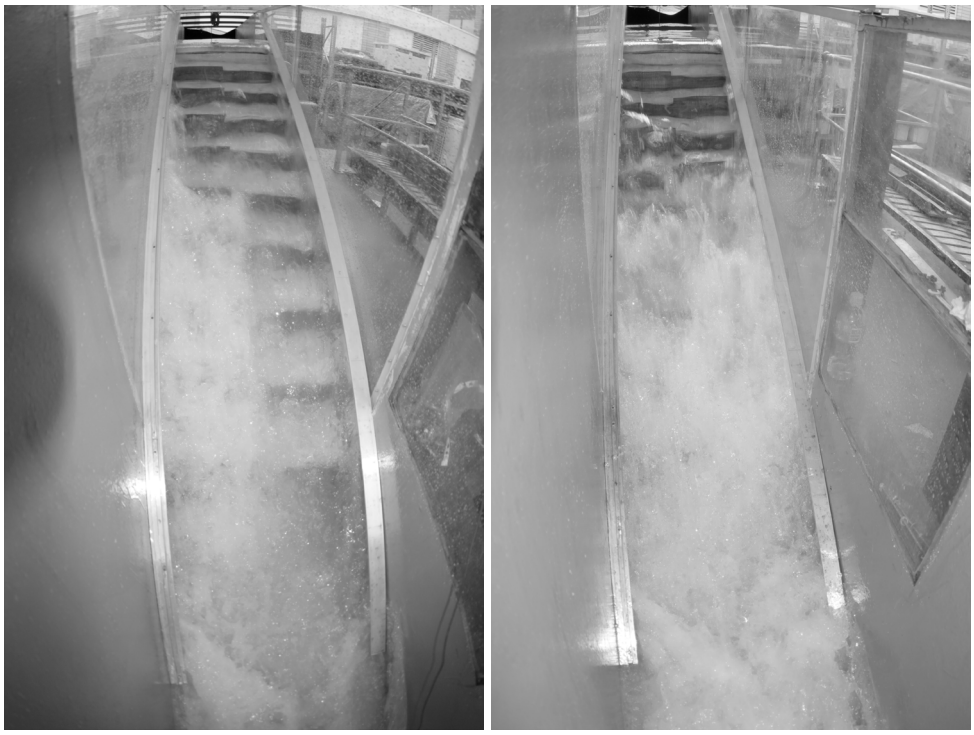

Figure 4. Three-dimensionless flow down the in-line and staggered configurations of flat and pooled steps - Left: in-line configuration, Q = 0.098 m^3/s, d_c/h = 1.54, Re = 7.6×10^5; Right: staggered configuration, Q = 0.090 m^3/s, d_c/h = 1.45, Re = 6.9×10^5

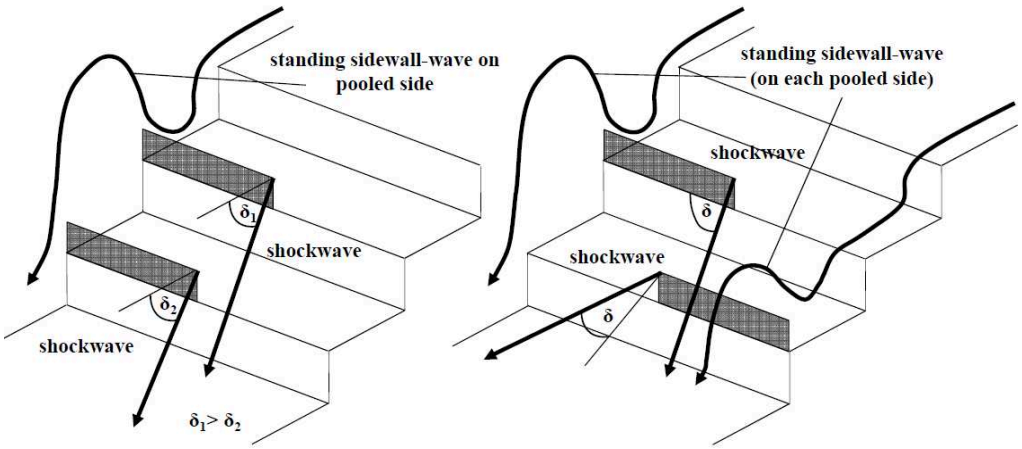

Figure 5. Sketches of sidewall standing waves and shock waves in stepped chutes with inline (Left) and staggered (Right) configurations of flat and pooled steps

On the in-line and staggered configurations of flat and pooled steps, the flow was highly three-dimensional (Fig. 4). Standing sidewall waves and shockwaves were observed along the sidewalls and on channel centreline respectively (Fig. 5), and these instabilities were associated with some strong splashing. On the in-line configuration, the pool weirs induced larger air-water depths at the pooled side of the

channel, and a faster flow motion was observed at the flat stepped side (Fig. 4, Left). The formation of nappe, transition and skimming flows could be determined separately on both sides. For small flow rates ($d_c/h < 0.46$), a nappe flow regime was observed on both sides of the spillway chute with plunging jets from step to step on the flat side and from pool to pool on the pooled side. Some transverse flow motions as well as strong droplet ejections were seen along the entire channel length. With increasing discharges ($0.46 < d_c/h < 0.57$), the flow became more unstable: it was characterised by plunging jets interacting on channel centreline together with a chaotic flow behaviour. The pools induced large flow disturbances and some three-dimensional flow motion was observed. For $0.57 < d_c/h < 0.86$, a transition flow regime was observed on both sides of the channel with some distinct droplet ejection downstream of the inception point of aeration. Some transverse flow interactions took place on channel centreline and yielded some three-dimensional flow motions along the entire channel. An intermediate flow regime ($0.86 < d_c/h < 1.03$) was characterised by a skimming flow regime on the pooled stepped side, and some transition flow on the flat stepped side of the spillway. Generally, the three-dimensional flow motion and flow disturbances caused by the pools became less significant with increasing discharges. For $d_c/h > 1.03$, a skimming flow was observed on both sides of the channel. The skimming flows showed some similarities to those observed on the flat stepped and pooled stepped spillways (Fig. 4, Left). The flow showed comparatively larger droplet ejections and the recirculation processes in the cavities appeared more irregular and disturbed compared to the uniform flat and pooled stepped spillways.

On the staggered stepped configuration, a nappe flow regime was observed at low flow rates ($d_c/h < 0.56$). A wavy flow appearance from side to side was observed along the entire channel length. The jets were highly aerated and showed some distinct plunge heights. For $0.56 < d_c/h < 0.92$, a transition flow occurred along the stepped chute. Some jets plunged over each second adjacent step edge. The step cavities of both flat and pooled steps showed no air pockets. The air-water mixture was highly aerated, showing some pseudo-chaotic pattern and transverse interactions on the channel centreline. The waving appearance of the flow from side to side became less significant than in the nappe flow regime. For $d_c/h > 0.92$, a skimming flow regime was observed (Fig. 4, Right). The recirculation in the step cavities was observed, although the recirculation processes were unsteady and disturbed by the staggered step configuration. The flow appeared highly aerated.

The stepped spillways with in-line and staggered configuration of flat and pooled steps showed some irregular occurrence of standing sidewalls and shockwaves for all flow regimes. The sidewall standing wave lengths and heights were comparable for both in-line and staggered configurations of flat and pooled steps. With increasing discharges, both wave height and length became smaller. The shockwaves occurred predominantly on the spillway centreline and the direction of the shockwaves differed between adjacent steps depending upon the configuration (Fig. 5). Further informations on the flow instabilities were reported by Felder et al. (2012).

4 CAVITY FLOW PROCESSES

On the flat and pooled stepped spillways, the cavity ejections were carefully observed. The recirculation processes were documented for each step cavity at and downstream of the inception point of free surface aeration. The clear-water surface upstream of the inception point appeared two-dimensional and parallel to the pseudo-bottom formed by the step edges and pooled weir edges respectively. Close to the inception point, the surface showed an irregular flapping mechanism which led to some waving behaviour. The surface tended to lean inward the cavity at irregular intervals and caused an air packet entrapment which was advected in the form of smaller and uniform shaped bubbles within the step cavities (Fig. 6, Left). This pattern was consistent with previous observations on stepped spillways (Chamani 2000, Chanson 2001, Toombes & Chanson 2007). With increasing discharge, the flapping mechanism of the free-surface became less distinct. Visually the flow resistance caused by the next downstream step, or pool edge, yielded some ejection processes close to the respective step or pool edge. Figure 6 illustrates the flapping mechanism and the cavity ejection processes on the flat and pooled stepped spillways. The cavity ejection processes were similar in appearance for the flat and pooled steps.

Basically the cavity recirculation observations highlighted some distinct ejection processes with inward and outward cavity flow motion. These occurred at irregular time intervals and led to some additional air entrainment. The ejections appeared to be sequential from upstream to downstream as illustrated by Djenidi et al. (1999) and Chanson et al. (2002). On average, the data indicated a slight increase in cavity ejection rate with increasing downstream distance for a given flow rate (Fig. 7, Left). The results are summarised in Figure 7 (Right) showing the median cavity ejection frequency as a function of the Rey-

nolds number. Indeed the ejection processes took place in regions of high shear stress where the Reynolds number was closely linked to turbulence properties.

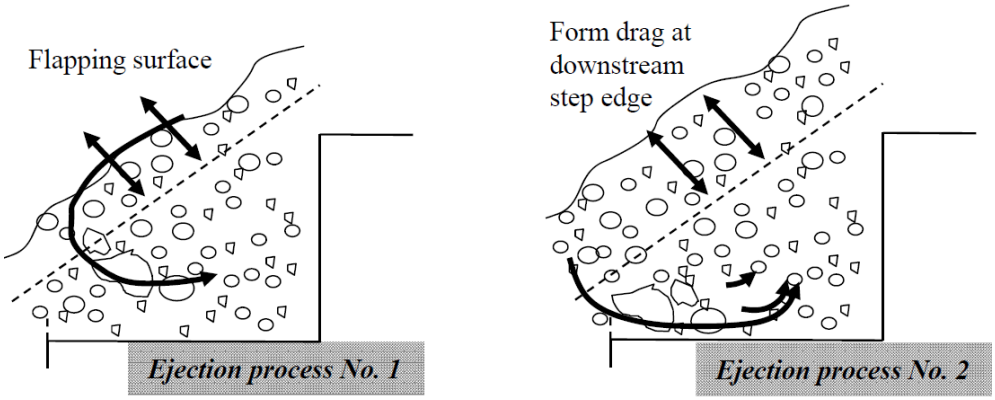

Figure 6. Sketch of cavity ejection processes on flat and pooled stepped spillways (θ = 26.6°)

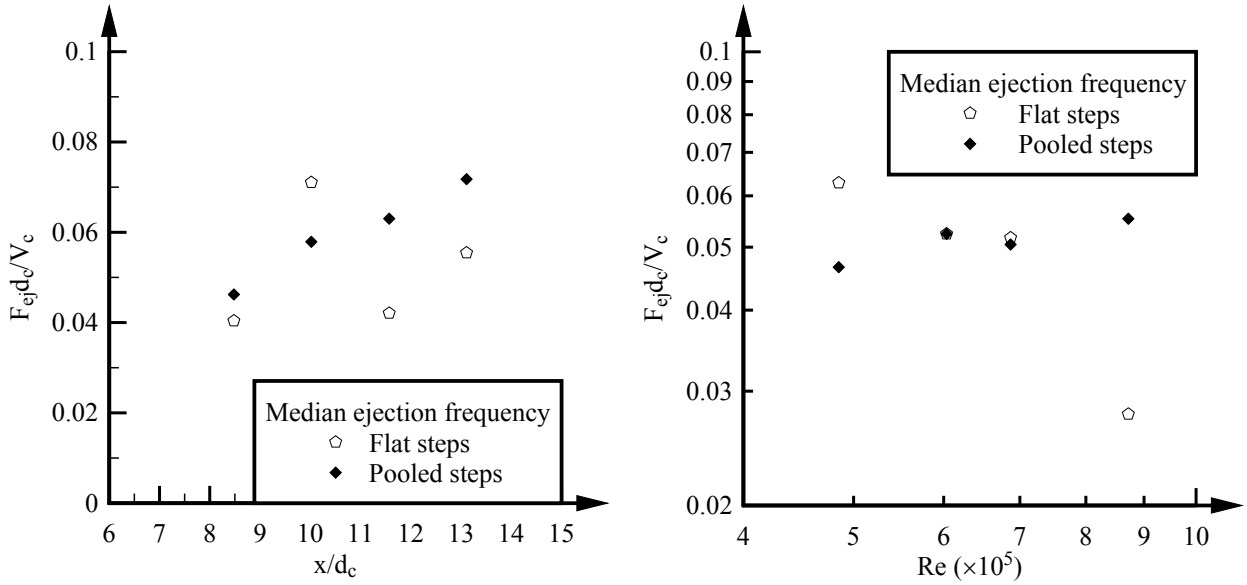

Figure 7. Dimensionless cavity ejection frequency $F_{ej}d_c/V_c$ on flat and pooled stepped spillways (θ = 26.6°) - Left: Longitudinal distribution in skimming flow (d_c/h = 1.45, Re=6.9×10^5); Right: median ejection frequency as a function of Reynolds number

The cavity ejection process in a skimming flow on stepped spillway may be analysed in term of energy considerations, assuming that all the energy losses took place by viscous dissipation in the cavity, with some energy exchange between the main stream and the recirculation by irregular fluid ejection. The results yielded an expression of the averaged ejection frequency F_{ej} as a function of the Darcy-Weisbach friction factor f_e:

$$\frac{F_{ej}\times(h\times\cos\theta)}{U_w}\approx\frac{f_e}{2\times\lambda\times\eta} \qquad (1)$$

where U_w = flow velocity, h = vertical step height, θ = angle between the pseudo-bottom formed by the step edges and the horizontal, λ = ratio of average fluid ejection volume to total cavity volume, and η = ratio of average ejection period to burst duration. Equation (1) was developed for a wide chute with flat horizontal steps assuming a gradually-varied flow motion close to uniform equilibrium. The reasoning may be extended to a pooled stepped chute:

$$\frac{F_{ej}\times(h\times\cos\theta)}{U_w}\approx\frac{f_e}{2\times\lambda\times\eta\times\left(1+2\times\frac{w}{h}\right)} \qquad (2)$$

where w = vertical pool height. Equation (2) is valid for a wide chute with horizontal steps and vertical pool walls.

Herein the average ejection period to burst duration was on average $\eta \approx 3.5$. While the video analyses did not provide accurate information about the average fluid ejection volume ratio, the combination of flow resistance data and the above equations (1) and (2) would yield meaningless values of λ (i.e. $\lambda > 1$). The result might suggest the over-simplification of Equations (1) and (2) to assume that "all the energy losses took place by viscous dissipation in the cavity".

5 AIR-WATER FLOW PROPERTIES

Detailed air-water flow measurements were performed for all four configurations. Overall the results highlighted the intense flow aeration. Downstream of the inception of free-surface aeration, the entire water column including the step cavities were aerated (Fig. 8). Figure 8 shows some dimensionless distributions of void fraction for all four stepped configurations. In Figure 8, y is the distance normal to the pseudo-bottom formed by the step edges with y = 0 at the step edges for flat steps and y = 0 at the weir edge for the pooled steps. The skimming flow data compared favourably with an analytical solution of the air bubble diffusion equation:

$$C = 1 - \tanh^2\left(K' - \frac{y/Y_{90}}{2 \times D_o} + \frac{(y/Y_{90} - 1/3)^3}{3 \times D_o}\right) \qquad (3)$$

where Y_{90} = characteristic distance where C = 0.90, and K', D_o = dimensionless functions of the depth-averaged void fraction C_{mean} (Chanson and Toombes 2002). Equation (3) is compared with experimental data in Figure 8.

Overall the void fraction data showed close results between flat and pooled steps within the main stream (Fig. 8, Top left). In skimming flows, the depth-averaged void fraction ranged between 0.3 and 0.35 for both geometries. On the in-line configuration of flat and pooled steps, the measurements showed some transverse differences (Fig. 8, Top right). The flow was significantly more aerated on the pooled side (z/W = 0.25) as illustrated by the photographs (Fig. 4 Left). On the staggered configuration of flat and pooled steps, the void fraction distributions were more uniformly distributed across the channel width, although the alternation of flat and pooled steps every second step edge induced locally some three-dimensional flow motion.

The interfacial velocity distributions (data not shown) exhibited a self-similar profile on both flat and pooled stepped spillways:

$$\frac{V}{V_{90}} = \left(\frac{y}{Y_{90}}\right)^{1/N} \qquad y/Y_{90} < 1 \text{ (4a)}$$

$$\frac{V}{V_{90}} = 1 \qquad y/Y_{90} > 1 \text{ (4b)}$$

with V_{90} = characteristic velocity at $y = Y_{90}$. The exact value of N varied slightly from one step to the next step for a given flow rate with a typical value N = 10, while Kökpinar (2004) observed N = 6 on flat and pooled stepped chutes ($\theta = 30°$).

On the in-line and staggered configurations of flat and pooled steps, the velocity distributions followed closely Equation (4a) for $y/Y_{90} < 1$ at all transverse locations, but velocity data in the spray region incl. $y/Y_{90} > 1$ were scattered. On the in-line configuration, the interfacial velocities were consistently larger on the flat stepped side than on the pooled stepped side of the chute. Some transverse flow motion was observed along the channel centreline with the staggered configuration of flat and pooled steps, leading to an alternation of transverse flow direction between each step.

6 ENERGY DISSIPATION

The rate of energy dissipation above the stepped chute and the residual energy at the downstream end of the stepped spillway are two key design parameters, especially for low-head weirs. In this study, the rate of energy dissipation and the residual energy were estimated for all stepped spillway configurations based upon the detailed air-water flow measurements. The residual head was estimated as:

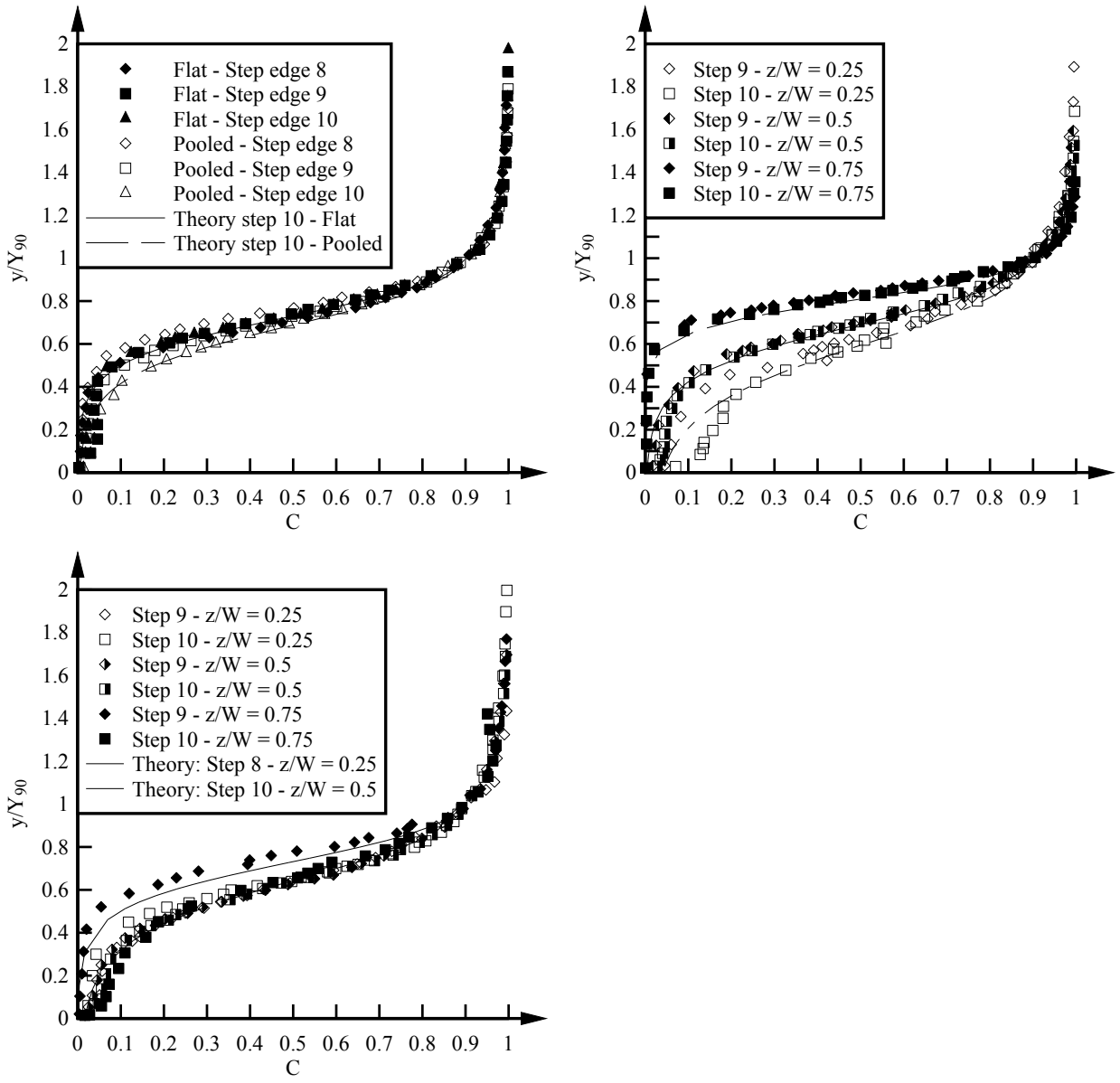

Figure 8. Dimensionless distributions of void fractions in skimming flows - Top left: flat and pooled steps, Q = 0.097 m^3/s, d_c/h = 1.52, Re = 7.4×10^5; Top right: in-line configuration, Q = 0.090 m^3/s, d_c/h = 1.45, Re = 6.9×10^5; Bottom: staggered configuration, Q = 0.113 m^3/s, d_c/h = 1.70, Re = 8.7×10^5

$$H_{res} = d\times\cos\theta + \frac{U_w{}^2}{2\times g} + w = \int_0^{Y_{90}} (1-C)\times\cos\theta\times dy + \frac{q^2}{2\times g\times\left(\int_0^{Y_{90}} (1-C)\times dy\right)^2} + w \quad (5)$$

where d = equivalent clear water depth, q = water discharge per unit width, U_w = flow velocity (U_w = q/d) and w = pool height (w = 0 for flat steps). On the in-line and staggered configurations of flat and pooled steps, the residual head was averaged in the transverse direction (Felder et al. 2012).

For the 10-steps chute, the rate of energy dissipation ranged from 45% to 90%, with decreasing rate of energy dissipation with increasing flow rate as previously observed by Chanson (1994) and Peruginelli and Pagliara (2000). For the design engineers, however, the dimensionless residual head H_{res}/d_c is a more pertinent design parameter. Present results implied that the dimensionless residual head was about $2.5 \leq H_{res}/d_c \leq 5$ (Fig. 9). In Figure 9, the dimensionless residual head is shown as a function of the dimensionless discharge d_c/h. The present data showed the smallest residual head for the flat stepped spillway: i.e., $H_{res}/d_c \approx 3.1$ on average in skimming flow. The residual head was larger on the pooled stepped spillway: i.e., $H_{res}/d_c \approx 3.7$. For the stepped spillways with in-line and staggered configurations of flat and pooled steps, larger residual head data were obtained, with some data scatter.

The data for the in-line and staggered configurations of flat and pooled steps must be considered with care. The results shown in Figure 9 were transverse averaged. Locally the residual head could be signifi-

cantly larger because of the three-dimensional flow motion. For example, on the in-line geometry, the dimensionless residual head H_{res}/d_c ranged from less than 2 to up to 17 locally, depending upon the transverse location and flow rate, while H_{res}/d_c varied within a factor 2 across the last step for a given flow rate on the staggered geometry.

Overall the present data ($\theta = 26.6°$) showed a larger rate of energy dissipation on the spillway with flat horizontal steps compared to all the other configurations in the skimming flow regime. The result was consistent with physical data down a 30° stepped chute (Kökpinar 2004), despite some quantitative difference in residual head levels with the present data (Fig. 9). The finding is contrary to observations on smaller slopes on which the largest rate of energy dissipation was observed with the pooled stepped design (Thorwarth 2008). Herein the designs with in-line and staggered configurations of flat and pooled steps did not provide any advantageous performances in terms of energy dissipation, while they were affected by flow instabilities and three-dimensional patterns leading to some flow concentration.

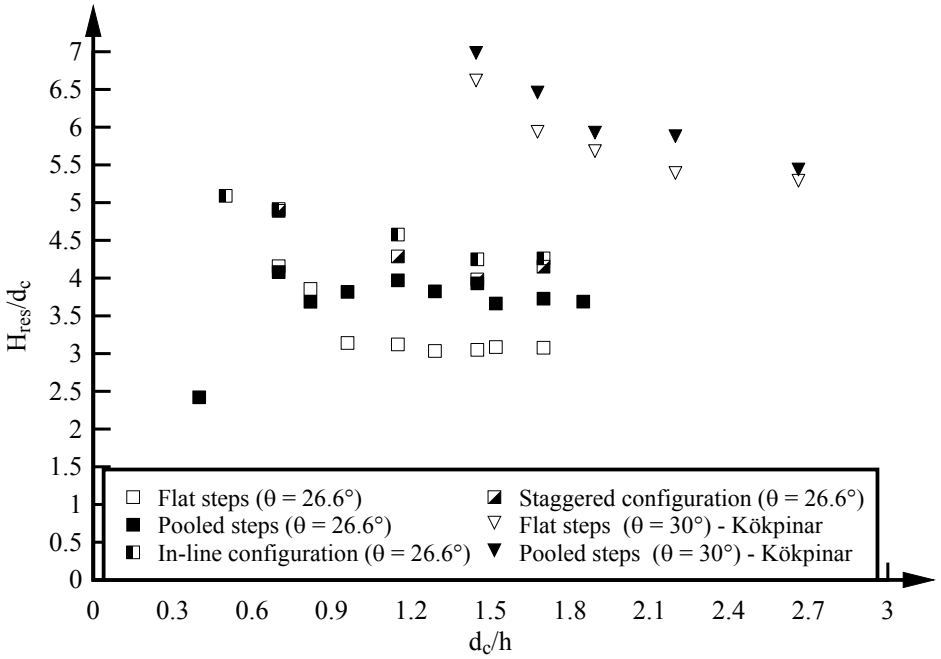

Figure 9. Dimensionless residual head at the downstream end of 10-steps stepped spillways - Comparison between flat stepped chute, pooled step chute, and in-line and staggered configurations of flat and pooled steps (Present study), as well as with the re-analysed data of Kökpinar (2004) - All data were estimated based upon detailed air-water flow measurements

7 CONCLUSION

A physical study was performed on flat and pooled stepped spillways for overflow weirs and embankments ($\theta = 26.6°$). While different stepped chute configurations were tested, the focus of the study was on the cavity flow processes, flow aeration and energy dissipation performances.

The flat stepped spillway showed some typical flow patterns with nappe, transition and skimming flow regimes depending upon the flow rate. Some similar flow regimes were observed on the pooled stepped spillway, although some pulsating flow was seen for some nappe flow rates associated with the downstream propagation of small instabilities. On the in-line and staggered configurations of flat and pooled steps, the flow was highly three-dimensional. Standing sidewall waves and shockwaves were observed along the sidewalls and on channel centreline respectively. These instabilities were instationary and associated with some strong splashing. Detailed air-water flow measurements were conducted downstream of the inception point of free-surface aeration for all configurations. The results highlighted the strong flow aeration. The residual head and energy dissipation rates at the stepped chute downstream end were calculated based upon the air-water flow properties. The results showed that the residual energy was the lowest for the flat stepped weir. The data for the stepped spillway configuration with in-line and staggered configurations of flat and pooled steps showed large differences in terms of residual head in the transverse direction. Altogether the present study demonstrated that, on a 26.6° slope stepped chute, the designs with in-line and staggered configurations of flat and pooled steps did not provide any advantageous performances in terms of energy dissipation and flow aeration, but they were affected by three-dimensional pat-

terns leading to some flow concentration. Another outcome is that some detailed physical investigations for complex stepped spillway designs are strongly recommended before any implementation into a prototype environment.

8 ACKNOWLEDGEMENTS

The authors thank Jason Van Der Gevel and Stewart Matthews (The University of Queensland) for their technical assistance. The financial support of the Australian Research Council (Grant DP120100481) is acknowledged.

REFERENCES

ASCE (1994). Alternatives for Overtopping Protection of Dams. ASCE, New York, USA, Task Committee on Overtopping Protection, 139 pages.

Chamani, M.R. (2000). Air Inception in Skimming Flow Regime over Stepped Spillways. proc. Intl Workshop on Hydraulics of Stepped Spillways, Zürich, Switzerland, Balkema Publ., pp. 61-67.

Chanson, H. (1994). Comparison of Energy Dissipation between Nappe and Skimming Flow Regimes on Stepped Chutes. Journal of Hydraulic Research, IAHR, Vol. 32, No. 2, pp. 213-218. Errata: Vol. 33, No. 1, p. 113.

Chanson, H. (1995). Hydraulic Design of Stepped Cascades, Channels, Weirs and Spillways. Pergamon, Oxford, UK, Jan., 292 pages.

Chanson, H. (2001). The Hydraulics of Stepped Chutes and Spillways. Balkema, Lisse, The Netherlands, 384 pages.

Chanson, H. (2009a). Embankment Overtopping Protections System and Earth Dam Spillways. in Dams: Impact, Stability and Design, Nova Science Publishers, Hauppauge NY, USA, Ed. W.P. HAYES and M.C. BARNES, Chapter 4, pp. 101-132.

Chanson, H. (2009). Turbulent Air-water Flows in Hydraulic Structures: Dynamic Similarity and Scale Effects. Environmental Fluid Mechanics, Vol. 9, No. 2, pp. 125-142 (DOI: 10.1007/s10652-008-9078-3).

Chanson, H., and Gonzalez, C.A. (2005). Physical Modelling and Scale Effects of Air-Water Flows on Stepped Spillways. Journal of Zhejiang University SCIENCE, Vol. 6A, No. 3, March, pp. 243-250.

Chanson, H., and Toombes, L. (2002). Air-Water Flows down Stepped chutes: Turbulence and Flow Structure Observations. Intl Jl of Multiphase Flow, Vol. 27, No. 11, pp. 1737-1761.

Chanson, H., Yasuda, Y., and Ohtsu, I. (2002). Flow Resistance in Skimming Flows and its Modelling. Can. Jl of Civil Engineering, Vol. 29, No. 6, pp. 809-819.

Djenidi, L., Elavarasan, R. and Antonia, R.A. (1999). The Turbulent Boundary Layer over Transverse Square Cavities. Jl of Fluid Mechanics, Vol. 395, pp. 271-294.

Felder, S., and Chanson, H. (2009). Turbulence, Dynamic Similarity and Scale Effects in High-Velocity Free-Surface Flows above a Stepped Chute. Experiments in Fluids, Vol. 47, No. 1, pp. 1-18 (DOI: 10.1007/s00348-009-0628-3).

Felder, S., and Chanson, H. (2012). Air-Water Flow Measurements in Instationary Free-Surface Flows: a Triple Decomposition Technique. Hydraulic Model Report No. CH85/12, School of Civil Engineering, The University of Queensland, Brisbane, Australia, 161 pages.

Felder, S., Guenther, P., and Chanson, H. (2012). Air-Water Flow Properties and Energy Dissipation on Stepped Spillways: a Physical Study of Several Pooled Stepped Configurations. Hydraulic Model Report No. CH87/12, School of Civil Engineering, The University of Queensland, Brisbane, Australia, 225 pages.

Gonzalez, C.A., and Chanson, H. (2008). Turbulence and Cavity Recirculation in Air-Water Skimming Flows on a Stepped Spillway. Jl of Hydraulic Research, IAHR, Vol. 46, No. 1, pp. 65-72.

Kökpinar, M.A. (2004). Flow over a Stepped Chute with and without Macro-Roughness Elements. Can. Jl of Civil Eng., Vol.. 31, No. 5, pp. 880-891.

Ohtsu, I., Yasuda, Y., and Takahashi, M. (2004). Flow Characteristics of Skimming Flows in Stepped Channels. Jl of Hyd. Engrg., ASCE, Vol. 130, No. 9, pp. 860-869.

Peruginelli, A., and Pagliara, S. (2000). Energy Dissipation Comparison among Stepped Channel, Drop and Ramp Structures. Proc. Intl Workshop on Hydraulics of Stepped Spillways, Zürich, Switzerland, Balkema Publ., pp. 111-118.

Peyras, L., Royet, P., and Degoutte, G. (1992). Flow and Energy Dissipation over Stepped Gabion Weirs. Jl of Hyd. Engrg., ASCE, Vol. 118, No. 5, pp. 707-717.

Pfister, M., and Chanson, H. (2012). Scale Effects in Physical Hydraulic Engineering Models. Journal of Hydraulic Research, IAHR, Vol. 50, No. 2, pp. 244-246.

Rajaratnam, N. (1990). Skimming Flow in Stepped Spillways. Jl of Hyd. Engrg., ASCE, Vol. 116, No. 4, pp. 587-591.

Takahashi, M., Yasuda, Y., and Ohtsu, I. (2008). Flow Patterns and Energy Dissipation over Various Stepped Chutes. Discussion. Jl of Irrigation and Drainage Engineering, ASCE, Vol. 134, No. 1, pp. 114-116.

Thorwarth, J. (2008). Hydraulisches Verhalten der Treppengerinne mit eingetieften Stufen – Selbstinduzierte Abflussinstationaritäten und Energiedissipation. (Hydraulics of Pooled Stepped Spillways – Self-induced Unsteady Flow and Energy Dissipation.) Ph.D. thesis, University of Aachen, Germany (in German).

Toombes, L., and Chanson, H. (2007). Surface Waves and Roughness in Self-Aerated Supercritical Flow. Environmental Fluid Mechanics, Vol. 7, No. 3, pp. 259-270 (DOI 10.1007/s10652-007-9022-y).

Wood, I.R. (1991). Air Entrainment in Free-Surface Flows. IAHR Hydraulic Structures Design Manual No. 4, Hydraulic Design Considerations, Balkema Publ., Rotterdam, The Netherlands, 149 pages.

IWLHS, 20-22/02/2013, Aachen - Bung & Pagliara (eds) - © 2013 Bundesanstalt für Wasserbau ISBN 978-3-939230-04-5

Air Entrainment and Energy Dissipation on Porous Pooled Stepped Spillways

S. Felder & H. Chanson
The University of Queensland, School of Civil Engineering, Brisbane QLD 4072, Australia

ABSTRACT: The hydraulics of stepped spillways with flat steps is well documented and some design guidelines exist for typical embankment dam slopes. On the other hand, alternative stepped designs are poorly understood. In the present study, some porous pooled stepped spillways were investigated with two different porosities of the pooled weir. The air-water flow patterns, air-water flow properties and the energy dissipation rate were observed and compared to the corresponding flat and pooled stepped spillways. The comparative study highlighted a larger interfacial velocity for the pooled step configurations. The largest residual energy at the downstream end was observed for the porous pooled steps which was associated with reduced cavity recirculation and form drag. Overall the porous pooled stepped design exhibited some more stable flow patterns than the pooled stepped design, but it was characterised by a lesser rate of energy dissipation than the flat step design for the investigated slope ($\theta = 26.6°$).

Keywords: Stepped spillways, Porous pooled steps, Pooled steps, Flow aeration, Energy dissipation, Flow resistance, Drag reduction

1 INTRODUCTION

Stepped spillways are an advantageous design for flood release facilities on embankment dam stepped spillways and low head hydraulic structures. The steps act as large rough elements increasing the air entrainment and energy dissipation performances compared to smooth chutes (Chanson 2001). The stepped spillway design is compatible with modern construction techniques including roller compacted concrete (RCC) and gabions. Further its selection reduces the cavitation risk and no damage has been reported. The stepped spillway design is often designed for skimming flows, and the aeration and energy dissipation performances are well documented for flat uniform stepped spillways with embankment dam slopes (Chanson 2001, Ohtsu et al. 2004, Gonzalez & Chanson 2007, Felder & Chanson 2009, Bung 2011).

The stepped spillway design is not limited to flat uniform steps and some prototype stepped chutes were designed with non-uniform steps (e.g. Tillot dam, France), downwards inclined steps (e.g. Brushes Clough Dam, UK), changing channel slope (e.g. New Victoria dam, Australia), pooled steps (e.g. Sorpe dam, Germany) and weir structures designed with gabion steps. An optimum design in terms of energy dissipation and air entrainment might not be known yet. Some studies provided some insights into some more complex dam designs (e.g. Gonzalez & Chanson 2008, Relvas & Pinheiro 2008, Felder & Chanson 2011). Peyras et al. (1992) studied the energy dissipation over gabion stepped weirs. In recent years, the air-water flows on pooled stepped spillways were researched with channel slopes of 14.6°, 18.6° and 30° (André 2004, Kökpinar 2004, Thorwarth & Köngeter 2006). Some self-induced instabilities on a pooled stepped spillway with $\theta = 8.9°$ were investigated in detail by Thorwarth (2008) and Felder & Chanson (2012). The instabilities comprised jump waves which traveled downstream and might cause a risk for safe discharge of the stepped chute.

In the present study, some further pooled step designs were tested for a stepped spillway with $\theta = 26.6°$ comprising flat, pooled and porous pooled stepped configurations with porosities $Po = 5\%$ and $Po = 31\%$. The investigations aimed to provide some insights on the flow patterns, as well as the aeration and energy dissipation performances for the (porous) pooled step designs.

2 EXPERIMENTAL CONFIGURATIONS AND INSTRUMENTATION

2.1 *Experimental facility and phase detection intrusive probes*

The experimental study was conducted in a large size stepped spillway facility with a 7 m long, 0.52 m wide test section with a slope of 26.6°. The channel consisted of 10 plywood steps with step height h = 10 cm and perspex sidewalls for flow visualization. Constant flow rates were supplied by a large upstream intake basin which supplied smooth waveless inflow into the test section through a long sidewall convergent with a 4.23:1 contraction ratio. At the upstream end of the test section, the flow was controlled by a broad-crested weir with height of 1 m, width W = 0.52 m and length L_{crest} = 1.01 m and an upstream rounded corner (r_{crest} = 0.08 m).

The air-water flow experiments were conducted with a double-tip conductivity probe (inner diameter $Ø$ = 0.25 mm). The leading and trailing tips of the probe were offset in longitudinal direction Δx = 7.2 mm with a transverse separation of Δz = 2.1 mm. The probe was supported by a trolley system and the positioning of the probes normal to the pseudo-bottom was performed with a Mitutoyo™ digital ruler mounted on a fine adjustment screw-drive mechanism. The error in the translation of the probe in the direction normal to the flow was less than 0.5 mm. The accuracy on the longitudinal probe position was estimated as Δx < +/- 0.5 cm. All measurements were conducted with an electronic system (Ref. UQ82.518) and the signal was acquired with a high speed data acquisition system (NI USB-6251) and a self-designed LabVIEW^{TM} data acquisition software. In a detailed sensitivity analysis, a sampling duration of 45 s and a sampling rate of 20 kHz were identified as optimum for the accurate recording of the air-water flow properties. More details about the stepped spillway facility were reported by Felder et al. (2012).

2.2 *Experimental configurations*

The experiments encompassed four uniform stepped spillway configurations, i.e. flat steps, pooled steps and porous pooled steps with Po = 5% and Po = 31% (Figure 1). The pool weir height for all pooled configurations was w = 3.1 cm. The pores on the porous pooled steps had a diameter $Ø$ = 5 mm and were distributed evenly on the pooled weir (Figure 2). Detailed visual observations of the flow patterns were conducted for all step configurations for a range of discharges per unit widths $0.003 \leq q_w \leq 0.282$ m^2/s. Some air-water flow measurements were performed with the double-tip conductivity probe downstream of the inception point of air entrainment for $0.025 \leq q_w \leq 0.250$ m^2/s. The main focus of the investigations was the porous pooled design and the flat and pooled step designs were used as reference configurations.

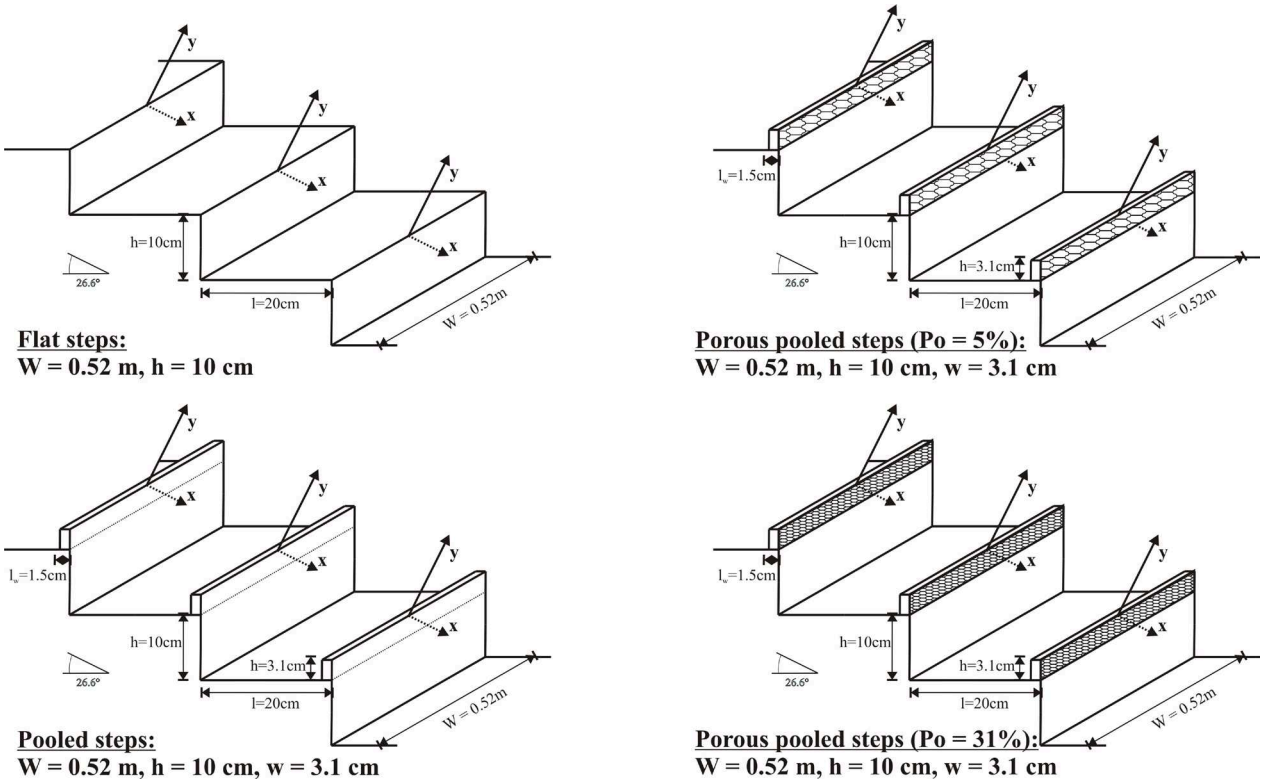

Figure 1. Detail of stepped spillway configurations with flat, pooled and porous pooled steps (θ = 26.6°); definition of first measurement position on flat and (porous) pooled steps (y = 0)

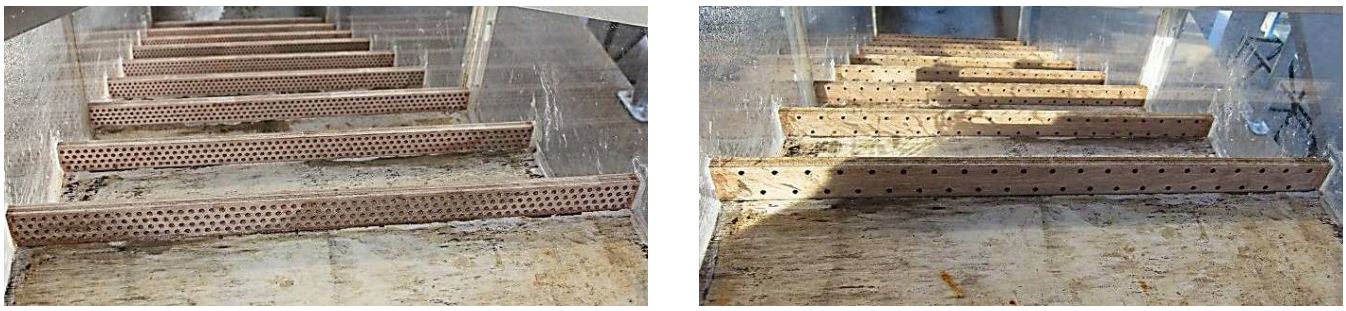

Figure 2. Photos of porous pooled stepped spillways with *Po* = 31% (Left) and *Po* = 5% (Right); Diameter of holes *Ø* = 5 mm

3 AIR-WATER FLOW PATTERNS

The air-water flow patterns on the flat and pooled stepped spillways exhibited some typical features with nappe, transition and skimming flow regimes clearly distinguishable with increasing discharge. The changes in flow regimes were in good agreement and compared well with previous studies on embankment dams (Felder & Chanson 2009). For the pooled stepped spillway, some small instabilities were observed within the nappe flow regime for dimensionless flow rates $0.3 < d_c/h < 0.45$ with d_c the critical flow depth. The instabilities resulted from a pulsating flow within the first step cavity which caused some small deviations of the free-falling nappes. The flow disturbances were much smaller compared to the observations of Thorwarth (2008) and Felder & Chanson (2012) on a pooled stepped spillway with $\theta = 8.9°$ and same ratio of pool weir height to step length ($w/l = 0.155$). For $d_c/h \geq 0.45$, no instabilities were observed. Some more details about the instabilities and the flow patterns on the flat and pooled stepped spillways can be found in Felder et al. (2012). The change from transition to skimming flow was observed for $d_c/h = 0.9$ on the pooled stepped spillway and for $d_c/h = 0.97$ on the flat steps.

The air-water flow patterns on the porous pooled stepped spillways with *Po* = 5% and *Po* = 31% respectively exhibited typical nappe, transition and skimming flow regimes. The observations were in good agreement with the observations on the pooled stepped spillway, but for all flow rates, some differences were caused by some small discharges through the pores in the pooled weirs. Some estimates of the discharge through the pores were conducted for the different flow rates using classical resistance coefficients (Idelchik 1994). The discharge through the pores was estimated based upon the energy equation between either sides of the porous pooled wall:

$$\Delta H = \frac{\zeta \times U_{Po}^{\ 2}}{2 \times g} \qquad (1)$$

where ΔH is the energy difference between the two sides of the porous wall (herein the difference in free-surface elevation between one pool weir height upstream and downstream of the pool wall, identified using visual observations), ζ is the resistance coefficient for an perforated thick plate (Idelchik 1994), g is the gravity acceleration constant and U_{Po} is the stream wise velocity of the discharge through the pores. The maximum discharges through the pores based upon stationary flow considerations were estimated at less than 7% of the total flow discharge for the porous configuration *Po* = 31% and much less than 1% for *Po* = 5%. The discharges for the transition and nappe flows were comparatively larger because the downstream side of the pooled weir was not submerged and a void existed. Note that the discharge calculation through the pores was a rough estimate and the recirculations within the cavity, the irregular cavity ejections, and the non-horizontal angle between flow and pool weir might affect the porous flow estimate.

For the smallest flow rates $d_c/h < 0.43$-0.46, a nappe flow regime was observed for both porous pooled configurations. The flow pattern was similar to the nappe flows on the pooled stepped spillway, but some flow occured also through the pores. Importantly, for the nappe flow regime on both porous pooled stepped spillways, no pulsations were observed in the first pooled cavity and no instabilities were present. The pores tended to balance the pressure between adjacent pooled cavities and increased the stability of the nappe flows. The transition flow regime showed some instable flow patterns which were similar to observations of transition flows on the flat and pooled stepped spillways (Figure 3). In Figure 3, a typical transition flow regime is shown for the porous steps with *Po* = 5% indicating a small air-water flow jet at the second pooled weir edge and some small instabilities and strong droplet splashing downstream. With increasing discharge, the instabilities decreased. With the disappearance of the jet at the second pooled step weir, the flow became stable in the skimming flow regime. The transition flow regime for the porous

pooled stepped spillway with Po = 31% was observed for 0.43 < d_c/h < 0.75 and for Po = 5% for 0.46 < d_c/h < 0.91. The larger porosity reduced the instable transition flow rates and provided more stable skimming flow conditions compared to the flat and pooled step configurations. The skimming flow regime was observed for d_c/h > 0.75 (Po = 31%) and d_c/h > 0.91 (Po = 5%) respectively. The flow patterns were very similar to typical skimming flows on the corresponding flat and pooled stepped spillways (Figure 4). The flow appeared very regular and some stable cavity recirculations were observed downstream of the inception point. Figure 4 highlights some details of the cavity processes and the air-water flows through the pores. It seemed that the cavity recirculations decreased with increasing porosity. Furthermore, the amount of air in the cavity appeared smaller for the porous pooled steps which indicated a smaller interaction between cavity and main stream flow and a lower air entrainment into the step niche. The flow through the pores decreased the size of the upward jet at the downstream end of the cavity compared to the pooled steps. The visual observations indicated that the pores affected the air-water cavity flows, but the overlying main stream flow patterns were very close to the corresponding flows on the flat and pooled stepped spillways.

The visual observations indicated that the air-water flows in the step cavity were affected by the pore discharges. Some similarities were observed to flows behind porous fences which lead to a reduced recirculation behind the fence with increasing fence porosity (Tsuhahara et al. 2012). It is believed, that the injection of fluid into the cavity reduced the drag coefficient. The drag reduction behind ventilated bodies was shown by several researchers (e.g. Abdul-Khader & Rai 1980, Suryanarayana et al. 1993, Naudascher & Rockwell 1994). A reduction in drag in the porous pooled stepped experiments would lead to a reduced flow resistance, an increased main stream velocity and a reduced energy dissipation rate.

Figure 3. Transition flow regime on porous pooled stepped spillway (Po = 5%): d_c/h = 0.51; q_w = 0.036 m^2/s; Re = 1.4 × 10^5

Figure 4. Cavity detail and flow through pores in skimming flow regime on porous pooled stepped spillways – Left: Po = 5%, d_c/h = 1.44; q_w = 0.171 m^2/s; Re = 6.8 × 10^5; Right: Po = 31%, d_c/h = 0.86; q_w = 0.079 m^2/s; Re = 3.1 × 10^5

4 AIR-WATER FLOW PROPERTIES

The air-water flow measurements with the double-tip conductivity probe were conducted at all step edges downstream of the inception point on the channel centerline. For the flat steps, the first vertical position

of the probe was at the step edge ($y = 0$) and for the pooled steps at the pool weir edge ($y = 0$). For all air-water flow properties, the graphs comprised dimensionless distributions as functions of the dimensionless distance from the pseudo-bottom formed by the step edges and pooled weir edges respectively (Figures 5-7). On the left hand side of the figures, the air-water flow properties are shown as a function of y/Y_{90}, where Y_{90} is the characteristic air-water flow depth where the void fraction $C = 90\%$. On the right hand side, the data are presented as a function of $(y + w)/d_c$ to highlight the effects of the pool weir upon the flow depth.

Some typical void fraction distributions are illustrated in Figure 5 for all stepped configurations showing some typical S-shapes which were observed in many previous studies on flat stepped spillways in transition and skimming flows (e.g. Chanson & Toombes 2002, Bung 2011). Little difference was visible between flat, pooled and porous pooled stepped spillways illustrated as functions of y/Y_{90}. The distributions of void fraction C matched well the advective diffusion equation of Chanson & Toombes (2002):

$$C = 1 - \tanh^2\left(K' - \frac{y/Y_{90}}{2 \times D_o} + \frac{\left(y/Y_{90} - 1/3\right)^3}{3 \times D_o}\right) \qquad (2)$$

where K' is an integration constant and D_o is a function of the mean air concentration C_{mean} only:

$$K' = 0.32745 + 1/2 \times D_o - 8/81 \times D_o \qquad (3)$$

$$C_{mean} = 0.762 \times (1.0434 - \exp(-3.614 \times D_o)) \qquad (4)$$

The mean air-concentration C_{mean} characterized the depth-average air content in terms of Y_{90}: $C_{mean} = 1 - d/Y_{90}$ where d is the equivalent clear water flow depth:

$$d = \int_{y=0}^{y=Y_{90}} (1 - C) \times dy \qquad (5)$$

For the graph showing the void fraction as function of $(y+w)/d_c$, the results showed also little difference between the data. However the void fraction profile for the pooled steps was shifted upward by w/d_c (Figure 5). The comparison of the (porous) pooled configurations showed a very good agreement between pooled and porous pooled configuration with $Po = 5\%$. The void fraction distributions for the porous pooled stepped spillway with $Po = 31\%$ were slightly lower and indicated some small differences in terms of flow depth which seemed to be linked with some discharges through the pooled weir pores (Figure 5).

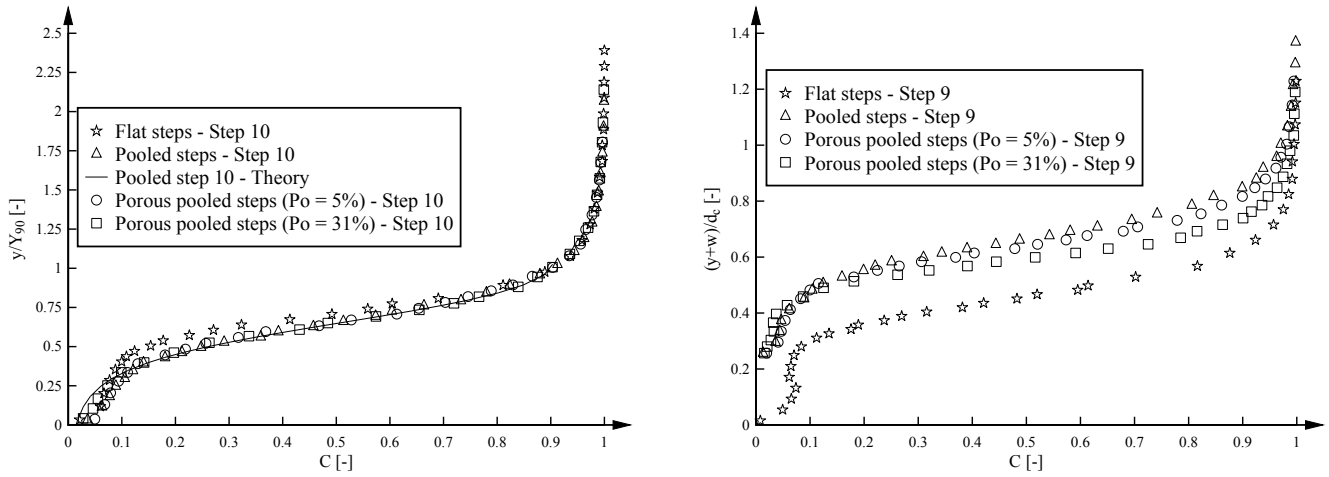

Figure 5. Comparison of void fraction distributions on the stepped spillways with flat, pooled and porous pooled steps – Left: $d_c/h = 0.96$; $q_w = 0.094$ m^2/s; Re = 3.7×10^5; Right: $d_c/h = 1.29$; $q_w = 0.144$ m^2/s; Re = 5.7×10^5; Comparison with advective diffusion equation (Equation (2))

The distributions of bubble count rate showed typical shapes with maxima in the intermediate flow region for void fractions of about $C = 0.4$ to 0.5 for all step configurations (Fig. 6). The number of entrained air bubbles was larger for the flat stepped spillway compared to the (porous) pooled step configurations. A close agreement in terms of bubble count rate distributions was observed for the pooled and porous pooled steps with $Po = 5\%$ for all discharges at all step edges. In contrast, a smaller bubble count rate was

observed on the porous pooled stepped spillway with Po = 31%. The differences in bubble count rate between these configurations tended to decrease with increasing distance from the inception point of air entrainment. In Figure 6, some typical dimensionless distributions of bubble count rate $F \times d_c/V_c$ in transition and skimming flows are shown as functions of y/Y_{90} and $(y+w)/d_c$ where V_c the was the critical flow velocity. Note that, for all experiments, the equilibrium flow conditions were not achieved and the bubble count rate increased monotonically with longitudinal distance on all configurations and for all flow rates.

For all step configurations, some typical distributions of the dimensionless interfacial velocity V/V_{90} and V/V_c respectively are shown in Figure 7 as functions of y/Y_{90} and $(y+w)/d_c$. For the comparison of dimensionless interfacial velocity V/V_{90}, all data for the flat, pooled and porous pooled stepped spillways were in good agreement and they compared very well with some self-similar relationships:

$$\frac{V}{V_{90}} = \left(\frac{y}{y_{90}}\right)^{1/N} \qquad y/Y_{90} \leq 1 \quad (6)$$

$$\frac{V}{V_{90}} = 1 \qquad y/Y_{90} > 1 \quad (7)$$

For $y/Y_{90} \leq 1$, the data agreed well with a power law with exponent of N = 10 (Eq. (6), Figure 7). The exact value of N may vary from one step edge to the next one for a given flow rate. For $y/Y_{90} > 1$, the velocity distributions had a pseudo-uniform profile although some scatter of the data was observed in the spray region.

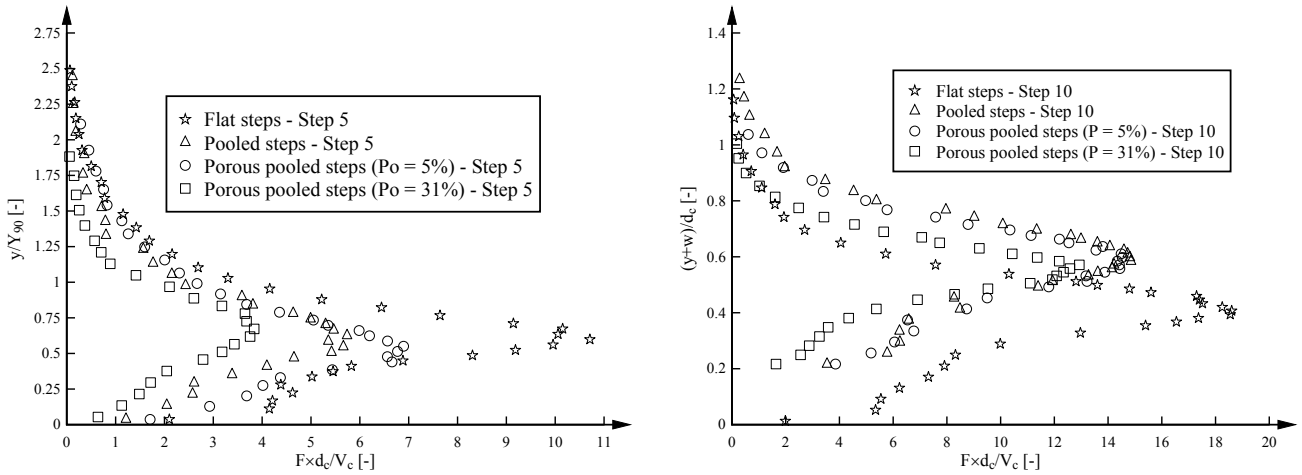

Figure 6. Comparison of bubble count rate distributions on the stepped spillways with flat, pooled and porous pooled steps – Left: d_c/h = 0.82; q_w = 0.073 m^2/s; Re = 2.9 × 10^5; Right: d_c/h = 1.52; q_w = 0.187 m^2/s; Re = 7.4 × 10^5

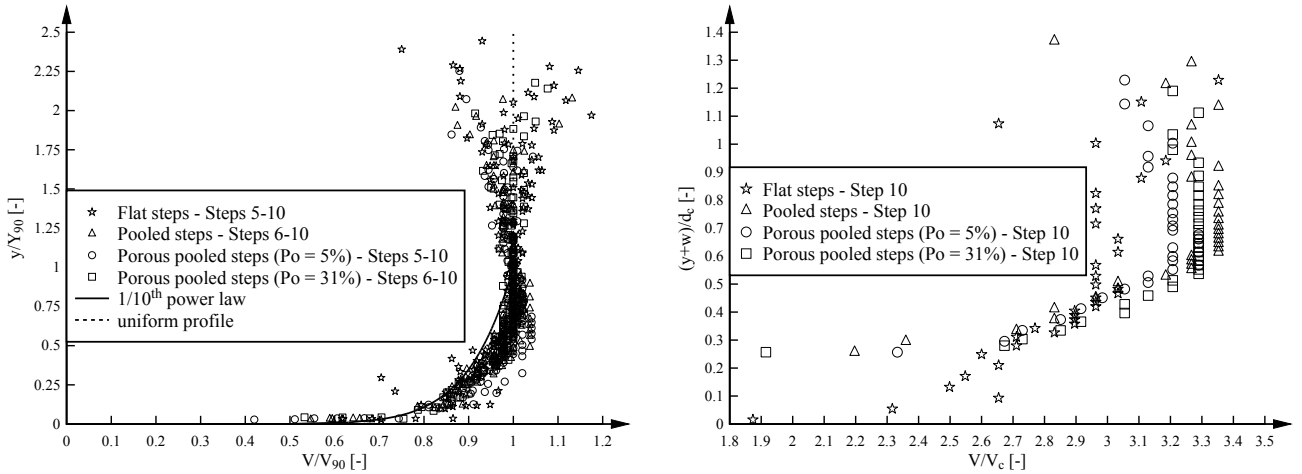

Figure 7. Comparison of interfacial velocity distributions on the stepped spillways with flat, pooled and porous pooled steps – Left: d_c/h = 0.96; q_w = 0.094 m^2/s; Re = 3.7 × 10^5; Right: d_c/h = 1.29; q_w = 0.144 m^2/s; Re = 5.7 × 10^5; Comparison with self-similar equations (Equations (6) & (7))

Some differences were however visible in terms of dimensionless interfacial velocity V/V_c (Fig. 7). For all present experiments, the data implied smaller interfacial velocities on the flat stepped spillway. This finding was counter-intuitive because it was assumed that the pooled steps increased the chute roughness and

would slow down the spillway flows. Nonetheless, the present observations showed consistently a faster flow motion down the (porous) pooled stepped chutes for a wide range of discharges in transition and skimming flows. For all configurations, the interfacial velocities increased with increasing distance from the inception point. The interfacial velocities for the porous pooled step configurations were in between the flat and pooled stepped spillway velocities. The velocities for the porous pooled steps with Po = 31% and for the pooled steps were very close for all discharges with some slightly larger velocities for the pooled steps. The interfacial velocities tended to increase with increasing porosity and the data for the porous pooled steps with Po = 5% were consistently smaller compared to the steps with Po = 31%. The observations of the velocities for the (porous) pooled configurations did not follow a clear trend and the reason for the largest interfacial velocities on the pooled step configuration remained unclear. Overall the the interfacial velocity data $V_{flat} < V_{(Po=5\%)} < V_{(Po=31\%)} < V_{pooled}$ for a given flow rate and for all discharges.

5 ENERGY DISSIPATION AND FLOW RESISTANCE

5.1 *Residual energy*

For a design engineer, it is important to quantify the energy dissipation rate and the residual energy at the downstream end of stepped spillways. The rate of energy dissipation and the residual energy were calculated herein at the downstream end for the flat and (porous) pooled stepped spillway configurations. The calculations were based upon the air-water flow measurements with the double-tip conductivity probe. The residual head H_{res} at the location of measurement at the downstream end was:

$$H_{res} = d \times \cos\theta + \frac{U_w^{\ 2}}{2 \times g} + w \qquad (8)$$

where U_w was the mean flow velocity $U_w = q_w/d$.

The observations of dimensionless residual head H_{res}/d_c at the last step edge or pool weir edge are illustrated in Figure 8 as a function of the dimensionless flow rate. Some differences in the residual head were observed for the different step configurations (8). The lowest residual head was achieved for the flat steps and the pooled steps exhibited a larger residual energy. This finding was surprising because it was expected that the pools would increase the energy dissipation along the pooled stepped chute as observed for flatter channel slopes (θ = 8.9°). The finding was consistent with the larger interfacial velocities on the pooled stepped spillway (Figure 7).

The largest residual energy was observed for the porous pooled stepped spillways with increasing residual head with increasing porosity. The larger residual energies for the porous pooled steps seemed to be linked with a reduced momentum exchange between the cavity and main stream flow caused by the pores in the pool weir. The pores in the pooled weir reduced both the energetic recirculation motions in the pooled step cavity and the form drag of the steps. Furthermore, some small discharge appeared through the pores and contributed to the reduced energy dissipation on the porous pooled stepped spillways. With increasing porosity, the energy dissipation performance decreased further.

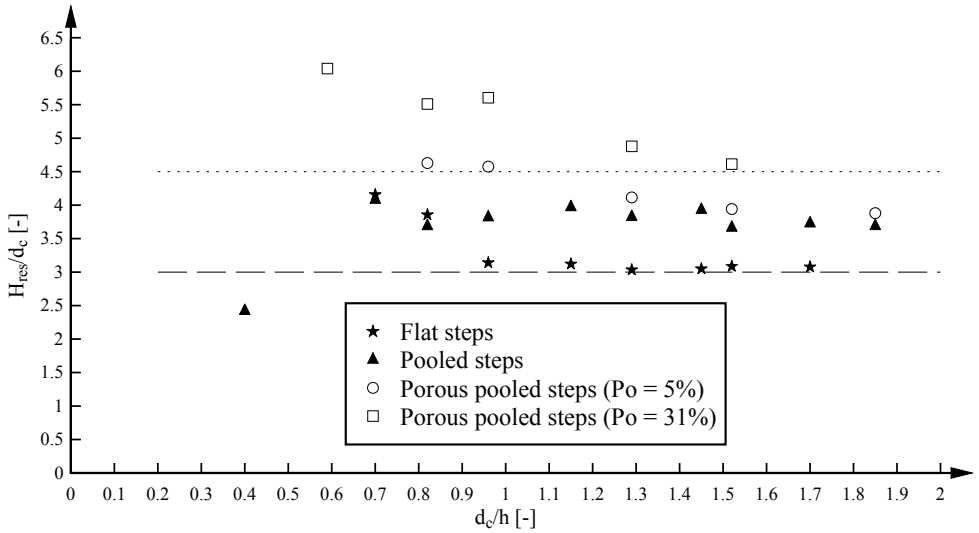

Figure 8. Comparison of dimensionless residual head at the downstream end on the stepped spillways with flat, pooled and porous pooled steps; Comparison with correlations of further stepped spillways with embankment dam slopes (dotted lines)

For all step configurations, the residual head decreased with increasing discharge for the smaller flow rates, while it was about constant for the largest flow rates. In Figure 8, the residual head data were compared with some simple design criteria for moderate slope-stepped spillways: the upper dotted line expressed the median residual energy of a number of experimental data obtained for flat stepped spillway slopes smaller than 15.9° and the lower dashed line the median values for flat stepped spillway data with slopes 21.8° < θ < 26.6° (Felder & Chanson 2009). Please note that the present flat stepped spillway data were not included in the median values. However, the present findings on the flat stepped spillway agreed very well with the previous physical studies on flat stepped spillways used for the median values shown in Figure 8. The residual energy for the (porous) pooled stepped spillways exceeded the correlations.

Note that, for the largest flow rates, the discharge was not fully developed at the downstream end of the spillway and the residual energy might be overestimated (Chanson 2001, Meireles & Matos 2009). The residual head at the downstream end of the stepped chute might be slightly larger than the specific energy at the start of the spillway apron. Hence, Figure 8 is suitable for design purposes including non-design flow conditions because it is conservative.

5.2 *Flow resistance*

On stepped spillways, some significant form losses are caused by the steps (Chanson 2001). Some additional flow resistance might be caused by the weir on pooled stepped spillways. The flow resistance is commonly expressed by the Darcy-Weisbach friction factor f_e (Rajaratnam 1990, Chanson 2001). The friction factor on a stepped spillway is quantified as the average shear stress in the air-water flow region downstream of the inception point. In the present study, no uniform equilibrium flow was achieved along the stepped chutes. Therefore the Darcy friction factor was calculated to quantify the average shear stress in the gradually-varied flow for the flat and pooled stepped spillways in the present study (Chanson et al. 2002):

$$f_e = \frac{8 \times \tau_o}{\rho_w \times U_w^2} = \frac{8 \times g \times S_f \times d}{U_w^2} \qquad (9)$$

where the friction slope equals $S_f = - \partial H/\partial x$, H is the total head and x is the distance in flow direction.

The experimental results for the flat and (porous) pooled stepped spillways are summarised in Figure 9, in which the friction factor is plotted as a function of the dimensionless step roughness height k_s/D_H with D_H the equivalent pipe diameter. Figure 9 includes all transition and skimming flow data for the flat and pooled step configurations. The data are compared with the solution of a simplified analytical mixing length model, which expressed the pseudo-boundary shear stress $f_d = 2 \times \pi^{0.5}/K$, where f_d is an equivalent Darcy friction factor estimate of the form drag and $1/K$ represents the dimensionless rate of expansion of the shear layer (Chanson 2001).

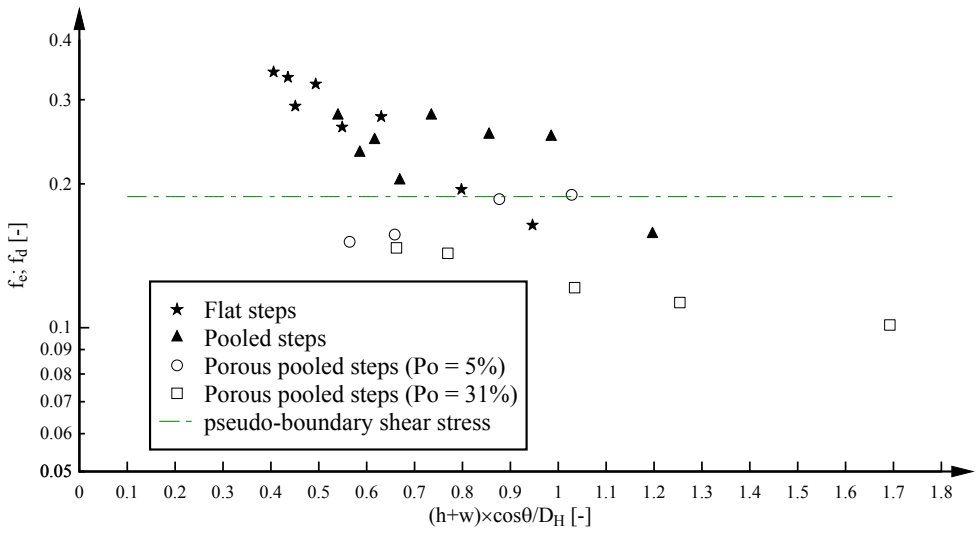

Figure 9. Comparison of Darcy friction factors on the stepped spillways with flat, pooled and porous pooled steps; Comparison with pseudo-boundary shear stress

Overall the stepped spillway data yielded Darcy-Weisbach friction factors between 0.1 and 0.34 (Figure 9). The findings were consistent with the reanalyses of flow resistance data showing variations of Darcy

friction factors between 0.1 and 0.35 for θ = 15.9° and θ = 21.8° (Felder & Chanson 2009). For the present data (θ = 26.6°), the smallest values of f_e were observed for the porous pooled steps which confirmed the reduction of form drag and momentum exchange by the pores.

6 CONCLUSION

A physical study was conducted on a relatively large stepped spillway with θ = 26.6° comprising four configurations with flat, pooled and porous pooled steps. The flow patterns showed a close agreement between the nappe, transition and skimming flow regimes for the flat and pooled stepped spillways. However, some small instabilities were observed for the pooled stepped spillway in nappe flows which was linked with pulsating flows in the first pool. The porous pooled stepped spillways showed similar flow patterns in the main stream flow, but some small differences were observed in the pool cavity region. Some discharge appeared through the pores, and decreased the cavity recirculations and air entrainment into the porous pooled step niche. The comparison of the air-water flow properties for the flat, pooled and porous pooled stepped spillways was conducted for transition and skimming flows. The comparative analyses showed a good agreement in most air-water flow property distributions including the void fraction and dimensionless interfacial velocity V/V_{90}. However, the pooled and porous pooled stepped spillways exhibited some larger interfacial velocities V/V_c for all flow rates, a result which was counter-intuitive. However, the comparison of the residual energy at the downstream end showed a smaller energy dissipation rate for the (porous) pooled stepped spillways. The pores decreased the momentum exchange between cavity recirculation and main stream flow and decreased the form drag which resulted in smaller friction factors.

The present testing provided some valuable design implications. The pooled step design showed some pulsating flow patterns for small flow rates which led to some small instabilities. The energy dissipation rate was smaller compared to the flat stepped design performances. The introduction of porosity to the pooled weir wall eliminated any flow pulsations and the flow patterns were stable for all flow discharges. However, the energy dissipation rate was much smaller compared to the flat and pooled step configurations. In summary the porous pooled step design was preferable to the pooled stepped design because the flow was more stable. The practical use of porous pooled steps in prototype requires some thorough physical modeling to ensure that the energy dissipation rate is accurately quantified. The porous pooled stepped spillway with Po = 31% had a porosity comparable to gabions, and the aeration and energy dissipation performance on hydraulic structures with gabion technique should be investigated before any implementation in a prototype environment.

7 ACKNOWLEDGEMENTS

The authors thank Jason Van Der Gevel and Stewart Matthews for their technical assistance. The financial supports through a UQ research scholarship and through the Australian Research Council (Grant DP120100481) are acknowledged.

NOTATION

C	void fraction or air content
C_{mean}	mean air concentration
D_H	hydraulic diameter
d	equivalent clear water flow depth
d_c	critical flow depth
F	bubble count rate
f_d	Darcy friction factor estimated of the form drag
f_e	equivalent Darcy friction factor
g	gravity acceleration constant
H	total head
H_{res}	residual energy
h	step height
K	expansion rate of shear layer
l	step length
N	power law exponent

Po	porosity of porous pooled steps
q_w	water discharge per unit width
S_f	friction slope
U_{Po}	flow velocity through pores
U_w	mean flow velocity
V	interfacial velocity
V_c	critical flow velocity
V_{90}	interfacial velocity where C = 90%
W	channel width
w	pool weir height
x	distance in flow direction
Y_{90}	characteristic flow depth where C = 90%
y	direction normal to the pseudo-bottom formed by the step edges
z	transverse direction
$Ø$	diameter of pores and probe tips
ΔH	energy difference between the two sides of the porous wall
Δx	longitudinal separation between probe tips
Δz	transverse separation between probe tips
ζ	resistance coefficient
θ	channel slope
τ	shear stress

REFERENCES

Abdul-Khader, M.H., Rai, S.P. (1980). A Study of Channel obstructions with a Longitudinal Slot. - Proc. 7th Australasian Hydraulics and Fluid Mechanics Conf., IEAust., Brisbane, Australia, pp. 175-178.

André, S. (2004). High velocity aerated flows on stepped chutes with macro-roughness elements., Ph.D. thesis, Laboratoire de Constructions Hydraulics (LCH), EPFL, Lausanne, Switzerland, 272 pages.

Bung, D.B. (2011). Developing flow in skimming flow regime on embankment stepped spillways., Journal of Hydraulic Research, Vol. 49, Issue 5, pp. 639-648.

Chanson, H. (2001). The Hydraulics of Stepped Chutes and Spillways., Balkema, Lisse, The Netherlands, 418 pages.

Chanson, H., Toombes, L. (2002). Air-Water Flows down Stepped chutes: Turbulence and Flow Structure Observations., Intl Jl of Multiphase Flow, Vol. 28, No. 11, pp. 1737-1761.

Chanson, H., Yasuda, Y., Ohtsu, I. (2002). Flow Resistance in Skimming Flows and its Modelling., Canadian Journal of Civil Engineering, Vol. 29, No. 6, pp. 809-819.

Felder, S., Chanson, H. (2009). Energy dissipation, flow resistance and gas-liquid interfacial area in skimming flows on moderate-slope stepped spillways., Environmental Fluid Mechanics, Vol. 9, No. 4, pp. 427-441.

Felder, S., Chanson, H. (2011). Energy Dissipation down a Stepped Spillway with Non-Uniform Step Heights., J. of Hydraulic Eng., ASCE, Vol. 137, No. 11, pp. 1543-1548.

Felder, S., Chanson, H. (2012). Air-Water Flow Measurements in Instationary Free-Surface Flows: a Triple Decomposition Technique., Hydraulic Model Report No. CH85/12, School of Civil Engineering, The University of Queensland, Brisbane, Australia, 161 pages.

Felder, S., Guenther, P., Chanson, H. (2012). Air-water flow properties and energy dissipation on stepped spillways: a physical study of several pooled stepped configurations., Hydraulic Model Report No. CH87/12, School of Civil Engineering, The University of Queensland, Brisbane, Australia, 225 pages.

Gonzalez, C.A., Chanson, H. (2007). Hydraulic Design of Stepped Spillways and Downstream Energy Dissipators for Embankment Dams., Dam Engineering, Vol. 17, No. 4, pp. 223-244.

Gonzalez, C.A., Chanson, H. (2008). Turbulence and cavity recirculation in air-water skimming flows on a stepped spillway., Journal of Hydraulic Research, Vol. 46, No. 1, pp. 65-72.

Kökpinar, M.A. (2004). Flow over a Stepped Chute with and without Macro-Roughness Elements., Can. Jl of Civil Engineering, Vol. 31, No. 5, pp. 880-891.

Meireles, I., Matos, J. (2009). Skimming Flow in the Nonaerated Region of Stepped Spillways over Embankment Dams., J. of Hydraulic Eng.- ASCE, Vol. 135, No. 8, pp. 685-689.

Naudascher, E., Rockwell, D. (1994). Flow-Induced Vibrations. An Engineering Guide. - IAHR Hydraulic Structures Design Manual No. 7, Hydraulic Design Considerations, Balkema Publ., Rotterdam, The Netherlands, 413 pages.

Ohtsu, I., Yasuda, Y., Takahashi, M. (2004). Flow Characteristics of Skimming Flows in Stepped Channels., Jl of Hydraulic Eng., ASCE, Vol. 130, No. 9, pp. 860-869.

Peyras, L., Royet, P., Degouette, G. (1992). Flow and Energy Dissipation over Stepped Gabion Weirs., J of Hydraulic Eng., ASCE, Vol. 118, No. 5, pp. 707-717.

Rajaratnam, N. (1990). Skimming Flow in Stepped Spillways., Jl of Hydraulic Eng., ASCE, Vol. 116, No. 4, pp. 587-591.

Relvas, T.R., Pinheiro, A.N. (2008). Inception Point and Air Concentration in Flows on Stepped Chutes lined with Wedge-shaped Concrete Blocks., J. of Hydraulic Eng., ASCE, Vol. 134, No.8, pp. 1042-1051.

Saryanarayana, G.K., Pauer, H., Meier, G.E.A. (1993). Bluff-Body Drag Reduction by Passive Ventilation., Experiments in Fluids, Vol. 16, No. 2, pp. 73-81.

Thorwarth, J. (2008). Hydraulisches Verhalten der Treppengerinne mit eingetieften Stufen – Selbstinduzierte Abflussinstationaritäten und Energiedissipation. (Hydraulics of Pooled Stepped Spillways – Self-induced Unsteady Flow and Energy Dissipation.); Ph.D. thesis, University of Aachen, Germany (in German).

Thorwarth, J., Köngeter, J. (2006). Physical Model Test on a Stepped Chute with Pooled Steps – Investigation of Flow Resistance and Flow Instabilities. - International symposium on Hydraulic Structures, Caracas, Venezuela:, pp. 477 – 486.
Tsukahara, T., Sakamoto, Y., Aoshima, D., Yamamoto, M., Kawaguchi, Y. (2012). Visualisation and laser measurements on the flow field and sand movement on sand dunes with porous fences., Experiments in Fluids, Vol. 52, No. 4, pp. 877-890.

IWLHS, 20-22/02/2013, Aachen - Bung & Pagliara (eds) - © 2013 Bundesanstalt für Wasserbau ISBN 978-3-939230-04-5

Stepped Spillway Downstream of a Piano Key Weir – Critical Length for Uniform Flow

A. Silvestri, S. Erpicum, P. Archambeau, B. Dewals & M. Pirotton
HECE Research group, Argenco Department,University of Liège, Belgium

ABSTRACT: Recent researches showed the rapid aeration of the flow downstream of piano key weirs. This could be related to the specific geometric features of the structure, creating several interacting flows and jets downstream. In order to validate this assumption, an experimental research has been carried out at the Laboratory of Engineering Hydraulics, University of Liège. The main objective of the study was to analyze the energy dissipation occurring in skimming flow conditions on a stepped spillway downstream of a piano key weir (PKW). Comparison with energy dissipation on a stepped spillway downstream of a standard ogee crested weir has been performed. An indirect method has been used to determine the residual energy at the spillway toe. The results show that uniform flow conditions are reached faster on a stepped spillway downstream of a PWK compared to the length needed downstream of a standard ogee crested weir. Extrapolation of the results to prototype flow conditions is also discussed with regards to scale effects influence.

Keywords: skimming flow, uniform flow, hydraulic jump, conjugate depths equation, local head loss

1 INTRODUCTION

Stepped spillways are used in dam construction to reduce the length or eliminate the stilling basin at the dam toe by dissipating energy along the spillway. They enable also to decrease the erosion risk due to cavitation by providing natural aeration. They are usually built downstream of standard ogee-crested weirs.

Two distinct flow regimes may occur on stepped spillways: nappe flow and skimming flow. In nappe flow the steps act as a series of overfalls with the water plunging from one step to another. In skimming flow, the water flows as a coherent stream over the pseudobottom formed by the outer step edges, without air pockets under the jets and with development of intense recirculating zones in the triangular cavities formed by the step faces and the pseudobottom. These vortices are maintained by the transmission of shear stress from the coherent stream over the pseudobottom and contribute significantly to the energy dissipation for this type of regime. The nappe flow is found for large steps and low discharge whereas the skimming flow appears for small steps and high discharge. Between these both flow regimes, there is a transition regime where both nappe and skimming flows occur simultaneously in different parts of the stepped spillway (Boes and Hager, 2003a).

For a stepped spillway with skimming flow regime, as studied in this paper, the free-surface of the flow is smooth in the early steps and no air entrainment occurs. Close to the bottom, turbulence is generated. When the outer edge of the turbulent boundary layer reaches the free surface, air entrainment occurs. Downstream of the point of inception of air entrainment, the flow becomes rapidly aerated. A mixture of air and water extends gradually through the fluid. Far downstream, the flow becomes uniform. From this moment, air concentration flow, velocity and water depth remain nearly constant along the spillway (Chanson, 1994). A criterion has been proposed by Boes et Hager (2003a) to predict the minimum vertical distance $H_{dam,u}$ from spillway crest needed to reach uniform flow depending on the critical depth h_c and the slope ϕ of the spillway:

$$\frac{H_{dam,u}}{h_c} = 24\left(\sin\phi\right)^{2/3}. \qquad (1)$$

When uniform flow conditions are reached on a stepped spillway, Boes and Hager (2003a) suggest to calculate the residual energy head $E_{f,u}$ at the spillway end as

$$\frac{E_{f,u}}{E_{\max}} = \frac{F}{\frac{H_{dam}}{h_c} + \frac{3}{2}}, \qquad (2)$$

where E_{max} is maximum reservoir energy head, H_{dam} is the dam height and F is a parameter related to the the bottom roughness. This relation has been established analytically from the general equation for water curves (Hager and Boes, 2000). Its validity has already been proven in several searches by comparison with experimental data.

Equation (2) is independent of the type of weir upstream of the stepped spillway as uniform flow characteristics are related to the discharge and the spillway features.

The specific geometric features of the piano key weirs create several interacting flows and jets downstream of the structure, enhancing thus the aeration of the flow. An experimental study has been conducted at the Laboratory of Engineering Hydraulics, University of Liège, to compare, in an idealized environment, the energy dissipation on a stepped spillway downstream a PKW and downstream of a standard ogee-crested weir. In particular, the study aims at verifying whether uniform flow conditions can be reached faster on stepped spillway placed downstream of the PKW than downstream of an ogee-crested weir.

First results were published by Erpicum et *al.* (2011). Two geometries of PKW were considered as well as a standard ogee-crested weir upstream of the same stepped spillway model. Thanks to sufficient length of the stepped spillway (H_{dam}/h_c=16.1 to 58.8), uniform flow conditions were reached at the spillway toe for almost the whole range of tested discharges. Therefore, the resulting energy at the spillway toe was equivalent downstream of the PKWs and downstream of the standard ogee crested weir. However, for the same specific discharge on the spillway, important differences in the flow features were observed. Indeed, with both PKW geometries, the flow was fully aerated immediately downstream of the PKW, while this was not the case downstream of the ogee-crested weir.

In the present study, the experimental facility used by Erpicum *et al*. (2011) has been modified to reduce the spillway length. Several spillway lengths have been tested to generalize criterion proposed by Boes and Hager (2003a) for stepped spillways downstream of PKWs.

Extrapolation of the results to prototype flow conditions is also discussed. Though not experimentally verified, scale effects are not anticipated due to criteria involving the Weber (Kobus, 1984) and Reynolds (Rutschmann, 1988 and Speerli, 1999) numbers.

2 EXPERIMENTAL FACILITY AND METHODOLOGY

Experimental data were obtained on a facility (Figure 1) made of a 0.494m wide stepped spillway with a slope of 52° and regular steps of 2.4cm in length and 3cm in height. The spillway is linked to an upstream reservoir and a 4.20m long downstream horizontal channel. Thanks to an adoptive support system, the length of the spillway can be easily modified from 0 to 1.30m. All the walls of the facility (sidewalls, channel bottom, weirs and spillway) are made of steel, PVC or Plexiglas in order to minimize friction effects. The upstream reservoir is fed by a regulated pump connected to a pressurized pipes network. The downstream extremity of the horizontal channel is equipped with an adjustable vertical gate.

Tested discharges ranged from 5l/s to 80l/s. They have been measured in the upstream pipe using an electromagnetic flow meter (accuracy of 1%). The water depths in the upstream reservoir and along the horizontal channel have been measured by ultrasonic probes (frequency of 10Hz, resolution of 0.025mm and accuracy of 2%). Because of small free surface oscillations, water depth measurements have been averaged on a period of 90s to define a single water depth value in each point.

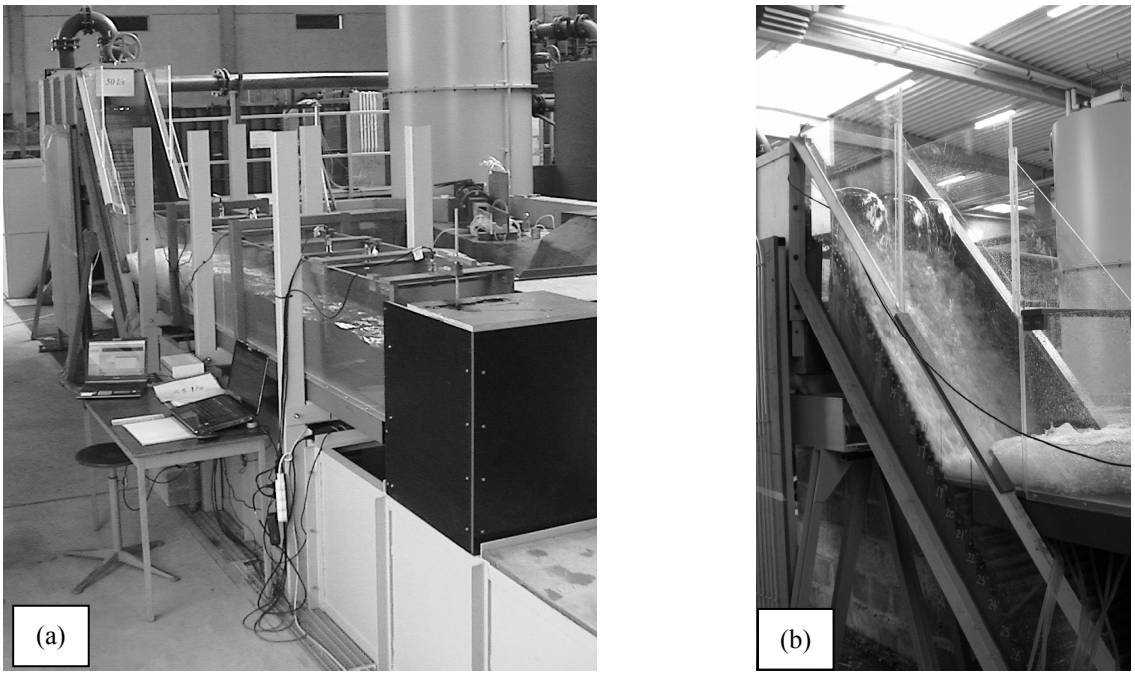

Figure 1: Global view of the experimental facility (a) and view of PKW_2 and spillway [Position II] (b).

In the present study, three different dam heights have been considered, namely Position I, Position II and Position III, corresponding to a spillway length of 1.27m, 1.04m and 0.62m respectively. Three different models of weir have been tested upstream of the stepped spillway: a standard ogee-crested weir (Dewals *et al*., 2004) and two geometries of piano key weirs, noted PKW_1 and PKW_2 (Erpicum *et al*., 2011). The dimensions of the PKW_2 are generally 1.6 times smaller than PKW_1 ones, except the spillway width and the walls thickness which are constant. PKW_1 represents 1.5 inlets and 1.5 outlets while PKW_2 represents 2.5 inlets and 2.5 outlets. Their dimensions are summarized in Table 1. They are both "modified type A PKWs", i.e. with downstream and upstream overhangs of different lengths. Steps have been built in the outlets to improve energy dissipation. The dam's heights (from crest of weir to spillway toe) are given in Table 2 for all combinations of weir's type and Position (I, II or III).

Table 1. General dimensions and aspect ratios of PKW_1 and PKW_2.

	W_i [cm]	W_0 [cm]	T_s [mm]	P [cm]	B [cm]	B_b [cm]	B_i [cm]	B_0 [cm]	W_i/ W_0 [-]	P/ W_i [-]	T_s/ W_i [-]	L_u/ W_u [-]
PKW_1	16.9	12.3	15	26.2	62.3	37.4	11	13.9	1.37	1.55	0.09	4.78
PKW_2	9.8	7.7	10	16.3	38.8	23.3	6.8	8.7	1.27	1.66	0.10	4.88

Table 2. Dam heights (H_{dam}) for all tested combinations of weir type and Position (I, II or III).

	Standard weir	PKW_1	PKW_2
$H_{dam,I}$	1.067	1.282	1.183
$H_{dam,II}$	0.887	1.102	1.003
$H_{dam,III}$	0.552	0.767	0.668

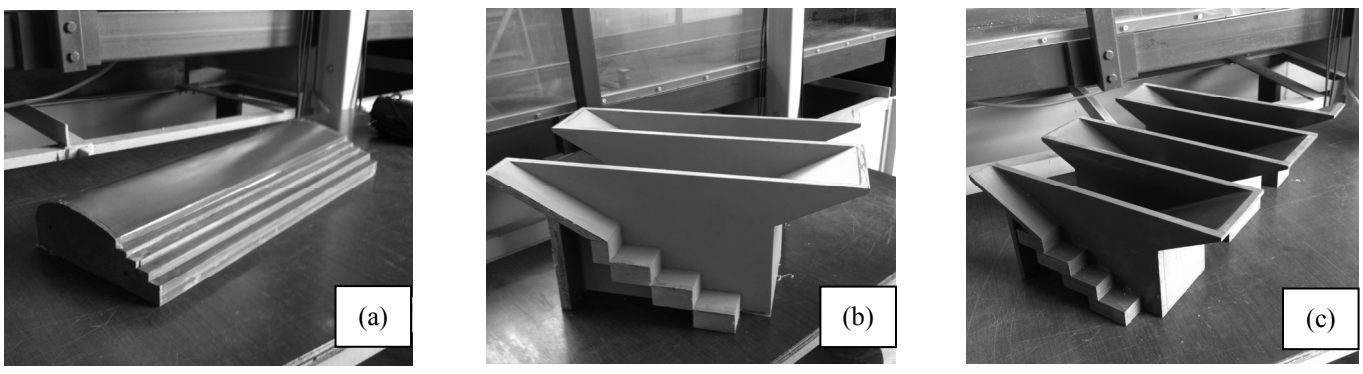

Figure 2: Pictures of standard ogee-crested weir (a), PKW_1 (b) and PKW_2 (c).

Experiments consisted in measuring and comparing, for constant discharges, the energy dissipation along the stepped spillway depending on the type of upstream weir. This energy dissipation has been calculated as the difference between the energy measured in the upstream reservoir E_0 and the energy at the spillway toe E_p.

Because of air entrainment and high flow velocity at the spillway toe, the residual energy E_p is difficult to determine accurately by a direct measurement of the water depth and flow velocity. Therefore an indirect method has been used; consistently with Matos and Quintela (2004), Shvainshtein (1999) or Erpicum *et al*. (2011). It consists in creating a hydraulic jump in the downstream horizontal channel by means of a gate, to measure the flow energy downstream of the jump, where flow depth varies less and aeration rate is smaller, and then to calculate the water depth at the spillway toe and the residual energy using the conjugate depths equation.

Tested discharge ranged from 5l/s to 80l/s (specific discharge from 0.02l/s to 0.162l/s). A sketch of the experimental facility is shown in Figure 4.

3 RESULTS AND DISCUSSIONS

3.1 *Qualitative observations*

The first result of the tests consist in a visual confirmation of previous observations by other researchers such as Erpicum *et al*. (2011) and Ho Ta Khanh *et al*. (2011). For the same specific discharge, important differences have been observed in the flow downstream of the spillway depending on the type of weir (Figure 3).

With both PKW geometries, the flow is fully aerated directly after the weir toe, while this is not the case with the ogee-crested weir. The inception point downstream of a PKW is significantly closer to the spillway crest than downstream of an ogee-crested weir. As a result, the energy dissipation on a stepped spillway downstream of a PKW should be different from downstream an ogee-crested weir. In the next subsection, we show that uniform flow conditions are reached faster downstream of a PKW than downstream of the ogee-crested weir. Another consequence of this higher aeration is a reduction of the cavitation risk, so that it should be possible to avoid the construction of aerators in the non-aerated region.

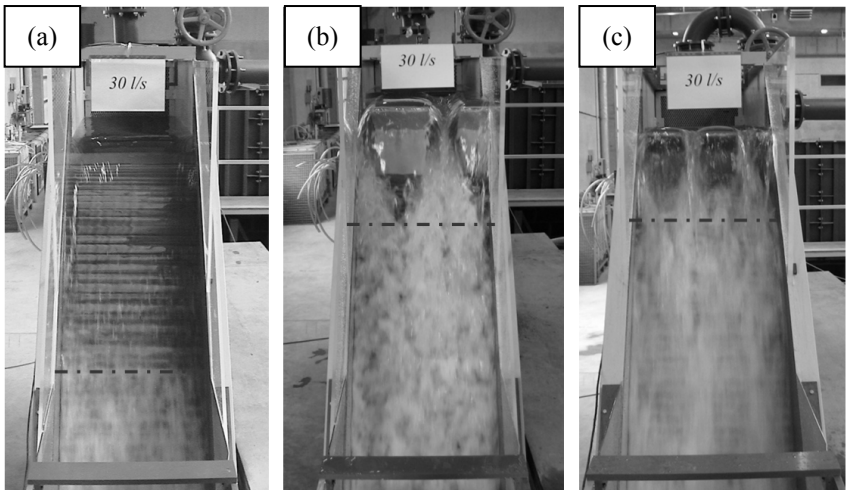

Figure 3: Change in the inception point location along the spillway between standard ogee-crested weir and PKWs (Position I, Q = 30 l/s, q = 0.06 m²/s): standard ogee-crested weir (a), PKW_1 (b) and PKW_2 (c).

3.2 *Quantitative analysis*

For a given discharge, upstream energy E_0 can be evaluated directly from the water depth h_0 measured by the ultrasonic probe in the upstream reservoir. Indeed, under the assumption of a uniform velocity distribution across the reservoir cross-section, E_0 is given by

$$E_0 = z + h_0 + \frac{v^2}{2g} \qquad (3)$$

where z is the reservoir bottom elevation from the downstream horizontal channel bottom level and v the mean velocity through the reservoir cross section. To be consistent with the uniform velocity assumption, the probe used to measure the water depth h_0 is located at a horizontal distance from the weir crest longer than twice the maximum head on the weir (Paternoster, 1963).

In all tests, the hydraulic jump was located exactly at the spillway toe (Figure 4 - b).

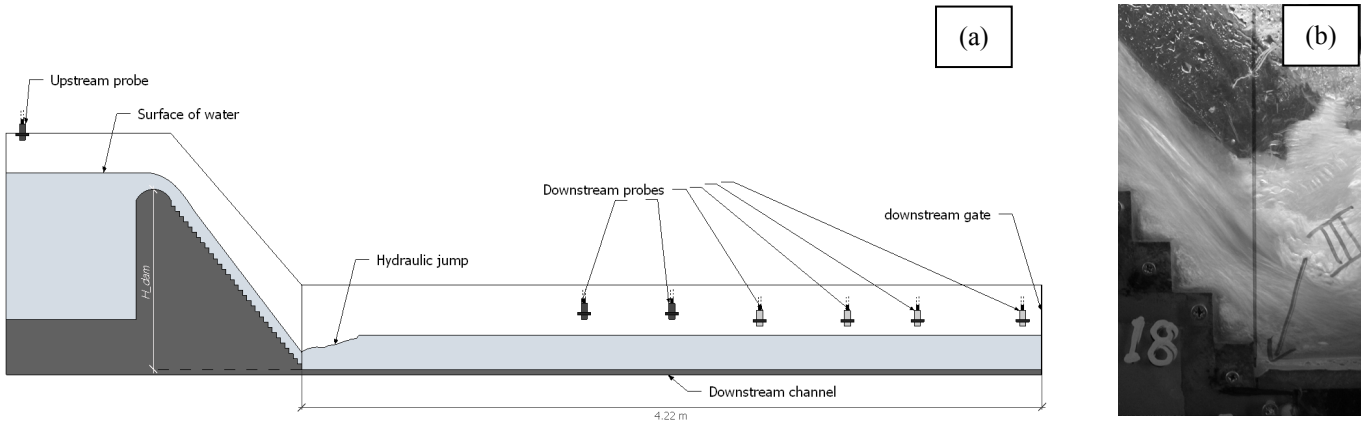

Figure 4: Sketch of the experimental facility (a) and localization of the hydraulic jump at the spillway toe (b).

The water depth at the spillway toe is thus equal to the first conjugate depth h_1 of the jump. To solve the conjugate depths equation (equation (4)), the second conjugate depth h_2 has been evaluated as the mean value measured using a maximum of six ultrasonic probes arranged along the downstream part of the channel. Indeed, friction effects along the subcritical section of the channel have been found to be negligible.

$$h_1 = h_2 \frac{\sqrt{1+8\left(\frac{h_c}{h_2}\right)^3}-1}{2}. \qquad (4)$$

The residual energy E_p in the horizontal channel at the spillway toe can be calculated from the first conjugate depth h_1 using equation (5), similar to equation (3).

$$E_p = h_1 + \frac{\left(q/h_1\right)^2}{2g}. \qquad (5)$$

To evaluate the residual energy at the spillway toe in the spillway, the local head loss due to the slope change at the horizontal channel inlet needs to be considered. To evaluate this local head loss, only the results of the tests carried out with the ogee crested weir and with an H_{dam}/h_c ratio higher than the limit provided by equation (1) have been considered. In practice, working with 90% of the limit given by equation (1) and with our geometry of facility, we had $H_{dam,u}/h_c$ equal to 18.4. For these tests, the flow in the spillway is uniform and the corresponding residual energy $E_{f,u}$ may be computed using equation (2). ΔE_{impact} may thus be simply computed as

$$\Delta E_{impact} = E_p - E_{f,u}. \qquad (6)$$

From ΔE_{impact} values and assuming a classical form for the local head loss equation, we obtain

$$\Delta E_{impact} = k\frac{\left(q/h_1\right)^2}{2g} \qquad (7)$$

where h_1 is the first conjugate depth giving by equation (4), a constant local head loss coefficient k equal to 0.627 is found (Figure 5).

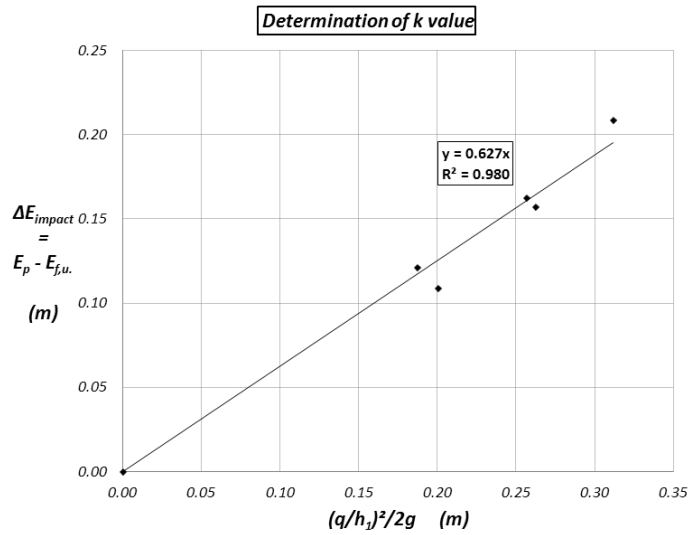

Figure 5: Determination of the local head loss coefficient k value at the spillway toe.

Whatever the discharge, the theoretical residual energy head in uniform flow conditions at the spillway toe in the horizontal channel E_p^{uni} may be calculated as

$$E_p^{uni} = E_{\max} \frac{F}{\frac{H_{dam}}{h_c} + \frac{3}{2}} - k \frac{\left(q/h_1\right)^2}{2g} . \qquad (8)$$

E_p^{uni} is only a function of the spillway characteristics and discharge, and not of the upstream weir type. The comparison of this theoretical value with the residual energy measured at the spillway toe is shown in Figure 6 for all the PKW geometries and discharges considered in this study.

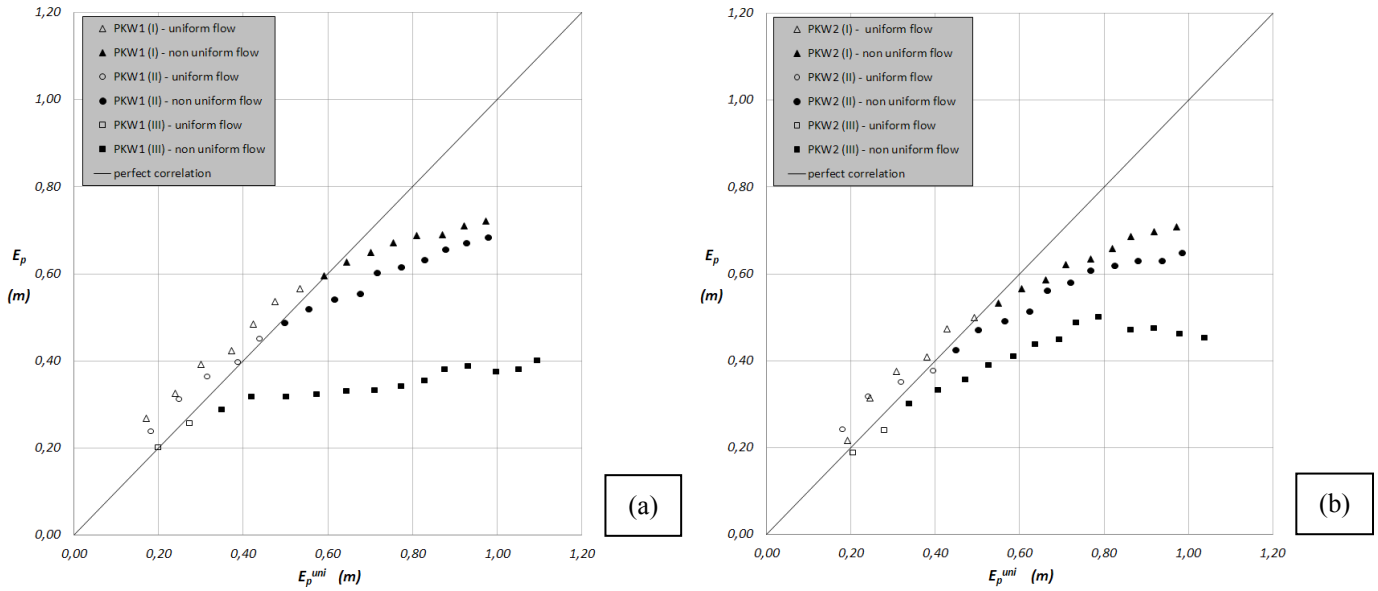

Figure 6: Correlation between the theoretical uniform energy at the spillway toe E_p^{uni} and the measured residual energy E_p for PKW configurations. White symbols for uniform flow energy and black symbols for non-uniform flow energy.

Figure 7 shows the ratio between E_p^{uni} and E_p as a function of $H_{dam,u}/h_c$. The critical dam height to reach uniform flow conditions downstream of the ogee-crested weir as defined by Boes and Hager (2003a) appears too high when the spillway is fed by means of a PKW. The limit ratio for stepped spillway fed by PKW is around 14.5. This value is valid for the tested spillway and weir geometry. Nevertheless, these results prove that using a PKW as upstream weir with a stepped spillway enables to reach uniform flow conditions on a shorter spillway compared to the length needed downstream of a standard ogee crested weir.

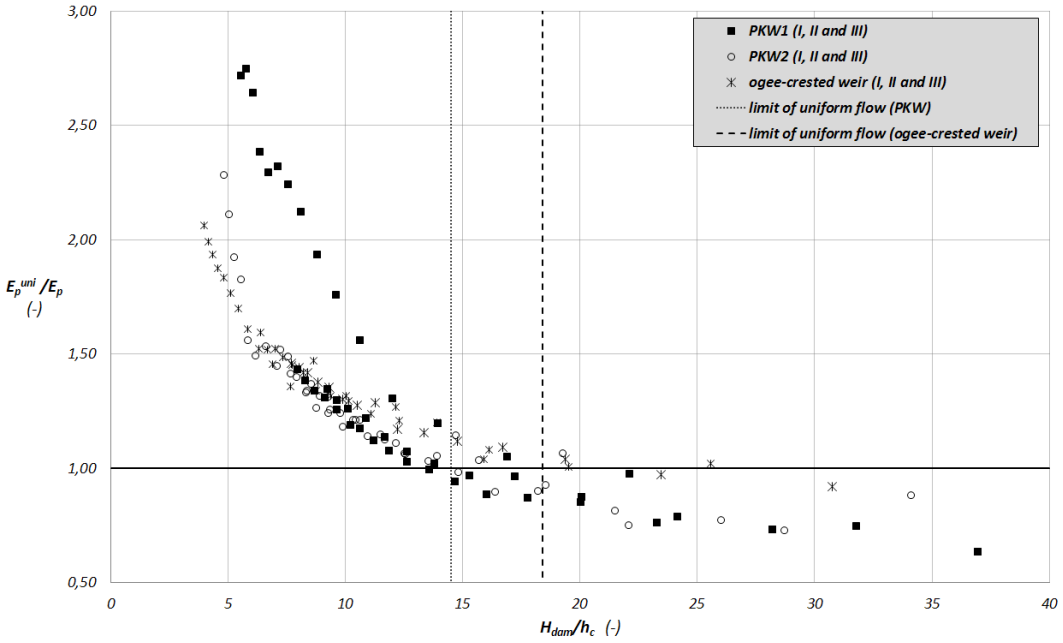

Figure 7: Ratio between theoretical uniform flow energy E_p^{uni} and measured residual energy E_p at the spillway toe as a function of non-dimensional dam height H_{dam}/h_c.

3.3 *Scale effects*

Scale effects have been analysed to evaluate whether the conclusions of the present study, resulting from scale model tests, can be upscaled to a prototype scale. Indeed, highly turbulent air-water flows cannot be modelled without scale effects when using Froude similitude, because of the significant role of viscosity and surface tensions (Boes and Hager, 2003b). For a true similarity of the aeration process between model and prototype, the Froude, the Reynolds and the Weber similarity laws should be fulfilled simultaneously (Kobus, 1984). Therefore, care must be taken when upscaling model results to the prototype scale.

Kobus (1984) proposes Reynolds numbers *Re* with flow depth as reference length (equation (9)) equal or higher to 10^5 to minimize viscous effects.

$$\mathrm{Re} = \frac{q}{\nu} > 10^5 \,. \qquad (9)$$

Rutschmann (1988) and Speerli (1999) concluded both that the Weber number *W*, with the flow depth as the reference length, should be at least 110 for surface tension effect to be negligible (where depth-averaged mixture velocity $\bar{u}_m$ is calculated with the critical depth h_c of the flow on the spillway and L_s is the distance between two successive edges step) – equation (10).

$$W = \frac{\bar{u}_m^2}{\frac{\sigma}{\rho L_s}} = \frac{\left(\frac{q}{h_c}\right)^2}{\frac{\sigma}{\rho L_s}} \geq 110 \,. \qquad (10)$$

Considering our geometry and the range of tested discharges, Reynolds number varies between 2.4 10^4 and 1.6 10^5 and Weber number varies between 179 and 716.2. Consequently, the results of the study can be extrapolated to a prototype scale without modification.

4 CONCLUSIONS

The present experimental research has been carried at the Laboratory of Engineering Hydraulics, University of Liège, with the main purpose to study the energy dissipation occurring in skimming flow conditions on a stepped spillway downstream of a piano key weir (PKW) by comparison with the theory for

stepped spillway downstream of a standard ogee crested weir. The results confirmed the rapid aeration of the flow downstream of piano key weirs due to the specific geometric features of the weir, creating several interacting flows and jets downstream of the structure. Indeed, with PKW geometry, the flow is fully aerated directly after the weir toe, while it is not the case with the ogee-crested weir. The inception point downstream of a PKW is significantly closer to the spillway crest than downstream of an ogee-crested weir.

The results showed that using a PKW as upstream weir enables to reach uniform flow conditions on a shorter stepped spillway compared to the length needed downstream of a standard ogee crested weir. The critical dam height to reach uniform flow condition downstream of the ogee-crested weir appears too high when the spillway is fed by a PKW. Indeed, with our geometry, the limit ratio $H_{dam,u}/h_c$, as defined by Boes and Hager (2003a), for stepped spillway fed by PKW is estimated around 14.5 whereas it is 18.4 downstream of the ogee-crested weir.

Finally, from criteria defined by Kobus (1984), Rutschmann (1988) and Speerli (1999) and having a Reynolds number which varies between 2.4 10^4 and 1.6 10^5, respectively Weber number, between 179 and 716.2, it can be concluded that scale effects have a limited influence in the tested configurations. Consequently, though not experimentally verified, scale effects are not anticipated.

The present experimental research has been carried on with goal to study the energy dissipation along a stepped spillway downstream of a PKW when the non-uniform flow conditions are installed.

NOTATIONS

g	gravitational acceleration
h_0	water depth in the upstream reservoir
h_1	first conjugate depth (supercritical)
h_2	second conjugate depth (subcritical)
h_c	critical depth (on the spillway)
$h_{w,u}$	uniform equivalent clear water depth
k	local loss coefficient
q	specific discharge
s	step height (stepped spillway)
v	flow velocity (hypothesis of uniform distribution on the section)
z	vertical distance between the floor of downstream horizontal channel and the bottom of the upstream reservoir
B	upstream-downstream length of the PKW $B = B_b + B_i + B_0$
B_0	upstream (outlet key) overhang crest length
B_i	downstream (inlet key) overhang crest length
B_b	base length
E_0	energy in the upstream reservoir
$E_{f,u}$	residual energy head at spillway end (uniform flow conditions established)
E_{max}	maximum reservoir energy head
E_p	energy at the spillway toe
F_*	roughness Froude number
H_{dam}	height of dam
$H_{dam,u}$	vertical distance from spillway crest to close uniform equivalent clear water flow
L_u	developed length of the PKW unit along the overflowing crest axis
L_s	$= s/\sin\phi$ distance between step edges, roughness spacing
P	height of the PKW
Re	Reynolds number
T_s	sidewall thickness
W	Weber number
W_u	width of a PKW unit
W_i	inlet key width (sidewall to sidewall)
W_0	outlet key width (sidewall to sidewall)
ΔE_{impact}	local head loss due to flow impact at the change of slope between spillway and downstream horizontal channel
ϕ	slope of stepped spillway
ν	kinematic viscosity of water
ρ	density of water
σ	surface tension between air and water

REFERENCES

Boes R.M. & Hager W.H. (2003a). Hydraulic design of stepped spillways. Journal of hydraulic engineering ASCE., Vol. 129, N°9, 671-679.

Boes R.M. & Hager W.H. (2003b). Two-Phase Flow Characteristics of Stepped Spillways. Journal of hydraulic engineering ASCE., Vol. 129, N°9, 661-670.

Chanson H. (1994). Hydraulics of skimming flows over stepped channels and spillways. Journal of Hydraulic Research, Vol. 32, N°3, 445-460.

Dewals B.J., André S., Schleiss A. & Pirotton M. (2004). Validation of a quasi-2D model for aerated flows over mild and steep stepped spillways. In Liong, Phoon & Babovic (eds). Proc. Of the 6th Int. Conf. on Hydroinformatics, Singapore. Vol. I, 63-70. World Scientific Publishing Company.

Erpicum S., Machiels O., Archambeau P., Dewals B. & Pirotton M. (2011). Energy dissipation on a stepped spillway downstream of a Piano Key Weir – Experimental study. Labyrinth and Piano Key Weirs-PKW 2011. Erpicum et al. (eds). Taylor & Francis Group, London, 105-111.

Hager W.H. & Boes R.M. (2000). Backwater and drawdown curves in stepped spillways flow. Proc. Int. Workshop on Hydraulics of Stepped Spillways, VAW, ETH Zurich, H.-E. Minor and W.H. Hager, eds., Balkema, Rotterdam, The Netherlands, 129-136.

Ho Ta Khanh M., Truong Chi Hien & Nguyen Thanh Hai. (2011). Main results of the PK Weir model tests in Vietnam (2004 to 2010). International Workshop on Labyrinth and Piano Key Weirs, Liège, Belgium..

Kobus H. (1984). Local air entrainment and detrainment. Proc. IAHR Symp. on Scale Effects in Modeling Hydraulic Structures (H. Kobus, ed.) Esslingen, Germany, 4.10: 1-10.

Matos J. & Quintela A. (1994). Discussion of jet flow on stepped weirs. Journal of Hydraulic Engineering, ASCE, Vol. 120, 443-444.

Paternoster C. (1963). Mécanique des fluides, La cinématique des fluides (Tôme 2). Editions Vyncke.

Rutschmann P. (1988). Belüftungseinbauten in Schussrinnen (Aerator devices in spillways). Doctoral Dissertation. Mitteilung N° 97, Versuchsanstalt für Wasserbau, Hydrologie und Glaziologie, ETH Zürich (in German).

Shvainshtein A.M. (1999). Stepped spillways and energy dissipation. Hydrotechnical construction. N°33(5), 275-282.

Silvestri A. (2012). Étude de la dissipation d'énergie sur un coursier en marches d'escalier en aval d'un évacuateur de crue de type PKW. Mémoire de fin d'études. Faculté des sciences appliquées, Université de Liège (URL : http://orbi.ulg.ac.be/retrieve/145402/198658/rapport%20TFE%20v.FINALE.v1.pdf).

Speerli J. (1999). Strömungsprozesse in Grundablasstollen (Flow phenomena in bottom outlets). Doctoral Dissertation. Mitteilung N° 163, Versuchsanstalt für Wasserbau, Hydrologie und Glaziologie, ETH Zürich (in German).

4 Ramps and Fishways

IWLHS, 20-22/02/2013, Aachen - Bung & Pagliara (eds) - © 2013 Bundesanstalt für Wasserbau ISBN 978-3-939230-04-5

In-Situ Measurements on Cross-Bar Block Ramps

M. Oertel

Hydraulic Engineering Section, Civil Engineering Department, FH Lübeck University of Applied Sciences, Full Professor, Prof. Dr.-Ing. habil., Mönkhofer Weg 239, 23562 Lübeck, Germany

ABSTRACT: Cross-bar block ramps can be used to conquer large river bottom steps with adequate flow velocities and water depths. Therefore, the slope will be reduced by arranging several basins with maximum drop heights of 0.2 m. By following general design guidelines acceptable energy dissipation can be achieved and fish climbing is possible. While the flow can be separated into basin, waved and channel flow regimes, the Poleni formula can be used to calculate water depths on the structure for basin flow regimes. With increasing discharges the flow changes into waved and finally into channel flow regime, where an approach using friction factors and the Darcy equation lead to good results for water depths calculations. To validate results for the basin flow regime, a measurement campaign was arranged on three varying cross-bar block ramps structures in North Rhine-Westphalia. The present paper compares example results and gives limiters for measurement purposes.

Keywords: Cross-Bar Block Ramp, in-situ measurement, MID, ADCP, flow regime

1 INTRODUCTION

In the wake of the European Water Framework Directive (EU-WFD 2000) all water bodies with significant anthropogenic impacts have had to be retreated into nature-orientated good ecological conditions. A standard solution for renaturing lateral structures is the arrangement of so called rough ramps or block ramps. Within these structures large boulders and bed roughness dissipate energy and reduce flow velocities, thus increase flow depth. A classification of block ramps can be done into (see Fig. 1)

- block carpets (interlocked blocks or dumbed blocks), and
- block clusters (structured, unstructured or self-structured blocks).

A special case of structured block ramps are so called cross-bar block ramps (Oertel and Schlenkhoff 2012). A step-pool-system reduced the bottom level difference from upstream to downstream while adequate flow velocities occur. Cross-bars are made of huge stones with diameters up to $D_B = 1.5$ m and more. Lower openings within the cross-bars guarantee minimum water depths and fish paths (Figs. 2 and 3). The structures can be arranged over the complete width (Fig. 4) as well as partially (Fig. 5).

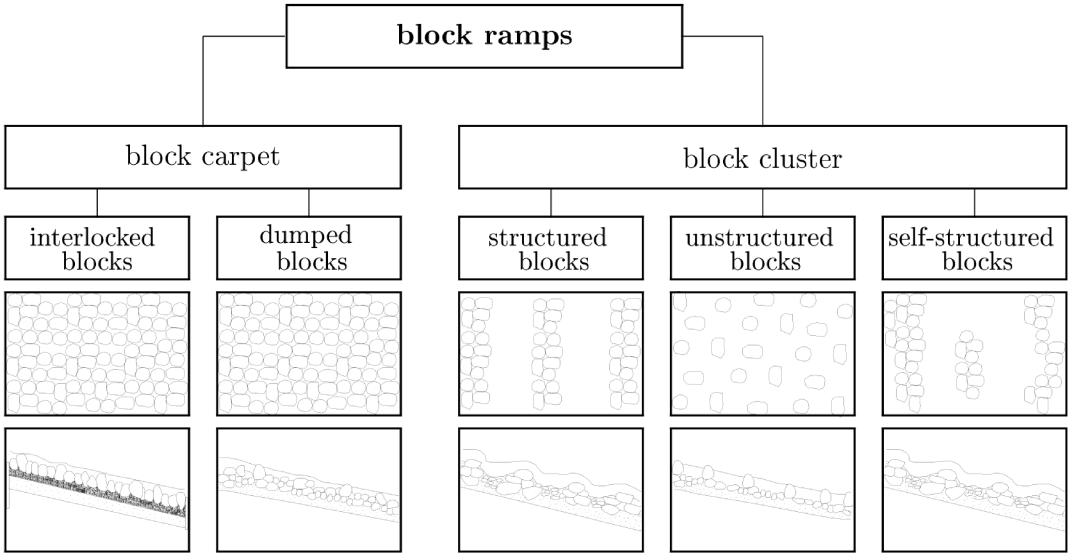

Figure 1. Block ramp design (Oertel 2012, Tamagni et al. 2010).

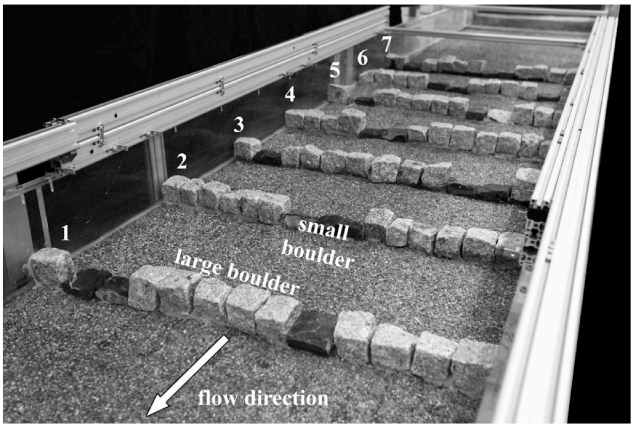

Figure 2. Example cross-bar block ramp model in laboratory, Q = 0 l/s, boulder arrangement (Oertel 2012).

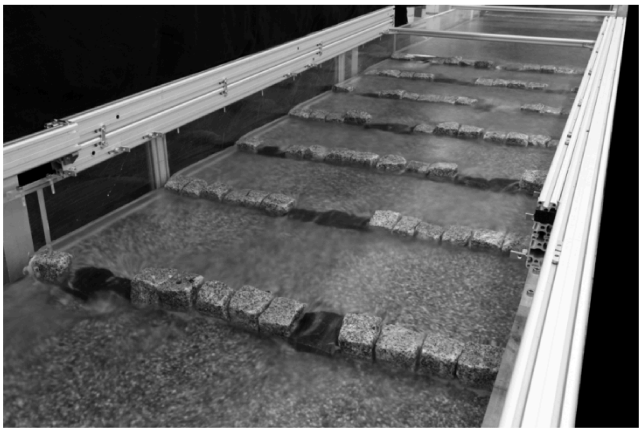

Figure 3. Example Cross-bar block ramp model in laboratory, Q = 5 l/s, basin flow regime (Oertel 2012).

Figure 4. Cross-bar block ramp (River Brückerbach, Düsseldorf, Germany).

Figure 5. Cross-bar block ramp (River Wupper, Wuppertal, Germany).

Current research investigations deal with flow characteristics, stability criteria and ecological aspects. Therefore, physical and numerical models were built up to analyze occurring flow (e. g. Pagliara and Chiavaccini 2006, Pagliara et al. 2008, Oertel and Schlenkhoff 2012, Oertel 2012). Thereby, Oertel (2012) separates three various flow regimes on cross-bar block ramps:

1 basin flow regime ($h < h_B$),
2 waved flow regime ($h_B < h < \sim 1.5h_B$), and
3 channel flow regime ($h > \sim 1.5h_B$),

where h = mean flow depth and h_B = large boulder height. For the basin flow regime the regular Poleni approach lead to acceptable results for flow depth calculations (see DVWK, DWA 2010):

$$Q = \frac{2}{3} C_w C_b C_s \sum W_w \sqrt{2g} h_w^{1.5} \qquad (1)$$

where: Q = discharge, C_w = 0.65 = overfall coefficient, C_b = 0.94 = backwater coefficient, C_s = 1.1 = stone factor, W_w = total opening width small boulders, g = acceleration due to gravity, h_w = overfall height small boulder. If Q increases, the flow changes into the waved flow regime and a research deficit can be identified. For the channel flow regime the water surface slope becomes equal to the bottom slope and flow depth can be calculated by using friction factors (Oertel 2012):

$$\sqrt{\frac{8}{f}} = \left(4.4 + \frac{0.09}{S}\right) \log\left(\frac{h}{h_B}\right) + \left(2.2 - \frac{0.0023}{S}\right) \qquad (2)$$

where: f = friction factor, S = ramp slope. In Eq. (2) h represents the water depth from basin bottom to water surface. Using the Darcy formula lead to mean flow velocities:

$$U = \sqrt{\frac{8}{f}} \sqrt{grS} \qquad (3)$$

where: U = mean flow velocity in x-direction, r = hydraulic radius. Figure 6 give example results for analytical approach, numerical model and laboratory measurements.

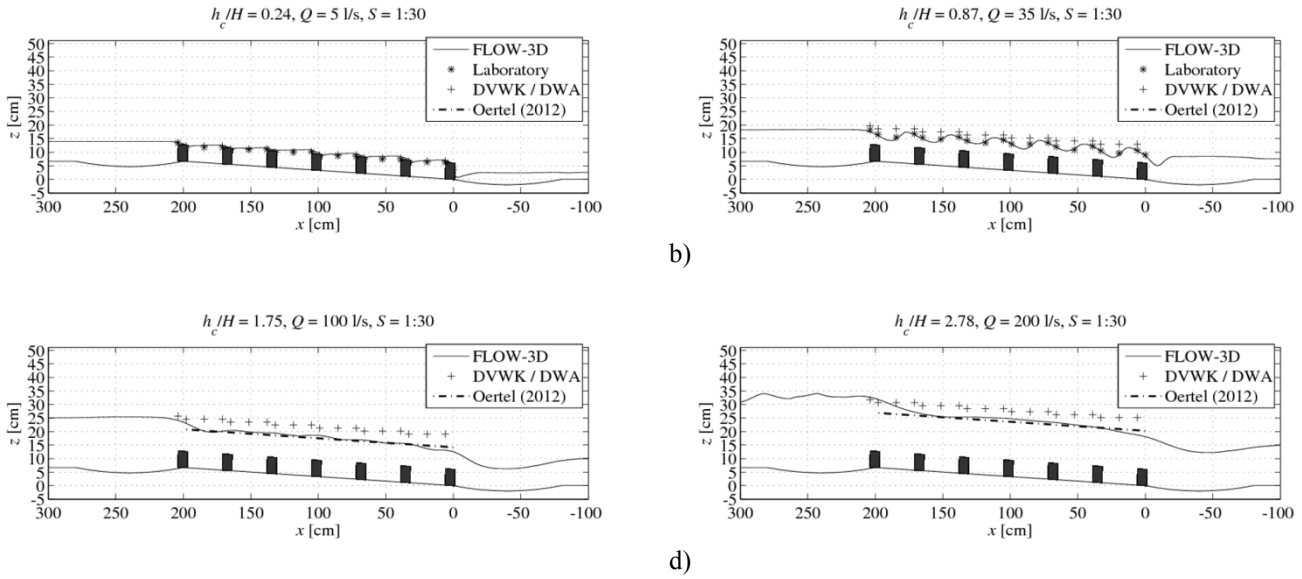

Figure 6. Example results for basin (a), waved (b) and channel (c, d) flow regime (Oertel 2012), with $h_c = (Q^2 g^{-1} b^{-2})^{1/3}$ = critical water depth and H = ramp height.

Generally, scaled physical model results of free surface flow will be transformed into prototype scale via Froude model (USBR 1980). Therefore, main boundary conditions must be considered – e. g. minimum water levels – to obviate scaling effects by surface tension or viscosity. To validate numerical and laboratory results, in-situ measurements will be necessary. It will be difficult to measure in field during flood events, thus to get results for channel flow regime. But for basin flow regime in-situ measurements are possible with adequate complexity. The present paper picks up this requirement and deals with in-situ measurements on cross-bar block ramps.

2 INVESTIGATION PROGRAM AND MEASURMENT TECHNIQUE

2.1 *River Ruhr*

To arrange field measurements on cross-bar block ramps, three varying ramps in North Rhine-Westphalia were selected. The first block ramp is a bypass channel at the River Ruhr next to the Harkort power plant

(Harkort reservoir), see Figs. 7 and 8. The ramp was built in 2004 and designed for Q = 700 l/s. The total length is L = ~375 m, partitioned into 57 basins. The level difference is approx. H = 6.8 m, the width around W = 6.0 m.

Figure 7. Bypass cross-bar block ramp Harkort reservoir (source: www.ruhrverband.de).

Figure 8. Bypass cross-bar block ramp Harkort reservoir, upstream ramp part.

2.2 *River Brückerbach*

The second chosen structure is located in Düsseldorf in the River Brückerbach and represents a cross-bar block ramp over the full channel width (Figs. 9 and 10). The ramp was built in 2009 and is made of 12 cross-bars on a total length of L = 58 m. The resulting basin length is L_b = 3.3 to 5.8 m. The ramp width varies between W = ~9.8 m in the upstream part and W = ~5.0 m in the downstream part.

2.3 *River Wupper*

The third investigated cross-bar block ramp was built in the River Wupper and is designed as a partial ramp (Figs. 11 and 12). The total channel width is ~25.5 m, while the ramp was constructed with a width of W = 10.5 m. The ramp length is L = 20.0 m and the height H = 1.0 m. Hence, the resulting slope is S = 1:20 with a drop of Δh = 0.2 m for each basin. Five cross-bars create L_b = 4.2 m long basins. Large stones are approx. h_B = 1.0 m in height and 0.6 m in width. The total opening width (small boulders) is W_w = ~3.25 m.

Figure 9. Full cross-bar block ramp, Brückerbach, upstream part.

Figure 10. Full cross-bar block ramp, Brückerbach, downstream part.

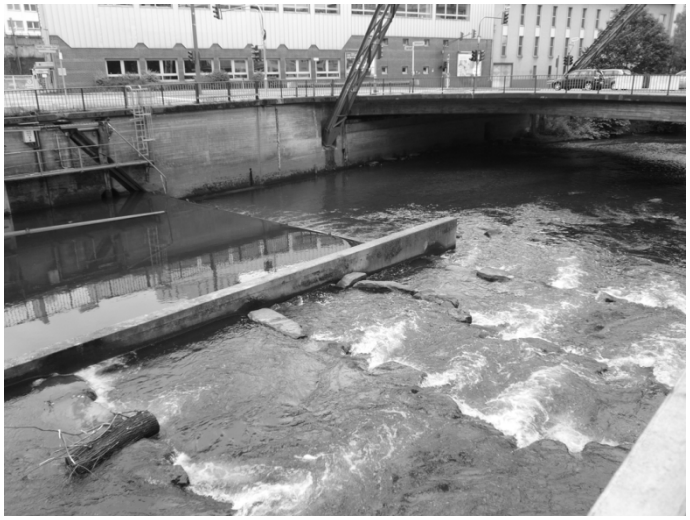

Figure 11. Partial cross-bar block ramp, Wupper.

Figure 12. Partial cross-bar block ramp, Wupper, measurement.

2.4 *Investigation program*

To analyze the flow on the structure, flow depths and flow velocities were measured in selected basins. Therefore, two to three cross-sections were selected (~1.0 m downstream the upstream cross-bar and ~1.0 m upstream the downstream cross-bar, and in between). Figure 13 shows example cross-section measurement points, where flow depths were collected at P1, P2, … , PX. Flow velocities were measured 5 cm under the free surface as well as 5 cm above the basin bottom. Between the water surface and basin bottom velocities were collected with a distance of approx. 20 cm.

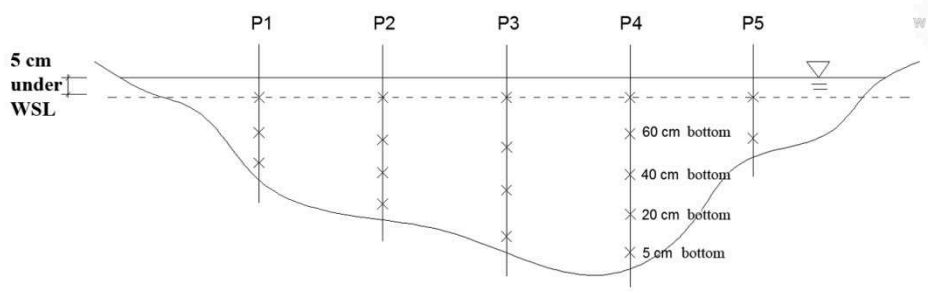

Figure 13. Example cross-section measurement points.

2.5 *Measurement technique*

Flow velocities were measured by using a portable velocity flow meter with electromagnetic sensor. Therefore, the *Flo-Mate 2000* (manufacturer: Hach) was chosen (Fig. 14). It is fully water resistant and the mobile measurement device allows data collection of mean values. Specifications can be found in Morgenschweis (2010).

Within the first basin of the cross-bar block ramp in the River Wupper a mobile Acoustic Doppler Current Profiler (ADCP) measurement was additionally carried out to compare results with those collected by electromagnetic measurements. Therefore, a *StreamPro* (manufacturer: RDI) was placed on a small boat (Fig. 15), which was pulled twice through the cross-section.

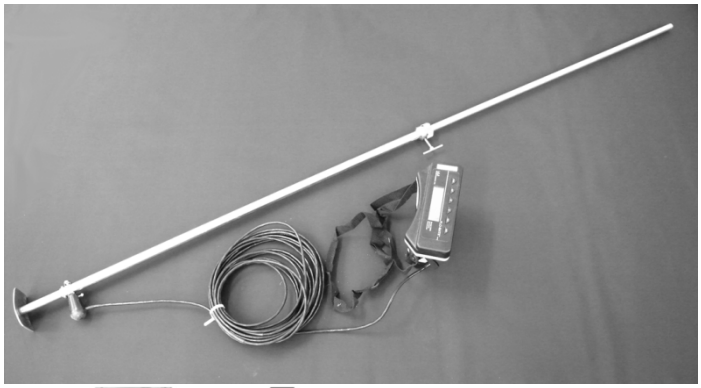

Figure 14. Flo-Mate 2000 MID (Morgenschweis 2004).

Figure 15. StreamPro ADCP.

3 RESULT ANALYSIS

3.1 *Discharge*

In the present paper, results will be presented only for the cross-bar block ramp in the River Wupper. Here, flow velocities determined via electromagnetic sensor will be analyzed in comparison with those measured by ADCP. Measurements were carried out in the first and second upstream basin (see Fig. 5). In both, two cross-sections were selected.

Measurements were carried out 12th June 2012. On that day a discharge of $Q_{river} = 4.0$ m^3/s was measured at gauge Kluserbrücke a few hundred meters upstream the ramp. Since the investigated cross-bar block ramp was partially built up, the flow is separated into the ramp and over the weir. The weir overfall height was measured with $h_w = 0.08$ m. An overfall discharge coefficient of $C_w = 0.8$ lead to the weir discharge $Q_{weir} = 2/3 \cdot C_w \cdot W_{weir} \cdot (2g)^{0.5} \cdot h_w^{1.5} = 2/3 \cdot 0.8 \cdot (25.5–10.5) \cdot (2 \cdot 9.81)^{0.5} \cdot 0.08^{1.5} = 0.80$ m^3/s. A power plant located next to the block ramp continuously extracts $Q_{powerplant} = 1.0$ m^3/s. Another part of the discharge is guided through a bypass ($Q_{bypass} = 0.8$ m^3/s). Hence, the total discharge on the cross-bar block ramp can be assumed as $Q_{ramp} = Q_{river} - Q_{weir} - Q_{bypass} - Q_{powerplant} = 4.0 - 0.8 - 0.8 - 1.0 = 1.4$ m^3/s.

Large boulders are marginally overflown and the lower opening ($h_w = 0.4$ m) represents the main flow area. Hence, using the Poleni formula (Eq. 1) for the given basin flow regime, the discharge can be calculated as:

$$Q_{ramp} = \frac{2}{3} C_w C_b C_s \sum W_w \sqrt{2g} h_w^{1.5} = \frac{2}{3} \cdot 0.65 \cdot 0.94 \cdot 1.1 \cdot 3.25 \cdot \sqrt{2 \cdot 9.81} \cdot 0.4^{1.5} = 1.63 \ \text{m}^3/\text{s}$$

Using the ADCP boat and pulling it twice through the cross-section, a discharge of $Q_{ramp} = 1.45$ m^3/s results. It can be shown, that theoretical approaches, ADCP measurements and gauge measurements give comparable results for discharge amounts on the cross-bar block ramp.

3.2 *Flow velocity*

Sectional flow velocities were measured via electromagnetic sensor. For one profile in the upstream basin, ADCP measurements were additionally carried out. It must be mentioned, that ADCP measurements can only be used if no major air entrainment occurs and a clear water surface is given. Otherwise, signals cannot be processed and errors are resulting. In contrast, MID measurements present the best way to detect flow velocities on these structures, even if air entrainment exists.

Figures 16 and 17 give results for flow velocities within the first two basins. It can be shown, that maximum values reach U = ~1.2 m/s downstream lower openings within the cross-bars. Maximum allowed velocities of U_{max} = 2.0 m/s (DWA 2010) were not detected. Due to displaced lower openings horizontal huge vortexes will be created, leading to negative flow velocities of few centimeters per second. Generally, areas with low flow velocities are created, generating rest areas for fish during climbing.

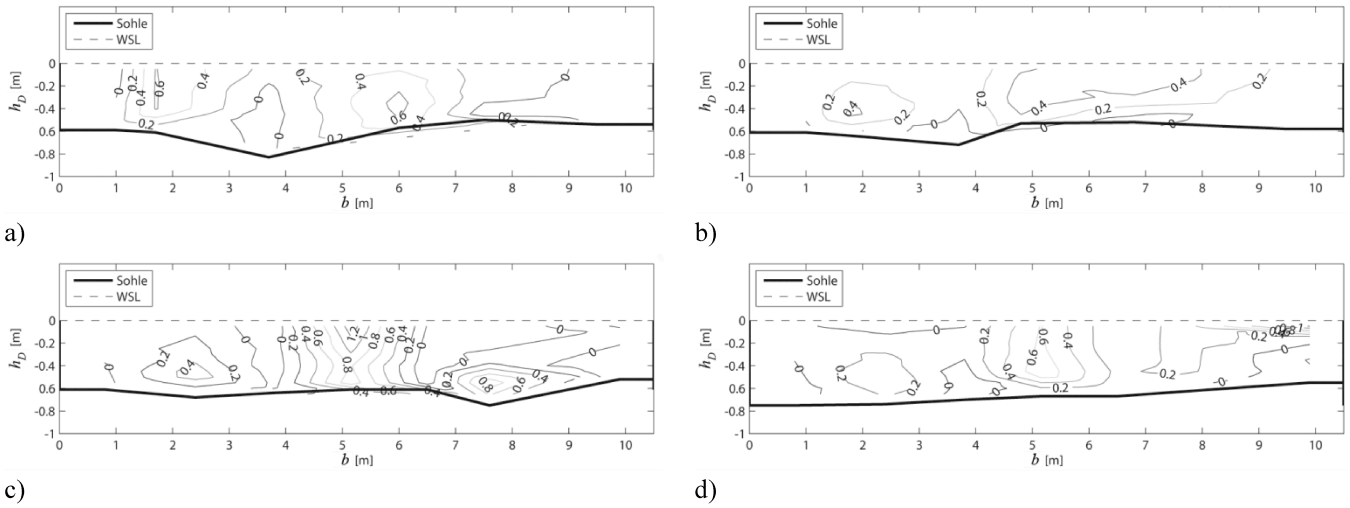

Figure 16. Flow velocities in [m/s] measured with electromagnetic sensor, (a) basin 1, cross-section 1, (b) basin 1, cross-section 2, (c) basin 2, cross-section 1, (d) basin 2, cross-section 2.

Comparing MID results with those determined by ADCP measurement (Fig. 18), a basically good agreement can be found. This was also confirmed by discharge measurements, where velocity profiles will be integrated over the flow area (see Section 3.1). Main differences come by averaging values from MID measurements. Here, the ramp bottom as well as ramp banks will not be detected exactly. Thus, Fig. 18 shows displaced minimum bottom depths over the width. Problems of ADCP measurements can be assumed due to negative flow velocities. Since negative values are very small, these were not reproduced well.

Summarizing, MID measurements represents a state-of-the-art solution for in-situ measurements on block ramps. Neither air entrainment nor huge flow velocities will influence measuring accuracy. Hence, MID sensors should be preferred for these structures.

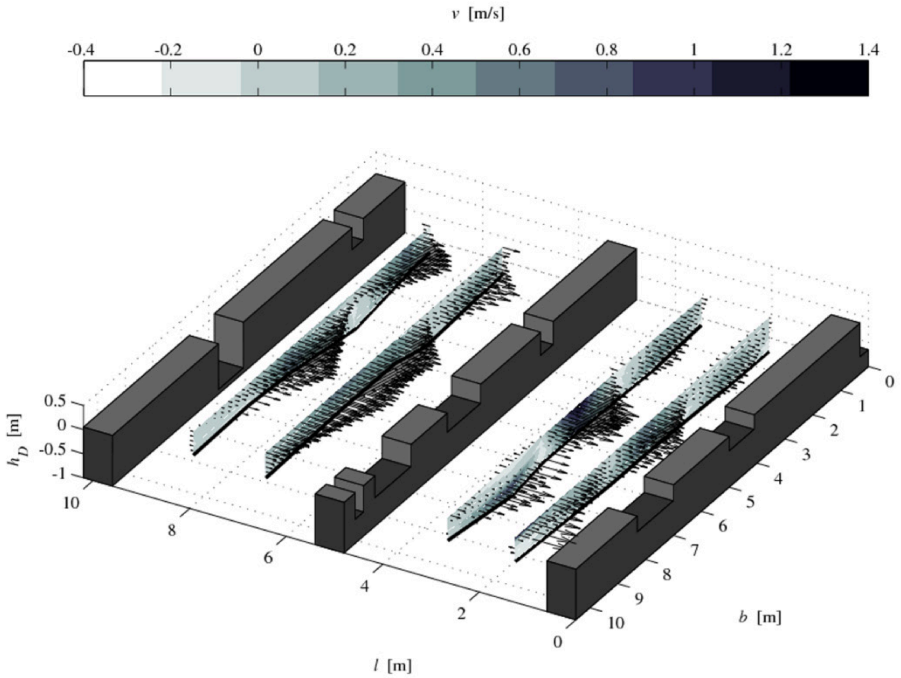

Figure 17. Flow velocities in [m/s], three dimensional view of all four measured cross-sections.

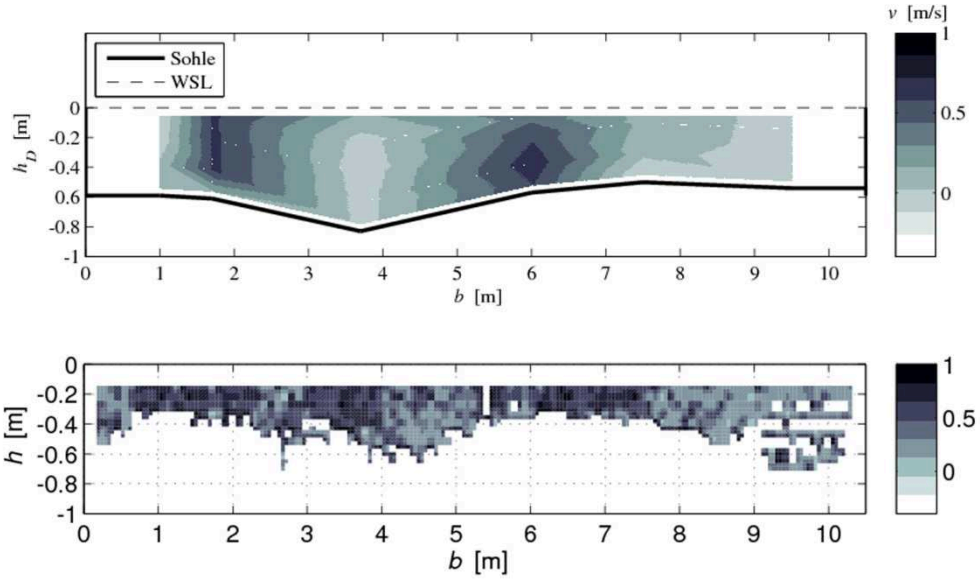

a)

b)

Figure 18. Comparison of flow velocities measured via electromagnetic sensor (a) and via ADCP (b).

4 SUMMARY AND CONCLUSION

4.1 *General*

Cross-bar block ramps separate large river bottom steps into several basins with adequate flow velocities and flow depths concerning fish climb capabilities. Hydraulic phenomena on those structures were frequently investigated during the last years. Formulas for flow resistance and energy dissipation were developed and flow regimes were defined as basin flow, waved flow, and channel flow. Usually, the basin flow regime occurs and flow depth calculations can be done by using the regular Poleni approach. For flood events the free water surface slope equals the ramp slope and developed friction factors lead to acceptable results. The waved flow regime is still investigated since a research leakage can be identified.

In-situ measurements confirm the applicability of the Poleni formula. Water depths within the basins can be described well. But for detailed flow velocity distribution in-situ measurements or numerical simulations are necessary. The present paper deals with in-situ measurements on cross-bar block ramps and results for an exemplary structure were presented.

4.2 *Outlook*

Further in-situ investigations will be necessary to confirm those approaches using friction factors for the channel flow regime during flood events. Collected data are rare, because measurements will be very difficult to arrange. Huge flow velocities and flow depths on the structure will increase the risk of measuring significantly. Hence, new ideas for measurement facilities are necessary.

NOTATION

C_w	overfall coefficient
C_b	backwater coefficient
C_s	stone factor
D_B	boulder diameter
f	friction factor
g	acceleration due to gravity
h	mean flow depth
h_c	critical water depth = $(Q^2 g^{-1} b^{-2})^{1/3}$
h_B	large boulder height
h_w	overfall height small boulder
H	ramp height
L	ramp length

L_b basin length
Q discharge
r hydraulic radius
S ramp slope
U mean flow velocity in x-direction
W ramp width
W_w total opening width small boulders

REFERENCES

DWA (2010). Fischaufstiegsanlagen und fischpassierbare Bauwerke – Gestaltung, Bemessung, Qualitätssicherung. DWA-M 509, Deutsche Vereinigung für Wasserwirtschaft, Abwasser und Abfall e. V., Hennef, Germany, in German.

Morgenschweis, G. (2004). Mobiler Einsatz von MID-Sonden. Proceedings Seminar „Neue Entwicklungen der Durchflussmessung in natürlichen und künstlichen Gerinnen“, 11th–12th March 2004, TU München. ATV-DVWK: Hennef, Germany [in German].

Morgenschweis, G. (2010). Hydrometrie – Theorie und Praxis der Durchflussmessung in offenen Gerinnen, Springer, Berlin, Germany [in German].

Oertel, M. (2012). Cross-Bar Block Ramps – Flow Regimes, Flow Resistance, Energy Dissipation, Stability. Habilitation Thesis, Bergische University of Wuppertal, Germany.

Oertel, M., Schlenkhoff, A. (2012). Crossbar Block Ramps – Flow Regimes, Energy Dissipation, Friction Factors, and Drag Forces. Journal of Hydraulic Engineering, ASCE, 138(5), pp. 440-448.

Pagliara, S, Chiavaccini, P. (2006) Energy Dissipation on Block Ramps. Journal of Hydraulic Engineering, ASCE, 132(1), pp. 41-48.

Pagliara, S., Das, R. Palermo, M. (2008). Energy Dissipation on Submerged Block Ramps. Journal of Irrigation and Drainage Engineering, ASCE, 134(4), pp. 527-532.

Tamagni, S., Weitbrecht, V., Boes, R. (2010). Design of unstructured block ramps – a state of the art review. Proceedings River Flow, Braunschweig, Germany, pp. 729-736.

USBR (1980). Hydraulic Laboratory Techniques. United States Department of the Interior, Water and Power Resources Service, Denver, Colorado, USA.

IWLHS, 20-22/02/2013, Aachen - Bung & Pagliara (eds) - © 2013 Bundesanstalt für Wasserbau ISBN 978-3-939230-04-5

Analysis of Chosen Hydraulic Parameters of a Rapid Hydraulic Structure (RHS) in Porębianka Stream, Polish Carpathians

A. Radecki-Pawlik & K. Plesiński
New Department of Hydraulic Engineering and Geotechnique
University of Agriculture in Kraków, Poland

B. Wyżga
Institute of Nature Conservation, Polish Academy of Sciences, Kraków, Poland

ABSTRACT: Application of grade correction of a channel using rapid hydraulic structures (RHS) is a new tendency in modern river training. These structures meet both technical and ecological requirements. They decrease the longitudinal slope of the stream, differentiate the flow regime and dynamics, recreate the braided pattern of the channel and do not stop the migration of fish and macroinvertebrates. Moreover, they mimic a pool and riffle channel morphology and thus conform with the requirements of the Water Framework Directive of the EU. In this paper, we analyse chosen hydraulic parameters of a rapid hydraulic structure constructed in a gravel-bed Porębianka Stream, Polish Carpathians.

Keywords: rapid hydraulic structure (RHS), hydrodynamic parameters, shear stress, velocity

1 INTRODUCTION

Pool and riffle morphology is one of a few channel pattern types found in mountain watercourses (Montgomery, Buffington 1997) and the one typical of inhabited, lower sections of mountain and piedmont valleys. Pool-riffle sequences occur with an average spacing of five to seven times the channel width (Gregory et al. 1994) and the regular downstream variability in bed morphology is associated with that in bed-material size, with coarser material forming the bed on riffles than in pools (Keller 1971, Milne 1982). According to the velocity reversal hypothesis (Keller 1971), the areal sorting of bed material in pool-riffle sequences reflects different patterns of flow velocity at discharges lower and higher than bankfull. Further studies confirmed the hypothesis, indicating that not only the zones of different velocity but also those of bed shear stress and unit stream power in pool-riffle sequences reverse as flow increases (e.g. Teisseyre 1984, Radecki-Pawlik 2002). The differentiation of channel bed into pools and riffles exerts a remarkable influence on physical and biotic patterns in mountain river channels. Areas with different hydrodynamic conditions along pool-riffle sequences provide habitats for varied benthic invertebrate communities (Pastuchová et al. 2008), with riffles supporting the communities especially rich in rheophilic taxa. The undulated morphology of streambeds enables the exchange of water between river channel and hyporheic zone, crucial to provide oxygen for incubating eggs and larvae of lithophilic fish spawning in river gravels (Boulton 2007).

In modern river engineering there is often a need to construct hydraulic structures which mimic the geometry of natural riffles, while protecting river bed against erosion, directing flow and reducing slope of the channel bed. Such structures are rapid hydraulic structures (called later along that paper RHS) with artificial roughness provided by the stones installed along the slope apron. In some countries such structures are called ramps. Hydrodynamic conditions of the flow conveyed over RHS are similar to those typifying natural riffles. RHS resemble natural riffles also in their high spatial diversity of hydraulic conditions (Radecki-Pawlik et al. 2010), a key factor in creating heterogeneity of physical habitat conditions for benthic invertebrate fauna (Kłonowska-Olejnik, Radecki-Pawlik 2000, Zasępa et al. 2006). The aim of this paper is to analyse chosen hydraulic parameters of a rapid hydraulic structure constructed in a gravel-bed Porębianka Stream, Polish Carpathians.

2 STUDIED STREAM AND FLOW CONDITIONS DURING MEASUREMENTS

Porębianka Stream is a 15.4 km long, 4th-order stream draining a flysch part of the Polish Carpathians. The area of its catchment amounts to 72 km^2, and the width of the channel varies from 1 m at the headwater part of the stream to 140 m at the mouth stretch. Average channel slope equals 56.9‰ (Korpak 2008). Hydrological characteristics of Porębianka were determined on the basis of records at a gauging station located in the middle course of the stream. The present morphology of the Porębianka channel is influenced by check-dams, with channel incision occurring downstream and bed aggradation upstream of the dams (Kościelniak 2004, Korpak 2007). Nowadays, the stream has a single, narrow and winding channel. At the beginning of the twentieth century the stream flowed in a a multi-thread channel. Later its channelization was carried out, with the stream course partitioned by check-dams, weirs and rapid hydraulic structures (ramps) and channel banks reinforced with riprap, gabions and retaining walls (Kościelniak 2004, Korpak et al. 2008). In the lower course of the stream, a grade correction with 25 rapid hydraulic structures (RHS) of high roughness was applied. While reducing channel slope, the structures operate similar to natural riffles and promote accumulation of bed material between them. The paper aims at the analysis of hydraulic parameters in the vicinity of one of the RHS.

Field measurements were made in three series in: April, June and October 2010. At the first series, the measurements were performed during the spring thaw, at the flow of $Q = 2.25\ m^3 \cdot s^{-1}$, higher than mean annual discharge $SSQ = 1.32\ m^3 \cdot s^{-1}$. Between the first and the second series of measurements, a flood with the discharge $Q = 55\ m^3 \cdot s^{-1}$ occurred. During the second series, the discharge amounted to $Q = 2.40\ m^3 \cdot s^{-1}$ and was also higher than the mean. This elevated flow was caused by long-lasting rainfall that occurred in May and at the beginning of June 2010. In October low flows occurred, reflecting low precipitation in the autumn. The discharge equalled then $Q = 1.15\ m^3 \cdot s^{-1}$.

3 METHODOLOGY

One of the rapid hydraulic structures of high roughness in Porębianka Stream was chosen for detailed investigations (Fig. 1). Velocity measurements were carried out upstream and downstream of the structure in the area of its influence and on the ramp itself. Depending on the configuration of channel bed and water stage, measurements were made at 63 measurement points in the first series, at 57 in the second one and at 37 in the third one (Fig. 2).

Figure 1. Studied rapid hydraulic structure (RHS) in Porębianka Stream

Momentary flow velocity was measured with OTT Nautilus 2000 electromagnetic current meter. Based on the measurements, velocity curves were drawn for the velocities over individual measurement points. The momentary flow velocity measurements made it possible to determine the following parameters: depth-averaged velocity, dynamic velocity, Reynolds number (vertical and so called particle one), Froude number, shear stress, Shields parameter.

The value of dynamic velocity was calculated from the velocity profile using the formula (1) (Gordon et al. 2007):

$$v_* = \frac{a}{5.75} \ [\mathrm{m \cdot s^{-1}}] \qquad (1)$$

where a is slope of the straight line v = f(h).

The calculated value of the dynamic velocity was used to determine the drag force acting on the channel bed, that is tangential stress, according to the formula (2):

$$\tau = \rho \cdot (v_*)^2 \ [\mathrm{N \cdot m^{-2}}] \qquad (2)$$

where $\rho = 1000$ kg $\cdot$ m^{-3} is water density.

Froude numbers at average and maximum depth were determined according to the formula (3):

$$\mathrm{Fr} = \frac{v}{\sqrt{gh}} \ [-] \qquad (3)$$

where v is flow velocity [m $\cdot$ s^{-1}], h is water depth [m], and g is gravitational acceleration [m $\cdot$ s^{-2}]. The obtained values of Fr showed whether the measurement was made in the layer of supercritical flow, subcritical flow and/or critical flow, with the critical Fr value equal 1.

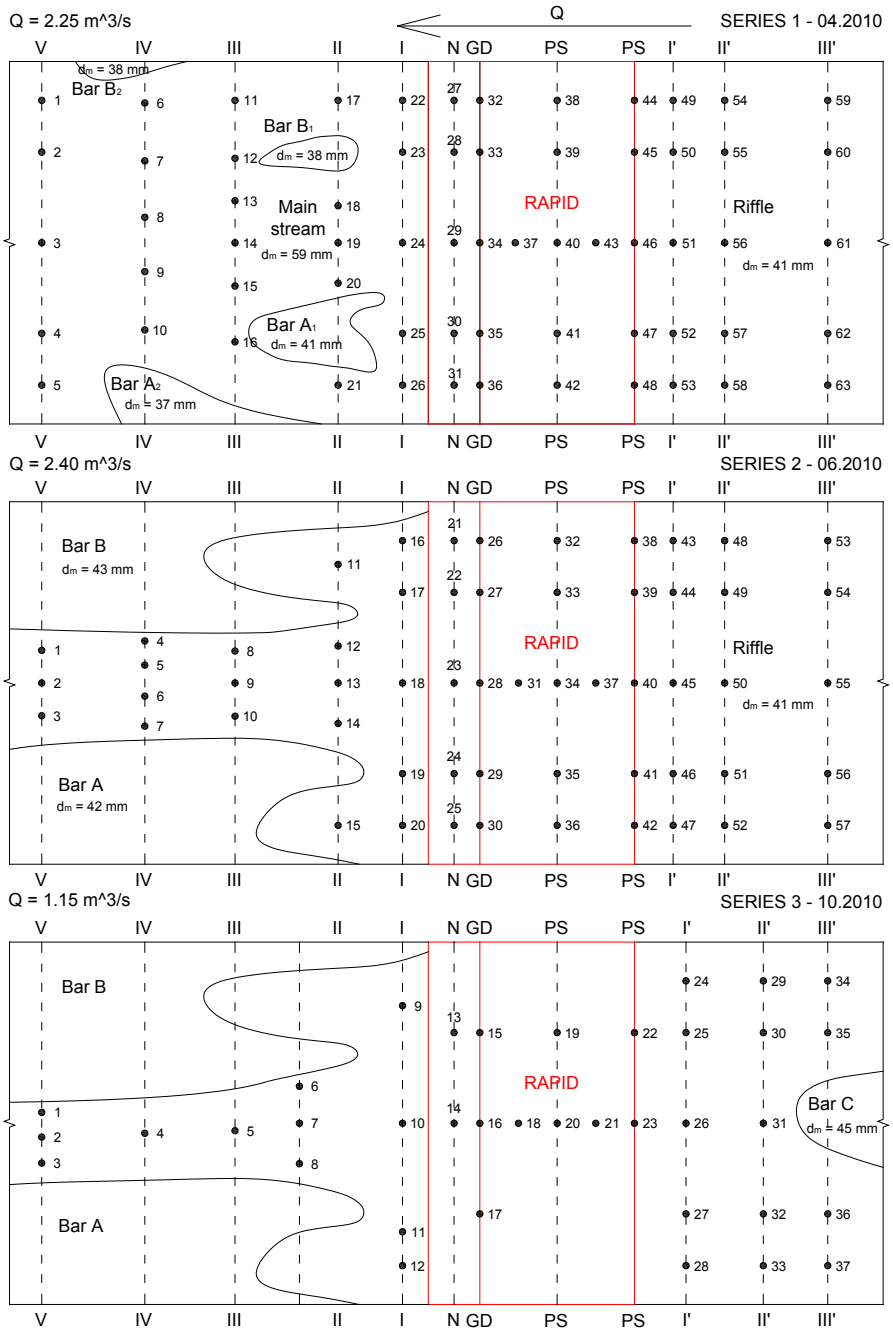

Figure 2. Arrangement of measurement points.

Reynolds numbers were obtained from the formula (4):

$$Re = \frac{v \cdot d}{\nu} \; [-] \qquad (4)$$

where v is flow velocity [m · s^{-1}], d is water depth or the diameter of grains on the bed surface [m], and ν is the coefficient of kinetic viscosity [m^2 · s].

Grain size of the bed material on bars and riffles was also measured. Surface bed material was sampled using the transect Wolman's method (Wolman 1954) and the effective grain sizes were calculated based on the measurements.

4 RESULTS AND DISCUSSION

Table 1 presents the results of hydrodynamic calculations based on data obtained in April 2010. The dynamic velocities and tangential stresses below the rapid hydraulic structure reached the highest values in the cross section "I – I", amounting to 0.029 m · s^{-1} and 0.86 N · m^{-2}, respectively. It reflected high velocity (v_{av} = 0.540 m · s^{-1}) and turbulence of the water flowing down the ramp and out of the energy-dissipating pool of the structure. Moreover, the highest values of the dynamic velocity and shear stresses occurred in the middle part of the channel (points 8, 13, 19). Reynolds numbers indicated that in all the measurement points flow was turbulent. The Froude numbers higher than 1 indicated the occurrence of supercritical flow on the ramp and in the middle part of the energy-dissipating pool.

Table 1: Hydrodynamic parameters (series 1).

Cross-section	Point number	h [m]	$v_{śr}$ [m · s^{-1}]	v_* [m · s^{-1}]	τ [N · m^{-2}]	Re [-]	Re_* [-]	Fr [-]	Fr_* [-]
V – V	1	0.04	0.036	0.007	0.05	1101	1065	0.06	0.005
	2	0.20	0.460	0.009	0.08	70331	1356	0.33	0.007
30 m downstream of the pool	3	0.12	0.352	0.003	0.01	32291	544	0.32	0.002
	4	0.18	0.470	0.012	0.14	64674	2472	0.35	0.007
	5	0.10	0.420	0.007	0.05	10091	1474	0.42	0.004
IV – IV	6	0.05	0.264	0.004	0.02	10091	503	0.38	0.003
	7	0.19	0.710	0.009	0.09	103127	1168	0.52	0.007
22 m downstream of the pool	8	0.20	0.450	0.012	0.15	68802	2523	0.32	0.007
	9	0.13	0.402	0.006	0.04	39951	755	0.36	0.005
	10	0.13	0.396	0.005	0.03	39355	656	0.35	0.004
III – III	11	0.08	0.264	0.005	0.03	16146	691	0.30	0.004
	12	0.05	0.302	0.016	0.26	11543	2019	0.43	0.013
15 m downstream of the pool	13	0.27	0.402	0.009	0.08	82975	1869	0.25	0.005
	14	0.22	0.650	0.017	0.29	109319	3575	0.44	0.010
	15	0.19	0.460	0.003	0.01	66814	343	0.34	0.002
	16	0.05	0.105	0.003	0.01	4013	363	0.15	0.002
II – II	17	0.20	0.212	0.003	0.01	32413	396	0.15	0.002
	18	0.23	0.354	0.014	0.20	62243	2962	0.24	0.009
8 m downstream of the pool	19	0.48	0.324	0.018	0.31	118890	3655	0.15	0.011
	20	0.45	0.334	0.011	0.13	114899	2366	0.16	0.007
	21	0.09	0.044	0.001	0.01	3027	215	0.05	0.001
I – I	22	0.35	0.338	0.009	0.08	90437	1142	0.18	0.007
	23	0.12	0.113	0.007	0.05	10366	903	0.10	0.006
4 m downstream of the pool	24	0.53	0.640	0.029	0.86	259307	6115	0.28	0.033
	25	0.19	0.101	0.004	0.02	14670	617	0.07	0.003
	26	0.09	0.216	0.011	0.13	14861	1653	0.23	0.008
N centre of the energy-dissipating pool	27	0.10	0.460	0.008	0.06	35166	2057	0.46	0.004
	28	0.13	0.400	0.010	0.11	39752	2769	0.35	0.006
	29	0.10	1.740	0.053	2.85	133017	14276	1.76	0.029
	30	0.15	0.206	0.010	0.10	23622	2685	0.17	0.005
	31	0.12	0.530	0.009	0.07	48620	2285	0.49	0.005
GD lower concrete sill of the RHS	32	0.08	0.630	0.003	0.01	38529	805	0.71	0.002
	33	0.04	1.480	0.012	0.14	45256	3215	2.36	0.006
	34	0.10	2.160	0.040	1.61	165125	10730	2.18	0.022
	35	0.03	0.840	0.013	0.18	19265	3564	1.55	0.007
	36	0.03	0.470	0.003	0.01	10779	870	0.87	0.002

Cross-section	Point number	h [m]	$v_{śr}$ [m · s^{-1}]	v_* [m · s^{-1}]	τ [N · m^{-2}]	Re [-]	Re_* [-]	Fr [-]	Fr_* [-]
PS	37	0.14	2.380	0.024	0.58	254721	6422	2.03	0.013
	38	0.08	1.150	0.009	0.08	70331	2382	1.30	0.005
ramp	39	0.08	1.140	0.008	0.06	69719	2089	1.29	0.004
of the RHS	40	0.10	2.450	0.036	1.28	187295	9567	2.47	0.019
	41	0.05	0.254	0.009	0.08	9709	2401	0.36	0.005
	42	0.03	0.950	0.009	0.08	21787	2382	1.75	0.005
	43	0.10	2.270	0.034	1.16	173534	9097	2.29	0.018
GG	44	0.05	0.540	0.014	0.19	41205	3704	0.77	0.007
	45	0.04	0.320	0.007	0.04	7935	1778	0.51	0.004
upper concrete sill	46	0.17	0.920	0.022	0.51	119563	6017	0.71	0.012
of the RHS	47	0.03	0.346	0.003	0.01	9785	870	0.64	0.002
	48	0.07	0.770	0.004	0.01	20641	1010	0.93	0.002
I' – I'	49	0.12	0.360	0.010	0.09	33025	1272	0.33	0.007
	50	0.10	0.212	0.038	0.01	18729	498	0.25	0.005
4 m	51	0.16	0.460	0.008	0.06	56265	1651	0.37	0.005
upstream	52	0.10	0.245	0.004	0.01	18729	524	0.25	0.003
of the RHS	53	0.12	0.185	0.002	0.005	16971	256	0.17	0.001
II' – II'	54	0.17	0.420	0.011	0.12	54583	1455	0.33	0.009
	55	0.14	0.410	0.011	0.13	43880	1489	0.35	0.009
8 m	56	0.17	0.530	0.017	0.31	68879	3651	0.41	0.011
upstream	57	0.06	0.161	0.005	0.03	7385	688	0.21	0.004
of the RHS	58	0.16	0.109	0.007	0.04	12499	909	0.09	0.005
III' – III'	59	0.07	0.010	0.001	0.005	535	43	0.01	0.001
	60	0.30	0.500	0.003	0.01	114670	385	0.29	0.002
15 m	61	0.14	0.396	0.010	0.10	42382	1304	0.34	0.008
upstream	62	0.12	0.220	0.0003	0.001	20182	45	0.20	0.001
of the RHS	63	0.05	0.224	0.005	0.03	8562	707	0.32	0.004

The highest values of depth-averaged velocity were recorded on the ramp of the structure in its central, lowered part, causing concentration of the flow. At points: 34, 37, 40 and 43, the velocities were above 2.00 m · s^{-1} (maximum 2.45 m · s^{-1} at point 40). Also in the energy-dissipating pool and in the marginal parts of the ramp, the velocities were quite high, amounting to 1.00–2.00 m · s^{-1}. At point 29 (in the central part of the energy-dissipating pool) the highest values of depth-averaged velocity and bed shear stress were observed, amounting to 0.053 m · s^{-1} and 2.85 N · m^{-2}, respectively. Also above, in the central, lowered part of the ramp (points 34, 40, 43), high values of shear stress (1.16–1.61 N · m^{-2}) were recorded. Among all the measurement points on the rapid hydraulic structure, the lowest values of tangential stress (0.01–0.51 N · m^{-2}) were those recorded on the upper concrete sill. The highest value of Froude number, 2.47, was recorded at point 40 (the middle of the ramp in its central, lowered part). Subcritical flow over the structure occurred at the points situated on the upper sill and at the marginal parts of the lower sill and the energy-dissipating pool.

Table 2: Hydrodynamic parameters (series 2).

Cross-section	Point number	h [m]	$v_{śr}$ [m · s^{-1}]	v_* [m · s^{-1}]	τ [N · m^{-2}]	Re [–]	Re_* [–]	Fr [–]	Fr_* [–]
V – V	1	0.40	0.780	0.014	0.20	238514	2060	0.39	0.010
30 m downstream	2	0.44	0.760	0.026	0.69	255638	5462	0.37	0.016
	3	0.30	0.530	0.031	0.94	121550	4350	0.31	0.023
IV – IV	4	0.05	0.264	0.028	0.77	10091	4090	0.38	0.020
22 m	5	0.50	0.780	0.024	0.58	298142	5005	0.35	0.015
downstream	6	0.28	0.570	0.017	0.28	122009	3513	0.34	0.010
of the pool	7	0.10	0.248	0.008	0.06	18959	1085	0.25	0.006
III – III	8	0.50	0.430	0.021	0.43	164361	3063	0.19	0.015
15 m	9	0.76	0.520	0.019	0.37	302118	4029	0.19	0.012
downstream	10	0.36	0.390	0.027	0.73	107331	3840	0.21	0.020
II – II	11	0.44	0.045	0.002	0.005	15136	250	0.02	0.002
	12	0.40	0.270	0.020	0.41	82562	4218	0.14	0.012
8 m	13	0.83	0.960	0.026	0.74	609128	12083	0.34	0.035
downstream	14	0.12	0.158	0.006	0.03	14494	1234	0.15	0.004
of the pool	15	0.50	0.074	0.011	0.13	28285	1261	0.03	0.009

Cross-section	Point number	h [m]	$v_{śr}$ [m · s^{-1}]	v_* [m · s^{-1}]	τ [N · m^{-2}]	Re [–]	Re_* [–]	Fr [–]	Fr_* [–]
I – I	16	1.05	0.010	0.001	0.001	8027	131	0.01	0.001
	17	0.16	0.128	0.008	0.06	15656	901	0.10	0.007
4 m	18	0.60	1.120	0.030	0.87	513722	6167	0.46	0.018
downstream	19	0.09	0.042	0.006	0.04	2890	698	0.04	0.005
of the pool	20	0.94	0.148	0.007	0.04	106353	737	0.05	0.005
N	21	0.10	0.770	0.016	0.27	58864	4388	0.78	0.009
centre of the	22	0.14	0.650	0.028	0.81	69567	7594	0.55	0.015
energy-dissipating	23	0.18	2.100	0.050	2.48	288969	13313	1.58	0.027
pool	24	0.15	0.330	0.009	0.07	37841	2308	0.27	0.005
	25	0.05	0.780	0.015	0.23	29814	4081	1.11	0.008
GD	26	0.08	0.770	0.006	0.04	47091	1661	0.87	0.003
	27	0.06	1.420	0.013	0.16	65133	3402	1.85	0.007
lower concrete sill	28	0.12	2.860	0.069	4.82	262365	18585	2.64	0.037
of the RHS	29	0.03	0.680	0.011	0.11	15595	2834	1.25	0.006
	30	0.06	0.860	0.012	0.15	39447	3257	1.12	0.007
PS	31	0.12	2.050	0.038	1.45	94030	10181	2.67	0.021
	32	0.08	0.960	0.013	0.16	58711	3360	1.08	0.007
ramp	33	0.08	1.140	0.040	1.57	69719	10605	1.29	0.021
of the RHS	34	0.10	1.980	0.051	2.59	105955	13615	2.39	0.027
	35	0.05	1.040	0.044	1.97	39752	11871	1.48	0.024
	36	0.05	0.930	0.025	0.60	35548	6566	1.33	0.013
	37	0.15	1.560	0.045	2.04	178885	12071	1.29	0.024
GG	38	0.08	0.870	0.014	0.20	53207	3820	0.98	0.008
	39	0.06	0.660	0.007	0.04	30273	1778	0.89	0.004
upper concrete sill	40	0.20	1.070	0.034	1.12	163596	8967	0.76	0.018
of the RHS	41	0.05	0.600	0.012	0.15	22934	3267	0.86	0.007
	42	0.05	0.570	0.007	0.06	21787	2006	0.81	0.004
I' – I'	43	0.21	0.400	0.024	0.56	64215	4954	0.28	0.015
	44	0.14	0.169	0.008	0.06	18087	1582	0.14	0.005
4 m	45	0.32	0.690	0.018	0.31	168794	3677	0.39	0.011
upstream	46	0.14	0.368	0.015	0.23	39385	3147	0.31	0.009
of the RHS	47	0.12	0.164	0.009	0.08	15045	1898	0.15	0.006
II' – II'	48	0.24	0.540	0.025	0.62	99075	5201	0.35	0.015
	49	0.10	0.330	0.012	0.13	25227	2425	0.33	0.007
8 m	50	0.20	0.530	0.015	0.23	81034	3194	0.38	0.009
upstream	51	0.15	0.246	0.012	0.15	28209	2515	0.20	0.007
of the RHS	52	0.12	0.152	0.008	0.06	13944	1670	0.14	0.005
III' – III'	53	0.28	0.680	0.012	0.14	145555	1592	0.41	0.009
	54	0.11	0.400	0.038	1.45	33637	5193	0.39	0.029
15 m	55	0.20	0.600	0.023	0.51	91736	4729	0.43	0.014
upstream	56	0.16	0.264	0.020	0.40	32291	2722	0.21	0.015
of the RHS	57	0.12	0.344	0.019	0.36	31557	2594	0.32	0.014

Table 2 presents hydrodynamic parameters determined during the second series of measurements in June 2010. During the flood in May 2010, the channel changed its geometry. Directly downstream of the RHS (cross-section "I – I"), pools formed at both sides of the channel (0.94 m and 1.05 m deep), with low values of depth-averaged velocity (0.148 m · s^{-1} and 0.010 m · s^{-1} for the right and left pool, respectively) and tangential stress (0.001 – 0.005 N · m^{-2} for the right pool and 0.04 – 0.13 N · m^{-2} for the left one). Downstream of the structure, dynamic velocity attained the highest values of the 0.026–0.031 m · s^{-1} and shear stress those of 0.69 – 0.94 N · m^{-2}. Closer to the banks, where the flow velocity was lower, the values of shear stress were lower than in the middle part of the channel (0.13 – 0.62 N · m^{-2}). Turbulent and subcritical flow occurred at all investigated points.

The highest values of depth-averaged velocity, 2.86 m · s^{-1}, and shear stress, 4.82 N · m^{-2}, were recorded on the lower sill (point 28). At the majority of the remaining points, high values of tangential stress occurred as well (2.48 at point 23 in the energy-dissipating pool, 1.45, 1.57, 2.59, 1.97 and 2.04 N · m^{-2} respectively at points 31, 33, 34, 35, 37 on the ramp and 1.12 N · m^{-2} at point 40 on the upper sill). The high values of this parameter are connected with the high values of depth-averaged and dynamic velocity, and the large water turbulence. Such conditions on the RHS were created pools to the lowering applied in

order to concentrate the stream. In the energy-dissipating pool, supercritical flow occurred only at two points (23, 25), at the remaining ones subcritical flow occurred.

Upstream of the structure, depth-average velocity varied between 0.164 and 0.690 $m \cdot s^{-1}$, dynamic velocity was in the range of 0.008 –0.038 $m \cdot s^{-1}$, and tangential stress – 0.06 – 0.62 $N \cdot m^{-2}$. Here, the highest value of the stress, 1.45 $N \cdot m^{-2}$, was recorded at point 54.

The whole set of hydrodynamic data collected during the third series of measurements is not presented in the paper but their analysis is presented below. Directly downstream of the RHS (cross-section "I – I"), further scour of the pools occurred between the second and the third series of measurements. In spite of the low water level, their depth increased (right pool) or remained the same (left pool) in comparison with the series 2. Now the smallest values of dynamic velocity and tangential stress occurred at the pools, and they equalled 0.001 $m \cdot s^{-1}$ and 0.001 $N \cdot m^{-2}$, respectively, for both pools. At the remaining points downstream of the structure, the values of tangential stress were lower than during the second series, which is connected with the lower discharge and and dynamic velocity. Here, the highest values of shear stress (0.38 $N \cdot m^{-2}$ at point 10 and 0.32 $N \cdot m^{-2}$ at point 4) were recorded in the thalweg. Turbulent flow occurred at all points except the pools in which transitional flow was observed. At all points below the structure, the Froude number was below 1, so the subcritical flow occurred. The highest depth-averaged velocity was recorded at point 18 (2.16 $m \cdot s^{-1}$) and point 20 (2.23 $m \cdot s^{-1}$). The highest dynamic velocity and tangential stress occurred on the lower sill and in the central, lowered part of the ramp, amounting to 0.062 $m \cdot s^{-1}$ and 3.90 $N \cdot m^{-2}$, respectively. At the remaining measurement points, the stress values varied between 0.21 and 0.91 $N \cdot m^{-2}$. The exception was point 24 in the energy-dissipating pool, where the value of this parameter equalled 0.03 $N \cdot m^{-2}$. The Reynolds number showed the occurrence of turbulent flow. Supercritical flow occurred almost on the whole ramp and the highest value of Froude number, 3.18, was recorded at point 20.

The values of Froude number, Reynolds number and flow velocity measured on the structure are very important for evaluation of the possibilities of migration of aquatic animals through the ramp. The ecological requirements that must be fulfilled by fish passes and similar structures, such as RHS, are formulated by DVWK (2002). The obtained data indicate that the RHS constructed on Porębianka Stream meets these requirements.

5 CONCLUSIONS

1 Hydrodynamic parameters in the area of the rapid hydraulic structures which mimic natural riffles in gravel-bed rivers depend closely on the location of the measurement point in relation to the individual parts of the structure.
2 Hydrodynamic conditions in the areas of rapid hydraulic structures are highly diversified, which increases heterogeneity of the habitat conditions for benthic invertebrate fauna.
3 The highest velocities were observed on the slope apron of the RHS in the place of flow concentration. At the same time, it is the place where fish and invertebrate can migrate along the structure under low-flow conditions.
4 The maximum, medium and dynamic velocities recorded upstream and downstream of the structure are similar, which shows the proper functioning of the RHS.
5 The values of the shear stress depend directly on flow velocity and water turbulence as well as on the dynamic velocity in all measured places of the investigated RHS.
6 Rapid hydraulic structures (sometimes called ramps) operate as low transversal structures mimicking natural riffles, and thus they conform with the requirements of the Water Framework Directive of the EU.

NOTATION

v	flow velocity [$m \cdot s^{-1}$]
h	water depth [m]
g	gravitational acceleration [$m \cdot s^{-2}$]
d	diameter of the grains on the channel bed [m]
ν	coefficient of kinetic viscosity [$m^2 \cdot s$]
v_{sr}	depth-averaged flow velocity [$m \cdot s^{-1}$]
Re*	particle Reynolds number
Fr*	particle Froude number

REFERENCES

Boulton, A.J. (2007). Hyporheic rehabilitation in rivers: restoring vertical connectivity. Freshwater Biology, 52, 632-650.

DVWK (2002). Fish passes – Design, dimensions and monitoring. Published by the Food and Agriculture Organization of the United Nations in arrangement with Deutscher Verband für Wasserwirtschaft und Kulturbau e.V. (DVWK), Rome, 2002.

Gregory, K.J., Gurnell, A.M., Hill, C.T., Tooth, S. (1994). Stability of the pool-riffle sequence in changing river channels. Regulated Rivers: Research and Management, 9, 35-43.

Gordon, N.D., McMahon, T.A., Finlayson, B.L., Gippel, C.J., Nathan, R.J. (2007). Stream Hydrology – an Introduction for Ecologists. Wiley and Sons. London.

Keller, E.A. (1971). Areal sorting of bed-load material: The hypothesis of velocity reversal. Bulletin of the Geological Society of America, 82, 753-756.

Kłonowska-Olejnik, M., Radecki-Pawlik, A. (2000). Zróżnicowanie mikrosiedliskowe makrobezkręgowców dennych w obrębie łach korytowych potoku górskiego o dnie żwirowym. XVIII Zjazd Hydrobiologów Polskich. Białystok.

Korpak, J. (2007). Morfologiczna rola budowli regulacyjnych w górskich systemach fluwialnych. Doctoral Thesis. Kraków. Manuscript.

Korpak, J. (2008). Rola maksymalnych wezbrań w funkcjonowaniu systemów uregulowanych koryt górskich. Landform Analysis. 8, 41-44.

Korpak, J., Krzemień, K., Radecki-Pawlik, A. (2008). Wpływ czynników antropogenicznych na zmiany koryt cieków karpackich. Infrastruktura i Ekologia Terenów Wiejskich 4, Kraków.

Kościelniak J. (2004). Zmiany funkcjonowania górskich systemów korytowych w wyniku przeprowadzonych regulacji hydrotechnicznych. Prace Geograficzne, 200.

Milne, J.A. (1982). Bed-material size and the riffle-pool sequence. Sedimentology, 29, 267-278.

Montgomery, D.R., Buffington, J.M. (1997). Channel-reach morphology in mountain drainage basins. Geological Society of America Bulletin, 109, 596-611.

Pastuchová, Z., Lehotský, M., Grešková, A. (2008). Influence of morphodynamic habitat structure on invertebrate communities (Ephemeroptera, Plecoptera and Trichoptera). Biologia, 63, 720-729.

Radecki-Pawlik A. (2002). The velocity-reversal hypothesis – implications for a mountainous stream bed morphology. Electronic Journal of Polish Agricultural Universities, 5(2).

Radecki-Pawlik A., Świderska K., Plesiński K. (2010). Zróżnicowanie parametrów hydraulicznych w rejonie bystrzy o zwiększonej szorstkości. Infrastruktura i Ekologia Terenów Wiejskich, 1, 25-38.

Teisseyre, A.K. (1984). The River Bóbr in the Błażkowa study reach (central Sudetes): A study in fluvial processes and fluvial sedimentology. Geologia Sudetica, 19(1), 8-65.

Wolman, M.G. (1954). A method of sampling coarse river-bed material. Transactions, American Geophysical Union, 35(6), 951-956.

Zasępa, P., Radecki-Pawlik, A., Kłonowska-Olejnik, M., Przybyła, K. (2006). Zróżnicowanie mikrosiedlisk makrobezkręgowców dennych w obrębie łachy bocznej potoku górskiego. Infrastruktura i Ekologia Terenów Wiejskich, 2(2), 5-16.

IWLHS, 20-22/02/2013, Aachen - Bung & Pagliara (eds) - © 2013 Bundesanstalt für Wasserbau ISBN 978-3-939230-04-5

Pilot Fish Protection System in NRW – Unkelmühle/Sieg Hydroelectric Plant

U. Dumont
Ingenieurbüro Floecksmühle GmbH, Aachen, Germany

ABSTRACT: The passability of river systems is a key prerequisite for the development of fish populations. Hence greater emphasis is being placed on keeping fish from entering water utilization systems that could harm them and on mechanisms enabling them to migrate downstream. In order to test and improve these techniques, the state of North Rhine-Westphalia constructed a pilot fish protection system at the Unkelmühle Hydroelectric Plant. The hydroelectric plant is owned by RWE Innogy and is located on the River Sieg, a key watercourse for salmon resettlement. The total flow of the plant's three turbines is 28 m³/s. Three 10 mm bar screens with state-of-the-art rake cleaners and bypasses near the surface and the bottom were installed. A biological and technical monitoring of the system for several years is planned once it has been put into operation.

Keywords: Fish protection, downstream migration, bypass, hydroelectric power, Atlantic Salmon

1 INTRODUCTION

The life cycles of diadromous fish populations are highly dependent on upstream and downstream passability of river systems: salmon and sea trout migrate upstream to their spawning grounds as adults and migrate downstream to the sea as juvenile smolts. In contrast inland watercourses are the growth habitat for eels, which then migrate to the sea as silver eels.

The River Sieg is of paramount importance to the state of North Rhine-Westphalia (NRW), as salmon and sea trout resettlement programs have been underway in this watercourse for some time. The dams and weirs in the vicinity of the Rhine have been equipped with upstream fish ladders in the scope of these programs. A monitoring station for upstream migration of adult salmon is in operation at the Buisdorf Weir.

Although substantial progress has been made in reestablishing upstream passability, there are considerable technical and economic risks associated with equipping hydroelectric plants with effective mechanical protection devices to keep downstream migratory stages out of turbines. In cooperation with the plant owner RWE, the state of NRW has therefore equipped the Unkelmühle Hydroelectric Plant (total capacity = 28 m³/s) with a 10 mm bar screen. Additionally, improvements were made to the upstream fish ladder and monitoring facilities were installed. The construction phase will be followed by a monitoring phase (for assessing the ecological and technical success of the project) of at least 3 years.

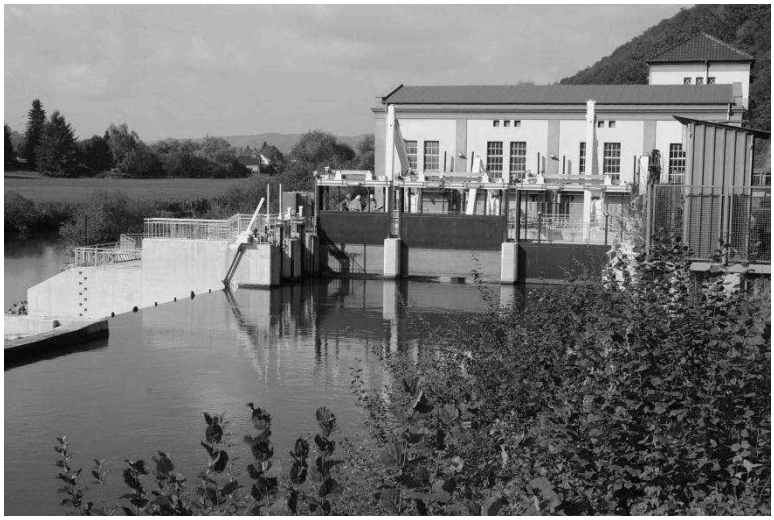

Figure 1. Unkelmühle/Sieg Hydroelectric Plant with new upstream bar screens, view from the upstream side.

2 IMPACT OF HYDROELECTRIC PLANTS ON FISH POPULATIONS

Lack of (upstream as well as downstream) passability impacts the life cycles of both diadromous and potamodromous fish populations. Because the migration routes of diadromous species by definition comprise the switch from the marine habitat to inland watercourses and also because the migration routes are frequently quite long, these species are subject to a particularly high risk of injury at each site through which they must pass. The historical trend in salmon populations and the hazard currently posed to eels are well-known examples of this impact.

As far as migration routes are concerned, particular consideration needs to be given to the following aspects:

In order for diadromous and potamodromous fish populations to complete their life cycles, it is essential that upstream passability be restored at every migration obstacle along the migration routes.

It is especially important that diadromous species are able to pass through migration obstacles such as hydroelectric sites with as little harm as possible during downstream migration.

Impoundment structures exert a cumulative effect on fish populations in both migration directions: the number of upstream migrants is successively thinned with each additional site that they need to pass through. The number of hydroelectric plants to pass through limits the overall survival rate of downstream migrants that reach the receiving watercourse. In each case the overall efficiency of migration plays a decisive role. A considerable amount of data on diadromous species has been obtained from detailed studies in river areas. For potamodromous species, however, there is a dearth of knowledge. Nevertheless migration efficiency has substantial impacts on these species as well.

A decisive factor in the upstream migration of diadromous species is how many fish starting from the sea are able to reach their spawning or growth habitats in a reasonable time and without expending too much energy. Overall efficiency is expressed as the accessibility index of the area. It declines in proportion to the number of transverse structures.

The sea accessibility index (= overall survival rate) is a decisive factor for diadromous species migrating downstream from freshwater habitats. As a rule the overall survival rate declines in proportion to the number of hydroelectric plants that must be passed through.

The accessibility index for salmon smolts migrating downstream from spawning area M9 of the Sieg is shown in Figure 2. 100 % start from the spawning area. There are losses at each passage of each hydroelectric plant; hence with the way the hydroelectric plants are currently designed, only 48 % of the salmon reach the Rhine alive.

But if all of the hydroelectric plants were equipped with 10 mm bar screens, the overall survival rate of salmon smolt would increase to 76 %.

The aforementioned interrelationships indicate that diadromous fish populations can only survive in areas where a maximum number of passage sites along the migration route is not exceeded. In addition it is necessary that certain material and structural requirements for the watercourses be fulfilled.

This knowledge is a direct indication of the need for identifying those watercourses in which diadromous species have a true chance for survival. These watercourses are potential habitats for development, and priority should be given to making them passable in both migration directions. In NRW, the Sieg was

selected as a priority anadromous watercourse. The furthest downstream hydroelectric plant on the Sieg is the Unkelmühle site. All downstream migrating fish have to pass through this site. The Unkelmühle plant thus plays a key role in the development of salmon populations. Hence in the scope of a joint project conducted by NRW and RWE it was equipped with an effective fish protection mechanism: a pilot facility for testing and improving protection and downstream passage systems.

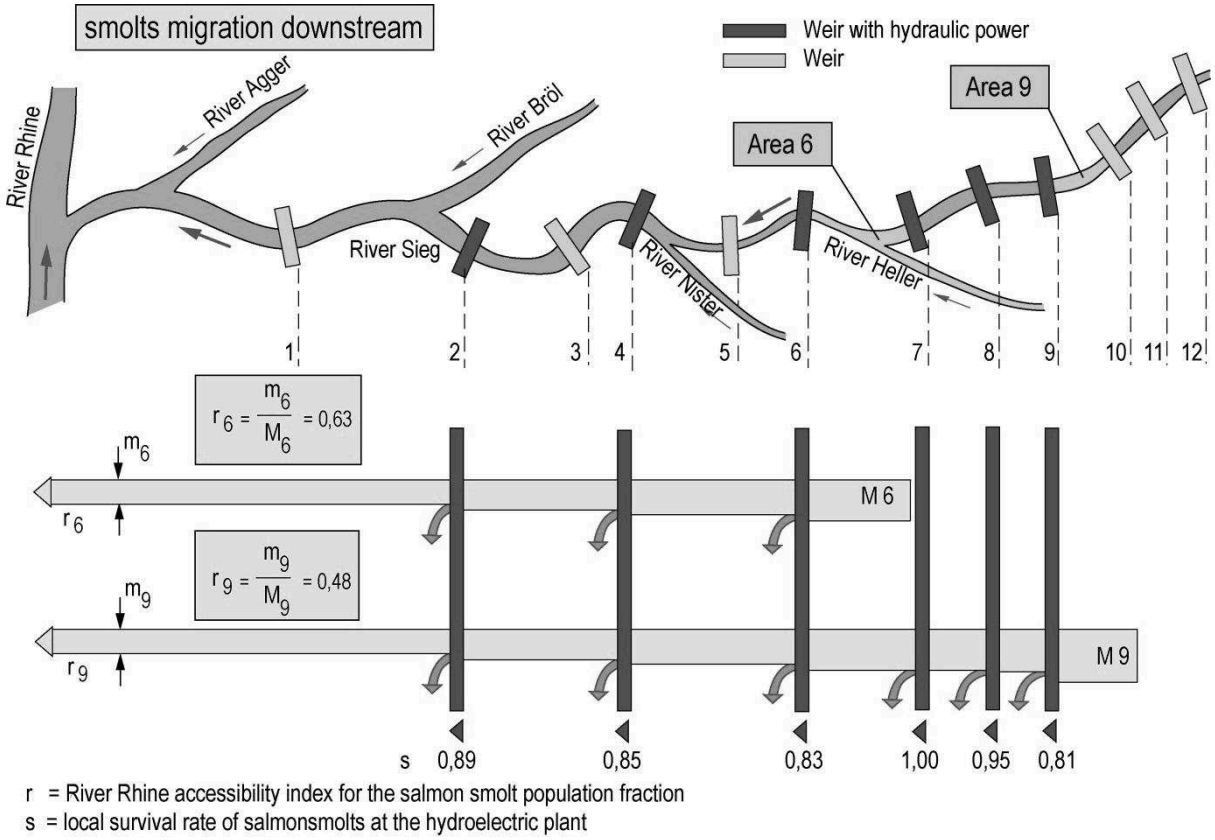

Figure 2. Current accessibility index of the River Rhine for salmon smolts migrating downstream from spawning areas M6 and M9 in the Sieg (present situation). The Unkelmühle Hydroelectric Plant is site 2.

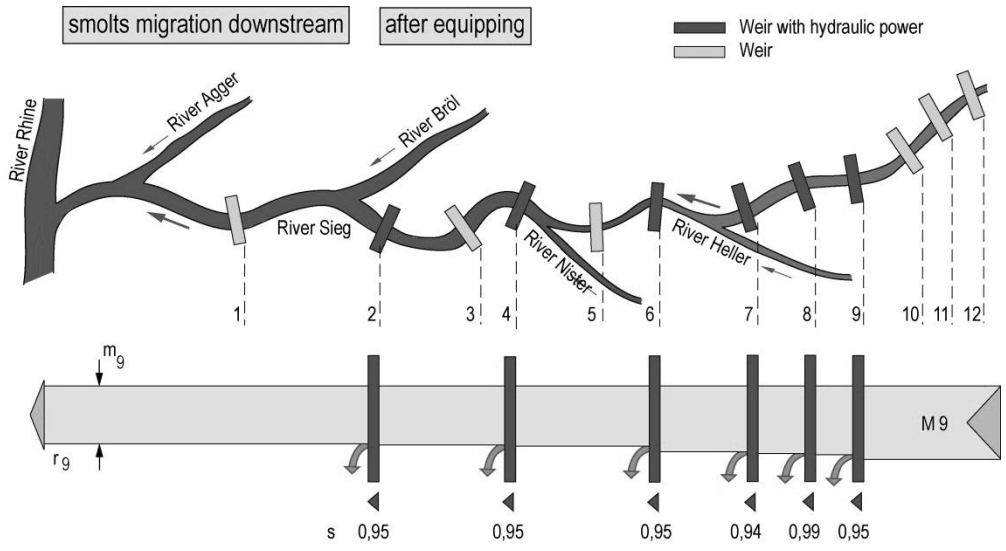

Figure 3. Accessibility index of the River Rhine for salmon smolts migrating downstream from spawning area M9 in the River Sieg after equipping all hydroelectric plants with fish protection systems.

3 MEASURES FOR FISH PROTECTION AND DOWNSTREAM MIGRATION

The present state of technology can be described as follows:

Fish protection systems (unlike upstream fish ladders) must always be designed with specific target species in mind. At each site and/or watercourse it is therefore necessary to determine first of all which species need to be protected and how effective the protection measures need to be in order to ensure the survival of the respective population.

The functionality of behavior barriers that make use of light, current, sound, and guide mechanisms has proven to be inadequate.

Effective fish protection is only achievable with mechanical barriers consisting of bar screens with narrowly-spaced bars. In Germany the primary emphasis is on protecting diadromous species, wherein the following design values must be applied (Arbeitsgemeinschaft Gewässersanierung (1998); Adam, B. et al (1999)):

- Inflow velocity in the channel leading to the bar screen: max. 0.5 m/s
- Bar spacing for protecting salmon smolts: max. 10 mm
- Bar spacing for protecting silver eels: max. 15 mm

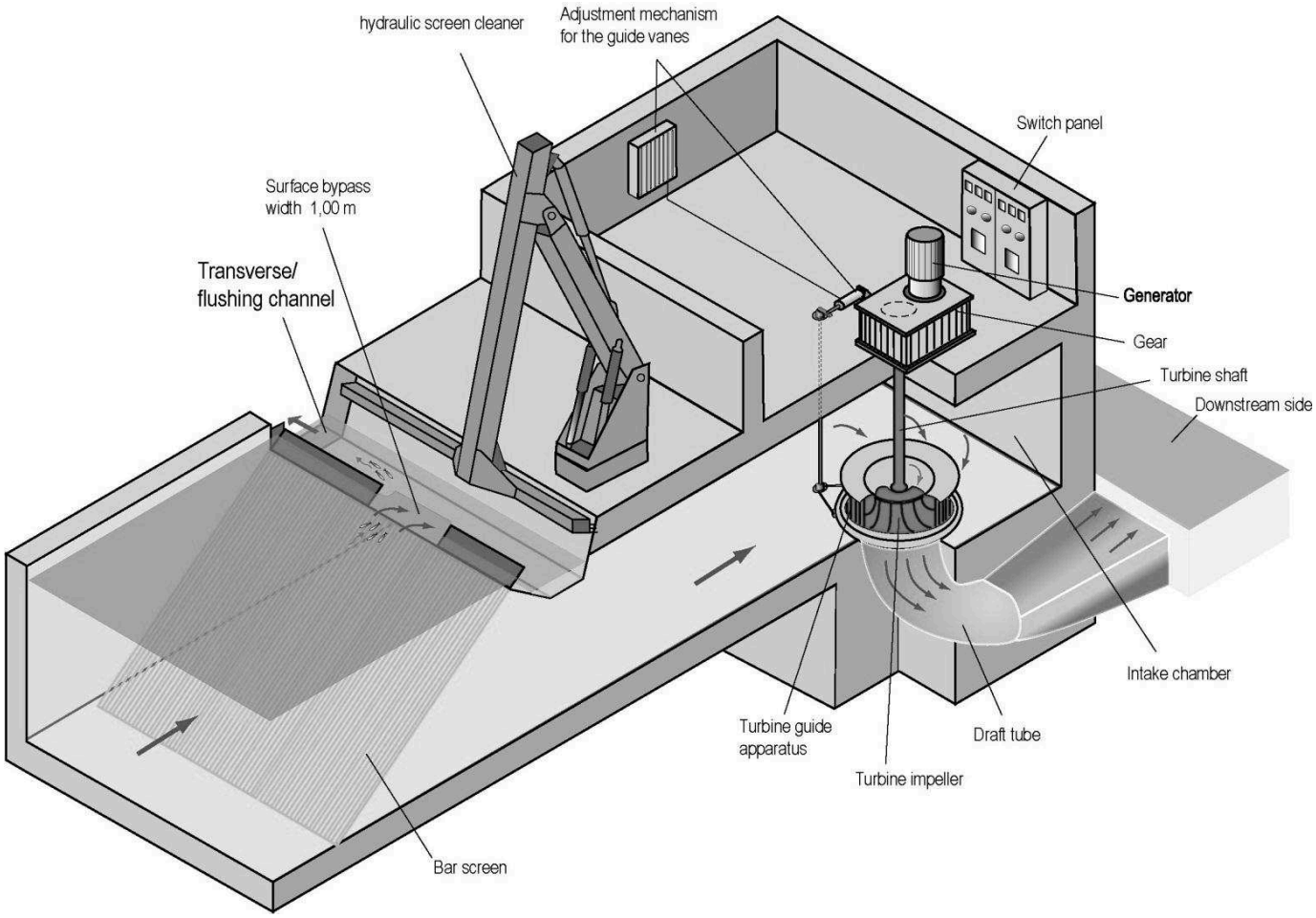

Figure 4. Schematic design of a 10 mm bar screen with screen cleaner and bypass channel at a hydroelectric plant.

For 10 mm bar screens with vertical bars (which as a general rule are actually inclined at an acute angle to the bottom), it is presently possible to construct screen units (including a screen cleaning machine) with flow capacities of up to ca. 30 m³/s. If such bar screen arrays are correctly designed and installed, they will not interfere with the operation of the hydroelectric plant. Sufficient practical experience has shown that losses at the bar screen can be minimized by providing a sufficiently large surface area, efficient screen cleaning machines and suitable screen profiles.

The flow capacity of 10 mm bar screens with horizontal bars is presently limited to ca. 50 m³/s per unit.

Bypass mechanisms suited to each target species must be provided. The latter can often be combined with mechanisms for ensuring the onward movement of floating debris.

4 ELEMENTS OF THE UNKELMÜHLE PILOT SYSTEM

The reconstruction of the hydroelectric plant consisted of the following measures:

The three bar screen arrays were equipped with 10 mm bar screens and state-of-the-art screen cleaners. The bar screen arrays were equipped with different screen profiles in order to study the hydrodynamic and biological suitability thereof.

The drive system channel was deepened in order to reduce the inflow velocity to 0.5 m/s.

Reinforcing structures were installed beneath the bar screens in order to enable them to withstand high compression stresses induced by a potential complete obstruction of the bar screen (due to a screen cleaner breakdown).

The bar screens are inclined at an acute angle to the horizontal and are equipped with a common flushing sluice across the top. This sluice ensures the forward movement of debris and also serves as a bypass for fish swimming near the surface.

A Bottom Gallery® opening into a lateral catch tank was installed in the bottom of the channel in front of the bar screen for fish swimming near the bottom (especially silver eels).

Upstream passability was improved by constructing a vertical slot fish pass to replace the selectively operating Denil-type fish pass.

Upstream and downstream migration monitoring stations were established.

Double protection systems (intake gates) were installed in front of the bar screen arrays so that the latter can be drained individually in order to perform inspections and make any necessary changes.

Lateral flushing sluices to ensure the removal and onward movement of debris. Flushing is especially necessary for bar screens with closely spaced bars in order to cut down on the volume of debris passing through the bar screen.

Two sluice gates were renovated, including the concrete construction.

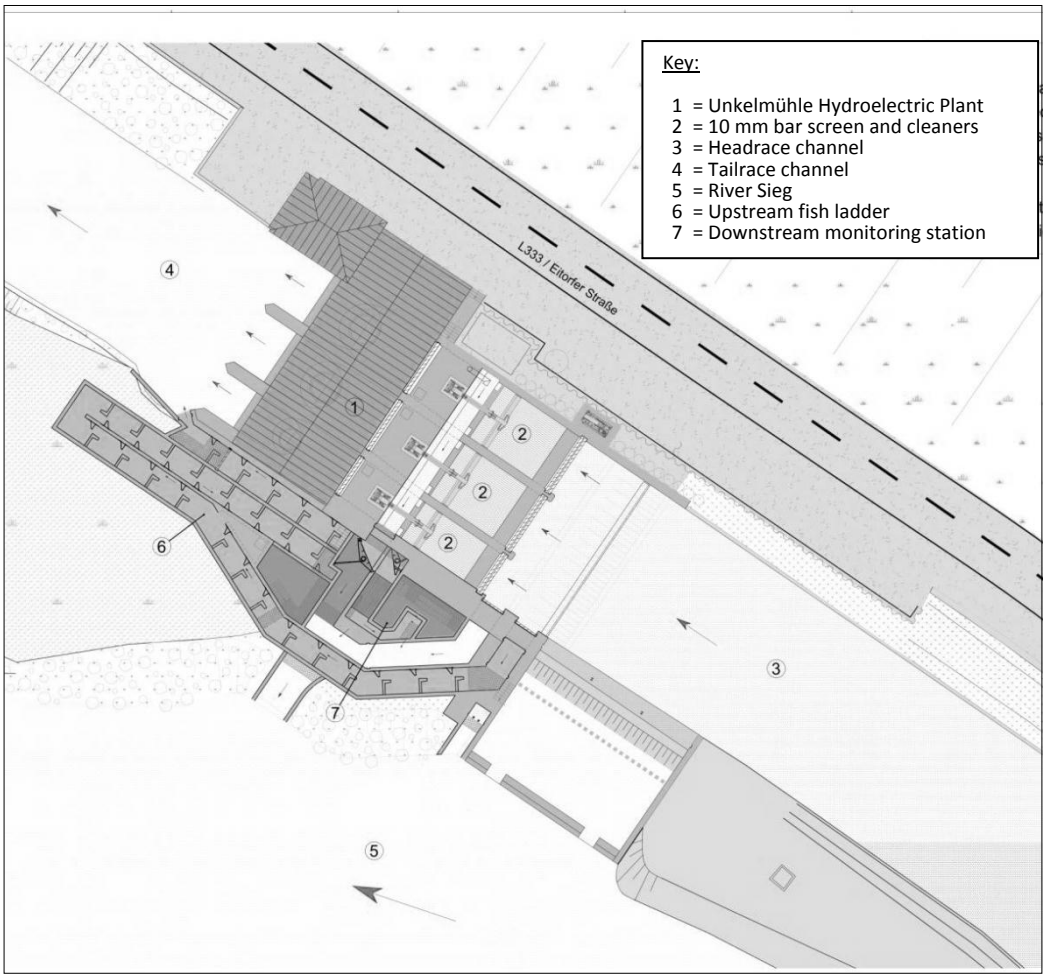

Figure 5. Layout of the Unkelmühle Hydroelectric Plant with vertical slot pass and three-bay 10 mm bar screen array.

Figure 6. Three-bay bar screen array with flushing channel in the back.

5 BYPASS MECHANISMS OF THE UNKELMÜHLE PILOT SYSTEM

The downstream passage mechanisms comprise the following elements:

Surface bypass openings for salmon smolts in the top area of the fish protection screens. Each bar screen array was equipped with two openings leading to the transverse flushing channel. Adaptors can be used to change the shape of the openings in order to permit optimum downstream migration of salmon smolts while at the same time minimizing the loss of water to run the turbines. The numbers of fish migrating downstream can be recorded at the downstream monitoring station.

Figure 7. Flushing channel and surface bypass openings for salmon smolts in the top area of the fish protection screens.

Three eel pipes staggered in height were arranged in the left bar screen chamber. Separate monitoring tanks make it possible to assess how effectively each pipe permits downstream passage of silver eels.

For the first time, a Bottom Gallery® was installed across the entire width of the bottom of the upstream channel. The latter was developed as a bottom bypass device for silver eels on the basis of behavioral observations. As they approach and/or come into contact with a bar screen, eels attempt to escape by swimming against the current. First they do a complete about-face on or in the vicinity of the bar screen surface. They then attempt to escape, usually by swimming close to the bottom. This flight reaction was observed in experimental flumes and has been generally confirmed in various studies in watercourses such as the Moselle. The Bottom Gallery® is patented.

The Bottom Gallery® exploits the observed behavior as follows:

At a certain distance in front of the turbine or pump screen, a barrier is created on the bottom where the silver eels fleeing against the current gather.

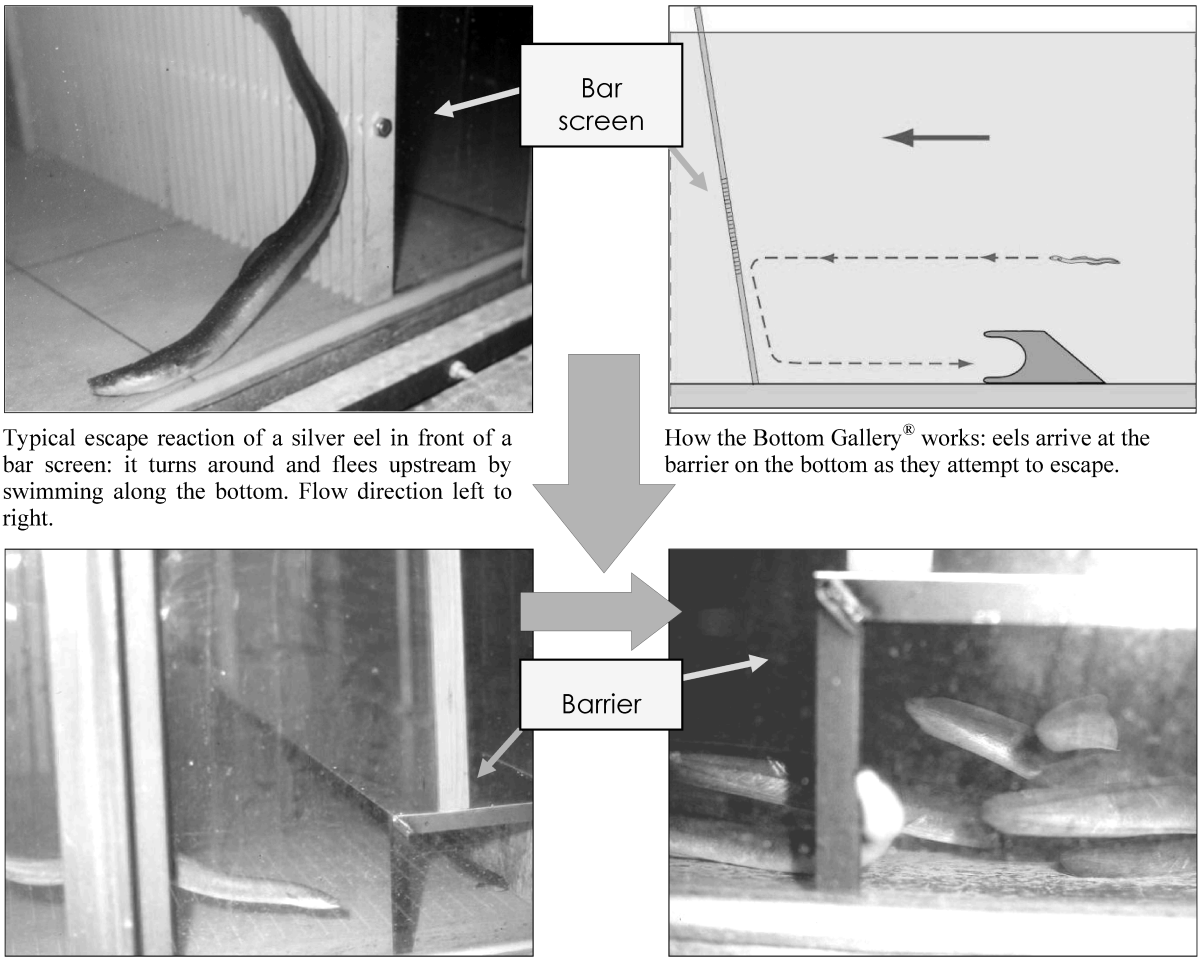

Typical escape reaction of a silver eel in front of a bar screen: it turns around and flees upstream by swimming along the bottom. Flow direction left to right.

How the Bottom Gallery® works: eels arrive at the barrier on the bottom as they attempt to escape.

The eel encounters the bottom barrier, which is open in the direction against the current.

Downstream migrating eels gather in the Bottom Gallery®.

Figure 8. How the Bottom Gallery® works.

Experiments have shown that silver eels tend to stay beneath the barrier and generally do not actively search for a lateral bypass to the downstream side. Hence the closing mechanism of the Bottom Gallery® consists of a trap door. The closed interior space of the Bottom Gallery® where the silver eels gather is hooked up to a bypass pipe. The unit has two operating modes:

Catching phase:
The closing mechanism is open, thus allowing the eels to swim into the Bottom Gallery®.

Flushing phase:
Opening the pipe creates a flow in the Bottom Gallery®, which flushes the silver eels through the bypass pipe and to the downstream side. The flushing process is started automatically. The flushing frequency depends on the downstream migration rate.

The functionality of the Bottom Gallery® can be assessed by means of a downstream monitoring chamber in which the migrating eels gather.

Figure 9. Monitoring station for fishes migrating downstream through the surface bypasses.

6 CONCLUSION

Hydroelectric plants have impacts on fish populations, particularly on diadromous populations because the migrating fish may be injured by turbines as they pass through. Various systems for minimizing the injury rate or to keep fishes from entering the turbines are currently under development. These protective mechanisms consist of screens with a narrow clearance between bars so that the fish are unable to pass through the barriers. For further developing and in particular for testing such fish protection mechanisms, the German state of North Rhine-Westphalia in collaboration with RWE Innogy installed the Unkelmühle pilot system on the Sieg. A screen with a 10 mm bar distance and a total flow of 28 m³ was installed there. Bypasses were also provided for the salmon smolts swimming near the surface and for the silver eels swimming along the bottom. The functionality of the system will undergo technical and biological testing in the scope of a multi-year monitoring.

REFERENCES

Dumont, U., Anderer, P., Schwevers, U. (2005). Handbuch Querbauwerke, Düsseldorf, Ministerium für Umwelt und Naturschutz, Landwirtschaft und Verbraucherschutz des Landes Nordrhein-Westfalen Editor, 213 pp. - Field manual transverse structures. (in German).

ATV-DVWK (Deutsche Vereinigung für Wasserwirtschaft, Abwasser und Abfall e.V., Editor) (2004): Fischschutz- und Fischabstiegsanlagen – Bemessung, Gestaltung, Funktionskontrolle, Hennef, 256 pp. – System for fish protection and downstream fish migration – design, arrangement, function control. (in German)

Arbeitsgemeinschaft Gewässersanierung (1998): Gutachten zur Wiederherstellung der Durchwanderbarkeit an der Staustufe Wahnhausen/Fulda. – Ingenieurbüro Floecksmühle & Institut für angewandte Ökologie. – Expertise on re-establishment of the possibility to cross the barrage Wahnhausen/Fulda. (in German)

Adam, B., Schwevers, U. & Dumont, U. (1999): Beiträge zum Schutz abwandernder Fische – Verhaltensbeobachtungen in einem Modellgerinne, Solingen, Verlag Natur & Wissenschaft, Bibliothek Natur & Wissenschaft 16, 63 pp. – Contributions to the protection of migrating fish – behavioral monitoring in a modell-channel. (in German)

Christen (1996): Literaturrecherche über Mortalität von Fischen in Kaplan - Turbinen. - Karlsruhe - Badenwerk AG. 29 S. - Literature research an mortality of fish in Kaplan-turbines. (in German)

Holzner, M. (1999): Untersuchungen zur Vermeidung von Fischschäden im Kraftwerksbereich dargestellt am Kraftwerk Dettelbach am Main/Unterfranken. – Schriftenreihe des Landesfischereiverbandes Bayern, Heft 1, 224 pp. – Analysis on avoidance of fish-damage in areal of an hydroelectric plant painted on hydroelectric plant Dettelbach am Main/Unterfranken – Scientific series of the Regional Association on Fisheries of Bavaria. (in German)

Larinier, M. & Dartiguelongue, J. (1989): La circulation des poissons migrateurs et transit à travers les turbines des installations hydroélectriques. – Bull. Fr. Peche Piscic. 312/313, 90 S.. – circulation of migrating fish and passing through traverse turbines of hydroelectric plants. (in French)

Montén (1985): Fish and turbines – Fish injuries during the passage through power station turbines. – Vattenfall, Stockholm. 111 S.

Ploskey, G.R., Carlson, T.J. (2004): Comparison of Blade-Strike Modeling results with Empirical Data. Pacific Northwest National Laboratory.

Schmalz, W. (2010): Untersuchungen zum Fischabstieg und Kontrolle möglicher Fischschäden durch die Wasserkraftschnecke an der Wasserkraftanlage Walkmühle an der Werra in Meiningen. Im Auftrag der Thüringer Landesanstalt für Umwelt und Geologie, -Breitenbach. – Analysis of Downstream migration of fish and controlling of possible damage to fish through the hydrodynamic srew at hydroelectric plant Walkmühle at the River Werra in Meiningen. (in German)

Turnpenny, A.W.H., Clough, S., Hanson, K.P., Ramsey, R. and McEwan, D. (2000): Risk Assessment for Fish Passage Through Small, Low-Head Turbines. Final Report. Energy Technical Support Unit, Harwell, Unites Kingdom.

UBA Texte (72/2011), UMWELTBUNDESAMT (Hrsg.): Erarbeitung und Praxiserprobung eines Maßnahmenplans zur ökologisch verträglichen Wasserkraftnutzung an der Weser, Dessau. – Elaboration and on-road test of an action plan for ecological compatible use of hydraulic energy at the River Weser. (in German)

5 Sewer Structures

IWLHS, 20-22/02/2013, Aachen - Bung & Pagliara (eds) - © 2013 Bundesanstalt für Wasserbau ISBN 978-3-939230-04-5

Characterization of the Flow in a Gully: Average Velocity, Turbulence and Air Entrainment

P. Páscoa
IMAR Researcher, Civil Engineering Department, University of Coimbra, Portugal

J. Leandro
Lecturer, Institute of Hydrology, Water Management and Environmental Techniques, Ruhr-University Bochum, 44780 Bochum, Germany, IMAR-CMA research centre member.

R. Carvalho
IMAR-CMA research centre member. Assistant Professor, Civil Engineering Department, University of Coimbra, Rua Luís Reis Santos, Pólo II, 3030-788 Coimbra,Portugal.

ABSTRACT: The goal of this work is to characterize the flow on a gully, occurring on both drainage and surcharged conditions. To do so, measurements of flow velocity were made using an acoustic Doppler velocimeter on a 1:1 scaled model of a gully, as well as video recordings. The flow fields and turbulence were quantified. In addition a qualitative analysis of the air inside the gully is given, based on the recordings. Similarities were found between the flow rates, for both drainage and surcharged flows, namely: for surcharged flow, a strong anticlockwise is observed on the left side of the gully, while the right side displays almost negligible velocities; for drainage flow there is one large vortex above the orifice, which ascends with the increase of the flow rate, and larger quantities of air are present which are then subsequently reduced with the increase of the flow rate; finally, for the drainage flow, the turbulence increases along the horizontal axis.

Keywords: urban drainage, gully, surcharged flow, direct flow

1 INTRODUCTION

A gully is one of the linking elements between the surface and the sewer of an urban drainage system. Its function is to conduct the excess rainfall from the surface to the sewer, but sometimes, when the incoming flow of an upstream sewer pipe is higher than the discharge capacity of the downstream sewer pipe, the flow is reversed. This may happen during an intense precipitation event or a flood. In this case, the drainage system will be contributing to the flood, instead of mitigating it. The study of a drainage system thus implies the study of its linking elements.

Several studies regarding gullies have been made. The hydraulic efficiency of gullies was studied by Goméz and Russo (2007) and Goméz and Russo (2009). The latter studied longitudinal gullies. These studies focused on the effect of the gratings on the hydraulic efficiency, but only for drainage conditions. Djordjević *et al.* (2011) used experimental results of drainage and surcharged flows to determine discharge coefficients and to compare with numerical simulations.

Under the Multiple Linking Elements project, taking place on the University of Coimbra, several numerical simulations have been made, including Carvalho *et al.* (2011) and Carvalho *et al.* (2012), who studied the hydraulic behavior of a gully with drainage and surcharged flow. Martins *et al.* (2012) and Lopes *et al.* (2012) presented 3D numerical simulations of the gully under drainage and surcharged flow conditions, respectively, whose results were compared with experimental water heights obtained on the 1:1 scaled model also used in this work.

Continuing the works above mentioned the present work aims to characterize the direct and reverse flow in a gully, using a 1:1 scaled model. Flow velocity was measured on several points inside the gully, using a Nortek AS® 10MHz acoustic Doppler velocimeter (NDV). This data was used to characterize the average flow velocity and turbulence of the flow, for the drainage flow. A qualitative analysis of the air entrainment is also presented, based on 30 s videos of each flow rate.

2 EXPERIMENTAL FACILITY

A 1:1 scaled model of a gully was set up inside the multipurpose hydraulic channel at the Hydraulics Laboratory on the Civil Engineering Department of Coimbra University. The water was supplied to the channel by a constant head tank, and then it flowed through a 50 cm wide, 50 cm deep and 10 m long acrylic channel, with a 1% slope. The gully model is a 30 cm wide, 30 cm deep and 60 cm long acrylic box, with a circular orifice at the center of the bottom of the box, 8 cm in diameter, and an additional 6 cm long tube connected to the orifice. The top opening is uncovered. When simulating the surcharged flow, a gate was set upstream the box, as well as a PVC pipe connecting the upstream flow to the gully orifice. Figure 1 presents a scheme of the experimental facility.

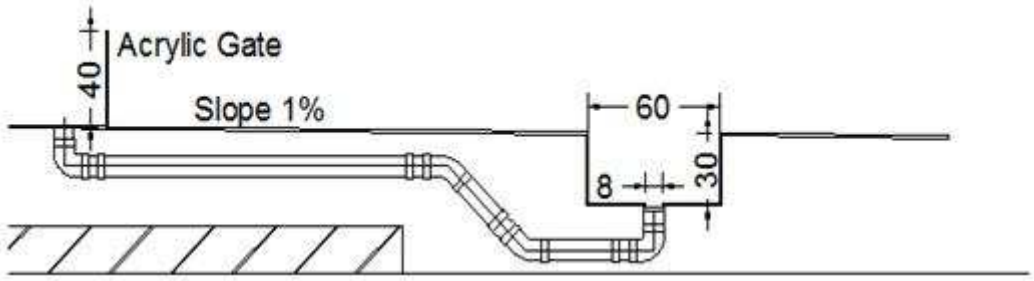

Figure 1. Experimental facility set up for surcharged flow. For drainage flow, the pipe and the gate are removed. The water flows from left to right.

3 METHODOLOGY

A 3D side looking Nortek AS® 10MHz acoustic Doppler velocimeter (NDV) was used to collect data to calculate the average velocity field and turbulence, for the central longitudinal plane. The sampling frequency was set to 1 Hz to the surcharged flow, and since this would return very low correlations for the drainage flow, it was set at 25 Hz for the latter. The sampling time was always 180 s. The mesh consists of points distanced 3 cm from each other. The NDV configuration did not allow measuring any point from the bottom up to 5 cm height. The highest points were measured at 29 cm, whenever possible. On the surcharged flow, the gully was always submerged, allowing these measurements, but for the drainage flows it was not always possible, since the water height inside the gully varied and in some cases it did not allow the NDV to be submerged. On the reverse flow the jet area presents high turbulence, making the NDV measurements less reliable. For this reason, the mesh was adapted and there are no points in the centre of the box and the two columns nearer the jet, one on each side, were moved 1 cm away from the jet, which means they are 2 cm away from the others, on the horizontal direction, as presented on Figure 2 (left).

The turbulence parameters were calculated only for drainage flow and for a smaller number of points: near the walls, at the center of the gully and at the center of each side of the gully and at 5, 14 and 23 cm height, as presented in Figure 2 (right). Considering that only the longitudinal plane is being studied, the turbulence was calculated only on the streamwise and the vertical directions.

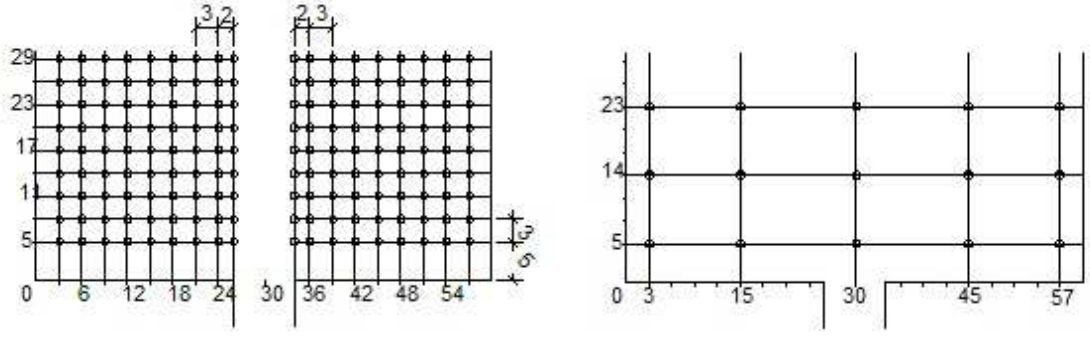

Figure 2. Mesh used for surcharged flow (left) and turbulence (right).

Videos of each flow rate were recorded, using a Panasonic DMC-FS16 camera with 14 Mega Pixels fixed on a tripod. The recordings were made on automatic mode with natural light. The frame rate was 30fps for the surcharged flow and 24 fps for the drainage flow; the shutter speed was always 1/30 s and the aperture varied from f/4 to f/4.8. The videos lasted 30 s and were used to analyze the air inside the gully, specifically the minimum and maximum air concentration observed.

The flow rates tested were 4, 5 and 6 l/s for the surcharged flow, and 15, 22, 32 and 42 l/s for the drainage flow. These choices depended on previous works and their conclusions. For the surcharged flow, flow rates lower than 4 l/s presented very low average velocities and the experimental facility limited the maximum flow rate. For flow rates lower than 15 l/s, the drainage flow presented an air concentration inside the gully so high that would not allow good measurements with the NDV. For flow rates higher than 42l/s, most of the water would flow across the gully, and the results would not return any additional information (Martins, 2011).

The Reynolds number (calculated as $Re = Ud/\nu$ and as $Re = UH_u/\nu$ for the drainage flow) varied from $6.4\text{x}10^4$ to $11\text{x}10^4$ for the surcharged and from $8\text{x}10^4$ to $11\text{x}10^4$ for the drainage flow, and the Froude number (calculated as $Fr = U/(gd)^{0.5}$ and $Fr = U/(gH_u)^{0.5}$ for the surcharged and drainage flow, respectively) was comprised between 0.90 and 1.34 for the surcharged flow and 1.80 and 2.00 for the drainage flow. The summary of the experimental conditions is shown on Table 1. The water depth was measured upstream, and the average velocity was calculated for the orifice with diameter d=0.08 m, on the surcharged flow, and upstream, on the drainage flow.

Table 1. Flow rate, water depth, average velocity, Reynolds number, Froude number, and sampling frequency and time for surcharged and drainage flow.

		Q (l/s)	H_u (m)	U (m/s)	Re (-)	Fr (-)	f (Hz)	t (s)
Surcharged	Q_4	4	0.76	0.80	$6.4\text{x}10^4$	0.90	1	180
	Q_5	5	0.825	0.99	$8.0\text{x}10^4$	1.12		
	Q_6	6	0.905	1.19	$9.5\text{x}10^4$	1.34		
Drainage	Q_{15}	15	0.030	0.99	$8\text{x}10^4$	1.80	25	
	Q_{22}	22	0.037	1.18	$9\text{x}10^4$	1.94		
	Q_{32}	32	0.047	1.36	$11\text{x}10^4$	2.00		
	Q_{42}	42	0.059	1.43	$11\text{x}10^4$	1.89		

The data obtained by the NDV were post-processed using WinADV, version 2.028 (Wahl, 2000). The post-processing included the elimination of spikes, using the phase-space threshold despiking method proposed by Goring and Nikora (2002) and modified by Wahl (2003), the elimination of points in the data series that presented a signal to noise ratio (SNR) lower than 5dB for the surcharged flow and 15dB for the drainage flow (Lohrman *et al.*, 1994), and the elimination of points that had lower correlation coefficients. For the calculation of the average velocity, the correlation coefficient can be as low as 30% (Sontek, 2001), but it was decided to apply a stricter filter first. For the calculation of the turbulence parameters, and considering that Wahl (2000) suggests that samples with correlation coefficients lower than 70% can provide good data when SNR is high and the flow is turbulent, samples with correlation coefficients as low as 50% were not eliminated, which is a similar approach to that of Romagnoli *et al*. (2012), who considered correlations as low as 45%.

4 RESULTS AND DISCUSSION

4.1 *Correlation coefficient*

The average correlation coefficients obtained during the samplings are presented in Figure 3. The values vary from more than 80% to as low as 20%, as seen on the surcharged flow. The presence of turbulence decreases the correlation coefficient. Its value was lower where it was expected the turbulence to be higher, namely near the jet, for the case of the surcharged flow, and near the surface. The areas where water is entering the box also present low correlations, specifically the upper left side for the surcharged flow and the side for the drainage flow. For all cases, the correlation coefficient is higher near the walls.

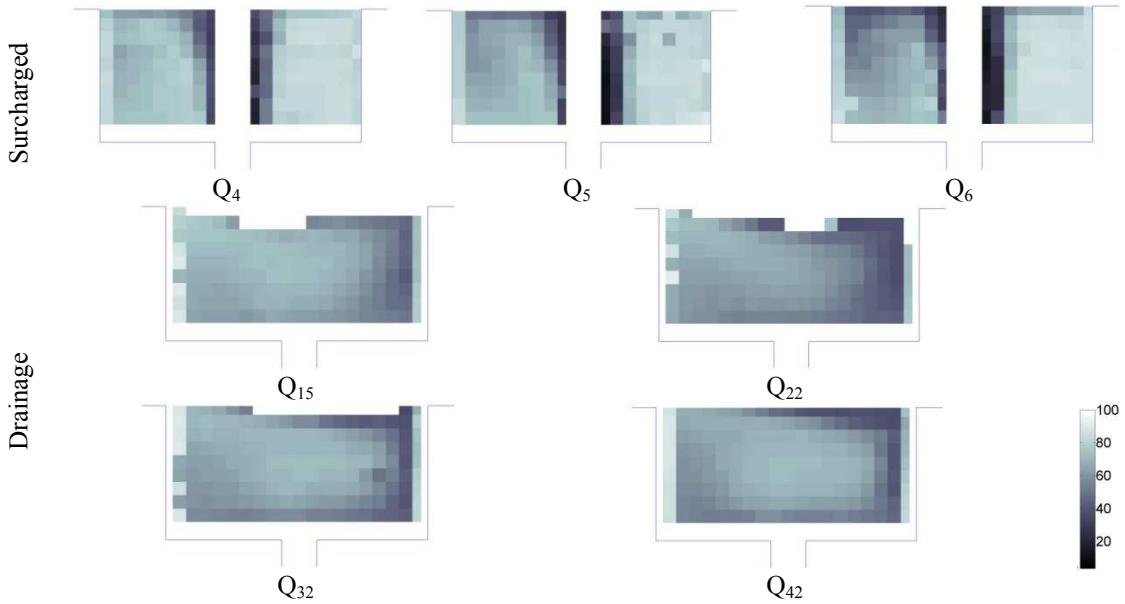

Figure 3. Correlation coefficients for surcharged (above) and drainage (below) flows.

4.2 *Average velocity field*

The average velocity fields are shown on Figure 4, for both surcharged and drainage flows. The maximum average velocity is presented for each flow rate. There is a similarity between the flow rates analyzed for the surcharged flow and for the drainage flow either.

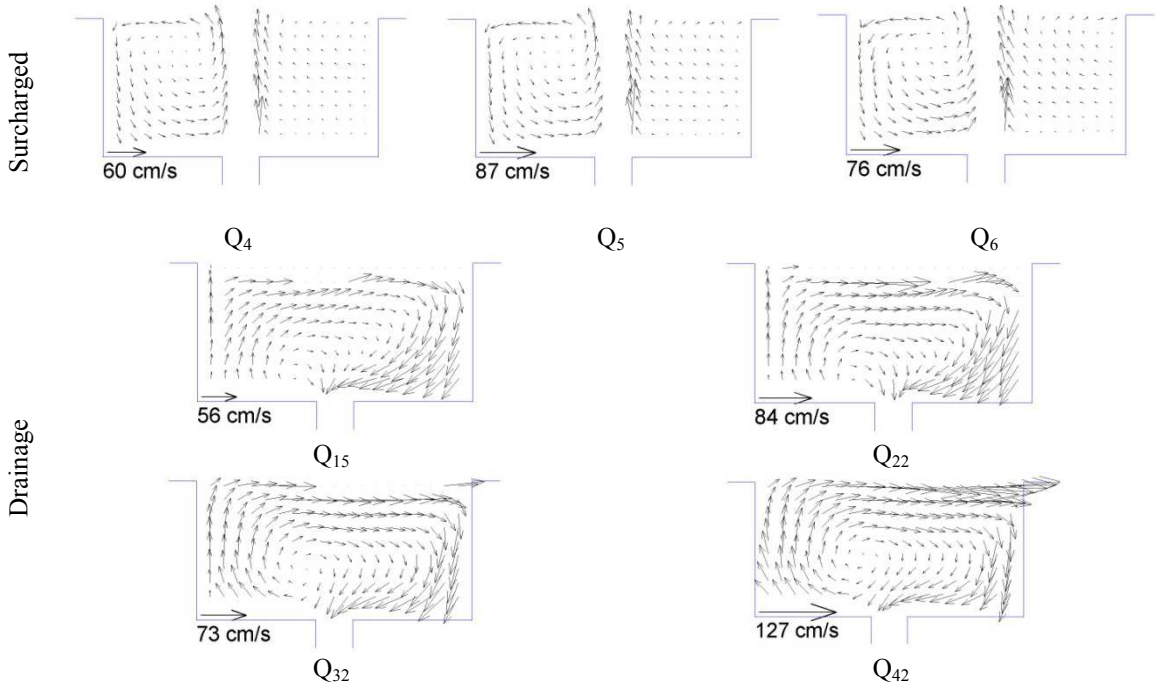

Figure 4. Average velocity fields for surcharged (above) and drainage (below) flows.

The surcharged flow presents an anticlockwise vortex on the left side of the box that illustrates the entrance of water in the gully. On the right side the velocities are quite low. Near the jet the velocities are almost vertical and are the highest on the gully. There is an increase on the average velocities with the increase on the flow rate, despite the fact that the highest maximum velocity was measured on Q_5 instead of Q_6, as expected. This could be explained with the fact that the maximum velocity is located near the jet, an area where the correlation coefficients are quite low, which makes the data less reliable.

The drainage flow is composed of only one clockwise vortex, and its center is located 20 to 25 cm away from the upstream wall. With the increase in flow rate the vortex center "ascends", and so do the horizontal velocities near the bottom, that then become visible. The water entering the gully flows across it, directly to the downstream wall. Here, part of it flows downwards into the gully, and the rest flows out of the gully. The former is the main contributor to the flow exiting through the bottom orifice. There is a

hydraulic jump and its position influences the velocity field. With the increase in flow rate, the jump moves downstream, causing the velocity near the surface to become more horizontal. The velocities increase with the flow rate, and the highest velocities are located on the surface and near the downstream wall. The highest velocity on Q_{22} is higher than on Q_{32}, but on this case this can be explained by the differences on the mesh used: it is possible that on the points that were eliminated (on the Q_{32} flow) the velocities were higher than the ones measured on both Q_{32} and Q_{22}.

4.3 *Air entrainment*

The qualitative analyses performed focused mainly on the maximum and minimum values observed and on the entrance points. Figure 5 consists of frames of the recording videos that were considered to best illustrate the variation of the air concentration inside the gully.

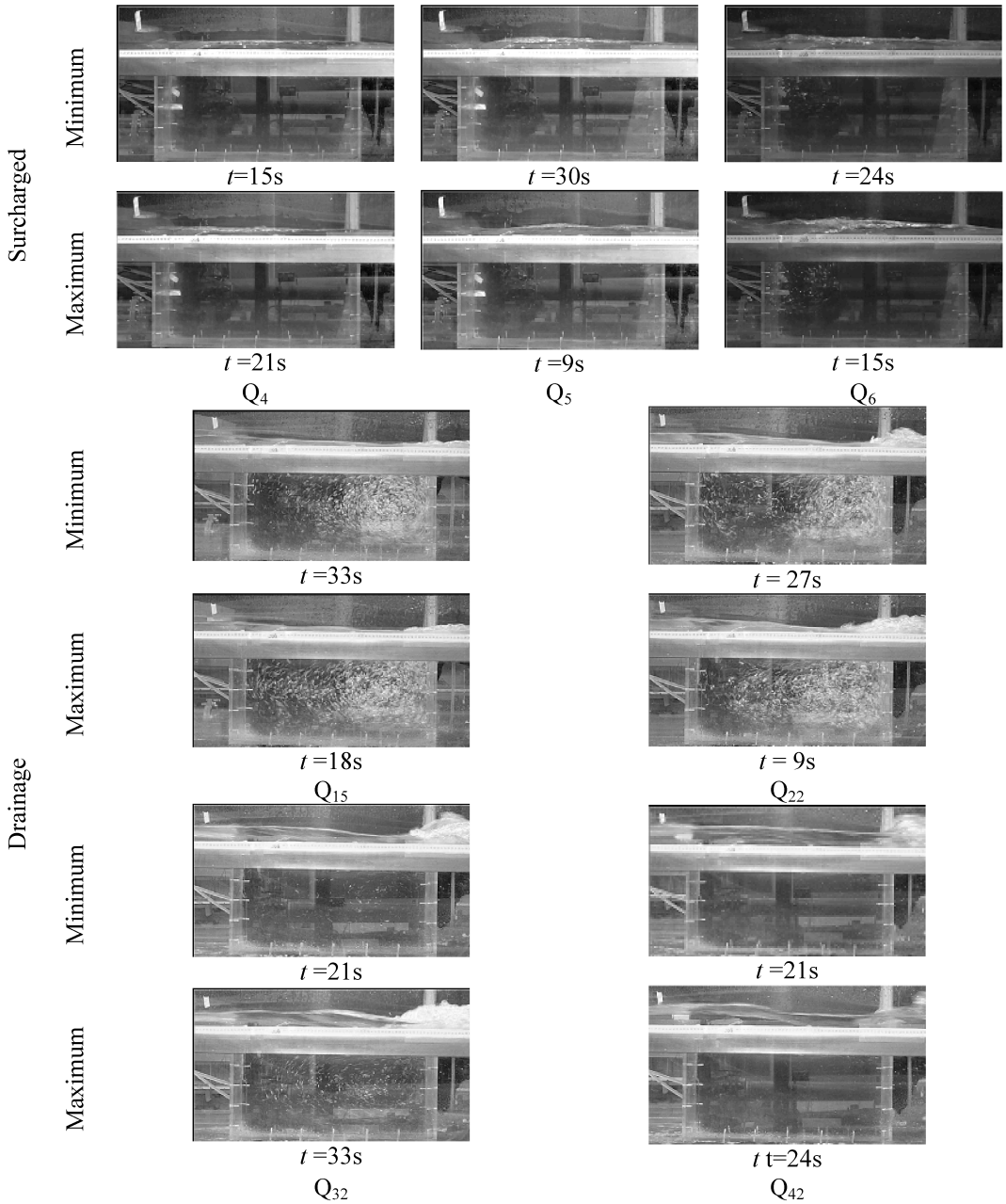

Figure 5. Air entrainment for surcharged (above) and drainage (below) flow. For each flow the minimum and maximum registered concentrations of air are presented.

Air enters the gully dragged by the water, so on the surcharged flow, it enters on the upper left corner, and on the drainage flow, it is dragged on the right side. The air quantity depends on the flow rate: on the surcharge flow, it increases with the flow rate, and for Q_4 there are no air bubbles inside the gully; Q_5 showed a few air bubbles, but on some occasions there are none visible; air was always present on Q_6, and it varied from some bubbles near the upstream wall to air occupying 20 cm (horizontally) of the gully. For the drainage flow, the opposite happens: the air concentration diminishes with the increase in

the flow rate, and this can be related with the position of the hydraulic jump, as well as the water height inside the gully.

The hydraulic jump also influences the air concentration variation for each flow rate. As it moves downstream, the air quantity entering the box diminishes, and for Q_{42} there were no air bubbles visible, but the increase in the water height had also an influence, since it made it difficult for the air to enter. The air distribution inside the gully depended on its quantity, and there was always air present on the right side of the box, whereas on the left side its presence was not constant.

4.4 *Turbulence*

Turbulence parameters were normalized with U^2, being U the average velocity as presented on Table 1. Normal stresses are presented on Figure 6, for the streamwise ($<u_xu_x>$) and the vertical ($<u_zu_z>$) direction. Shear stresses ($<u_xu_z>$) and turbulent kinetic energy (k) are shown on Figure 7. Like it was previously mentioned, the turbulence parameters were calculated for three different heights and for five points on the horizontal direction.

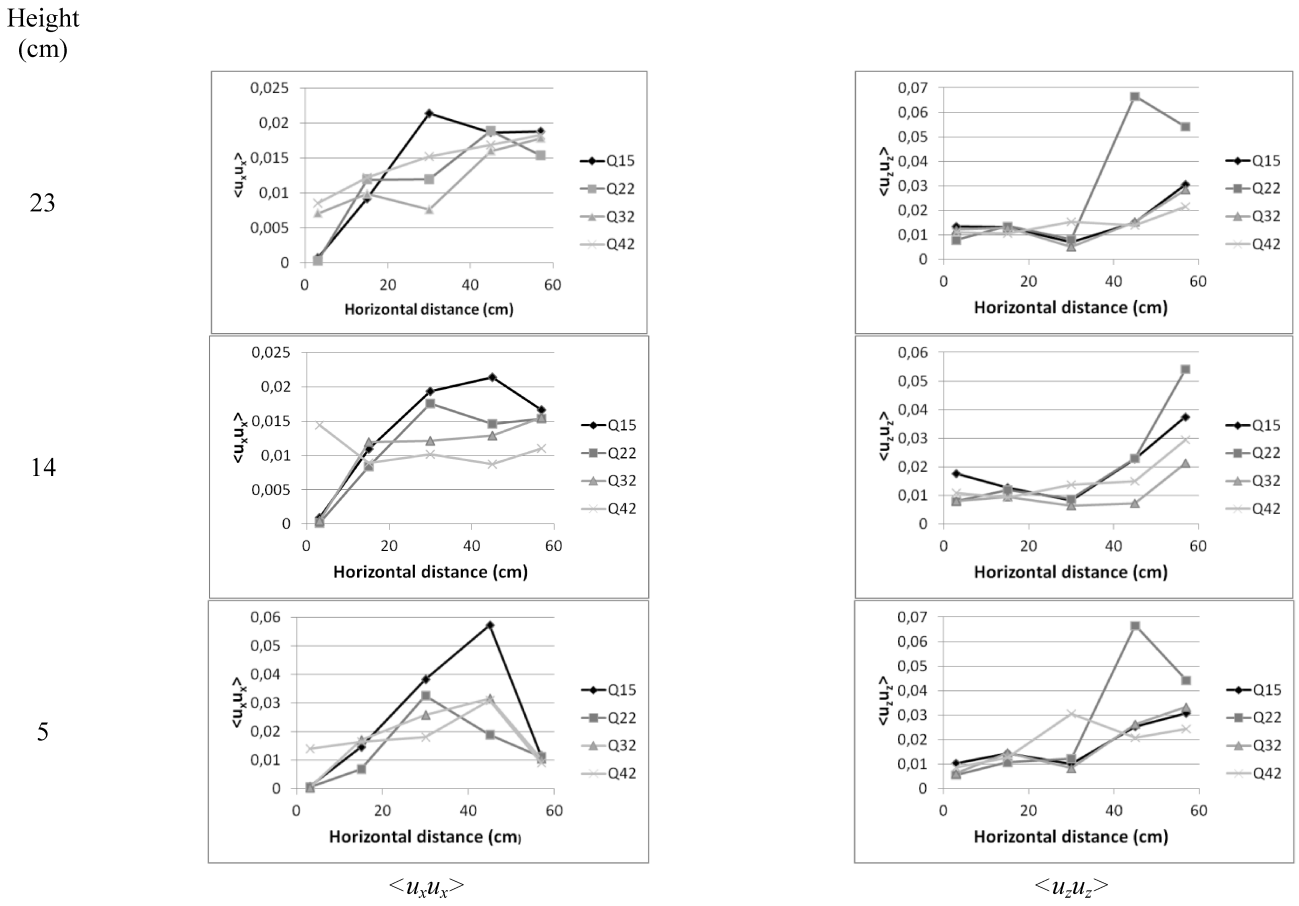

Figure 6. Normal stresses: streamwise (left) and vertical direction (right).

Considering the evolution along the horizontal distance, there is an increase in the normal stress for all four flow rates, although the maximum doesn't take place in the downstream wall, with the exception of normal stress in the vertical direction at 14 cm height, as seen in the centre right chart. In fact, the maximum value is mostly on the point distancing 45 cm from the upstream wall.

Streamwise stresses tend to assume a concave growth, while the vertical stresses present a convex growth. Streamwise stresses, for 5 cm and 14 cm height show a decrease on the turbulence with the increase on the flow rate, but there is no clear pattern for the other cases, although the maximum value for the vertical stresses always occurs for Q_{22}, while for streamwise stresses it is always Q_{15} that present it.

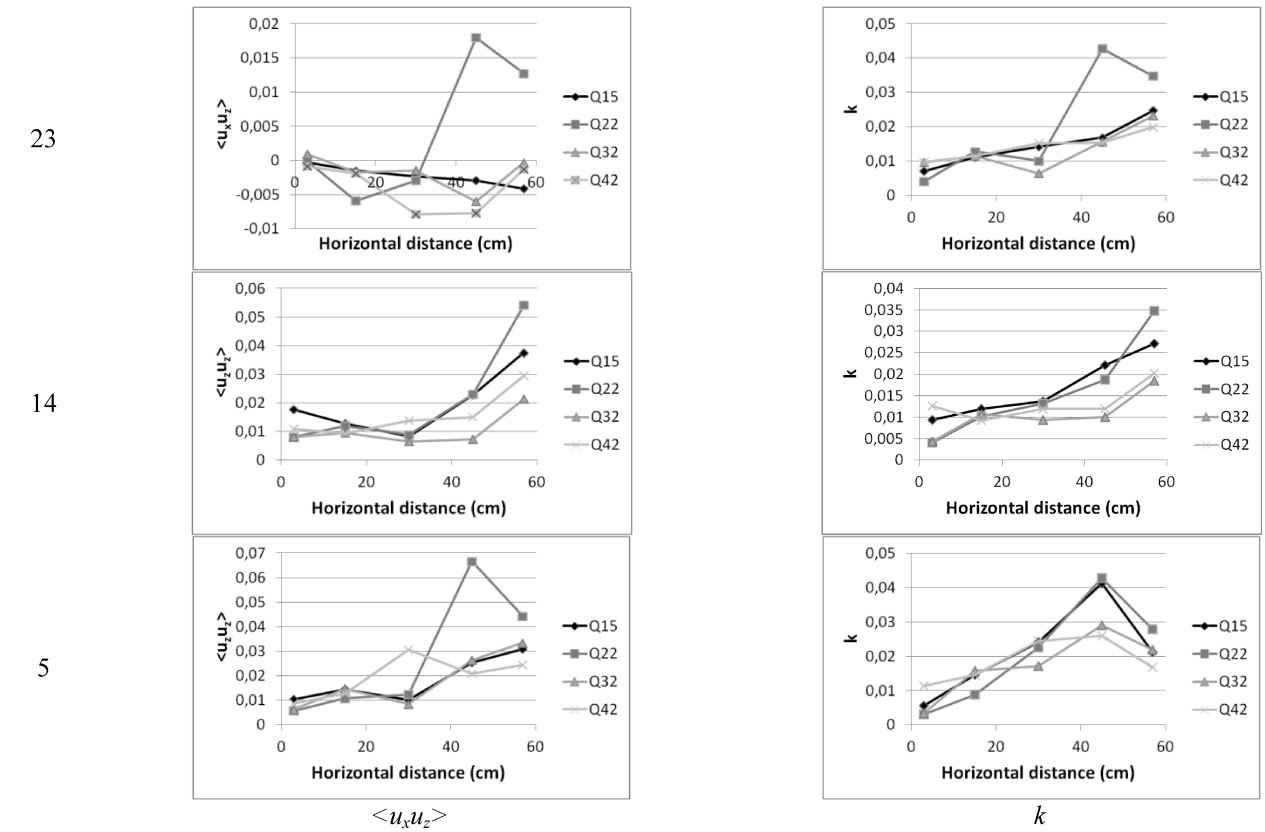

Figure 7. Shear stresses (left) and turbulent kinetic energy (right).

Like normal stresses, shear stresses and turbulent kinetic energy present an increase in turbulence along the horizontal distance, except for 23 cm height, where there is no clear pattern, as seen in Figure 7, top left. For both parameters, Q_{22} presents the maximum value, located near the downstream wall at 14 cm height (centre charts) and distanced 45 cm on the top and bottom of the gully.

5 CONCLUSION

The flow occurring on a gully was characterized, for both surcharged and drainage conditions. The average velocity fields were analyzed and a qualitative study of the air inside the gully was performed, as well as the turbulence characterization for the drainage flow. Several flow rates were studied, which showed similarity on their behavior.

- On the surcharged flow there is an anticlockwise vortex on the left side of the gully, whilst on the right side flow velocities are quite low.
- Drainage flow exhibits a big quantity of air drawn into the inside of the gully, but it diminishes with the increase of the flow rate, due to the displacement of the hydraulic jump or the increase of water depth.
- There is only one visible vortex on the drainage flow, clockwise, and its centre is located near the orifice, but it ascends as the flow rate increases.
- Turbulence increases along the horizontal distance, but no clear pattern was identified between the flow rates.

These results are quite important and highlight instabilities that may occur in gullies. They may be used to calibrate and validate numerical models that simulate gullies. This study should be extended in order to integrate channel and buried pipes.

NOTATION

$<u_i u_j>$	Reynolds stresses
d	orifice diameter
f	NDV sampling frequency
Fr	Froude number for the orifice
g	acceleration due to gravity
H_u	water height upstream the gully
k	turbulent kinetic energy
Q	flow rate
Re	Reynolds number
t	time
U	average velocity
ν	kinematic viscosity

ACKNOWLEDGEMENTS

The authors would like to acknowledge financing through the FCT ("Fundação para a Ciência e Tecnologia") and the COMPETE ("Programa Operacional Temático Factores de Competitividade"), supported by FEDER ("Fundo Europeu de Desenvolvimento Regional") through projects PTDC/AAC-AMB/101197/2008 and PTDC/ECM/105446/2008. The authors also thank Mr. Joaquim Cordeiro da Silva for the help provided during the experiments and the students Joana Pião and Pedro Lopes as well as Marín Romagnoli who made previous measurements in the channel.

REFERENCES

Carvalho, R., Leandro, J., David, L., Martins,R., Melo,N. (2011a). Numerical research of the inflows into different gullies outlets. Computing and control for the water industry. 5-7 September, 2011, Exeter, UK.

Carvalho, R., Leandro,J., Martins,R., Abreu,J., de Lima,J. Lopes, P. (20121b). 2DV numerical modelling of diferente flows occurring in gullies. 12th International conference on urban drainage. 11-16 Sepember, 2011, Porto Alegre, Brazil.Numerical study of the flow behavior in a gully. 4th International Symposium on Hydraulic Structures, 9-11 February 2012, Porto, Portugal.

Djordjević,S., Saul, A.J., Tabor, G.R., Blanksby, J., Galambos, I., Sabtu, I., Sailor, G. (2011). Experimental and numerical investigation of interactions between above and below ground drainage systems. 12th International conference on urban drainage. 11-16 Sepember, 2011, Porto Alegre, Brazil.

Goméz,M., Russo,B. (2007). Hydraulic efficiency of macro-inlets. Proc. Novatech, pp. 1157-1164.

Goméz,M., Russo,B. (2009). Hydraulic efficiency of continuous transverse grates for paved areas. Journal of Irrigation and Drainage Engineering, Vol.135:2, pp.225-230.

Goring, D., Nikora, V. (2002). Despiking acoustic Doppler velocimeter data. Journal of Hydraulic Engineering, Vol. 128, pp. 117-126.

Lopes,P., Leandro,J., Carvalho, R., Martins, R. (2012). Hydraulic behaviour of a gully under surcharged conditions. 9th international Joint IWA/IAHR Conference on Urban Drainage Modelling. 3-7 September, 2012, Belgrade, Serbia.

Martins, R. (2011); Estudo do comportamento hidráulico se sumidouros em modelo numérico OpenFOAM. FCTUC. Coimbra.

Martins,R., Leandro,J., Carvalho,R. (2012). Hydraulic behaviour of a gully under drainage conditions: numerical vs. experimental. 9th international Joint IWA/IAHR Conference on Urban Drainage Modelling. 3-7 September, 2012, Belgrade, Serbia.

Romagnoli, M., García, C., Lopardo, R. (2012). Signal processing technique and uncertainty analysis of ADV turbulence measurements on free hydraulics jumps.

Sontek (2001). SonTek/YSI ADVField/Hydra Acoustic Doppler Velocimeter (Field) Technical Documentation. SonTek/YSI, San Diego, USA.

Wahl,T. (2000). Analyzing ADV data using WinADV. ASCE Joint Conference on Water Resources Engineering and Water Resources Planning and Management, Minneapolis, July 30–August 2, 2000, USA.

Wahl,T. (2003). Discussion of "Despiking acoustic Doppler velocimeter data" by G. Goring and Vladimir I. Nikora." Journal of Hydraulic Engineering, Vol. 129, pp. 484-487.

IWLHS, 20-22/02/2013, Aachen - Bung & Pagliara (eds) - © 2013 Bundesanstalt für Wasserbau ISBN 978-3-939230-04-5

Exploring the Underlying Physics of the Double Vortex Insert Device by CFD

A. Malekpour & B. Karney
University of Toronto, Toronto, Canada

R. St-Aubin
IPEX Inc., Toronto, Canada

D. Radulj
HydraTek & Associates Inc., Toronto, Canada

ABSTRACT: The "double vortex" is a patented device originally invented by Dr. Eugene Natarius in order to efficiently admit and mix air into sewer systems. Examination of the general flow pattern via both a conceptual and CFD model revealed that this device does indeed possess considerable potential to admit and mix a large amount of air. This study explores and seeks to understand the flow mechanism through which air is admitted and mixed. To this end, the program Fluent is utilized to perform a three-dimensional two-phase flow analysis. Numerical experiments show that the device's elbow shape establishes a negative pressure at a high point inside the device, and that this mechanism is mainly responsible for admitting air into the system, while its double vortex rotation by enhancing water and air mixing assists in downstream air movement. The negative pressure is primarily induced by the profile that causes the hydraulic grade line to fall below the pipe's centerline. To better understand the original device, the alternative of a simple elbow with an air vent to admit flow to the top of a drop shaft is also numerically investigated. The results show that this simple assembly also admits considerable amount of air into the system through the same mechanism, although the large quantity of air intrusion constraints the flow and causes air to partly separate from the water flow.

Keywords: Double Vortex, Aeration, Sewer System, CFD

1 INTRODUCTION

In general, vertical drop shafts are commonly used as compact hydraulic structures that safely connect a higher energy flow upstream to a lower downstream energy level. These structures at least partly function as energy dissipators where an annular hydraulic jump forming at the bottom of the shaft is a key component in this mechanical energy dissipation. Moreover, in wastewater systems they also function as an aerator to increase the oxygen dissolved in the wastewater, which in turn helps to alleviate pipe corrosion and odour problems (Natarius 2000).

The most important opportunity and challenge of these structures is the formation of large air pockets in the vertical water column resulting from chaotic shaft water motion, which is then forced into the downstream conduit. Air pocket that coalesce in the downstream conduit is often problematic and may result in intermittent flow or even blowback if the buoyancy force acting on the air pocket exceeds the flow-induced drag force (Falvey 1980). Moreover high levels of flow agitation in these structures enhance the emission of hydrogen sulphide (H_2S), which could worsen odour issues locally (Churchill and Elmer 1999).

To cope with the problems associated with vertical drop shafts, an innovative device like the vortex drop structure with the Vortex Insert Assembly (VIA) was developed by Dr. Eugene Natarius (Natarius 2000). The VIA is a simple, pre-fabricated insert for existing or new drop structures. It has been shown to appreciably reduce odour and corrosion issues on all types of sewer drops.

Recently a new type of drop shaft with a Double Vortex Inlet (DVI) assembly was proposed by the same inventor to improve the performance of the VIA. This assembly works with fully pressurized flow and is believed to require a lower drop height in order to perform well and to achieve the desired results. Although this new assembly has not been field tested, the observations made on the performance of a

small-scale physical model revealed good potential for sewer aeration and that the device could be effectively employed to alleviate the odour and corrosion issues in sewer systems. Unfortunately, little is presently known about the underlying physics driving the direct air entry into the system, which in turn complicates the setup of the design criteria for real applications and sometimes leaves designers leery to try something that they do not completely understand. Thus, this study aims to shed light on the mechanism under which air could be sucked or drawn into the system. A better understanding of the underlying physics would make it easier to refine and apply design criteria for field applications.

A brief overview of the mechanism governing the traditional vortex inlet drop shaft is a good departure point toward the physical understanding of DVI drop shaft structure.

2 VORTEX INLET DROP SHAFTS

A typical schematic of a (single) vortex inlet drop structure is shown in Figure 1. The open channel flow approaching the structure contracts at the entrance by passing into the region of reduced cross-sectional area. This section is designed such that a flow control section is established at the entrance. The critical flow section hydraulically isolates the effluent system from the performance of the drop shaft structure. The flow passing through the control section switches from subcritical in the effluent conduit to supercritical in the steep-sloped vortex channel where the flow is accelerated to achieve the required vortical strength. The vortex flow causes the water to cling to the drop shaft's walls and produces a well-defined and stable air cone at the middle of the shaft. In such a design, the air column is not blocked anywhere between the upstream and downstream ends of the vertical shaft, and thus large scale air intrusion to the downstream conduit is avoided. Moreover, the vertical velocity of the water column motivates slight negative pressures that in turn induce a weak air flow below the shaft. This flow can effectively limit the development of unfavourable odours. The vortex nature of the flow also causes an inner pressure gradient to be established just below the downstream water surface, and this is directly due to the annular hydraulic jump. The inward pressure gradient causes the air bubbles to move to the center of the shaft and thus leaves the water to the air cone (Zhao et al. 2006). Another important superiority of the vortex drop shaft over plunge-flow models is the enhancement and predictability of energy dissipation in the vortex drop as the flow clings to the wall and gives rise to skin friction loss (Jain 1988). Although the energy loss is less than that produced by the annular hydraulic jump, it can still reduce the force imposed by the fluid on the bottom face of the drop shaft. In summary, vortex inlet drop structures can appreciably reduce odour and corrosion problems in sewer systems through increasing the oxygen dissolved in the sewer flow, and by reducing the turbulence-based agitation in the drop structure (Moeller and Natarius 2000).

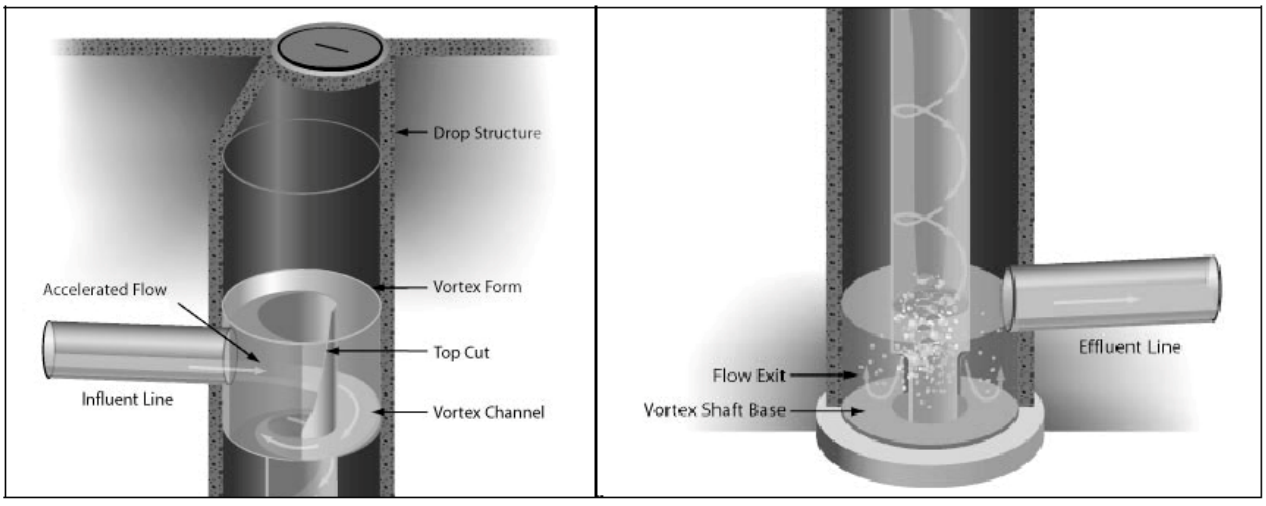

Figure 1. Typical vortex inlet drop shaft (left- inflow; right-outflow)

3 DOUBLE VORTEX INLET DROP SHAFT

The double vortex inlet drop shaft (hereafter often referred to as DVI), is naturally related to the device just described in the previous section, but it also differs from it in several key ways as well. First, the new device is designed to work under fully pressurized flow and it is believed to require a lower drop height in order to perform as designed. Unfortunately, little information is presently available regarding the performance of the DVI structure, with the exception of a video showing a small-scale model of the device. The track/path of the flow in the structure/system can be explained by considering geometrical drawings of the double vortex inlet device (Figure 2).

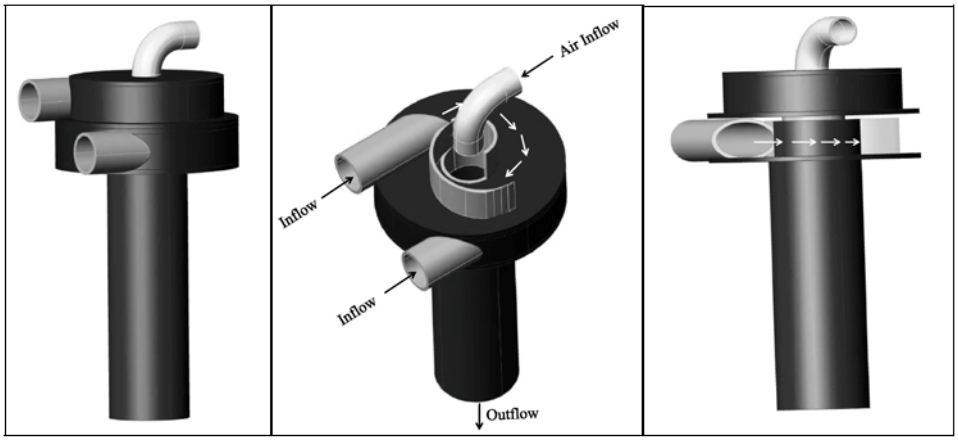

(A) (B) (C)

Figure 2. Three dimensional geometrical model of DVI: (A) general view, (B) flow path in upper chamber, and (C) flow path in lower chamber

The effluent conduit is split into two pipes at the entrance of the device and each pipe then feeds a distinct chamber in such a way that the flow in the upper chamber rotates in the opposite direction to the flow in the lower chamber. The upper chamber flow is discharged to a sinkhole at the chamber's center where the flow is delivered to a vertical pipe collecting the flow from the lower chamber. An air vent at the top of the upper chamber admits air into the system.

The experiments made on a small scale model of the DVI drop shaft show that the device does admit the desired large quantity of air into the system; however, the air intrusion mechanism has never actually been properly explained and/or documented. Figure 3 presents a few snapshot pictures from a video demonstrating the performance of the model device. The flow is completely air free when the air vent is plugged (left picture) whereas it develops a bubbly flow with its characteristic milky colour once the air vent is unplugged (right picture).

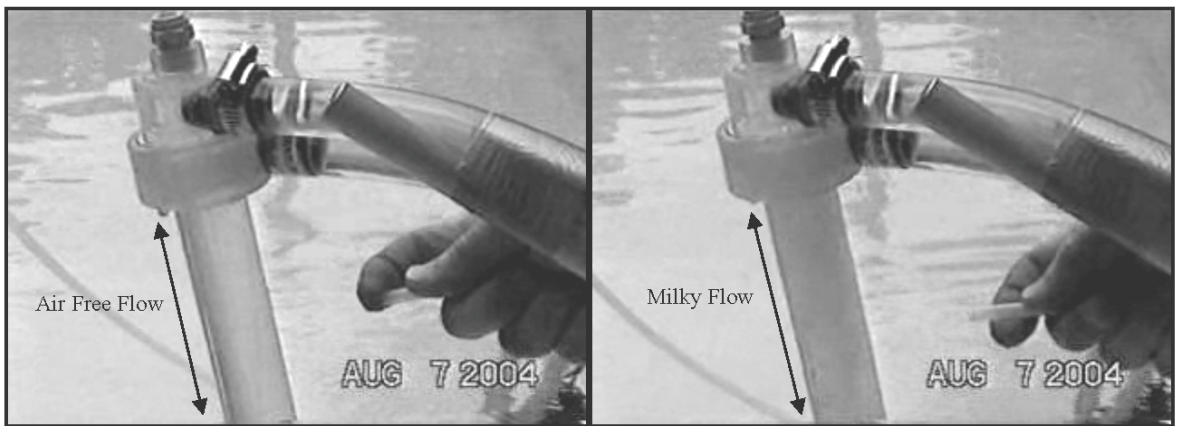

Figure 3. DVI device performance pictures

The key question that arises is whether the double vortex created in the chambers is responsible for the significant air intrusion, or whether or not other factors/mechanisms are at play. Certainly, the pressure in the upper chamber is obviously less than atmospheric since it allows air into the system. The next question is therefore whether the double vortex formation in the chamber can produce negative pressures in the upper chamber, or whether any other mechanism induces the sub-atmospheric pressure at that point.

To answer this crucial question, one should first consider the operational circumstances under which the negative pressures could be induced in such a pipe system.

4 ORIGINS OF NEGATIVE PRESSURE

Negative or sub-atmospheric pressures can be induced in closed conduit systems under two fundamentally different conditions. First, it can occur if the system velocity locally increases due to a decrease in the cross-sectional area. The velocity at which the negative pressure is created depends on the system pressure and flow conditions; the higher the original pressure, the higher the required velocity. An example of this phenomenon is the pressure drop at the throat of a venturi tube in which the velocity increase gives rise to a pressure reduction.

The negative pressure at the throat section can more easily be achieved when the upstream pressure decreases due to a velocity increase in the throat section. The simple mechanism of a venturi has made it an ideal device for the injection of Chlorine or other gases into closed conduit pipe systems. This mechanism is also useful for water pipe system aeration. Baylar et al. (2009) experimentally measured the amount of air that intrudes into a venturi tube through the orifices installed at the throat. These authors found that the device can perfectly admit air to the system provided that a negative pressure is established in the throat section. However, this device can really only be implemented low pressure pipe systems because in the case of high pressure systems, the velocity required to bring the hydraulic grade line (HGL) below the throat's elevation is typically impractically high.

The second condition that could potentially induce a negative pressure in a pipe system occurs when the HGL falls below the pipeline elevation profile. As an example, in a sufficiently long gravity system where the pressure at the outlet section is equal to the atmospheric pressure, the HGL in the pipe system can be obtained with fairly good accuracy by connecting the end of the pipe to the water surface of an upstream reservoir. The HGL in such a typical pipe system that discharges water to the atmosphere through a short-vertical elbow is shown in Figure 4. As shown, the negative pressure can be expected across a wide range of the system, with the maximum negative pressure value occurring at the end of the pipe and this value is essentially equal to the height of the elbow, denoted by "h".

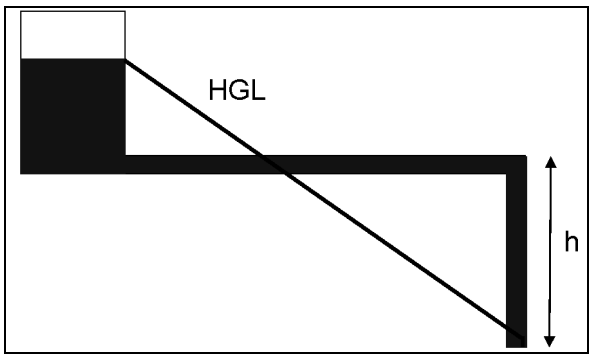

Figure 4. Negative pressure establishments in a typical pipe system

An easy way to investigate whether a high velocity is the source of the negative pressure in the double vortex device is to inspect the flow path cross-sectional area through a three-dimensional geometrical model. Figure 2 presents a geometrical model of the DVI device, as developed based on the available device prototype drawings. Flow paths are shown by arrows in the upper and lower chambers, and it is relatively clear that the potential flow cross-sectional area in the chambers is not reduced when compared to the pipes feeding the chambers. Although non-uniform flow distribution caused by the vortex action in chambers may still increase the velocity beyond that of the entrance pipes, the vortex flow is not strong enough to give rise to a considerable velocity increase. This can be easily shown by applying the free vortex concept on the simplified flow pattern inside the chambers, as shown in Figure 5.

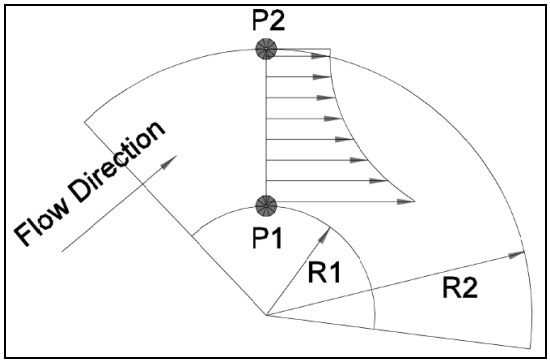

Figure 5. Schematic velocity distributions inside the double vortex chambers

The free vortex flow assumption insists that the production of tangential velocity and curvature radius of flow is constant, such that:

$$VR = C \tag{1}$$

In the current case, the constant on the right hand side of the above equation can be easily calculated by applying the mass conservation law. The flow through the section P1-P2 can be calculated by the following equation:

$$Q_{P1-P2} = \int_{R1}^{R2} VHdr = \int_{R1}^{R2} \frac{HCdr}{r} = HC \ln\left(\frac{R_2}{R_1}\right) \tag{2}$$

where H = the height of chamber, $R1$, $R2$ = the radius of inner and outer chamber walls, C = vortex constant value, V = tangential velocity, R = streamline curvature radius.

Mass conservation requires that the flow passing through section P1-P2 is exactly equal to flow entering the system via the inlet pipe. Therefore, the constant coefficient, C, can be calculated as follows:

$$C = \frac{Q_I}{H \ln\left(\frac{R_2}{R_1}\right)} = \frac{\pi D^2 V_I}{4H \ln\left(\frac{R_2}{R_1}\right)} \tag{3}$$

where Q_I = inlet pipe discharge, V_I = inlet pipe velocity, and D = inlet pipe diameter.

The above equation can be applied on the given example in order to investigate how the velocities change inside the chambers. To this end, a DVI is considered with: D = 7.5 cm, upper chamber R1 and R2 = 5, and 15 cm respectively, lower chamber R1 and R2 = 7.5, and 17.5 cm respectively, upper and lower chamber H = 7.5 cm. With this information the maximum velocities inside the upper and lower chambers for different inlet velocity are calculated by using Equations 1 to 3, and the results are summarized in Table 1.

As shown, the velocities in the upper chamber are just slightly greater than the inlet velocity, whereas the velocities in the lower chamber are lower than the inlet velocity. It is evident that such velocity changes cannot be responsible for the negative pressure and air intrusion to the system, particularly when the extra turbulence induced by the interaction of the opposite rotating flow in the chambers that is not considered in this simplified approach, acts to make the velocity field more uniform. While this is partially evident in the simple model, a more precise determination of the cross-sectional flow area is more readily obtained through the use of a three-dimensional numerical analysis via computational fluid dynamics (CFD).

Table 1. Maximum velocity in upper and lower chambers

Inlet velocity (m/s)	Maximum velocity in upper chamber (m/s)	Maximum velocity in lower chamber (m/s)
2	2.14	1.85
3	3.22	2.78
4	4.30	3.70
5	5.36	4.63
6	6.44	5.56

Based on hydraulic laws, the provisional conclusion at this point is that the significant air intrusion into the DVI is likely primarily due to the device's elbow shape profile rather than the direct action of the swirling flow formed in the chambers. A CFD analysis is an excellent tool for confirming this concept because it can act to provide a precise velocity field within the DVI; information from which it is subsequently possible to justify the conclusions obtained from the simplified analysis. Furthermore, if the elbow shape of the DVI is the dominant cause of air intrusion, a CFD analysis of both a DVI and a simple elbow with an air vent at the top, should ultimately yield similar results.

5 CFD ANALYSIS

5.1 *Governing physics and employed model*

The device's geometry ensures that the true flow pattern in the system has strong three-dimensional characteristics and thus that pattern could be determined by a three dimensional hydraulic analysis, in which all flow channels formed by internal and external walls of the device must be considered. Moreover, in order to consider the air flow in the system, a two phase flow model is also critical.

Generally speaking, several different types of two phase flow regimes can potentially occur in systems, including bubbly flow, droplet flow, slug flow, and stratified flow (Falvey 1980). Visual observations of the double vortex device (see Figure 3) reveal that air does indeed move within the system and this is most evident through the presence of the large number of small and diffused bubbles. Several different types of two phase flow models exist, including: the volume of fluid (VOF), Eulerian, and mixed flow models. The mixed flow model is the most compatible model that can be used to resolve bubbly flow motion and therefore is the preferred and employed model for this study. This numerical approach can model the water and air phases by solving momentum and continuity equations for mixture, the volume fraction equation for the air phase, and the algebraic expressions for the relative velocity.

In this research the proven CFD software, Fluent V6.3 (Fluent Inc. 2006), is employed as the numerical tool of choice. A three dimensional algebraic model with slip velocity and with the standard k-ε turbulence model is selected as the computational model within Fluent.

5.2 *Numerical results*

A DVI device with the same properties discussed in the simplified hydraulic analysis is directly considered within the CFD analysis. A vertical pipe with an internal diameter of 15 cm and a height of 1.5 m is assumed to collect water at the bottom of the lower chamber. The air vent size is 5 cm and the operating flow rate is assumed as 17.7 L/s, such that the velocity in each inlet pipe is 2 m/s. For the sake of comparison, the internal diameter, vertical height, air vent diameter, and flow rate for the simple elbow model are considered to be similar to those assumed for the DVI device. With this assumption, the entrance velocity to the elbow is 1 m/s.

In order to observe the hydraulic performance of the two different devices, a hydraulic model without ventilation is first considered. In order to achieve this effect the air vent surface is blocked in both cases, and a three dimensional hydraulic analysis is carried out for each case. Subsequently and in order to examine the potential for air intrusion and mixing, the air vent surfaces are unblocked and a two phase flow model simulation is carried out for each case. The following sections discuss these two sets of numerical results.

5.2.1 *Without ventilation*

To examine the hydraulic performance of the system in the absence of air intrusion, both the DVI device and the simple elbow device were simulated in the single phase mode by considering the ventilation surfaces as isolated walls. In order to verify that a velocity increase in the upper and lower chambers of the DVI is not the main cause of the induced negative pressure and subsequent air intrusion, the velocity fields in the upper and lower chambers were inspected and are shown in Figure 6. It can be seen that in general velocities in the upper chamber are higher than those in the lower chamber, and this is also predicted by the analytical model (see Table 1). Furthermore, it is evident that the velocities in both chambers do not significantly exceed the entrance velocity of 2 m/s; a result which is again in line with the analytical results. Figure 6 shows that the velocities in both chambers increase with the distance away from the outer wall and closer to the inner walls. This confirms our earlier assumption that the free vortex

motion is dominant within the chambers. Overall, the numerical results confirm that the velocity change is in itself not high enough to induce negative pressure and the air intrusion into the DVI device.

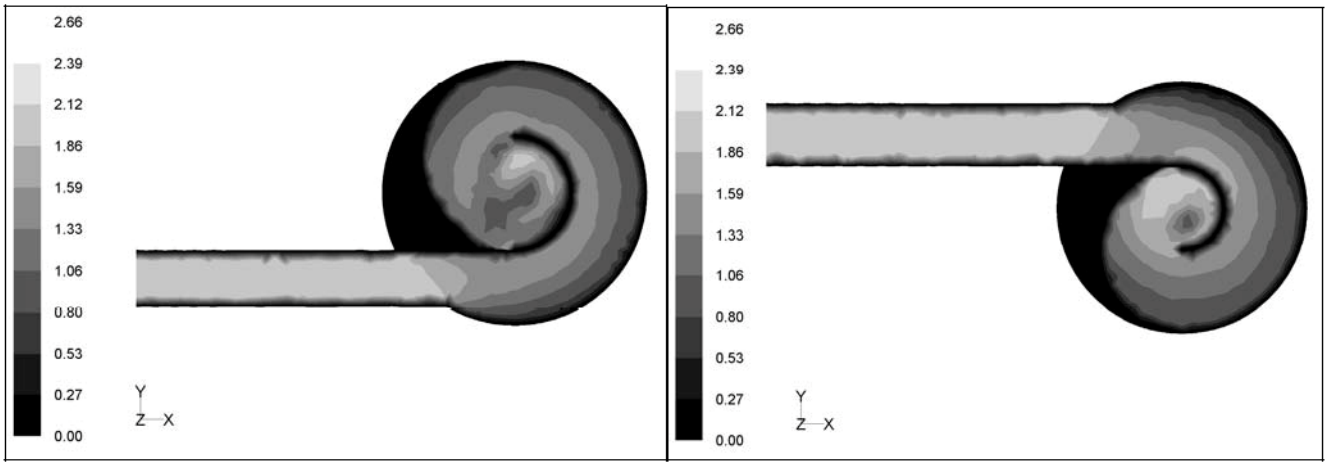

Figure 6. Velocity fields (in m/s) in the lower chamber (left) and upper chamber (right) of the DVI device

An inspection of the pressure distribution along both the DVI and the simple elbow devices reveals that the shape of the profile is likely the key cause of the negative pressures. Figure 7 depicts the predicted pressure distribution along the simple elbow and DVI devices. As shown, negative pressures having the same distribution are evident in both devices. As expected, the negative pressures increase as one moves vertically upwards towards the crown of each device. Since the velocities and the resulting head losses are low in both cases, the negative pressure heads at each point are almost equal to the elevation of the point relative to the elevation of the outlet section, or in other words to the height of the vertical section.

5.2.2 *With ventilation*

A two phase flow model simulation was performed for both the simple elbow and the DVI device in order to investigate the potential for air intrusion and mixing. The numerical results show that in both cases a significant amount of air is entrained into the system via the air vents. The total air flow rates that intrude into the DVI and simple elbow devices are predicted as 35.2 and 52.8 L/s respectively, and these are therefore almost 2 and 3 times higher than the system flow rate, respectively. These air flow rates produce high velocities of 18 and 27 m/s within the vent pipes of the DVI and simple elbow devices, respectively. Thus, not surprisingly, a small vent pipe could be used to create a flow restriction that could limit the air flow into the DVI. In general and somewhat less expected, the predicted air flow in the simple elbow is much higher than that in the DVI device. This result can be explained by considering the pressure distribution that is established within the devices, and these are shown in Figure 8.

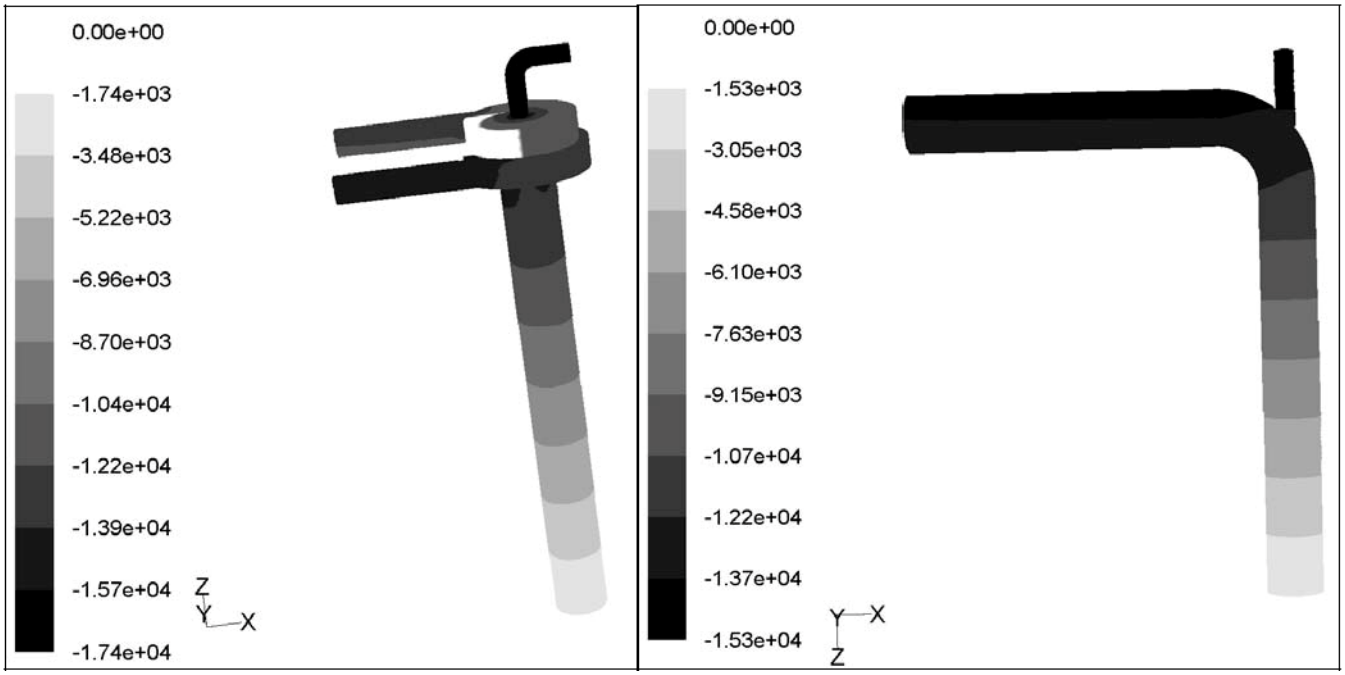

Figure 7. Pressure (in Pascals) distribution along the DVI devices, and simple elbow without aeration

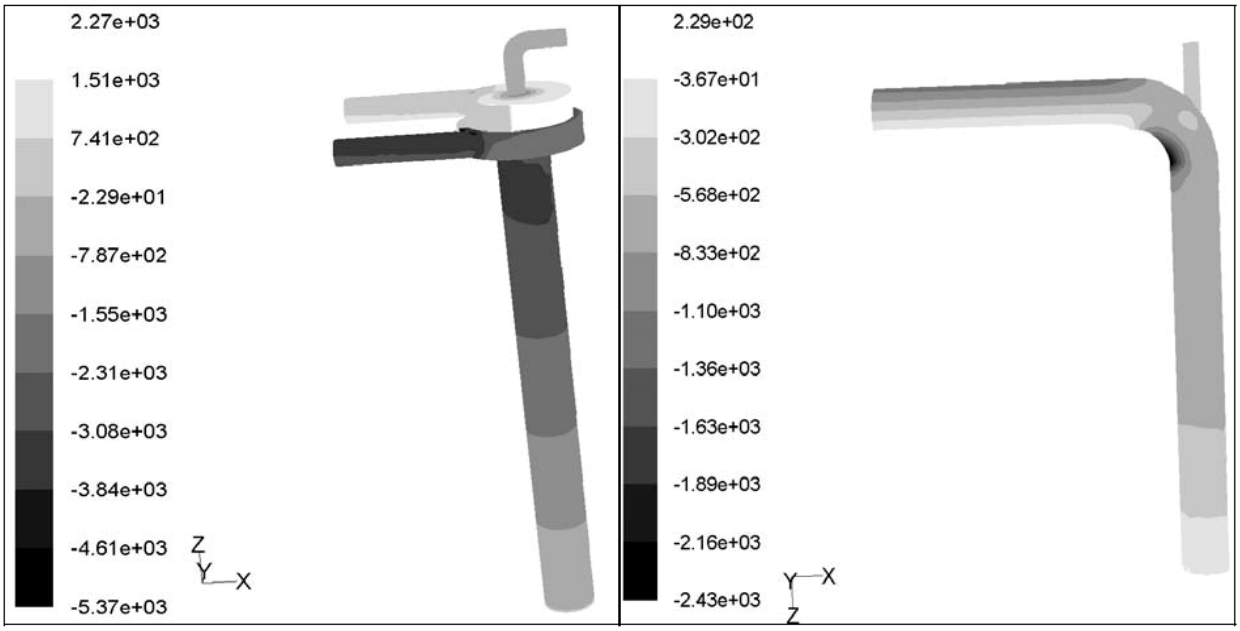

Figure 8. Pressure distributions in the DVI and simple elbow devices with aeration

As shown, the top and bottom faces of the lower chamber of the DVI experience different pressures in the range of 1510 to 714 Pa in the top face, and 741 to -22.9 Pa in the bottom face. The difference is primarily due to the head loss that occurs when the flow in the upper chamber and lower chamber are united. It is also evident that the backup pressure required to push the flow through the sink hole affects the pressure at the air vent surface. The results show that the average pressure at the air vent surface of the DVI device is -212 Pa (-0.022 m), whereas it is approximately -492 Pa (-0.05 m) at the air vent surface of the simple elbow. This small pressure difference has a significant impact on the air flow, and thus makes the simple elbow device more capable of inducing a larger air flow rate. This result is physically quite meaningful since a small vacuum pressure can yield large air flow in the air vents.

Further consideration of the pressure fields in the two devices shows that in both cases the air intrusion acts to maintain most of the pressures at almost atmospheric, although residual negative pressures still exist in both cases and are slightly greater in the DVI device because of the higher air flow in the simple elbow.

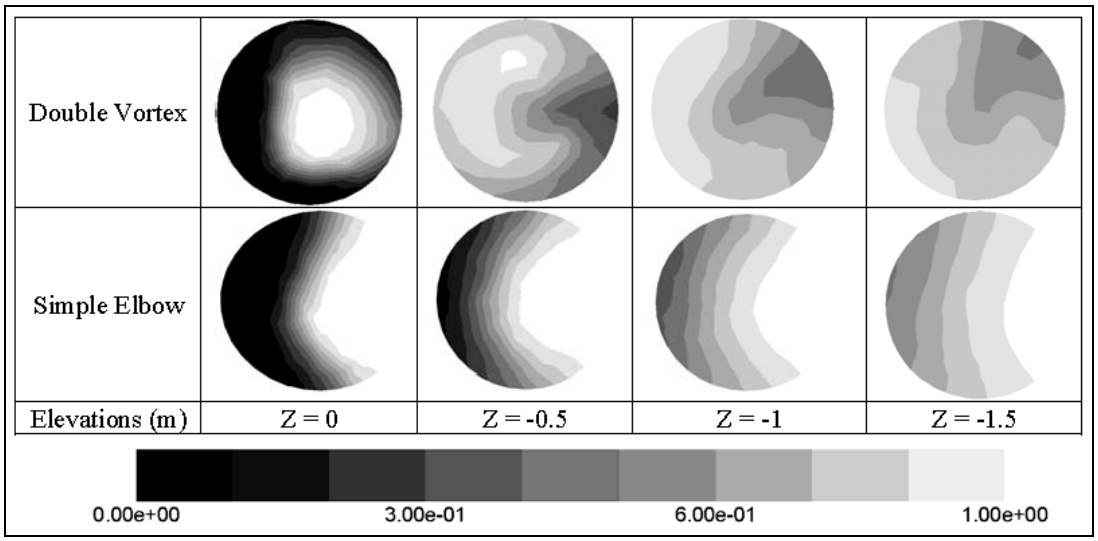

Figure 9. Air void fraction in the different cross sections of the vertical pipes of the DVI and simple elbow devices

In order to investigate the air mixing capability of the two devices, the distribution of the air void fraction across the vertical pipes was reviewed. Figure 9 compares the air void fraction across different cross sections of the vertical pipe of both devices. As can be seen at the top of the vertical pipes, the mixing is generally poor and in both cases water and air are moving in distinct layers. Air in the DVI pipe tends to flow in the middle and is also slightly deflected to the outer wall of the vertical pipe due to the action of the swirling flow. In the simple elbow case, the air flows in a distinct layer near the outer wall. Improved mixing is observed in both devices as the flow descends the vertical pipe, although in the simple elbow a

distinct air flow layer tends to moves in the outer wall of the pipe. It is also worth noting that in the DVI, the highest air void fraction zone in the cross section rotates counter-clockwise as the flow descends the vertical pipe. This is due to the swirl flow that originates at the chambers and that subsequently propagates into the vertical pipe. Furthermore, in the cross sections where the flow leaves the device (i.e., Z = -1.5 m), the air void fraction varies between 1 and 0.5 in both devices. However, in the simple elbow case, a good portion of the pure (i.e., non-mixed) air leaves the system in a single distinct layer.

Overall, the mixing appears to be better in the DVI device than in the simple elbow. Nonetheless, this fact still cannot prove the superiority of the DVI over the simple elbow, because first the amount of air flow in the simple elbow is much greater than that in the DVI and this can potentially compensate for the difference in the air form that leaves the device. Second, in both cases the air flow that enters the devices (i.e., up to 2-3 times the total system flow) significantly exceeds the amount by which air can be dissolved into water (i.e., 3-4% of the total system flow). Lastly, the overall simplicity may recommend the simple device like an elbow in some applications.

6 SUMMARY AND CONCLUSION

The performance of the double vortex insert (DVI) device is analytically and numerically explored. Using the basic hydraulic principles, it is analytically shown that the device's ability to entrain a large amount of air is due to the elbow like profile of the device, and not due to the action of swirling (vortex) flow in the chambers, as originally assumed. A 3-D CFD analysis further confirms this result. The analysis also confirms that the vortices in the upper and lower chambers are not in themselves strong enough to increase the velocities in the chambers to a level that would yield negative pressures and lead to air intrusion. Furthermore, the results confirm that the elbow shape of the device is the key component in the establishment of workable negative pressures.

In order to evaluate the air intrusion and mixing capabilities of the device, and in order to make sure that the elbow profile shape of the device is the main cause of the air intrusion, a three dimensional two phase flow analysis is performed for both the DVI device and a simple elbow with an air vent having similar geometrical and hydraulic parameters. The analysis results clearly show that both devices allow a large amount of air to intrude into the system, thereby reconfirming the crucial role of elbow shape to the DVI air intrusion behaviour. Furthermore, the results also surprisingly demonstrate that the potential air flow in the simple elbow is significant. This can be explained by considering the resulting backup pressure in the upper chamber that is established in order to compensate for the head loss that occurs when the upper chamber flow is united with the lower chamber flow within the sink hole. This backup pressure partially increases the pressure at the air vent surface which in turn causes the reduction in the air flow.

Inspection of the air void fraction in the vertical pipes of both the DVI and the simple elbow device shows that the DVI produces better mixing than the simple elbow. This is because the swirling flow that propagates from the lower chamber to the vertical pipe and more efficiently mixes the air and water, while a significant portion of air flow in the simple elbow tends to flow and leave the vertical pipe in a distinct layer and without interacting with water.

ACKNOWLEDGEMENT

The funding for this research is provided by IPEX Inc. and is gratefully acknowledged.

NOTATIONS

Q	discharge
V	velocity
R_1	the radius of the inner wall of the double vortex's chambers
R_2	the radius of the outer wall of the double vortex's chambers
H	the height of the double vortex's chambers
C	free vortex constant

REFERENCES

Baylar, A., Aydin, M. C., Unsal, M., and Ozkan, F. (2009). Numerical Modeling of Venturi Flows for Determining Air Injection Rates Using Fluent v. 6.2., Mathematical and Computational Applications, 14(2), 97-108.

Churchill, P., and Elmer, D. (1999). Hydrogen Sulfide Odor Control in Waste Water Collection Systems. NEWEA Journal, 33(1).

Falvey, H. T. (1980). Air-Water Flow in Hydraulic Structures. USBR, Denver, Colorado.

FLUENT Inc. (2006). Fluent 6.3 User Guide. FLUENT Inc.

Jain, S. C. (1988). Air Transport in Vortex-Flow Drop-Shafts. Journal of Hydraulic Engineering, 114(12), 1485–1497.

Moeller, W. P., and Natarius, E. M. (2000). The Vortex Drop Structure Inspection for Odor and Corrosion Control. WEFTEC.

Natarius, E. M. (2002). Vortex Insert Assembly Controls Odors and Corrosion in Sewer Drops, WEF Odors and Toxic Air Emissions Conference.

Zhao, C., Zho, D. Z., Sun, S., and Liu, Z. (2006). Experimental Study of Flow in a Vortex Drop Shaft. Journal of Hydraulic Engineering, 132(1), 61-68.

6 Experimental Studies

IWLHS, 20-22/02/2013, Aachen - Bung & Pagliara (eds) - © 2013 Bundesanstalt für Wasserbau ISBN 978-3-939230-04-5

V-Notch Weir Overflow: an Unsteady Calibration

H. Chanson & H. Wang
The University of Queensland, School of Civil Engineering, Brisbane QLD 4072, Australia

ABSTRACT: Thin-plate V-notch weirs are commonly used as measuring devices in flumes and channels. Herein, the discharge calibration of a large 90º V-notch weir was performed using an unsteady volume per time technique. The weir overflow was initially shut. The sudden opening of the gate was associated with an initial phase of transient water motion associated with a negative wave propagating in the reservoir and the free-falling motion of a mass of fluid in the close proximity of the overflow behind the initial wave. This initial phase was followed by a more gradual overflow motion which was affected by the seiche in the upstream reservoir. The integral form of the continuity equation was used to derive the relationship between flow rate and upstream water depth. The findings showed that the unsteady discharge calibration of the V-notch weir yielded similar results to a more traditional calibration approach based upon steady flow experiments, while allowing the rapid testing of a wide range of discharges.

Keywords: V-notch weirs, Unsteady calibration, Transient flow motion, Seiche, Physical tests

1 INTRODUCTION

A weir is a structure placed across a channel which raises the upstream water level and may be used to measure the flow rate. A range of measuring weirs were developed (Darcy and Bazin 1865, Bos 1976, Ackers et al. 1978). The V-notch thin-plate weir, also called triangular weir, has an overflow edge in the form of an isosceles triangle. The Australian Standards (1991) expresses the discharge calibration of the V-notch weir in the form:

$$Q = C_d \times \frac{8}{15} \times \tan\alpha \times \sqrt{2 \times g \times h^5} \qquad (1)$$

where Q = water discharge, C_d = dimensionless discharge coefficient, α = notch opening angle, g = gravity acceleration, h = upstream water depth above the notch (Fig. 1).

The contribution herein presents a novel approach to calibrate a large 90º V-notch weir using a volume per time approach. A series of relatively large-size tests were conducted to measure the upstream water level at high frequency following a sudden overflow opening. The results demonstrate the application of the technique while they highlight the effects of seiche motion in the upstream reservoir.

2 PHYSICAL FACILITY AND INSTRUMENTATION

2.1 *Equipment and instrumentation*

New experiments were performed in a 2.36 m long, 1.66 m wide and 1.22 m deep reservoir with a 400 mm high 90° V-notch thin-plate weir located at one end (Fig. 2). The weir was made out of brass and designed based upon the Australian Standards (1991) and International Organization for Standardization (1980). The notch was located 0.82 m above the reservoir invert. The weir overflow was initially closed with a fast-opening gate hinging outwards and upwards (Fig. 2 & 3).

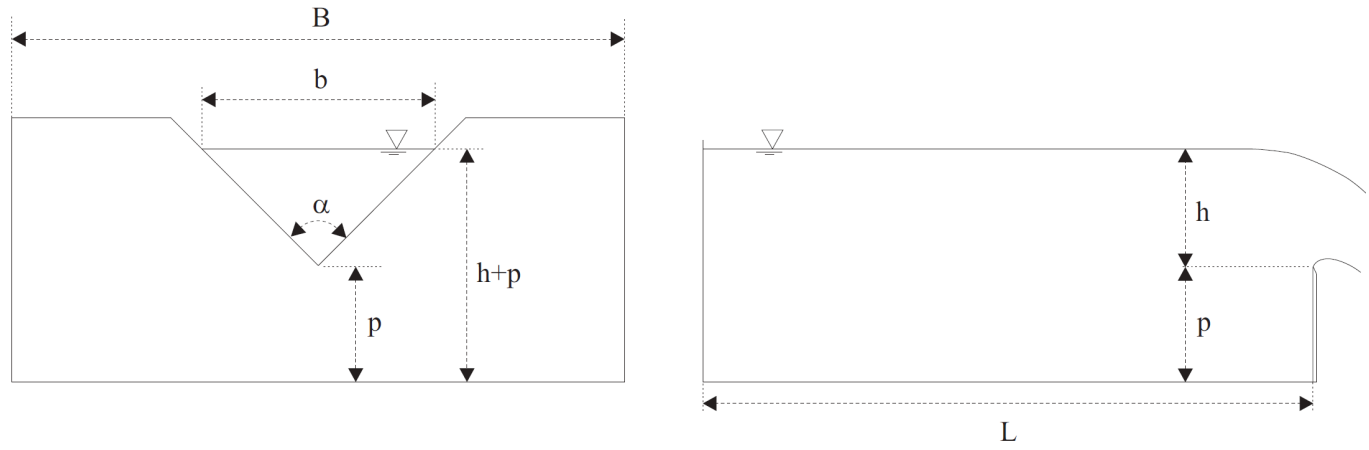

Figure 1. Definition sketch of a V-notch weir overflow

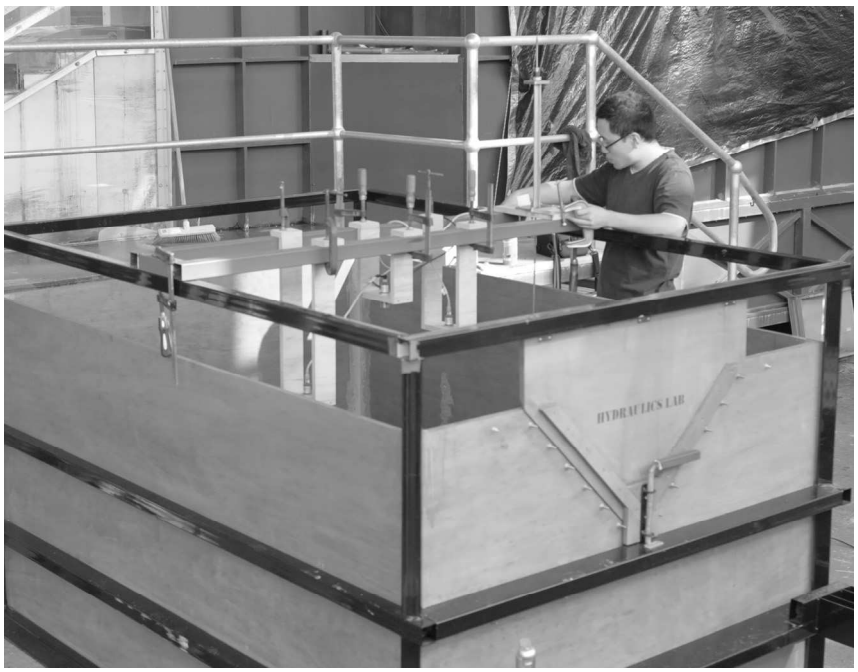

Figure 2. Reservoir and V-notch overflow, with the V-notch overflow gate closed (foreground right) - The displacement meters are mounted above the reservoir

The water depth was measured using a pointer gauge in steady flow conditions. The unsteady water depth was measured with three acoustic displacement meters Microsonic^{TM} Mic+25/ IU/TC. The sensors were located 1.11 m upstream of the weir. Their range was 250 mm and they were positioned in an overlapping fashion to cover the full height of the weir (400 mm). The data accuracy and response of the sensors were 0.18 mm and 50 ms respectively (http://www.microsonic.de). All the displacement sensors were synchronised and sampled simultaneously at 200 Hz. Additional visual observations were recorded with two HD digital video cameras, two dSLR cameras and a digital camera. The cameras were placed around the reservoir at various locations to cover both the water motion in the reservoir and the weir overflow during each run. Further details on the experiments, including some digital video movies, were reported in Chanson and Wang (2012).

2.2 *Physical investigations*

Prior to each run, the reservoir was filled slowly to the brink of the brass plate. The water was left to settle for at least 5 minutes prior to start. The experiment started when the gate was opened rapidly and the water level was recorded continuously for 500 s. The gate opening motion was recorded at 60 fps and the opening time was less than 0.15 s to 0.2 s. Such a rapid opening time was small enough to have a negligible effect on the water motion in the reservoir. After the sudden opening, the gate did not intrude into the overflow flow as illustrated in Figure 3.

Altogether five runs were conducted starting with an initially steady water level h_o above the lower edge of the notch: $h_o = 0.400 \pm 0.002$ m. The measured fluctuations in initial upstream water level were less than 0.3 mm prior to the gate opening.

Figure 3. Overflow sequence (Run 1) - Camera: Pentax K-7, lens: Pentax FA31mm f1.8 Ltd, shutter 1/80 s - From Left to Right, Top to Bottom: $t = t_o$, t_o+0.19 s, t_o+0.38 s, t_o+0.58 s, t_o+8 s, t_o+18 s

3 BASIC OBSERVATIONS

The gate opening was rapid. Figure 3 illustrates a typical overflow sequence. The unsteady overflow consisted initially of a transient phase followed by a gradually-varied overflow motion. The sudden gate opening caused the generation of a negative wave propagating upstream into the reservoir (Fig. 4) and a free-falling motion in the close vicinity the overflow behind the wave. Figure 4 illustrates an instantaneous snapshot. The initial phase lasted less than 0.45 s: that is, for $t \times (g/h_o)^{1/2} < 2.23$ with $t = 0$ at the start of the gate opening. Only a limited mass of water was reached by the initial wave; the rest of reservoir was still unaffected by the sudden opening. The negative wave leading edge had a quasi-circular arc shape illustrated in Figure 4. The resulting equipotential lines in a plan view highlighted the flow contraction under the action of gravity. The free-surface shape appeared somehow similar to the inlet shape of a minimum energy loss (MEL) structure with its curved profile (Apelt 1983). The design of a MEL struc-

ture was developed to pass large floods with minimum energy loss, hence with minimum upstream flooding (Chanson 2003). The MEL weir inlet is curved in plan to converge smoothly the chute flow (Fig. 5). Figure 5 shows the inlet of a minimum energy loss (MEL) spillway inlet. Note the analogy of shape between Figures 4 and 5.

Figure 4. Negative wave and initial free-falling motion behind observed for $t\times(g/h_o)^{1/2} < 2.2$ (Run 1) - The arrow points to the negative wave leading edge

Figure 5. Inlet of the minimum energy loss (MEL) weir spillway of Lake Kurwongbah (Petrie QLD, Australia) on 22 May 2009 during a small overflow

The initial phase was followed by a gradually-varied phase during which the overflow presented a quasi-steady flow motion. Some typical time-variations of the upstream water depth are illustrated in Figure 6. The ensemble-averaged water depth data were best fitted by:

$$\frac{h}{h_o} = \frac{12.72}{\left(t\times\sqrt{\frac{g}{h_o}} + 37.62\right)^{0.696}} \quad \text{for } 2.5 < t\times(g/h_o)^{1/2} < 2{,}400 \quad (2)$$

with a normalised correlation coefficient of 0.9999. During the initial phase, the time-variation of the water depth exhibited a different shape as shown in Figure 6 (Right).

The rapid gate opening generated some disturbance in the reservoir with the propagation of a three-dimensional wave illustrated in Figure 4. The reflections of the negative wave on sidewalls and end walls yielded some complicated three-dimensional wave motion associated with some seiche. Both longitudinal

and transverse sloshing motions were observed. Figure 7 presents a typical water depth signal. The data highlighted some pseudo-periodic oscillations about a mean data trend (Fig. 7). Some frequency analyses of the de-trended water depth signals were performed. The results compared favourably with the first mode of natural sloshing in the longitudinal and transverse directions of the intake basin, whose frequencies were respectively:

$$F_L = \frac{2 \times L}{\sqrt{g \times (p + h)}} \qquad (3A)$$

$$F_B = \frac{2 \times B}{\sqrt{g \times (p + h)}} \qquad (3B)$$

where L = reservoir length, B = reservoir width and p = notch elevation above reservoir invert (Fig. 1).

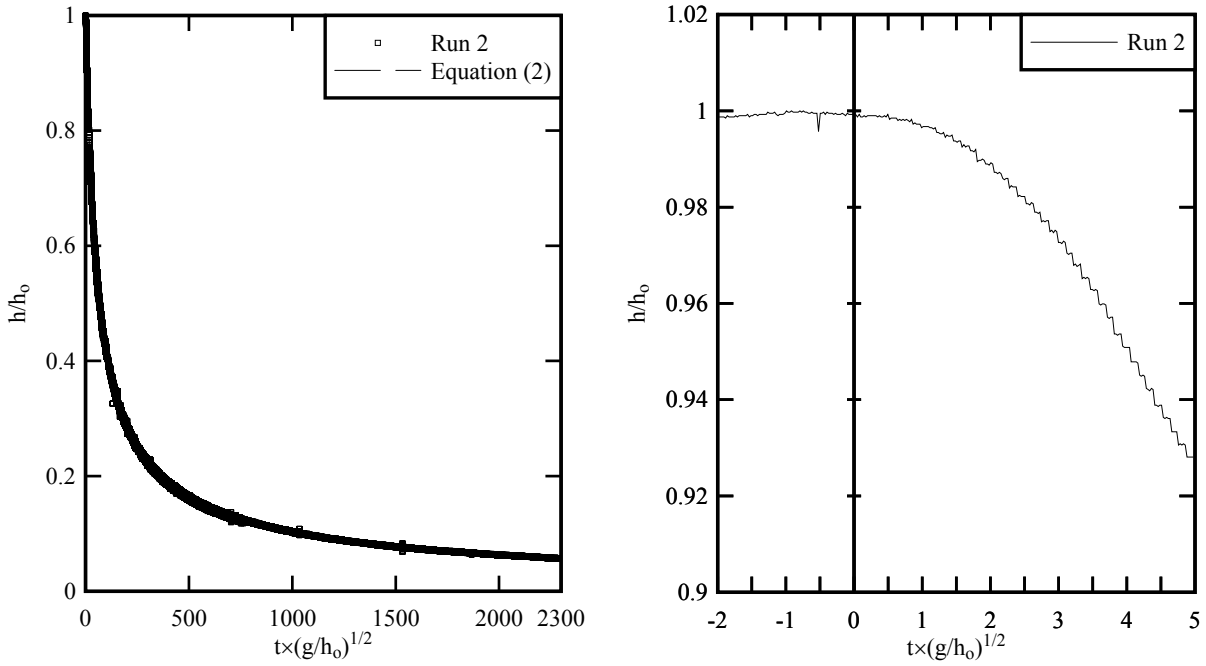

Figure 6. Dimensionless time-variations of the upstream water depth (Run 2) - Left: comparison between data and Equation (2); Right: Details of the initial instants

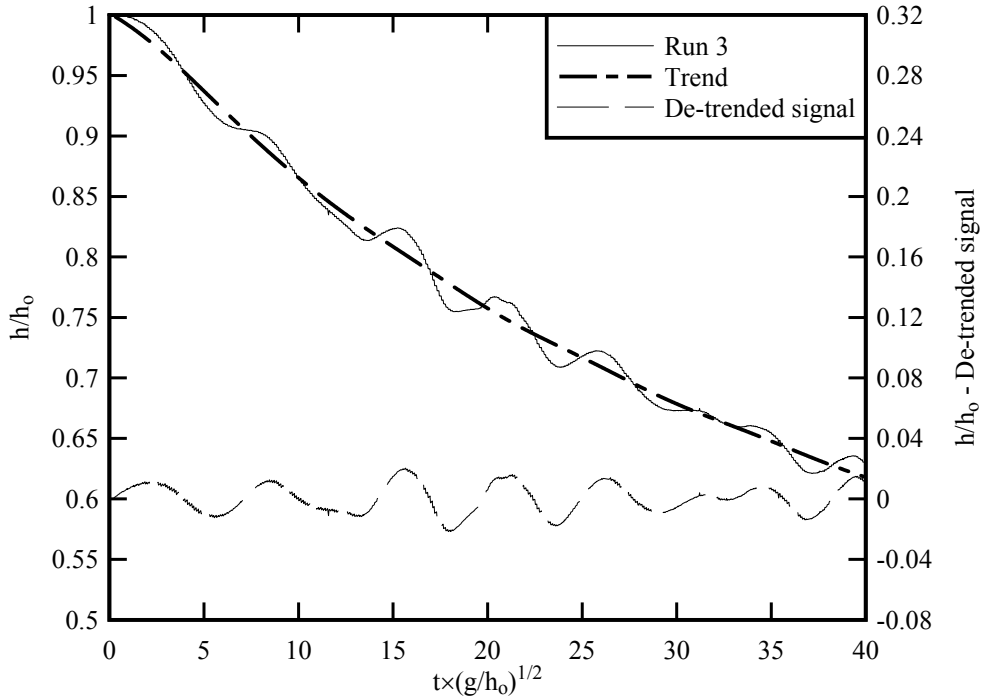

Figure 7. Dimensionless time-variations of the upstream water depth: raw signal and de-trended water depth signal (Run 5)

4 DISCUSSION

The instantaneous discharge Q through the V-notch weir was estimated using the integral form of the equation of conservation of mass for the water reservoir:

$$\frac{dVol}{dt} = -Q \qquad (4)$$

where t = time and Vol = instantaneous volume of water in the reservoir:

$$Vol = L \times B \times (h + p) \qquad (5)$$

with p = weir notch height above invert (Fig. 1). Equation (5) implicitly assumes that the reservoir free-surface was horizontal and neglects the local drop in water surface in the close vicinity of the overflow where the fluid particles are accelerated. The approximation was deemed reasonable considering the large reservoir surface area. Combining Equations (4) and (5), this gives an expression for the instantaneous overflow discharge:

$$Q = -L \times B \times \frac{d\,h}{dt} \qquad (6)$$

In the present study, Equation (6) was calculated based upon the smoothed water depth data. All the data are presented in Figure 8 by preserving every Nth point where N is the smoothing window size in points: e.g., N = 300 for a smoothing window of 300 points. Chanson and Wang (2012) tested systematicaly three smoothing window sizes: 300, 600 and 1,200 points. Qualitatively a smoothing window of 300 points was relevant immediately after the gate opening, while a smoothing window of 1,200 points was best suited during the gradually-varied phase.

Overall the data were best correlated by:

$$\frac{Q}{\sqrt{g \times h_o} \times {h_o}^2} = 0.58 \times \frac{8}{15} \times \sqrt{2 \times \left(\frac{h}{h_o}\right)^5} \qquad (7)$$

and Equation (7) is shown in Figure 8.

The data analysis yielded basically a dimensionless discharge coefficient $C_d = 0.58$. The result was close to a number of earlier studies in steady flow conditions (Lenz 1943, Trokolanski 1960, Herschy 1995). Simply the present findings showed that the unsteady discharge calibration of the V-notch weir yielded similar results to a more traditional calibration approach based upon steady experimental conditions.

For completeness, some unsteady experiments were conducted with a large two-dimensional orifice flow discharging vertically (Chanson et al. 2002). The results followed closely the following discharge equation:

$$\frac{Q}{\sqrt{g \times h_o} \times A} = C_d \times \sqrt{2 \times \frac{h}{h_o}} \qquad (8)$$

where A = orifice cross-section area and $C_d = 0.58$ (Chanson et al. 2002). Since $A = h^2$ for a 90° V- notch weir, Equation (8) yields a result somehow similar to Equation (7).

Note that the present approach enabled the calibration of the weir over a relatively wide range of water discharges (Fig. 8). Lastly, the physical tests were conducted for 0.022 m < h < 0.40 m. Although the results herein focused on water depths within the range 0.025 m < h < 0.40 m, the Reynolds number became less than 1×10^4 for h < 0.038 m. It is conceivable that viscous scale effects might affect the findings for the smallest water discharges.

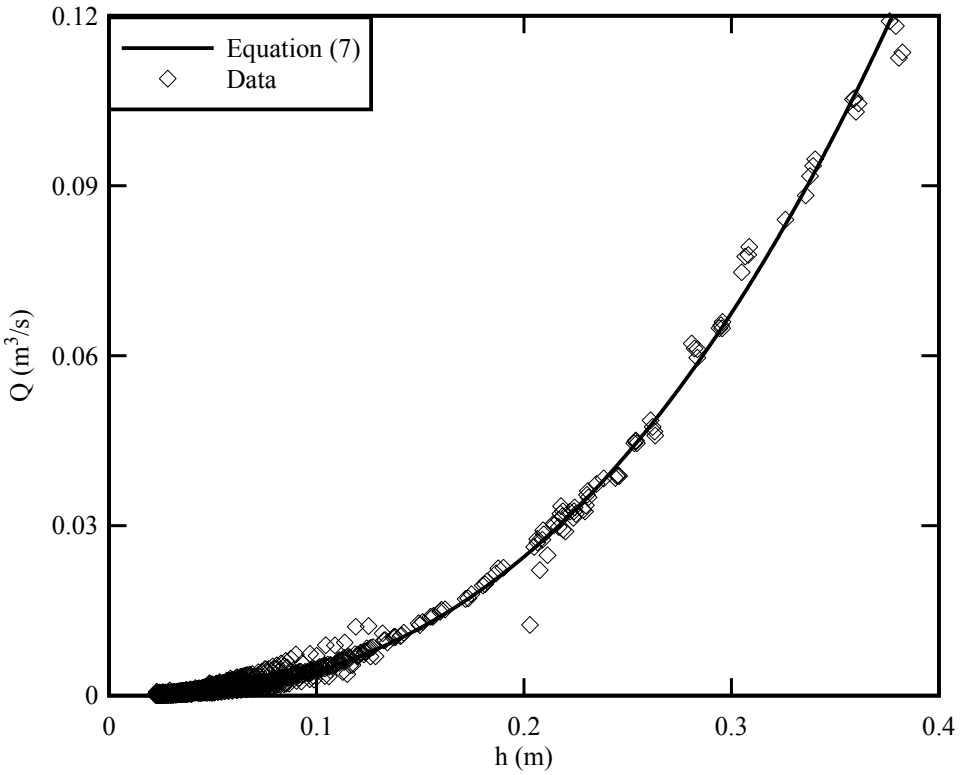

Figure 8. Relationship between instantaneous discharge Q and upstream water depth h - Comparison between data and Equation (7)

5 CONCLUSION

A large 90º V-notch thin plate weir was calibrated using an unsteady volume per time technique. The V-notch weir overflow was initially closed. The sudden opening of the overflow gate induced an initial phase dominated by the upstream propagation of a negative wave into the reservoir and the free-falling motion of a volume of fluid in the vicinity of the overflow. The water volume affected by the sudden opening was encompassed by a quasi-circular free-surface arc. Later the overflow motion became gradually-varied while some seiche was observed in the reservoir. The dominant frequencies of the water depth fluctuations compared favourably with the first mode of natural sloshing in the longitudinal and transverse directions of the reservoir, even though the wave motion was three-dimensional.

The relationship between water discharge and upstream water depth was derived from the integral form of the continuity equation based upon high-frequency water depth signal. The results yielded a dimensionless discharge coefficient $C_d = 0.58$ close to previous studies of 90º V-notch weirs and to an unsteady orifice experimental study. The present findings showed that the unsteady discharge calibration of the V-notch weir yielded similar results to a more traditional calibration approach based upon steady flow experiments. The present technique enabled further a calibration of the weir for a relatively wide range of upstream water levels.

ACKNOWLEDGEMENTS

The authors thank Dr Oscar Castro-Orgaz (IAS-CSIC, Spain) and Professor John Fenton (TU Wien, Austria) for helpful comments. They thank all the people who assisted with the large-scale experiments, especially the technical staff of the School of Civil Engineering at the University of Queensland. The financial support of the Australian Research Council (Grant DP120100481) is acknowledged.

NOTATION

C_d	dimensionless discharge coefficient
B	reservoir width
F_B	frequency of first mode of natural sloshing in the transverse direction
F_L	frequency of first mode of natural sloshing in the longitudinal direction
g	gravity acceleration
h	upstream water depth measured above the notch
h_o	initial upstream water depth measured above the notch
L	reservoir length
p	notch elevation above reservoir invert
Q	water discharge
t	time since gate opening start
Vol	water volume in the reservoir
α	opening angle of the notch
ρ	fluid density

REFERENCES

Ackers, P., White, W.R., Perkins, J.A., and Harrison, A.J.M. (1978). "Weirs and Flumes for Flow Measurement." John Wiley, Chichester, UK, 327 pages.

Apelt, C.J. (1983). "Hydraulics of Minimum Energy Culverts and Bridge Waterways." Australian Civil Engineering Transactions, I.E.Aust., Vol. CE25, No. 2, pp. 89-95

Australian Standards (1991). "Measurement of Water Flow in Open Channels. Part 4: Measurement using Flow Gauging Structures. Method 4.1: Thin-Plate Weirs." Australian Standard AS 3778.4.1-1991 (ISO 1438/1-1980), Council of Standards Australia, 34 pages.

Bos, M.G. (1976). "Discharge Measurement Structures." Publication No. 161, Delft Hydraulic Laboratory, Delft, The Netherlands (also Publication No. 20, ILRI, Wageningen, The Netherlands).

Chanson, H. (2003). "History of Minimum Energy Loss Weirs and Culverts. 1960-2002." Proc. 30th IAHR Biennial Congress, Thessaloniki, Greece, J. Ganoulis and P. Prinos Editors, Vol. E, pp. 379-387

Chanson, H., Aoki, S., and Maruyama, M. (2002). "Unsteady Two-Dimensional Orifice Flow: a Large-Size Experimental Investigation." Journal of Hydraulic Research, IAHR, Vol. 40, No. 1, pp. 63-71.

Chanson, H., and Wang, H. (2012). "Unsteady Discharge Calibration of a Large V-Notch Weir." Hydraulic Model Report No. CH88/12, School of Civil Engineering, The University of Queensland, Brisbane, Australia, 50 pages & 4 movies (ISBN 9781742720579).

Darcy, H.P.G., and Bazin, H. (1865). "Recherches Hydrauliques." ('Hydraulic Research.') Imprimerie Impériales, Paris, France, Parties 1ère et 2ème (in French).

Herschy, R. (1995). "General Purpose Flow Measurement Equations for Flumes and Thin Plate Weirs." Flow Measurements & Instrumentation, Vol. 6, No. 4, pp. 283-293.

International Organization for Standardization (1980). "Water Flow Measurement in Open Channels using Weirs and Venturi Flumes-Part 1: Thin-Plate Weirs." ISO 1438/1-1980, International Organization for Standardization.

Lenz, A.T. (1943). "Viscosity and Surface Tension Effects on V-Notch Weir Coefficients." Transactions, ASCE, Vol. 108, paper 2195, pp. 759-782. Discussion: Vol. 108, pp. 783-802.

Troskolanski, A.T. (1960). "Hydrometry: Theory and Practice of Hydraulic Measurements." Pergamon Press, Oxford, UK, 684 pages.

IWLHS, 20-22/02/2013, Aachen - Bung & Pagliara (eds) - © 2013 Bundesanstalt für Wasserbau ISBN 978-3-939230-04-5

Scour at Foundations of Rock Made Low-Head Structures

S. Pagliara & M. Palermo
Department of Energy, Systems, Territory and Constructions Engineering (DESTEC), University of Pisa, Pisa, Italy

ABSTRACT: Low-head control structures are widely used for river restoration problems. Their main function is to control sediment transport. In the last decades, the increasing environmental sensibility has forced hydraulic engineers to find solutions which could be able to solve the cited problem and, at the same time, to assure a reduced environmental impact. Thus, several eco-friendly structural typologies were tested. Mainly, this type of structures are made of natural elements disposed in different configurations and geometries and are not rigid like classical transverse concrete check dams, i.e. they can easily adapt to the modified in situ conditions. Among these structure typologies, rock grade control structures and stepped gabion weirs, in different hydraulic and boundary configurations, were analyzed. As all other stream restoration structures, they have to be correctly designed in order to avoid structural problems and assure their hydraulic functioning. One of the main problem is the stability of the toe. Thus a detailed analysis was performed resulting in relationships by which it is possible to estimate the scour depth at the toe of tested structures which was found quite close to the maximum scour depth in the stilling basin.

Keywords: Erosion, Rock grade control structures, Stepped Gabion Weirs, Structural stability

1 INTRODUCTION

Low-head structures have been widely used for river restorations purposes. In particular, they have the function to regulate and control the sediment transport in natural rivers and, at the same time, they constitute a discontinuity in natural river morphology contributing to dissipate flow energy.

In the last decades, the increasing environmental sensibility forced hydraulic engineers to find solutions which could be suitable in terms of both hydraulic and structural efficiency and, at the same time, eco-friendly. Thus, the actual tendency is to find and build structures whose impact on the surrounding environmental contest is reduced. In particular, among this hydraulic structure typology, in the last decades "elastic" or "flexible" structures have assumed a great importance, i.e. structures which are characterized by the possibility to adapt to the in-situ conditions when changed. Generally, this type of structures are made of rocks of various dimensions which can be arranged either in loose configuration or in selected one and are also used to re-convert traditional concrete check dams. Block ramps, stepped gabion weirs, rock grade-control structures, block sills, etc., are typical examples of flexible rock made structures. Their advantage respect to traditional concrete structures is to be more easily adaptable to various contests, especially in mountain streams. In addition, the surface roughness, due to protruding elements, is a key peculiarity which contributes to make these structures more efficient in terms of energy dissipation. However, they present some peculiar and characteristic flow structures and their stability required a considerable attention in order to prevent collapse and assure hydraulic functionality. Thus, several studies dealing with hydraulic performances and scour mechanisms occurring in the downstream stilling basin were carried on. Nevertheless, despite the quite conspicuous technical literature present about block ramps (see for example Whittaker and Jäggi (1986), Pagliara and Palermo (2008), Pagliara et al. (2008), Pagliara et al. (2009), Pagliara and Palermo (2011) and Pagliara et al. (2011)), there is still a lack of knowledge about both the hydraulic and scour processes involving gabion stepped weirs and rock grade-control structures.

These two last structures present several similarities (in terms of flow characteristics on the structure itself) with stepped concrete chutes. Significant contribution are present in literature dealing with flow regimes occurring on stepped chutes. In particular, Chanson (1994) distinguished three different flow regimes: *Nappe Flow*, *Transition Flow* and *Skimming Flow*. Several Authors analyzed the transition between the different regimes and contributed to furnish a clear description of the parameters influencing the phenomenon in the presence of stepped chutes (among these Rajaratnam (1990), Essery and Horner (1978), Peyras et al. (1992), Chanson (1996), Othsu et al. (2000), Ohtsu et al. (2001), Boes and Hager (2003) and Ohtsu et al. (2004)). Whereas, relatively few studies are analysing the flow characteristics on the stepped gabion weirs and rock grade control structure (see for example Peyras et al. (1992), Chinnarasri et al. (2008) and Mohamed (2010)).

But, according to the Authors' knowledge, there are very few studies which take into consideration both the flow pattern (on the structure itself and in the stilling basin) in the presence of a downstream movable bed. Just recently, Pagliara and Palermo (2012) analysed both rock grade control structures and stepped gabion weirs, investigating both the flow characteristics on the structures and the hydraulic jump forming downstream of them. They conducted experiments in a large range of conditions testing different structure boundary configurations. In particular, they also analysed the scour process, proposing relationship by which, for each tested structure configuration, it is possible to estimate maximum scour depth and scour hole length. However, for practical purposes, another important parameter needs to be analysed: the scour depth at the toe of the structure. This parameter results to be very important in order to correctly design the structure. In fact, an excessive scour at the toe of the structure can lead to a structural collapse.

Thus, the aim of this paper is to analyse the scour at the toe of both rock grade control structures and stepped gabion weirs in different hydraulic conditions and for different boundary configurations of the structure. The analysis highlighted that there is a close relationship between the maximum scour depth and the scour at the toe of the structures. Simple relationships are proposed in order to estimate the maximum scour at the toe of the analysed structures, both in terms of maximum scour depth and in terms of non dimensional parameters.

2 EXPERIMENTAL SET-UP

Two series of experiments were conducted at PITLAB, the hydraulic laboratory of the University of Pisa. Experiments were carried out using two different models and, for each model, different boundary structure conditions were tested. Models were located in a channel 0.30 m wide, 0.60 m deep and 6 m long.

The first series of experiments was conducted using a model simulating a rock grade control structure. The model was built using uniform crushed rocks whose average diameter was D_{50}=7 cm. Several rock layers were located in the channel in such a way that the downstream face of the structure was characterized by a 45° slope. In addition, the rock layers were linked together using a silicon glue, thus the resulting permeability of the structure is practically negligible. In order to test structure height effect on both flow pattern and scour process, two different structure heights H were tested. The height of the structure was measured from the original initial bed level. The two grade control structures tested were termed $B1$ and $B2$, and their height was 10.3 and 13.7 cm, respectively. Nevertheless, the analysis was conducted varying both hydraulic parameters and boundary structure configuration. In particular, a filtering layer made by the same material constituting the stilling basin (trapped in an opportunely shaped 2x2 mm squared holes iron net) was located upstream of the structure. The filtering layer had the same height of the tested structure and the granulometric characteristics of the material by which it was filled were: d_{50}=4.78 mm, d_{90}=5.7 mm, where d_{xx} is the granular material diameter for which xx% is finer, non uniformity coefficient $\sigma=(d_{84}/d_{16})^{0.5}$=1.2 and density ρ=2645 kg/m^3. In the presence of the filtering layer, two different structure boundary conditions were tested, i.e. B_f and $B_{f\text{-}imp}$, respectively, where the subscript f indicates the presence of a filtering layer upstream of the structure and the subscript imp means that an impermeable covering was adopted to make the filtering layer impermeable. Thus, in synthesis the following grade control structure configurations were tested: $B1$ and $B2$, i.e. grade control structure with different height but without any filtering layer upstream of them; B_f, i.e. grade control structure and upstream filtering layer; $B_{f\text{-}imp}$ grade control structure and upstream impermeable filtering layer. Figure 1a illustrates the tested configurations and reports the main hydraulic and geometric parameters. Namely, H is both the structure and filtering layer height (when present), h the upstream water depth (measured from the horizontal plane passing through the top of the structure), h_0 the downstream water depth, z_{max} the maximum scour hole depth, and z_f the scour depth at the structure toe.

The second series of experiments were conducted in the presence of a stepped gabion weir. Two base stepped gabion weirs were tested and termed GW_0 and GW_{imp}. They were both simulated using superimposed layers of squared holes 1 cm x 1cm prismatic gabions, located in such a way that the downstream pseudo bottom of the structure had a slope equal to 45° (see Figure 1b). The height of the structure measured from the original bed level was H=15.4 cm. The prismatic gabions were filled using rounded uniform stones whose average diameter was d_{50}=1.2 cm. In addition, the steps were shaped in such a way that their length (w_s) and height (h_s) was both equal to 5.13 cm. The main difference between the base structure configurations tested is constituted by the presence of an impermeable covering (opportunely shaped) on the upstream part of the structure. In fact, the structure GW_0 was a simple gabion stepped weir, in which the upstream flow could filter inside the structure also from the upstream side, whereas the structure GW_{imp} had an impermeable steel covering on its upstream part, thus water filtration could not occur from the upstream side.

Also in this case, a filtering layer with the same structure height and containing the same stilling basin material (as specified above) was used in order to simulate different boundary conditions. In particular, in the presence of the base configuration GW_0, a permeable filtering layer was adopted, thus obtaining the configuration termed (GW_f). Whereas, for the base configuration GW_{imp}, the filtering layer adopted had an impermeable covering in order to not allow water filtering inside the structure from the upstream. In synthesis, the tested structure configuration characteristics are the following: gabion stepped weir GW_0, i.e. base configuration with no impermeable covering on the upstream part of the structure; gabion stepped weir GW_{imp}, i.e. base configuration characterized by the presence of impermeable covering on the upstream part of the structure; gabion stepped weir GW_f, i.e. configuration characterized by the presence of an upstream filtering layer, but no impermeable coverings are present, neither on the upstream part of the structure nor on the filtering layer; gabion stepped weir $GW_{f\text{-}imp}$, i.e. configuration characterized by the presence of an upstream filtering layer, with impermeable coverings both on the upstream part of the structure and on the filtering layer.

For the present experiments, the discharge Q ranged between 4 l/s and 11 l/s. Tests were conducted varying the downstream water level h_0 in the range $0.25<h_0/H<0.82$ and they lasted up to 120 minutes in order to reach the equilibrium scour configuration. The hydraulic parameters were selected in order to avoid live-bed conditions, i.e. a ridge was always present downstream of the scour hole. Both the water depths and the scour lengths were measured using a point gauge 0.1 mm precise. In Figure 2a-b two pictures are reported, showing a rock grade control structure and a stepped gabion weir, respectively.

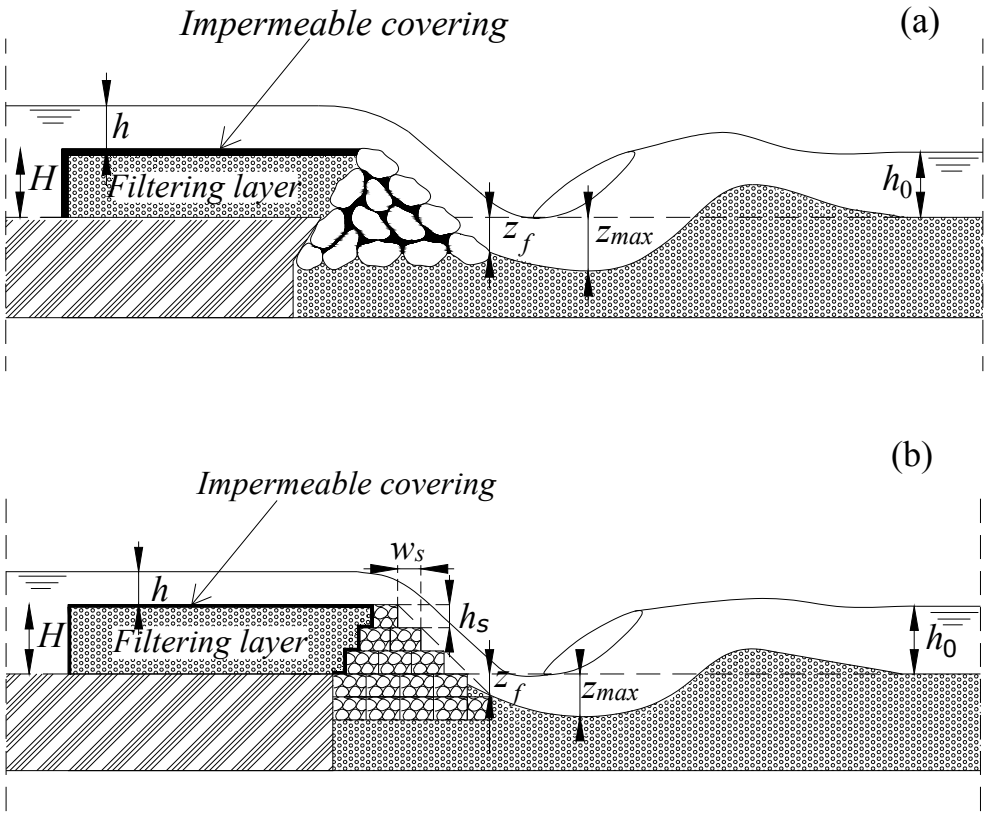

Figure 1. Diagram sketch of (a) rock grade control structures and (b) stepped gabion weirs including the main geometric and hydraulic parameters for various tested configurations

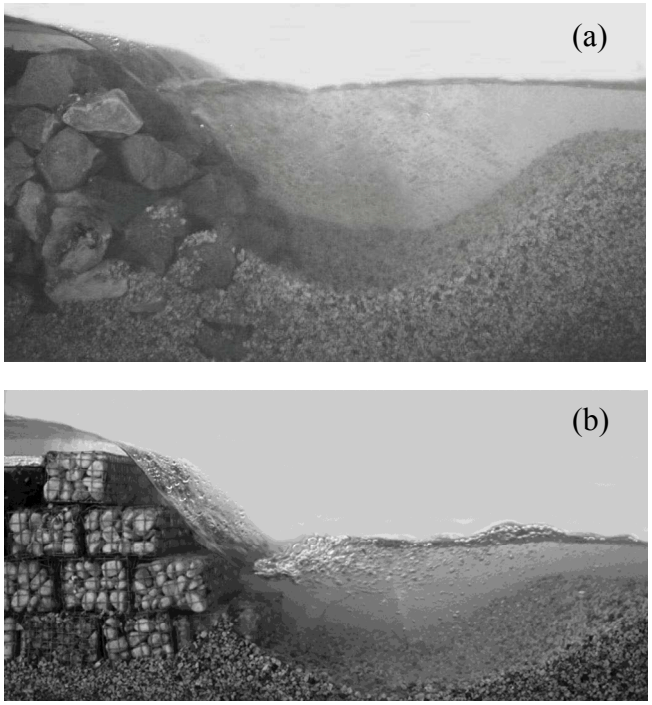

Figure 2. Picture of (a) rock grade control structure and (b) stepped gabion weir

3 RESULTS AND DISCUSSION

3.1 *Flow characteristics on the structures*

The close analysis of the flow structure on both stepped gabion weirs and rock grade control structures showed several similarities with stepped spillways, for which mainly three different flow regimes can be distinguished: *Nappe Flow*, *Transition Flow* and *Skimming Flow*. *Nappe flow* regime is characterized by a succession of plunging jets; whereas, in the case of *Skimming Flow*, the flow streams on a pseudo-bottom, below which vortex re-circulation takes place. The *Transition Flow* regime occurs when the water surface is quite undular and neither a direct jet impinging on the successive step nor a coherent flow stream on the structure occur. It means that for this last regime the flow structure shows intermediate characteristics between *Nappe* and *Skimming Flow* regimes. An example of *Skimming Flow* regime occurring on both a rock grade control structure and a stepped gabion weir is reported in Figure 2a-b, respectively.

Pagliara and Palermo (2012) analyzed the onset conditions characterizing the various regimes. In particular they specialized the analysis of Ohtsu et al. (2001) for the tested structure typologies. Namely, Ohtsu et al (2001) proposed a classification of the various flow regimes valid for stepped chutes based on two non-dimensional parameters: h_s/k_c and tanα, where h_s is the step height, k_c the critical flow depth and tanα is the slope of the chute. They concluded that for tanα=1 (i.e. the case in which α=45°, the same structure surface slope tested in the present study), the transition between *Nappe* and *Skimming Flow* occurs for $1<h_s/k_c<1.6$. But, it has to be noted that the conclusion of Ohtsu et al (2001) are valid just for the case in which the downstream water level does not submerge the structure. For the present tests, this condition is not preserved as several tailwaters were tested up to h_0/H=0.82.

Pagliara and Palermo (2012) specialized the analysis of Ohtsu et al (2001) for the tested structures including the effect of the previous parameter (h_0/H). They concluded that for rock grade control structures, assuming $h_s=D_{50}/2$ (as stones are partially protruding), the transition between *Nappe Flow* regime and *Skimming Flow* regime occurs for $0.9<h_s/k_c<1.1$. Furthermore, they experimentally proved that the influence of both the parameter h_0/H and the structure boundary configuration are relatively negligible on the transition between the two regimes. This is mainly due to the fact that the tested rock-grade control structures are practically impermeable as stones are linked by using a silicon glue, thus no filtration process from upstream can occur in the body of the structure.

Nevertheless, the authors conducted the same analysis for stepped gabion weirs concluding that *Transition Flow* regime mainly occurs for $1.1<h_s/k_c<1.5$ for all the tested structure boundary conditions, even if certain differences between the structure configurations (due to the fact that for some tested configura-

tions the structure is not impermeable) can be noted varying h_0/H values. In synthesis, it can be noted that the classification valid for the tested structures appears very similar to that proposed by Ohtsu et al (2001) in the case in which tanα=1.

3.2 *Hydraulic jump features*

Two hydraulic jump typologies can be distinguished downstream of these structure typologies in the tested range of parameters. Namely, based on the hydraulic jump analysis performed by Pagliara (2007), Pagliara and Palermo (2012) stated that the hydraulic jump in the stilling basin can be either F_{MB} or S_{MB}. F_{MB} type is characterized by a clock wise flow circulation in the stilling basin. Furthermore, the sediment transport in the scour hole is directed both downstream and upstream. This occurrence contributes to have less scour depth respect to the case in which an S_{MB} hydraulic jump takes place. In fact, this last jump is characterized by a counter clock wise flow circulation and at the same time the sediment transport is practically completely directed downstream.

The analysis performed by Pagliara and Palermo (2012) contributed to classify and distinguish these hydraulic jumps typologies in terms of two non-dimensional parameters: h_0/H and A_{50}. This last parameter is equal to $q/[H\cdot[g\cdot d_{50}\cdot(\Delta\rho/\rho)]^{0.5}]$ (D'Agostino and Ferro, 2004), in which q is the unit discharge, g is the acceleration due to gravity, $\Delta\rho=\rho_s-\rho$, where ρ_s is the sediment density and ρ the water density. The analysis of experimental data showed that the transition between F_{MB} and S_{MB} occurs for $h_0/H>0.5$. In fact, being constant all the other parameters, an increase of the tailwater level contributes to submerge the jump, thus an S_{MB} type takes place.

3.3 *Scour depth analysis*

One of the most important parameter, in the case of movable stilling basin bed, is the maximum scour depth. A detailed analysis for the tested configurations was conducted by Pagliara and Palermo (2012). They selected several non-dimensional parameters on which the erosive phenomenon depends and, after having analyzed the experimental data, they concluded that, for each tested configuration of both rock grade control structures and stepped gabion weirs, the non dimensional maximum scour depth z_{max}/E_0, for practical purposes, can be expressed as only function of the non dimensional parameter A_{50}, i.e. the following functional relationship:

$$\frac{z_{\max}}{E_0} = f\left(A_{50}\right) \qquad (1)$$

Note that E_0 is the total energy head upstream of the structure. For each tested configuration, it was experimentally proved that the effect of the parameter h_0/H is negligible in terms of practical applications. But a clear difference in data trend was observed for the various flow regime. For example, the following Figure 3, valid for rock grade control structure $B_{f\text{-}imp}$, reports the experimental data clearly showing that passing from *Nappe* to *Skimming Flow* regime the scour depth increases faster. The transition between the two regimes generally occurs for $0.5<A_{50}<0.7$.

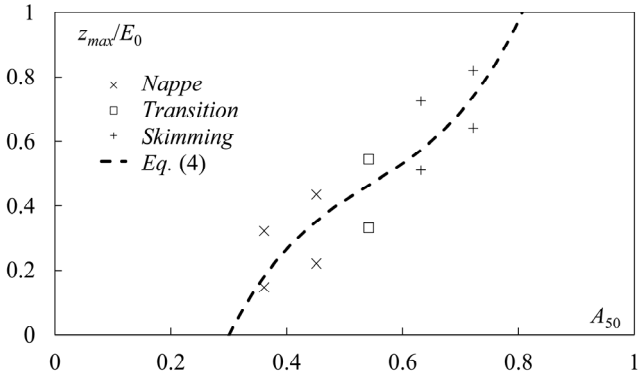

Figure 3. Non dimensional scour depth as function of A_{50} for different flow regimes and rock grade control structure $B_{f\text{-}imp}$

Pagliara and Palermo (2012) proved that, for rock grade control structures, the maximum non dimensional scour depth can be satisfactorily predicted by the following equations valid for grade control structure $B1$-$B2$ (Eq. 2), B_f (Eq. 3) and $B_{f\text{-}imp}$ (Eq. 4):

$$\frac{z_{max}}{E_0} = 3.28A_{50}^3 - 6.28A_{50}^2 + 4.74A_{50} - 0.95 \qquad (2)$$

$$\frac{z_{max}}{E_0} = 3.46A_{50}^3 - 6.96A_{50}^2 + 5.42A_{50} - 1.09 \qquad (3)$$

$$\frac{z_{max}}{E_0} = 13.46A_{50}^3 - 22.02A_{50}^2 + 13.12A_{50} - 2.32 \qquad (4)$$

For stepped gabion weirs, the analysis of experimental data showed that one unique equation is able to predict the totality of data, i.e. for practical purposes one single equation is able to catch the behavior of all the tested structures. Thus, Pagliara and Palermo (2012) proposed the following general equation valid for stepped gabion weirs GW_{imp}, GW_f, $GW_{f\text{-}imp}$:

$$\frac{z_{max}}{E_0} = 7.53A_{50}^3 - 11.53A_{50}^2 + 6.66A_{50} - 1.16 \qquad (5)$$

3.4 *Scour at the toe of the structures*

In terms of practical applications, the maximum scour depth at the toe of the structure is extremely important. In fact, the hydraulic functionality of the structure is assured if it remains stable. It implies that the foundation of the structure (i.e. a layer of stones (or more than one) in the case of rock grade control structures or layers of prismatic gabions for stepped gabions weirs) should not be affected by the erosive phenomenon occurring in the stilling basin. Namely, the scour depth at the toe of the structure has not to be so prominent to remove sediment at the base of the structure.

In this perspective it is clear that the knowledge of the maximum scour depth occurring at the toe of the structure is of fundamental importance for a correct design. The aim of this paper is to furnish quantitative criteria to estimate the maximum scour depth at the toe of the tested structure, based on the previous observations and deductions of Pagliara and Palermo (2012) which have been briefly synthetized in previous sections.

In the tested cases, once the scour hole equilibrium was reached, the stilling basin morphology was carefully measured. In particular, for both the structural typologies the maximum scour depth at the structure toe z_f was analyzed. In the case of rock grade control structure, the foundation was made of stones layer having the same average diameter (i.e. the usual methodology to build this type of structure), which were located in such a way that the average downstream structure surface slope (45°) was preserved. Thus, the maximum scour depth at the toe z_f was assumed as the minimum distance of the scoured sediment surface covering the structure foundation from the original bed level (see Figure 1a). For stepped gabion weirs, the foundation was made of prismatic layers having the same characteristics specified in Experimental Set-up section. Thus, the plane passing through the steps edge, including those belonging to the foundation, had a slope equal to 45°. This occurrence led us to assume z_f as the distance from the original bed level of the interception of the virtual plane passing through the steps edges with the scoured surface (see Figure 2b). Note that the assumed z_f is also the minimum distance between the scoured sediment surface and the step surface of the eventual covered foundation layer. This choice implies coherent values of z_f for both tested structure typologies. Furthermore, for stepped gabion weirs it takes into account the most dangerous conditions in terms of stability, as it considers the minimum sediment covering of the prismatic foundation.

The analysis of experimental data were based on two observations: Breusers and Raudkivi (1991) proved that the scour hole geometry can be expressed by only function of its maximum scour depth and Pagliara and Palermo (2012) proved that there is a scour hole profile similitude for the tested configurations, i.e. the non dimensional profiles for each structure typology are essentially the same (same non dimensional scour hole profiles for all the tested configurations of rock grade control structures and same non-dimensional scour hole profiles for all the tested stepped gabion weirs). These two observations allow to asses that the non-dimensional scour depth at the toe of the structure can be expressed as function of the maximum non-dimensional scour depth in the scour hole. Data were analyzed for each structure configuration, considering also the non dimensional structure submergence and the flow regime occurring. Figure 4a-d illustrates the relationship between z_f/E_0 and z_{max}/E_0, for different h_0/H and flow re-

gimes, for structure $B1$, $B2$, B_f and $B_{f\text{-}imp}$, respectively. It was experimentally proved that the for all the tested structures, the effect of flow regime and h_0/H on data trend is negligible, thus confirming the observations of Pagliara and Palermo (2012) and Breusers and Raudkivi (1991). In addition, there is no detectable difference between the various rock grade control structures in terms of the ratio z_f/z_{max}. In fact, one unique linear relationship can be used to interpolate the experimental data for all tested rock grade control structures (Figure 4a-d), whose expression is

$$\frac{z_f}{E_0} = 0.9\frac{z_{\max}}{E_0} \qquad (6)$$

This occurrence proves that the scour depth at the structure toe is almost 90% of the corresponding maximum scour hole depth. Thus, for practical applications, z_{max} can be considered as the main parameter to design structure foundations. The same analysis was conducted for stepped gabion weirs (see Figure 5a-c). Also in this case, a direct proportional relationship between z_f and z_{max} was found. Namely, the analysis was conducted for stepped gabion weirs GW_{imp}, GW_f and $GW_{f\text{-}imp}$ (Figure 5a, 5b and 5c, respectively) and it was found that the following expression can satisfactorily interpolate all experimental data.

$$\frac{z_f}{E_0} = 0.84\frac{z_{\max}}{E_0} \qquad (7)$$

Note that in this case the scour depth at the structure toe is almost 84% of the corresponding maximum scour hole depth, i.e. less than the previous case. This relatively slight difference between stepped gabion weirs and rock grade control structures in terms of z_f/z_{max} can be explained considering that the foundation of stepped gabion weirs is made of prismatic layers which furnish higher protection for the scour at the structure toe due to vortexes formations below the pseudo bottom. Furthermore, the structure itself is always permeable, whereas rock grade control structures are made gluing stones thus the internal structure permeability is practically negligible and less flow energy loses occur. Figure 5d illustrates the comparison between the measured and calculated values of the variable z_f/E_0 (using Eq. 6 for rock grade control structures and Eq. 7 for stepped gabion weirs). A good agreement was found between measured and calculated data. In synthesis, it can be concluded that for both the structure typologies the maximum scour depth can be assumed as reference parameter in order to correctly design the structure foundations, as it results to be very close to the scour depth at the toe of the structures.

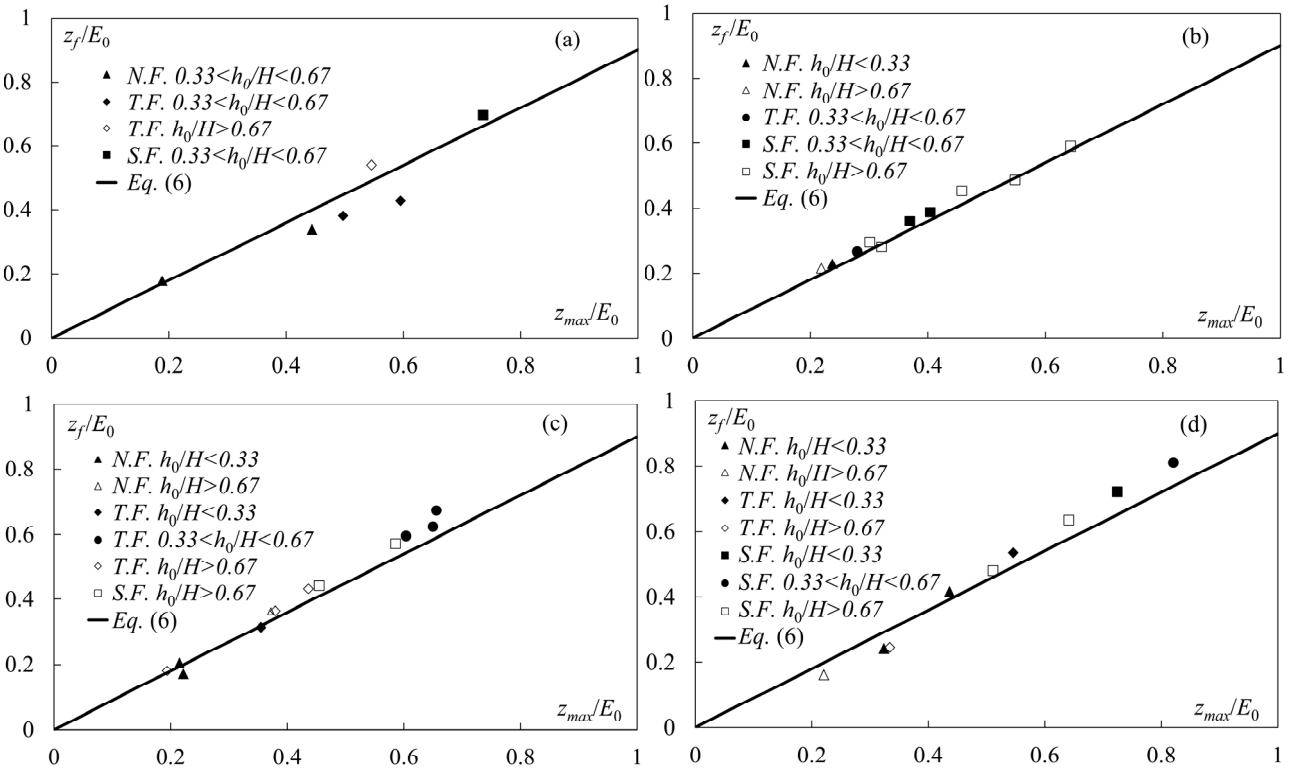

Figure 4. z_f/E_0 versus z_{max}/E_0 for different flow regimes (N.F.=Nappe Flow, T.F. Transition Flow, S.F.=Skimming Flow) and relative submergence and for rock grade control structure (a) $B1$, (b) $B2$, (c) B_f and (d) $B_{f\text{-}imp}$

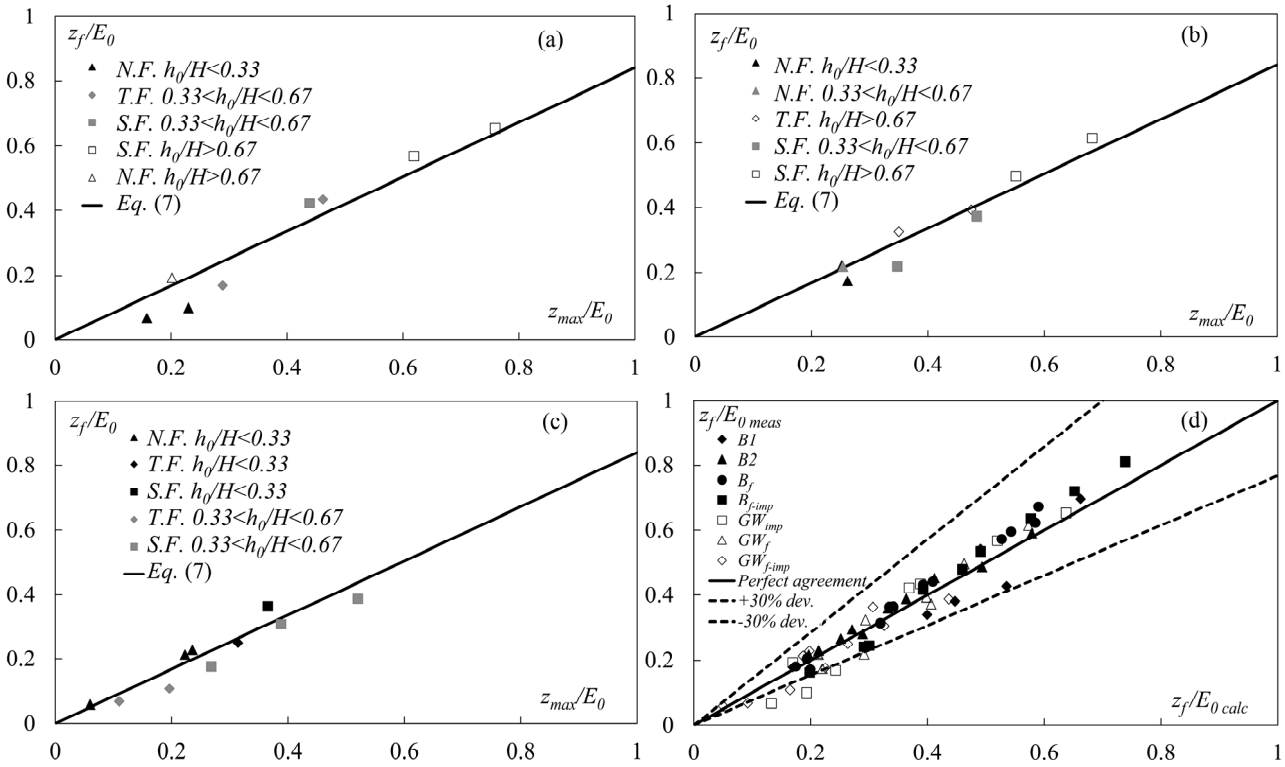

Figure 5. z_f/E_0 versus z_{max}/E_0 for different flow regimes (N.F.=Nappe Flow, T.F. Transition Flow, S.F.=Skimming Flow) and relative submergence and for stepped gabion weirs (a) GW_{imp}, (b) GW_f, (c) $GW_{f\text{-}imp}$. (d) Comparison between measured and calculated values of z_f/E_0 using Eq. (6) (rock grade control structures) and Eq. (7) (stepped gabion weirs)

4 CONCLUSIONS

An analysis of scour at foundations of low-head rock made structure was performed. Namely, the scour at the toe of rock grade control structures and stepped gabion weirs was analyzed in different hydraulic conditions and configurations. In particular different structure boundary configurations were tested for various submergence conditions. It was experimentally proved that the scour depth at the toe of the structure is almost 90% of the maximum scour hole depth occurring in the stilling basin in the case of rock grade control structures, whereas for stepped gabion weirs it is almost 84%. These occurrences allow to asses that for these structure typologies, the maximum depth in the scour hole can be considered as the reference parameter to correctly design the structure foundations in order to avoid structural risks and assure their stability. Furthermore, it was experimentally proved that this occurrence is not depending on both the submergence conditions and the flow regime occurring on the structure itself.

NOTATION

$A_{50} = q/[H\cdot[g\cdot d_{50}\cdot(\Delta\rho/\rho)]^{0.5}]$ non dimensional group.
D_{50} average diameter of rock grade control structure material
d_{xx} diameter of the channel bed and filtering layer material for which xx% of sediment is finer
d_{50} diameter of the channel bed material and filtering layer for which 50% of sediment is finer
d_{90} diameter of the channel bed material and filtering layer for which 90% of sediment is finer
E_0 total energy head upstream of the structure
f function of
g gravitational acceleration
h_0 tailwater level
h water depth measured from the horizontal plane passing through the top structure
h_s height of the steps
H structure height
k_c critical depth
Q water discharge
q unit discharge
w_s length of the steps
z_{max} maximum scour hole depth

$\Delta\rho = (\rho_s - \rho)$ reduced sediment density
ρ_s sediment density
ρ water density
$\sigma = (d_{84}/d_{16})^{0.5}$ sediment non uniformity parameter.

REFERENCES

Boes, R.M., Hager, W.H. (2003). Hydraulic design of stepped spillways. J. of Hydraulic Eng., ASCE, Vol. 129, No. (9), pp. 671-679.

Breusers, H.N.C., Raudkivi, A.J. (1991). Scouring. Balkema, Rotterdam NL.

Chanson, H. (1994). Hydraulics of skimming flows over stepped channels and spillways. J. of Hydraulic Res., IAHR, Vol. 32, No. 3, pp. 445-460.

Chanson, H. (1996). Prediction of the transition nappe/skimming flow on a stepped channel. J. of Hydraulic Res., IAHR, Vol. 34, No. 3, pp. 421-429.

Chinnarasri, C., Donjadee, S., Israngkura, U. (2008). Hydraulic characteristics of gabion-stepped weirs. J. of Hydraulic Eng., ASCE, Vol. 134, No. 8, pp. 1147-1152.

D'Agostino, V., Ferro, V. (2004). Scour on alluvial bed downstream of grade-control structures. J. of Hydraulic Eng., ASCE, Vol. 130, No. 1, pp. 24-37.

Essery, I.T.S., Horner, M.W. (1978). The hydraulic design of stepped spillways. CIRIA, Report n° 33, 3rd Edition, Jan, London, UK.

Mohamed, H.I. (2010). Flow over gabion weirs. J. of Irr. and Drain. Eng., ASCE, Vol. 136, No. 8, pp. 573-577.

Ohtsu, I., Yasuda, Y., Takahashi, M. (2000). Discussion of "Hydraulics of skimming flow on modeled stepped spillways" by Pegram, G.G.S, Officer, A.K, and Mottram, S.R.. J. of Hydraulic Eng., ASCE, Vol. 126, No. 12, pp. 950-951.

Ohtsu, I., Yasuda, Y., Takahashi, M. (2001). Discussion of "Onset of skimming flow on stepped spillways" by Chamani, M.R., and Rajaratnam, N.. J. of Hydraulic Eng., ASCE, Vol. 127, No. 6, pp. 522-524.

Ohtsu, I., Yasuda, Y., Takahashi, M. (2004). Flow characteristics of skimming flows in stepped channels. J. of Hydraulic Eng., ASCE, Vol. 130, No. 9, pp. 860-869.

Pagliara, S. (2007). Influence of sediment gradation on scour downstream of block ramps. J. of Hydraulic Eng., ASCE, Vol. 133, No. 11, pp. 1241-1248.

Pagliara, S., Palermo, M. (2008). Scour control and surface sediment distribution downstream of block ramps. J. of Hydraulic Res., IAHR, Vol. 46, No. 3, pp. 334-343.

Pagliara, S., Das, R., Palermo, M.(2008). Scour control and surface sediment distribution downstream of block ramps. J. of Irr. and Drain. Eng., ASCE, Vol. 134, No. 4, pp. 527-532.

Pagliara, S., Palermo, M., Carnacina, I. (2009). Scour and hydraulic jump downstream of block ramps in expanding stilling basins. J. of Hydraulic Res., IAHR, Vol. 47, No. 4, pp. 503-511.

Pagliara, S., Palermo, M. (2011). Effect of stilling basin geometry on clear water scour morphology downstream of a block ramp. J. of Irr. and Drain. Eng., ASCE, Vol. 137, No. 9, pp. 593-601.

Pagliara, S., Palermo, M., Carnacina, I. (2011). Expanding pools morphology in live-bed conditions. Acta Geophysica, Vol. 59, No. 2, pp. 296-313.

Pagliara, S., Palermo, M., (2012). Rock grade control structures and stepped gabion weirs: scour analysis and flow features. Acta Geophysica, DOI: 10.2478/s11600-012-0066-0.

Peyras, L., Royet, P., Degoutte, G. (1992). Flow and energy dissipation over stepped gabion weirs. J. of Hydraulic Eng., ASCE, Vol. 118, No. 5, pp. 707-717.

Rajaratnam, N. (1990). Skimming flow in stepped spillways. J. of Hydraulic Eng., ASCE, Vol. 116, No. 4, pp. 587-591.

Whittaker, W., Jäggi, M. (1996). Blockschwellen. Mitteilung 91, Versuchsanstalt für Wasserbau, Hydrologie und Glaziologie. ETH Zurich, Zürich, Switzerland [in German].

IWLHS, 20-22/02/2013, Aachen - Bung & Pagliara (eds) - © 2013 Bundesanstalt für Wasserbau ISBN 978-3-939230-04-5

Using Genetic Programming to Predict Scour Downstream Rapid Hydraulic Structures from Experimental Results

A. M. Abdel Sattar
German University in Cairo, Egypt – on leave from Department of Irrigation & Hydraulics, Faculty of Engineering, Cairo University, Egypt

A. Radecki-Pawlik
Department of Hydraulics Engineering and Geotechnic, Agricultural University of Cracow, al. Mickiewicza 24/28, 30-059 Kraków

R. Ślizowski
Department of Sewage Systems and Water Management, Agricultural University of Cracow, al. Mickiewicza 24/28, 30-059 Kraków

ABSTRACT: Rapid hydraulic structures are used in Poland Stream Mountains excessively to regulate flow by changing its slope at certain locations while allowing for fish passage. Local scour downstream the rapid is an important issue regarding its safety. This paper presents experimental investigation for scour holes downstream a rapid structure using a small scale physical model. Results are used with other data presented in literature for similar structures to develop an equation for the prediction of maximum scour hole downstream rapids. For this purpose Genetic Programming (GP) is utilized as a tool for developing the required relation. It is shown that GP could produce formulae relating scour hole depth and various rapid parameters with less error than some of available regression equations.

Keywords: Rapid hydraulic structures, low head structures, scour, Genetic Programming

1 INTRODUCTION

There is very often a necessity to regulate a river or a stream by changing its slope (what is called: river training works), especially in mountain regions where streams are characterized by high gradients and heavy scouring and erosion tend to occur. In such cases designing and constructing of hydraulic structures has been advised for stabilizing a riverbed and riverbanks (Rhone 1977, Ratomski, 1992). Usually such structures are drop hydraulic structures. Their construction is well known to designers and they are described in detail in the professional literature (e.g. Shields and Cooper 1995, Rosgen 2001, Scurlock and Thornton 2011 and 2012). Unfortunately in many places, if a structure is built, it can spoil the natural beauty of a mountain stream. If it functions properly in terms of hydraulics, it is rarely similar to the natural geomorphological features of a stream (Ratomski, 1992). Construction of rapid hydraulics structures (RHS) similar to natural river riffles is advised when considering a channel slope reduction (Kajak, 1992, Ślizowski, 1993). Such hydraulic structures are environmentally friendly, since they simulate a natural river bed and river bed forms (riffles), do not require additional fish passage consideration, and aerate flowing water naturally (Bhuiyan and Wormleaton 2007, Novak et al. 1996). Above all they are similar to natural river features and do not disturb a river cross-section appearance when well-constructed (see Figure 1).

The process of creating local scour resulting from water and debris is one of the least to identified problems in the rapid hydraulic structure systems. So far, there is no sufficiently precise mathematical description of the process of local erosion arising downstream the rapid structure. Developing fully reliable predictions on the basis of laboratory tests has often been impossible because of the time required to obtain experience the so-called final scour. However, Mason and Arumugan (1985) provided comprehensive data analysis in available literature to demonstrate the validity of the ultimate scour hole concept. Lack of understanding of the process of creating local scour below the rapid structure is the main reason for failure of structure in various studies (e.g. Bormann and Julien 1991). Scour downstream similar structures (e.g. block ramps and grade-control structures) has been carried out by various researchers. Veronese (1937) conducted one of the first studies on scour downstream hydraulic structure. The characteristic parameters defining scour hole downstream hydraulic structure have been experimentally studied by Hassan and Narayanan (1985) and Farhoudi and Smith (1985). Bormann and Julien (1991) used a large

scale experiment to investigate the scour downstream a grade control structure with a unit discharge of 2.5m^2/s. Mossa (1998) and D'Agostino and Ferro (2003) analyzed the scour formation downstream grade control structures. Lenzi and Comiti (2003) analyzed scour hole formation downstream 29 drop structures, Marion et al. (2004) experimentally analyzed the effect of bed sill spacing and sediment grading on potential erosion by jets over fills. Ben Meftah and Mossa (2006) analyzed the formation of scour holes downstream bed sills in low gradient channels. Pagliara and Hager (2004) conducted experimental work to study the scour process and characteristics downstream a block ramp in case of uniform bed material. More recently, Pagliara (2007),and Pagliara and Palermo (2008) investigated the scour mechanics downstream a block ramp and examined the influence of sediment gradation on the scour mechanism using two physical models. Scurlock and Thornton (2012) studied the equilibrium scour formation downstream three dimensional grade control structures.

Figure 1. RHS on the Krzczonowski stream (photo by A. Radecki-Pawlik)

Most of the previous experimental studies aimed at characterizing the scour hole downstream grade control structure by a maximum scour depth, which is a function of the incoming flow conditions and soil parameters representative of bed particle size distribution (e.g. Mason and Arumugam 1985, Bormann and Julien 1991, Lenzi and Comiti 2003, Marion et al. 2004 and Pagliara 2007). However, there are no reliable equations for calculating scour downstream rapid hydraulic structures and thus it is of usual practice to adopt scour formulae developed for other structures under different hydraulic conditions. While these formulae provide estimates for the required scour depth, they might have some deficiencies in capturing accurately the scour downstream rapid hydraulic structures. Errors in prediction of scour hole using some of these formulae can reach 300%. Thus, it is required to have specific equations developed mainly for rapid hydraulic structures considering real measured rapid parameters.

Recently, evolutionary algorithms have been used as a superior alternative for regression analysis and artificial neural networks, for finding relations between various parameters and producing a higher R-squared value and less mean error in prediction using newly developed equation. Genetic programming (GP) is known as a technique with the capability of generating mathematical equations, which are able to define models for the given training data. Genetic programming was proposed by Koza (1992). GP is founded on the basic principle of Darwin's theory of evolution in nature. GP attempts and succeeds at applying the evolutionary theory in order to find the best or the most appropriate equation (solution)for a problem. The motivation of using a GP approach is its ability to evolve a model based entirely on prior data without the need of making underlying assumptions.

Applications of evolutionary algorithms, especially genetic programming (GP) in water and environmental engineering is not as much as the other soft computing tools of artificial neural networks. They are restricted to relatively fewer sub-areas including; rainfall-runoff relationship and unit hydrographs in catchments (Aytek and Alp 2008, Wigham and Crapper 2001, Savic et al. 1999, Keijer and Babovic 2002, Dorado et al. 2003, and Rabunal et al. 2006), sewer and water supply networks (Dorado et al. 2002, Babovic et al. 2002), river flow and water quality in watersheds (Drunpob et al. 2005, Harris et al. 2003, Giustolisi 2004, Preis and Otsfeld 2008), oceanic and sea coastal waves (Gaur and Deo 2008, and Ghorbani et al. 2010), irrigation planning (Raju and Kumar (2004), river channel scour downstream spillway

(Azamathulla et al. 2008), pan evaporation and evapotranspiration (Guven & Guani 2008, and Shiri and Kisi 2011), and suspended sediment transport in open channel (Ayetk and Kisi 2008). Guven & Guani (2008) utilized the gene expression programming approach for prediction of local scour downstream sharp crested control grade structure. They provided a complicated equation relating various parameter to maximum scour hole depth.

This paper aims at utilizing the power of the genetic programming to develop relations to predict scour hole depth downstream rapid hydraulic structures as a function of incoming flow conditions, rapid geometric characteristics and soil parameters using experimental data measured by the authors in an experiment to simulate real rapid structures and other published data of similar hydraulic investigations performed by Pagliara (2007). First an overview of the basic theory of genetic programming is given accompanied by implementation technique steps. Afterwards, a description for the experimental setup used to collect scour data is given with the results. Finally, the GP is utilized to develop empirical relationships between various controlling parameters and the maximum scour depth downstream a rapid hydraulic structure. The developed relation is compared to other available relations.

2 EVOLUTIONARY ALGORITHMS

Evolutionary Algorithms (EAs) is a class of solving technique based on the Darwinian theory of evolution which involves the search of a population of solutions and not only one. A possible and acceptable solution i.e. a member of the population is called an individual. Each iteration of an EA involves a competitive selection that weeds out poor solutions through the evaluation of a fitness value that indicate the quality of the individual as a solution to the problem. The evolutionary process involves at each generation a set of genetic operators that are randomly applied on the individuals, typically recombination (or crossover) and mutation.

2.1 *Genetic Programming (GP)*

Genetic programming is an extension to Genetic Algorithms (GA). GA is an optimization and search technique based on the principles of genetics and natural selection. A GA allows a population composed of many individuals (chromosome) to evolve under specified selection rules to a state that maximizes the "fitness" (i.e. minimizes the cost function). The GP is similar to genetic algorithms but unlike the latter its solution is a computer program or an equation as against a set of numbers in the GA.

In GP, a random population of individuals (equations or computer programs) is created, the fitness of individuals is evaluated and then the 'parents' are selected out of these individuals. The parents are then made to yield 'offspring's' by following the process of reproduction, mutation and crossover. The creation of offspring's continues iteratively until a specified number of offspring's in a generation are produced and further until another specified number of generations are created. The resulting offspring at the end of all this process is the solution to the problem. The GP transforms one population of individuals into another one in an iterative manner by following the natural genetic operations like reproduction, mutation and crossover. Each individual contributes with its own genetic information to the building of new offspring adapted to the environment with higher chances of surviving. The solution for the problem provided by the GP algorithm is a tree as seen in Figure 2.

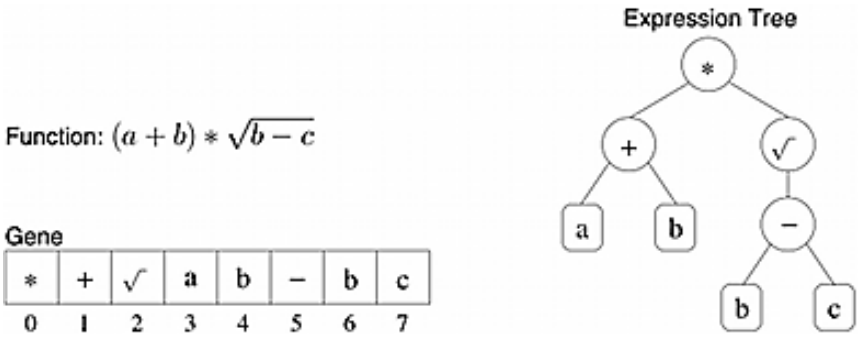

Figure 2. Tree representation for a GP function

A tree is a model representation that contains nodes and leaves. Nodes are mathematical operators (multiplication, subtraction, etc.). Leaves are terminals and trees are manipulated through genetic operators. The

crossover operator points a tree branch and exchanges it with another branch and obtains new trees. The mutation operator changes the branch for a random new branch. Reproduction means exact duplication of the program if it is found to be accepted by the fitness criteria (Figure 3). Fitness functions are employed to select various individuals for crossover, mutation, reproduction and to determine how good the individuals are at solving the given problem. The fitness function assesses how an individual is fitted to the environment of a domain problem, after calculating the fitness for all individuals. Many varieties of fitness function can be applied for evaluating performance of generated computer program. GP evolves computer programs to solve problems by executing the following steps using GPLAB Code (El-Sayed 2011);

Step1: One or more initial population of individuals is randomly generated with functions and terminals related to the problem domain.

Step2: The implementation of GP iteratively performs the following steps until the termination criterion has been satisfied

i. The fitness value of every individual is estimated according to a selected fitness measure
ii. All individuals in the population are sorted based on their fitness values
iii. The next generation is produced using the genetic operations (reproduction, crossover and mutation)
iv. The termination criterion is checked. If it is not satisfied, the next iteration is performed if satisfied go to step 3.

Step3: The result may be a solution to the problem domain.

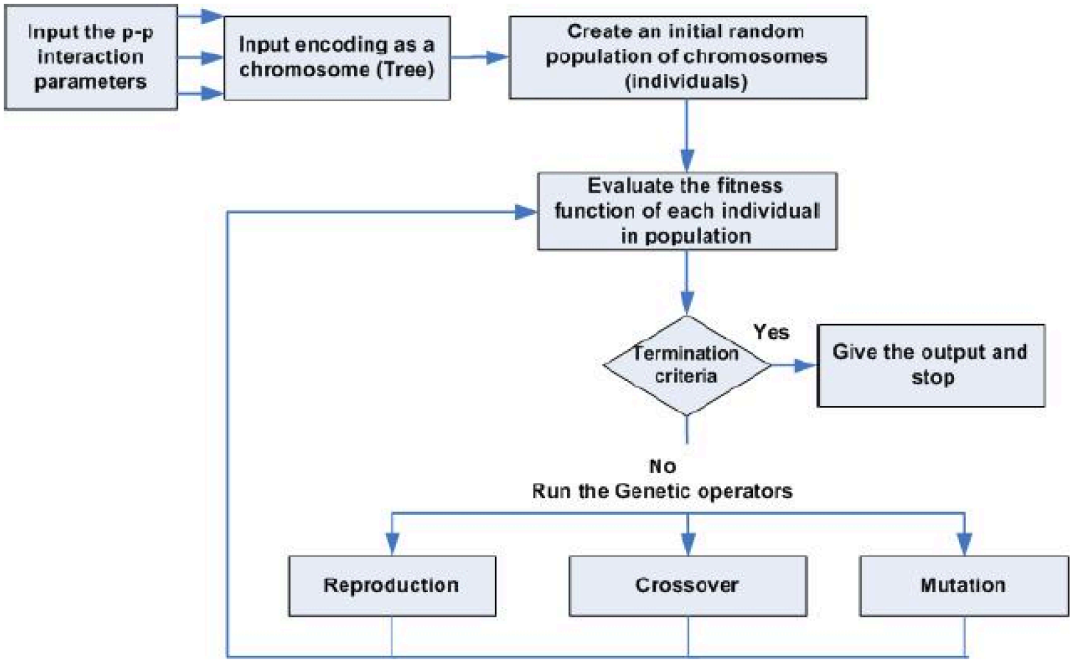

Figure 3. Genetic programming flow chart

3 EXPERIMENTAL SETUP

The experiment was carried out in the laboratory flume at the Department of Hydraulics Engineering and Geotechnic, Agricultural University of Cracow (see Figure 6).The banks and a bed of the model were stable and wash-resistant. The model has and upstream water tank with calibrated notch weir, at the downstream of the weir a water-wave calming device (honeycomb) is installed. In the middle of the channel, the rapid structure module is installed and mobile bed material is placed all over the flume bed. Measurement devices include; velocitimeters, pin-gauges, and calibrated notches

The study adopted the simplest design solution rapids on the crown straight sill height of 0.06 m drop across the same longitudinal length. Known from the literature are other smart structures, such as perfecta curved crown rapids; alternating elongated drop, and a curved cross section, but these structures are recommended for larger widths of the troughs. Because it was assumed that the study will only affect mountain streams generally characterized by a small width, the ratio $B / h < 4.5$ is recommended for such

streams and respected in the current study. Aim of the study carried out by analyzing six models of rapid structure design with increased roughness (2A - 8A).

Model rapids of natural stone are made in 1:10 scale in the riverbed hydraulic dimensions: length 25.00 m, width 0.60 m, depth 0.80 m (Fig. 4 shows a schematic of the rapid experiment). Section of the canal above and below the rapids was made of concrete sand bed as armoring layer. Only a section of the channel immediately below the rapids on the length of 4.50 m made as to observe the resulting scour hole. The channel was filled with sediment of characteristic diameter d_{90} = 0.003 m

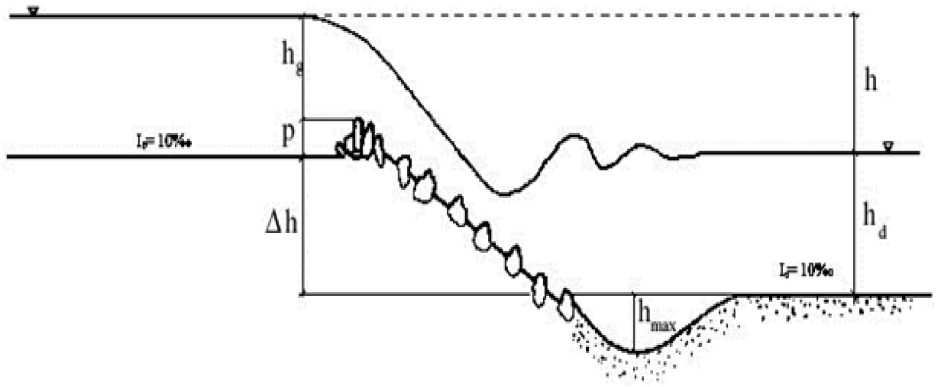

Figure 4. Sketch of the rapid structure with artificial roughness

In order to increase roughness and bring it to the roughness in a mountain stream, the bottom was lined with fine grit stone that protruded above the bottom line of about = 0.01 m Model rapids were made as part of removable concrete slab with inserted natural stones protruding more than the bottom line of rapids with 0.045 m stones arranged in a checkerboard pattern in the front row of 0.05 m, the distance between rows 0.075 m to backpressure water table position at the inlet of the upper rapids made the threshold with a height of 0.06 m . Experiments were carried out for a rapid drop slopes of 1:4.5, 1:6, 1:10 and height 0.10 and 0.30 m and for flow rates ranging 0.0245m^3/s, 0.0490m^3/s, and 0.0735m^3/s. Figure 6 shows the contour plot of scour downstream the rapid structure under the flow of 0.0735m^3/s. Experimental measurements are presented in Table 1.

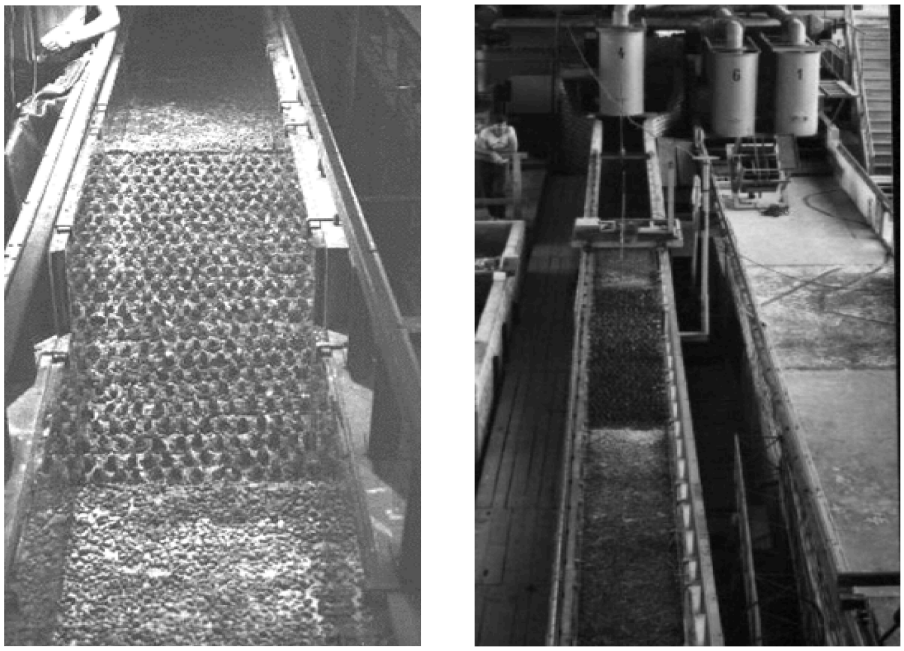

Figure 5. Model of rapid structure in laboratory flume

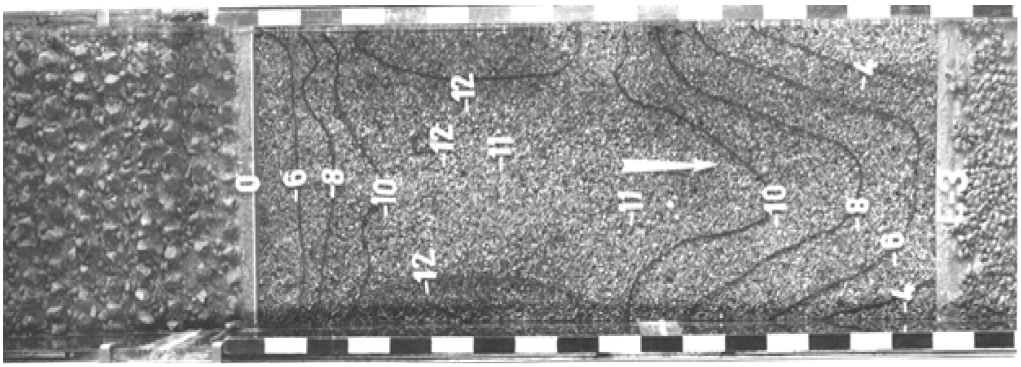

Figure 6. Contour plot of scour below rapid 3A: Q = 0.0735 m^3/s, *s* = 1:6, *h* = 0.10 m

Table 1. Scour depth from model studies according to rapid parameters

Rapid	Rapid discharge Q (m^3/s)	Rapid velocity v (m/s)	Height difference h (m)	Rapid slope, s	Scour depth h_{max} (m)
2A	0,0245	1.20	0.1424	0.22	0.07
	0,0490	1.445	0.1442	0.22	0.12
	0,0730	1.710	0.1441	0.22	0.15
3A	0,0245	1.100	0.1434	0.167	0.08
	0,0490	1.630	0.1454	0.167	0.10
	0,0730	1.945	0.1454	0.167	0.14
4A	0,0245	1.220	0.1481	0.10	0.08
	0,0490	1.750	0.1525	0.10	0.10
	0,0730	1.805	0.1524	0.10	0.12
6A	0,0245	1.290	0.3485	0.22	0.06
	0,0490	2.190	0.3454	0.22	0.13
	0,0730	2.440	0.3463	0.22	0.18
7A	0,0245	1.160	0.353	0.167	0.06
	0,0490	1.650	0.3551	0.167	0.13
	0,0730	2.050	0.3531	0.167	0.17
8A	0,0245	1.100	0.3654	0.10	0.06
	0,0490	1.480	0.3695	0.10	0.12
	0,0730	1.880	0.3703	0.10	0.12

These experiments are similar to those performed by Pagliara (2007) and Bormann and Julien (1991). Pagliara (2007) performed experimental investigations on block ramps to determine the impact of bed material gradation on the formation of the scour hole downstream the structure under various flow conditions. On the other hand, Bormann and Julien (1991) performed experimental investigation on large scale flume to determine the scour hole characteristics downstream a sloping ramp. Both studies provide additional important information with respect to having various rapid slopes, rapid discharges, various sizes and gradation for bed material and large scale rapid very similar to that of mountain streams. Table 2 shows the range of various rapid related parameters as measured in current study and obtained from Pagliara (2007) and Bormann and Julien (1991).

Table 2. Range of various parameters controlling the scour holes considered

Study	Rapid discharge Q (m3/s)	Sediment size d_{90} (m)	Rapid slope, s	Scour depth h_{max} (m)	Coff. of uniformity ($\sigma = \sqrt{d_{84}/d_{16}}$)
Current study	0.02 to 0.07	0.003	0.10 to 0.22	0.06 to 0.18	1
Pagliara (2007)	0.00148 to 0.073	0.016 to 0.0097	0.083 to 0.25	0.0056 to 0.18	1.2 to 2.8
Bormann & Julien (1991)	0.26 to 2.25	0.00158 to 0.00171	0.33 to 1.00	0.10 to 1.52	1
Overall	0.00148 to 2.25	0.00158 to 0.016	0.083 to 1.00	0.0056 to 1.52	1 to 2.8

4 GP MODELS FOR SCOUR PREDICTION

Pagliara (2007) stated that the scour-hole characteristics are related to the ramp slope, water flow discharge, and to the granulometric characteristics of the stream bed material represented as d_{90}. Thus; the maximum scour depth can be written as;

$$h_{max} = f(Q, s, d_{90}, \sigma) \quad (1)$$

Pagliara (2007) introduced a dimensionless parameter Z_{max}, defined as the ratio of the measured maximum cross sectional scour depth and the approaching flow depth at the ramp, h_1 such that;

$$Z_{max} = f\left(F_{d_{90}}, s, \sigma\right) \quad (2)$$

where $F_{d_{90}}$ is the densimetric Froude number, $F_{d_{90}} = \sqrt{v_1/g'\,d_{90}}$, v_1 = average approaching flow velocity, d_{90} = channel bed sediment diameter, $g' = [(\rho_s - \rho)/\rho]g$, and ρ_s = channel bed sediment density. Both of these two relations shall be used to develop a GP-based model for prediction of maximum scour hole depth. Data included 18 points from this study, 49 points from Pagliara (2007) and 45 points from Bormann and Julien (1991) with a total of 112points. 80% shall be used for training the model (89 points) and 20% shall be used for testing (23 points).

To apply the GP, we need to define the learning environment using a fitness function. The fitness function defined here is the mean squared error (MSE); it helps an efficient evolution for the model and allows it to travel fitness landscape until it finds an optimal solution for the given problem. The mean square error E_i of an individual program i is defined by the following equation;

$$E_i = \sqrt{\frac{\sum_{j=1}^{n}\left(P_{(ij)} - T_j\right)^2}{\sum_{j=1}^{n}\left(T_j - \bar{T}\right)^2}} \quad (3)$$

where $P_{(ij)}$ is the value predicted by the program i for fitness case j; T_j is the target value for fitness case j; and $\bar{T} = 1/n\sum_{j=1}^{n} T_j$. For a perfect fit E_i=0, and thus the index of RRSE ranges from 0 to infinity, with zero corresponding to the ideal. Thus the fitness of an individual model f_i can be calculated from the following equation which ranges from 0 to 1000, with 1000 corresponding to perfect fit; $f_i = 1000 \times 1/(1 + E_i)$. It is important to choose the set of functions that will create the chromosomes. These functions are the essence of evolution of the GP; they allow modifications without restrictions leading to compact correct programs for a specific function. The choice of an appropriate function set is not the same for every problem and depends mainly on the program performance with some chosen arguments. If the evolution is not satisfactory, one can use a wider set of functions until optimum fitness is achieved. However, a professional approach would be to initially use the basic mathematical operators (+, -, *, /) to allow for production of simple models. A second run of GP is performed using a different set of functions as shown in Table 3. Then, we have to set the linking function, which is the interaction between all subexpression trees of the model, these linking functions can be addition, subtraction, division, and multiplication. The choice of linking functions depends on the complexity of the problem and the experience of the model user and for simpler models for a certain problem, addition or subtraction would be appropriate. The last step is to set the values controlling various genetic operations controlling the evolutionary process of GP. The most efficient operator in GP are the mutation and cross over rates; which causes populations of individuals to adapt very efficiently, allowing for the evolution of good solutions to all problems. Values assigned for all genetic operators are shown in Table 3 for various GP models. To test the performance of the developed model, the mean square error MSE, mean absolute error MAE, and relative squared error RSE were used as indicators, as calculated from the following equations respectively;

$$MSE_i = 1/n\sum_{j=1}^{n}\left(P_{(ij)} - T_j\right)^2 \quad (4)$$

$$MAE_i = \frac{1}{n}\sum_{j=1}^{n}\left|\frac{P_{(ij)} - T_j}{T_j}\right| \quad (5)$$

$$RSE_i = \frac{\sum_{j=1}^{n}\left(P_{(ij)} - T_j\right)^2}{\sum_{j=1}^{n}\left(T_j - \bar{T}\right)^2} \quad (6)$$

Table 3. Optimal Parameter settings for the GP Algorithms

Parameters	Settings-GPI-h_{max}
Number of generations	100
Number of populations	500
Function set	+, -, *, /
Terminal set	Q, s, d_{90}, σ
Fitness function error type	MSE
Selection method	Tournament
Mutation rate	0.01
Crossover rate	0.9

Based on the optimal parameter settings in above table, the following GP-based equations were developed and are considered to be valid within the ranges given back in Table 2. The best individual for all generations for GPI-h_{max} can be presented as;

$$h_{max} = 0.38Qs - Q + \frac{d_{90}}{0.50-Q} + (1.92 - \sigma)(d_{90} + Q) \qquad (7)$$

Using the performance indicators discussed before, MSE, MAE, RSE and R-squared, Table 4 shows the comparison between developed GP-model and similar equations (Veronese, Martin, Mason, and Pagliara) for prediction of scour holes downstream ramp structures.

Table 4. Performance of developed equations for h_{max} versus some available equations

	GPI		Veronese	Martin	Mason	Pagliara (2007)
	train	test				
R-Square	0.88	0.84	NA	NA	NA	NA
MSE	0.0259	0.029	0.69	0.55	3.3	NA
MAE	0.087	0.110	0.90	0.99	0.75	33.3
RSE	0.116	0.255	27.1	13.9	60.99	NA

It is noticed that the developed GP relation had the highest representation of scour database, which resulted in highest value of R-squared and lowest values for errors. All existing formulae deviated in their predictions from measurements with huge RSE reaching 60.99 for Mason and 27.1 for Veronese. Due to huge errors in predictions of many of the existing formulae, the R-squared could not be calculated meaning that they do not represent measured data of rapid structures at all. This is mainly attributed to the presence of large scale experimental data, which are outside the limits of values used in developing most of these equations. Thus, this shows the importance of including the measured data from large scale experimental tests that are similar to real rapids on mountain streams. Results show also that genetic programming (GP) is capable of mapping data into a high dimensional feature space with variety of methods to find relations and trends in data. The following figures show the predictions of h_{max} as calculated by the developed GP model versus measured values for both training and testing datasets.

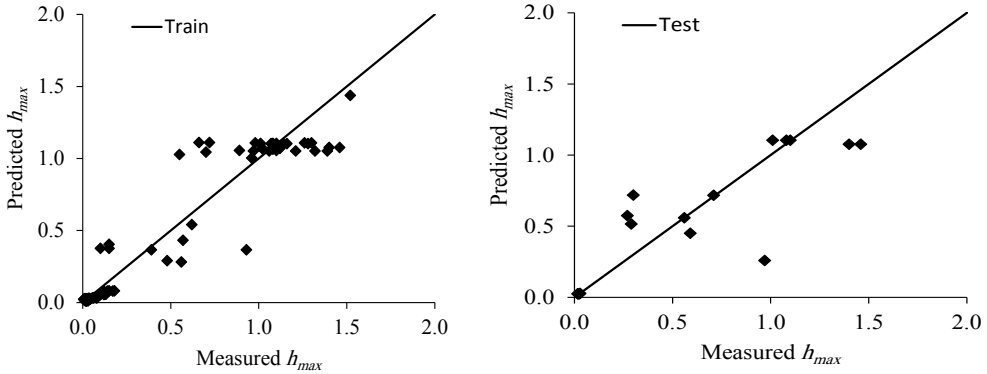

Figure 7. R^2 for training and testing data sets for GPI model for h_{max}

For risk assessment studies, the uncertainties of many influencing parameters have to be included. Thus; Wahl (2004) provided quantitative assessments for the uncertainty in breach parameter prediction using many of the available prediction relations on 108 documented dam failure case studies. In this part of the study, Wahl (2004) approach is adopted to test the ability of the developed GP models to predict scour hole depth. The analysis is applied to the dataset of 112 scour hole measurements including the measurements on large scale experiments. While this could provide some advantages for the GP model, it provides fair indication for comparison of ability of prediction for various equations (Wahl 2004). The uncertainty analysis defines the error in as; $e_{ij} = P_{ij} - T_j$, and then calculates main indicators defined as; mean prediction error ($\bar{e} = \sum_{j=1}^{n} e_{ij}$), width of uncertainty band, $B_{ub} = \pm 2S_e$ and the confidence band around the predicted value $\{\bar{e} + 2S_e, \bar{e} - 2S_e\}$, where S_e is the standard deviation of prediction errors. It is shown that the mean prediction error of developed GP model is -0.192 with prediction error standard deviation of 0.336 and width of uncertainty band of $\pm$0.67, while the prediction error interval ranged from -0.48 to 0.87. Unfortunately, other formulae produced large errors mainly due to the presence of large scale experiments in the used data base, which likes outside their applicable limits. Thus, this confirms the necessity to include more data related to large scale experiments in order to increase the range of applicability of various prediction equations for scour hole downstream rapid hydraulic structures.

5 CONCLUSIONS

Despite being important river training low head structures, there has not been much experiments on rapid hydraulic structures on large scale. However, many experimental studies are available for similar structures with ramps. This paper presents experimental work on rapid hydraulic structures investigating the characteristics of the downstream scour hole. Experimental data from this study have been used with other experimental data for similar ramp structures capturing the rapid and flow main characteristics with a total of 112 points including experimental data from large scale experiments on rapids. Genetic programming has been used to develop a relation for predicting maximum scour depth as a function of various rapid and flow parameters. Developed relation gave reasonable score in various indicators; it gave 0.84 in R-squared and 0.02 MSE with lowest errors amongst some of the available equations. While more data is still needed to enhance the prediction capability of the developed relation, however it can be used as preliminary estimates for scour hole formation downstream rapids while considering that errors are expected and shall have an uncertainty band of $\pm$0.67 orders of magnitude.

NOTATION

B	Rapid width
B_{UB}	Width of uncertainty band
d_{90}	Bed sediment size
F_{d90}	Densimetric Froude number
e	prediction error
h	Height difference between upstream and downstream of rapid
h_{max}	Maximum score hole depth
ρ	Water density
ρ_s	Sediment density
Q	Flow across rapid
g'	reduced gravity acceleration
S	rapid slope
Se	Standard deviation of prediction error
v	Flow velocity through rapid
σ	Coefficient of sediment variation

REFERENCES

Attari J., Arefi F., Golzari F. (2002). A review of physical models of scour holes below large dams in Iran. W: Rock Scour due to Falling High-Velocity Jets. Red.Schleiss, Bollaert.Swets and Zeitlinger, Lisse, Szwajcaria, 73-80.

Aytek, A. and Alp, M. (2008).An Application of Artificial Intelligence for Rainfall Runoff Modeling. Journal of Earth Syst. Sci., 117(2), 145-155.

Aytek, A., and Kisi, O. (2008).A Generic Programming Approach to Suspended Sediment Modeling.Journal of Hydrol. (Amsterdam), 351(3-4), 288-298.

Azamathulla H., Ghani A., Zakaria N., Lai S., Chang C. Leow C., and Abuhasan Z. (2008). Genetic Programming to Predict SkuJum Bucket Spillway Scour.Journal of Hydrodynamics. 20(4): 477-484.
Babovic, V., Drecourt, J.P., Keijzer, M., Hansen, P.F. (2002). A data mining approach to modeling of water supply assets. Urban Water 2002 (4), 401–414.
Ben Meftah, M. and Mossa, M. (2006). Scour Holes Downstream of Bed Sills in Low-Gradient Channels. J. Hydr. Res., 44(4), 497-509.
Bhuiyan, F., Hey, R. D. and Wormleaton, P. R. (2007). Hydraulic Evaluation of W-Weir for River Restoration. J. Hydraul. Eng., ASCE, 133(6), 596-609.
Bormann, N. E. and Julian, P. Y. (1991). "Scour Downstream of Grade-Control Structures." J. Hydraulic. Eng. ASCE,117(5), 579-594.
D'Agostino, V., and Ferro, V. (2003). "Scour on Alluvial bed downstream of grade-control structures." J. Hydraul. Eng., 130_1_, 1–14.
Dorado J et al. (2002). Prediction and modeling of the flow of a typical urban basin through genetic programming, Cagnoni S et al (eds): EvoWorkshops 2002, LNCS 2279, Springer-Verlag, 2002, pp190-201.
Drunpob, A., Chang, N.B., Beaman, M. (2005).Stream flow rate prediction using genetic programming model in a semi-arid coastal watershed. In: Walton, R. (Ed.), Proceedings, World Water and Environmental Resources Congress-2005. ASCE, Anchorage, Alaska, pp. 15–19.
El-Sayed, A.E. (2011).Application for Genetic Programming for Proton-Proton Interactions. Central European Journal of Physics, 9(3), 874-883.
Farhoudi, J., Smith, K.V.H. (1985). Local scour profile downstream of hydraulic jump. J. Hydr. Res. 23(4), 343-358.
GuvenA., and Gunai M. (2008). Genetic Programming Approach for Prediction of Local Scour Downstream of Hydraulic Structures. Journal of Irrigation and Drainage Engineering, 134(2), 241-249.
Ghorbani, M.A., Khatibi, R., Aytek, A., Makarynskyy, O., and SHiri, J. (2010). Sea Water Level Forecasting using Genetic Programming and Comparing the Performance with Artificial Neural Networks. Comput.Geosci., 36(5), 620-627.
Giustolisi, O. (2004). Using Genetic Programming to Determine Chezy Resistance Coefficient in Corrugated Channels. Journal of Hydroinformatics, 6, 157-173.
Guar S. and Deo, M.C. (2008). Real Time Wave Forecasting using Genetic Programming, Ocean Engineering, Vol.35, 1166-1172.
Harris, E.L., Babovic, V., and Falconer, R.A. (2003).Velocity Predictions in Compound Channels with Vegetated Flood Plains using Genetic Programming. Int. J. River Basin Manage., 1(2), 117-123.
Hassan, N.M.K.N., Narayanan, R.(1985). Local scour downstream of an apron. J. Hydr. Engng. 111(11), 1371-1385.
Kajak Z. (1992). Ecological results of river training works for a stream. XII OgólnopolskaSzkołaHydrauliki, Międzyzdroje, 21-25 września.MateriałySzkoły, p. 17-36. [In Polish]
Keijer, M. and Babovic, V. (2002).Declaratibe and Preferential Bias in GP-based Scientific Discovery.Genet.Program.Evolv. Mach., 3(1), 41-79.
Koza J. (1992). Genetic Programming: On the Programming of Computers by means of Natural Selection, MIT Press, Cambridge, MA.
Lenzi, M. A., and Comiti, F. (2003). Local scouring and morphological adjustments in steep channels with check-dam sequences." Geomorphology, 55_1–4_, 97–109.
Marion, A., Lenzi, M. A., and Comiti, F. (2004). Effect of sediment size grading and sill spacing on scouring at grade-control structures. Earth Surface Processes and Landforms, 29_8_, 983–993.
Mossa, M. (1998). Experimental study on the scour downstream of grade-control structures. Proc. 26th Convegno di Idraulica e Costruzioni Idrauliche, Catania, 581–594.
Novak P., Moffat AI.B., Nalluri C. (1996). Nayaranan R., Hydraulic Structures, Chapman and Hall, London.
Pagliara, S., Hager, W.H. (2004) Scour downstream of block ramps. Proc. 2nd Intl. Conf. Scour and Erosion, Singapore 2, 215-222.
Pagliara, S. (2007). Influence of Sediment Gradation on Scour Downstream of Block Ramps. J. Hydraul. Eng., ASCE, 133(11), 1241-1248.
Pagliara, S. and Palermo, M. (2008). Scour Control Downstream of Block Ramps. J. Hydraul. Eng., ASCE, 134(9), 1376-1382.
Preis, A., and Otsfeld, A. (2008). A Coupled Model Tree Genetic Algorithm Scheme for Flow and Water Quality Predictions in Watersheds. Journal Hydrol., 349(3-4), 364-375.
Rabunal, J.R., Puertas, J., Suarez, J., and Rivero, D. (2006).Determination of the Unit Hydrograph of a Typical Urban Basin using Genetic Programming and Artificial Neural Networks.Hydrol.Process., 27(4), 476-485.
Ratomski J. (1992). Pro-ecological elements in river training works. In Polish: Proekologicznazabudowarzekipotokówgórskich. XII OgólnopolskaSzkołaHydrauliki, Międzyzdroje, 21-25 września.MateriałySzkoły p. 59-68.
Rhone J.T. (1977).Baffled apron as spillway energy dissipator, Journal of Hydraulic Division, 12, p.1391-1401.
Rosgen, D.L. (2001). The Cross-Vane, W-Veir and J-Hook Vane Structures: Their Description, Design and Application for Stream Stabilization and River Restoration. Proc., Wetland Engineering and River Restoration Conf.(CD-ROM), ASCE, Reston, Va.
Scurlock, S.M., Thornton, C. I. and Abt S. R. (2011). One-Dimensional Modelong Techniques for Energy Dissipation in U-Weir Grade-Control Structures. World Environmental and Water Resources Congress, ASCE, 2496-2507.
Scurlock, S.M., Cox, A. L., Thornton, C. I. and Baird, D. C. (2012). Maximum Velocity Effects from Vane-Dike Installations in Channel Bends. World Environmental and Water Resources Congress,, ASCE, 2614-2626.
Scurlock, S.M., Thornton,C. I. and Abt S. R. (2012). "Equilibrium Scour Downstream of Three-dimensional Grade-control Structures." J. Hydraul.Eng., ASCE, 138(2), 167-176.
Savic, A.D., Walters, A.G., and Davidosn, J.W. (1999).A Genetic Programming Approach to Rainfall-Runoff Modeling. Water Resources Management, 13(3), 219-231.

Shiri, J., and Kisi, O. (2011).Application of Artificial Intelligence to Estimate Daily Pan Evaporation Using Available and Estimated Climatic Data in the Khozestan Province (South Western Iran). Journal of Irrigation and Drainage Engineering, 137(7), 412-425.

Shields, F. D., JR, Knight, S. S. and Cooper, C. M. (1995). Incised Stream Physical habitat Restoration with Stone Weirs. Regulated rivers: Research and Management, Vol. 10, 181-198.

Singh K.Y.H. (1983). Fundamentals of Irrigation Engineering .Nemchand, Roorkee.

Ślizowski R. (1993).Rapids with artificial roughness as an element used in river training works. In Polish: Bystrza o zwiększonejszorstkościjako element zabudowypotokówgórskich, Rozpr. hab. nr 181, Zesz. Nauk. AR, Kraków.

Veronese, A. (1937). Erosioni di fondo a valle di uno scarico. Ann. Lavori Pubbl. 75(9), 717-726, 1937 [in Italian].

Whigham P.A. and Crapper P.F. (2001).Modeling rainfall-runoff using genetic programming, Mathematical and Computer Modelling, 33, pp707-721.

IWLHS, 20-22/02/2013, Aachen - Bung & Pagliara (eds) - © 2013 Bundesanstalt für Wasserbau ISBN 978-3-939230-04-5

A Comparison between Inclined Hydraulic Jumps over a Thin Wall and a Step

J. Demetriou
Dr Civil Engineer, Associate Professor (RD), National Technical University of Athens, School of Civil Engineering, JD Research Hydrolab – A non Profit Foundation, 12, Polykarpou St., N. Smyrni, Athens 17123, Greece

E. Retsinis
Civil Engineer, National Technical University of Athens, Postgraduate Student, National Technical University of Athens, JD Research Hydrolab – A non Profit Foundation, 12, Polykarpou St., N. Smyrni, Athens 17123, Greece

ABSTRACT: In this study, which is based on previous experimental data by the authors, a comparison is attempted between inclined hydraulic jumps over a thin wall, and a step- which is followed by a raised floor. The water free surface profiles, the dimensionless lengths and dimensionless conjugate depths are examined and the results are compared and discussed. The two flow cases appear to have some similarities between the flow lengths, but they present considerable differences in the descending part of the water free surface profiles and the conjugate depths. Some explanations are offered in order to compare the two flow structures. The results of this investigation may be useful to the hydraulic engineer when designing the pertinent open channel-especially for low head-works.

Keywords: Hydraulic Jumps, Thin Walls, Abrupt Steps, Low Head.

1 INTRODUCTION

The stable horizontal or inclined (angle φ) water flows over a thin wall (w), perpendicular to the channel floor, and over a step (w) - with following raised floor - which has its upstream face perpendicular to the channel floor, are two interesting and comparable hydraulic problems, where the two flow obstacles are often called “sills”. In both cases an incipient hydraulic jump is present, which is stable and may be used to dissipate the jump’s mechanical excessive energy.

Figs. 1 and 2 show the basic flow characteristics of the two water flows, within the inclined rectangular channel. Both structures are mainly linked to rather low water heads because of their natural characteristics, where the low heads are important here.

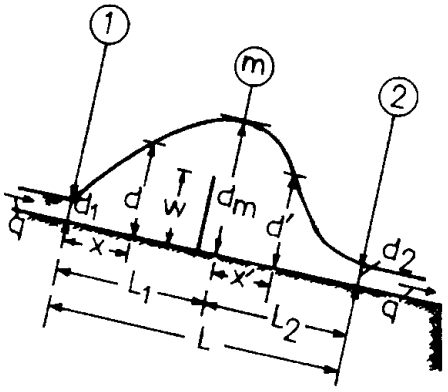

Figure 1. Jump over a thin wall.

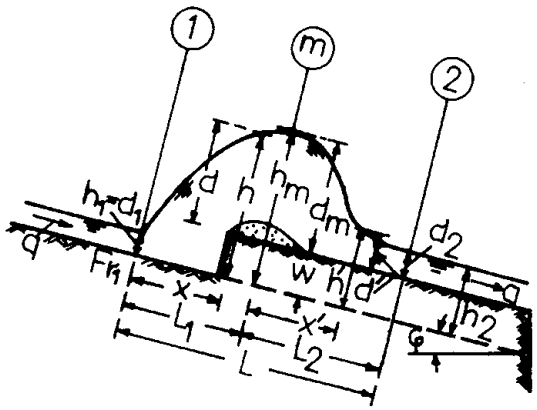

Figure 2. Jump over a step.

In both jump cases-of rather low head-there are three important flow cross sections: Section 1 (of uniform flow) with depths d_1 (Fig. 1) and d_1 (=h_1), Fig. 2, section m (of non uniform flow) with depths d_m (Fig. 1) and h_m, (or d_m), (Fig. 2), and section 2 (of uniform flow) with depths d_2 (Fig. 1) and h_2 (or d_2), Fig. 2, where $h_m=d_m+w$ and $h_2=d_2+w$. At a distance x the flow depth is d (Fig. 1) and h (or d), Fig. 2, while at distance x' (from section m) corresponding depths are d' (Fig. 1) and h' or d' (Fig. 2). The respective lengths (Figs. 1 and 2) are L_1, L_2, with $L= L_1+L_2$, the discharge (per unit channel width) is q, while in the case of the jump over a step an air pocket may be present, which has not been observed in the case of the jump over a thin wall. The max depths (d_m in Fig. 1 and h_m in Fig. 2) may appear close upstream, on, or – usually – close downstream the wall and the step face correspondingly.

The main flow parameter is the Froude number at section 1,

$Fr_1=q\cdot g^{-1/2}\cdot d_1^{3/2}$,

which is bigger than 1, since in both cases the upstream flow is supercritical, while the downstream flow ends up (here) to a channel *drop*.

Demetriou et al (2008), and (2010), have performed a large number of experimental measurements for flows over thin walls, Demetriou et al (2010), are also dealing with the jump over a step, while Hager (1992), is presenting a wide summary of both flows in exclusively horizontal channels. For the jumps over a thin wall the measurements are extended to $0^o\le\varphi\le14^o$, while for the jumps over a step it is $0^o\le\varphi\le8^o$.

All laboratory Runs were twice performed in a rather small perspex flume, suitable for non uniform flow phenomena measurements.

2 PREVIOUS DATA

2.1 *Flow Profiles*

2.1.1 *Jumps Over Thin Walls*

In order to determine the surface water profiles, $d(x)$ and $d'(x')$, the dimensionless terms

$\bar{d}=(d-d_1)/(d_m-d_1)$ vs $\bar{x}=x/L_1$,

$\bar{d}'=(d_m-d')/(d_m-d_2)$ vs $\bar{x}'=x'/L_2$

are used for upstream and downstream profiles, while d_m-w are the water hydraulic heads.

The experimental results gave the profiles' empirical equations, Demetriou et al (2008),

$$\bar{d}\cong(7.48-4.76\cdot e^{J_o})\cdot(\bar{x})-(6.48-4.76\cdot e^{J_o})\cdot(\bar{x})^{1.5} \qquad (1)$$

where, J_o=channel slope=sinφ and $0^o\le\varphi\le14^o$, $0.14\le d_1/w\le1$, $2\le Fr_1\le7.2$, and

$$\bar{d}'\cong a\cdot(\bar{x}')^{1.5}-b\cdot(\bar{x}')^3 \qquad (2)$$

where a, b, are arithmetic coefficients, with particular values for each angle φ. The approximate values of a, b, are presented in Table 1. In these profiles, for $\bar{x}=0$ it is $\bar{d}=0$ (or $d=d_1$) and for $\bar{x}=1$ it is $\bar{d}=1$ (or $d=d_m$), while for $\bar{x}'=1$ it is $\bar{d}'\cong1$ (or $d'\cong d_2$) and for $\bar{x}'=0$ it is $d'=d_m$.

Table 1. Arithmetic coefficients.

φ	a	b	$(a-b)=$
0^o	1.93	0.91	1.02
2^o	2.04	1.03	1.01
4^o	2.14	1.12	1.02
6^o	2.16	1.14	1.02
8^o	2.26	1.23	1.01
	Eq. (2)		

2.1.2 *Jumps Over Steps*

The corresponding water profiles' dimensionless terms are, Demetriou et. al (2010),

$\bar{h} = (h - h_1)/(h_m - h_1)$ vs $\bar{x} = x / L_1$,

$\bar{h}' = (h_m - h')/(h_m - h_2)$ vs $\bar{x}' = x'/L_2$ while the water hydraulic heads are h_m-w.

The experimental results gave the profiles' empirical equations (φ in degrees)

$$\bar{h} \cong (2.85 - 0.09 \cdot \varphi) \cdot \bar{x} - (1.85 - 0.09 \cdot \varphi) \cdot (\bar{x})^{1.5} \qquad (3)$$

$$\bar{h}' \cong 4.48 \cdot (\bar{x})^{1.5} - 3.48 \cdot (\bar{x})^2 \qquad (4)$$

i.e. the downstream profile is a unique curve – independent of angle φ. Actually, there are various profiles, but they are so dense (within the present flow parameters) that they can be represented by a single line. The above equations hold for $3 \le h_m/h_1 \le 31$, $1.5 \le h_m/h_2 \le 5$, $0.2 \le h_1/w \le 6.7$ and $1.1 \le Fr_1 \le 9.5$. In these profiles, for $\bar{x} = 0$ it is $h=h_1$ and for $\bar{x} = 1$ it is $h=h_m$, while for $\bar{x}' = 0$ it is $h' = h_m$ and for $\bar{x}' = 1$ it is $h' = h_2$.

2.2 *Jumps' Lengths*

2.2.1 *Jumps Over Thin Walls*

The dimensionless lengths $(L_1\text{-}w)/d_m$ vs Fr_1 and angle φ ($0^o \le \varphi \le 14^o$) were measured by Demetriou (2010), for $0.14 \le d_1/w \le 1$ and $2 \le Fr_1 \le 7.2$. These results were suitably adjusted here in order to compare with the present results for the jumps over steps.

2.2.2 *Jumps Over Steps*

Demetriou et al (2010), have experimentally determined the dimensionless lengths $(L_1\text{-}w)/d_1$ vs Fr_1 and angles φ ($0^o \le \varphi \le 8^o$), while they have also measured h_m/d_1 vs Fr_1 and angles φ (same range). Thus, dividing $(L_1\text{-}w)/d_1$ to h_m/d_1 the ratio $(L_1\text{-}w)/h_m$ can be received.

2.3 *Jumps' Conjugate Depths*

In a wide view, d_m (Fig. 1) and h_m (or d_m) – Fig. 2, may be considered as conjugate depths in relation to d_1 and h_1 ($=d_1$) respectively.

2.3.1 *Jumps Over Thin Walls*

Demetriou et al (2010), have measured $(d_m\text{-}w)/d_1$ vs Fr_1 ($1.5 \le Fr_1 \le 7.2$) and angle φ ($0^o \le \varphi \le 14^o$).

These results are slightly modified here in order to compare with the corresponding quantities of the jumps over steps.

2.3.2 *Jumps Over Steps*

Demetriou et al (2010), have also measured $(h_m\text{-}w)/d_1$ vs Fr_1 ($2 \le Fr_1 \le 8.5$) and angle φ ($0^o \le \varphi \le 8^o$).

3 COMPARISONS. RESULTS AND DISCUSSION

The comparison between the geometrical elements of both jumps is restricted here to corresponding water free surface profiles along the entire lengths L, the dimensionless lengths along the ascending parts of these profiles, L_1, and the conjugate depths ratios.

Figs. 3, 4 present the flow profiles for the jumps over a thin wall and over a step correspondingly, while Fig. 5 presents a comparison between these profiles, with solid lines two limit profiles for φ=0° and φ=14° (jumps over walls) and with dashed lines two limit profiles (jumps over steps) for φ=0° and φ=8°. The use of only two couples of limiting profiles in Fig. 5 (and not of all profiles – as in Fig. 3 and 4) is due to the narrow space in this figure.

As it is clear from Fig. 5, along L_1 the ascending flow profiles may compare among them, showing that from this point of view the two jumps, over a thin wall and a step, appear to have a similar structure. On the contrary, along L_2 the descending free surface water profiles are clearly different in the two flow phenomena: Just after the thin wall the water is dropping down, mainly because of gravity, while after the step the flow is continued along the raised floor. Perhaps this behavioral difference is also responsible for the existence or no of an air pocket in the two flow cases.

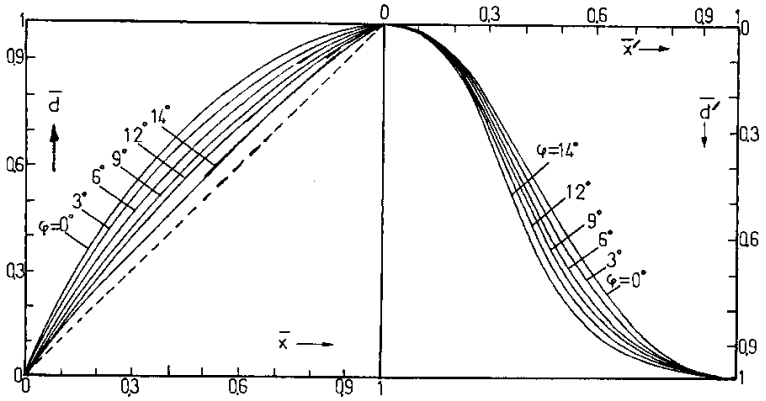

Figure 3. Flow profiles for jumps over a thin wall.

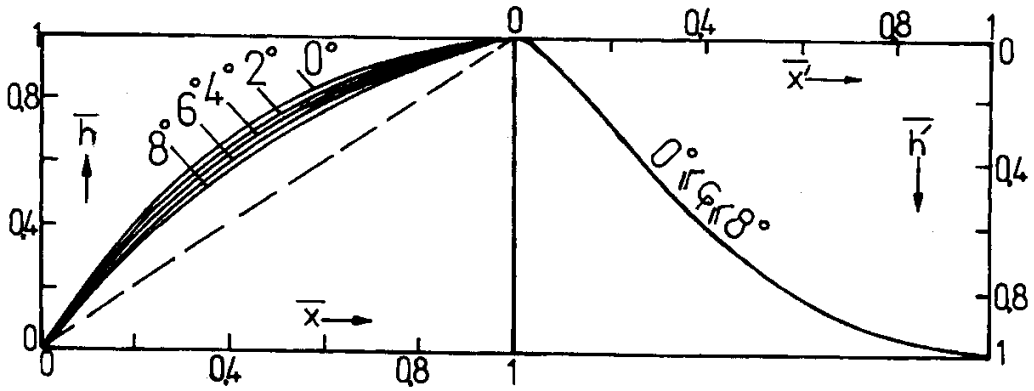

Figure 4. Flow profiles for jumps over a step.

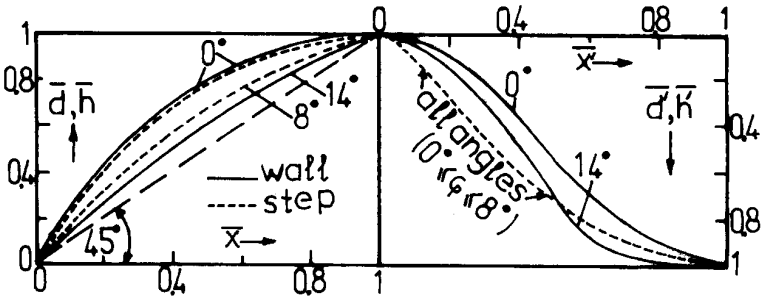

Figure 5. Comparison of flow profiles for jumps over a thin wall and over a step.

Fig. 6 presents the dimensionless lengths $(L_1 - w)/d_m$ vs Fr_1 and angle φ for the jump over a thin wall, Fig. 7 shows the lengths $(L_1 - w)/h_m$ vs Fr_1 and angle φ, for the jumps over a step, while Fig. 8 presents a comparison between corresponding lengths, where for $w \to 0$ (no wall and no step) $d_m \to d_1$ (Fig. 1), $h_m \to h_1$ (Fig. 2) and $L_1 \to 0$, i.e. both families of lines tend to the infinity.

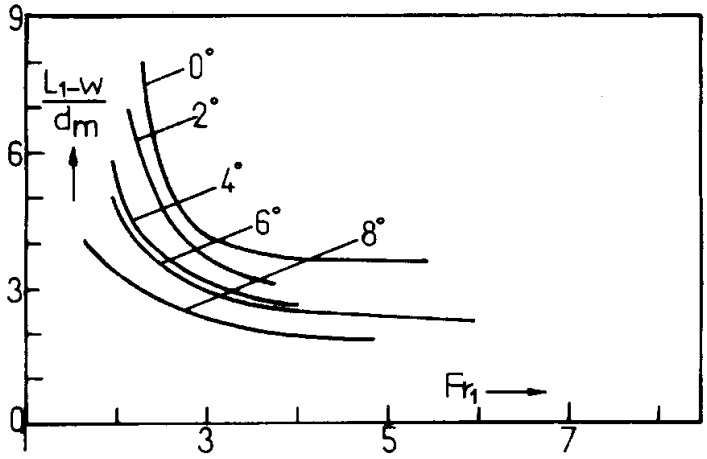

Figure 6. $(L_1 - w)/d_m$ vs Fr_1 and angle φ for jumps over a thin wall.

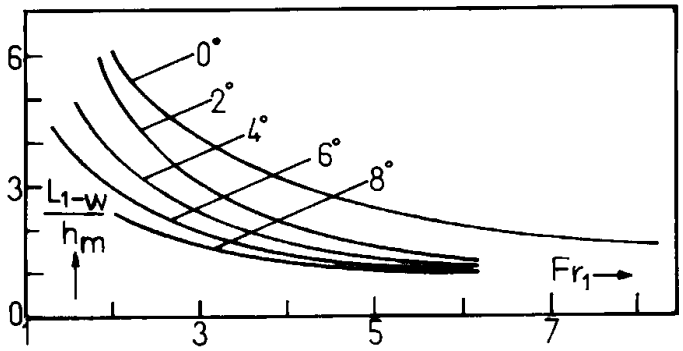

Figure 7. $(L_1 - w)/h_m$ vs Fr_1 and angle φ for jump over a step.

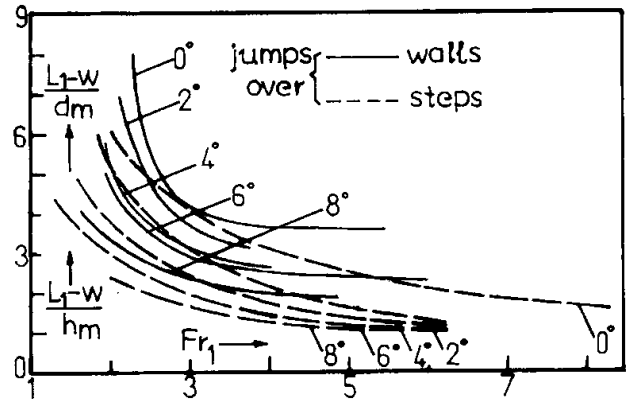

Figure 8. Comparison of flow lengths for jumps over a thin wall and over a step.

From Fig. 8 it is clear that, although any wall length curves (solid lines) lie over corresponding step – length curves (dashed lines), the two families of lines are similar and almost of the same order of magnitude. From this point of view both jumps (over a thin wall and over a step) appear to have a comparable structure.

Next figures compare the dimensionless conjugate depths for both inclines jumps.

Fig. 9 shows a diagram between $(d_m - w)/d_1$ vs Fr_1 and angles φ for jumps over a thin wall, Fig. 10 presents $d_m/h_1 = (h_m - w)/h_1$ vs Fr_1 and angle φ for jumps over a step, while Fig. 11 attempts a comparison between corresponding quantities of the two jumps (solid lines for jumps over a thin wall and dashed lines for jumps over a step).

For $w \to 0$ (no wall and step) $d_m \to d_1$ (or $d_m/d_1 \to 1$) and $h_m \to h_1$ (or $h_m/h_1 \to 1$), i.e. the horizontal line (Fig. 11) through $(d_m - w)/d_1$ or $(h_m - w)/h_1$ is the lower limit of all curves of Fig. 11, independently of angle φ and Fr_1.

As it clear from Fig. 11, for same w and initial depths (d_1, h_1) the jump over a step appears to have much larger conjugate depths than respective jump over a thin wall (for same angle φ and Fr_1). Especially for larger angles φ the dimensionless conjugate depth is enormously larger in the case of jumps over steps than in the case of jumps over thin walls.

The above behavior shows that the presence of a step (and following raised floor) produces a much larger effect on the flow, than the presence of a thin wall – especially in larger angles φ and Froude numbers Fr_1. If this result is combined with the profiles' result of Fig. 5 – along L_2, then the final conclusion may be that the raised floor (in the case of the jump over a step) makes the main difference of the two flow cases. This difference is primarily expressed in the quantities which are perpendicular to the flow direction (conjugate depths, $\bar{d}'$, $\bar{h}'$) and not parallel to the flow (jumps' dimensionless lengths).

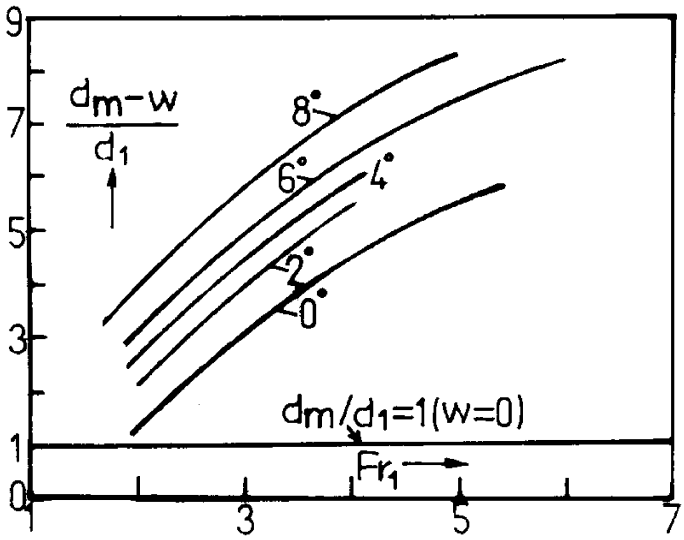

Figure 9. $(d_m - w)/d_1$ vs Fr_1 and angle φ, over a thin wall.

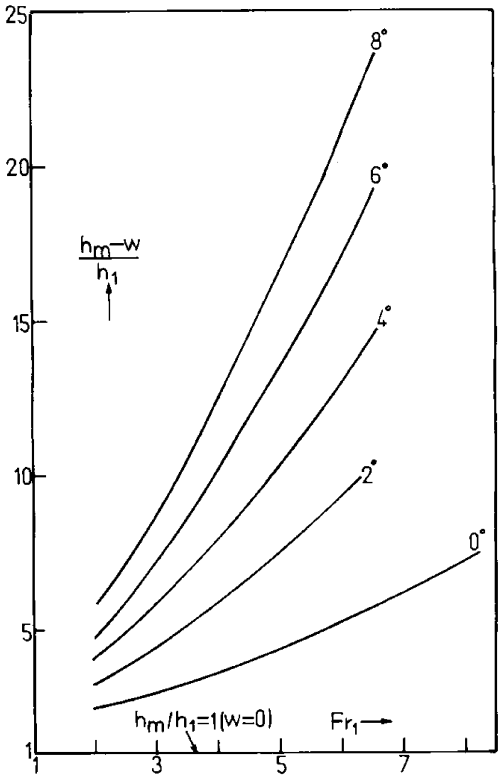

Figure 10. $(h_m - w)/h_1$ vs Fr_1 and angle φ, over a step.

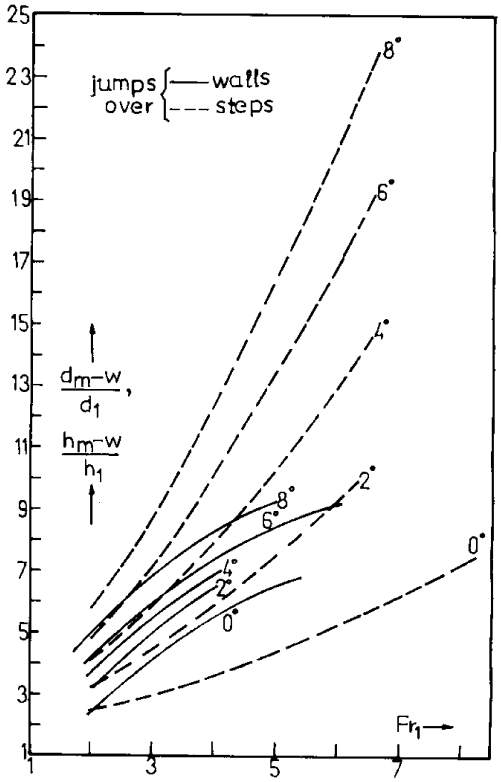

Figure 11. Comparison of conjugate depths for jumps over a thin wall and over a step.

In Figs. 9, 10 and 11 the dimensionless water heads $(d_m\text{-}w)/d_1$ and $(h_m\text{-}w)/d_1$ appear to have small or larger values, depending on Fr_1, angle φ and d_1. The last depth is quite small and this is why some large dimensionless water heads are present in these Figs. Actually all heads $(d_m\text{-}w)$ and $(h_m\text{-}w)$ are low when compared to w, for $0^o \leq \varphi \leq 8^o$ and $2 \leq Fr_1 \leq 7$, as they were preliminary measured by the authors.

4 CONCLUSIONS

In this study, which is based on previous experimental data by the author et al, a comparison is attempted between inclined (angle φ) hydraulic jumps over a thin wall (w) and a step (w). The water free surface profiles, the dimensionless lengths and dimensionless conjugate depths are compared in order to show the similarities and differences of the two flow cases. The main conclusions are: (1) The ascending parts of the water free surface profiles appear to have a similar behavior in structure and order of magnitude. (2) The descending parts of the water free surface profiles present considerable differences between them. (3) These differences are mainly due to the raised floor – following the flow over the steps. (4) The dimensionless lengths of both flows are comparable between them. (5) The dimensionless conjugate depths of both flows are quite different in magnitude. (6) The latter difference appears as a result of the raised floor – following the jump over a step. (7) The difference between the two flow cases is primarily expressed in the quantities which are perpendicular to the floor, while the quantities along the flow are almost of a similar behaviour. The results of this investigation may be useful to the hydraulic engineer when designing pertinent open channel works-especially in lower water heads cases.

NOTATION

q	discharge per unit channel width
g	gravity acceleration
d	water profile and specific depths
h	water profile and specific depths
x	longitudinal coordinate
φ	channel angle (degrees)
J_o	channel slope
Fr	Froude number
$\bar{x}$	dimensionless longitudinal coordinate
$\bar{d}$	dimensionless water profile
$\bar{h}$	dimensionless water profile

REFERENCES

Demetriou J., Hadjieleftheriou S. (2008). Inclined Jumps Over Sills. Part 1, Upstream Geometry, 16th IAHR-APD Congress/ 3rd IAHR – ISHS Symposium, October 20-23, Nanjing, China, 6 pages.

Demetriou J. (2008). Inclined Jumps Over Sills. Part 2, Downstream Geometry, 16th IAHR-APD Congress/3rd IAHR – ISHS Symposium, October 20-23, Nanjing, China, 6 pages.

Demetriou J. (2008). Overall Geometry of an Inclined Jump Over a Sill, 8th Int. Hydrogeological Congress, October 7-10, Athens, Greece, 9 pages.

Demetriou J. (2008). Predifiction of Forces Along inclined Jumps Over a Sill, 2nd Int. Conf. on RAEFM, Andra-Pradesh, India, 3-6 March, 8 pages.

Demetriou J. (2010). Conjugate Depth Comparisons Among Free, Repelled and Over Sills Inclined Hydraulic Jumps, Flow 2010, 7th Greek Congress, Thessaloniki, Greece, 12-13 Nov., 7 pages.

Demetriou J., Retsinis E., Dimitriou D. (2010). Profiles of Inclined Water Jumps Over Positive Channel Steps, Parts 1,2, 9th Int. Scientific-Practical Conf., 22-23 April, St. Petersburg, Russia, 25 pages.

Demetriou J., Dimitriou D. (2010). Overall Geometry of an Inclined Jump Over a Step, SWARM, Surathkal, Karnataka, India, 7-9 Jan., 7 pages.

Demetriou J. (2010). Length Comparisons Among Free, Repelled and Over Sills Inclined Hydraulic Jumps, 1st European IAHR Congress, Edinburgh, UK, 6 pages.

Hager W. (1992). Energy Dissipators and Hydraulic Jump, Kluwer Academic Publishers, Dordrecht/Boston/London.

IWLHS, 20-22/02/2013, Aachen - Bung & Pagliara (eds) - © 2013 Bundesanstalt für Wasserbau ISBN 978-3-939230-04-5

Study of Hydraulic Properties and Design Criteria for a River Subsurface Intake without Cut Off

R. Mansouri[1], A. N. Ziaei[2], K. Esmaili[3],
1 MSc. Student, Water Eng. Dep., Ferdowsi University of Mashhad, Iran, 2, 3 Assist. Prof., Water Eng. Dep., Ferdowsi University of Mashhad, Iran

ABSTRACT: In this study a subsurface intake introduced. This intake acts as a river drainage network. In this study an experimental model of the subsurface intake was constructed and the effective parameters such as upstream discharge, installation depth, and drains interval were evaluated. The results showed that the water diversion mostly influenced by the upstream flow rate. Small drain interval caused the discharge of each drain to be reduced. It was also revealed that the total drained discharge in the very transmitting media was mostly controlled with the number of drain and drain interval did have a marginal effect. Finally the regression equations were established to estimate the discharge of each drain based on dimensional analysis, which facilitate the design of this structure.

Keywords: subsurface intake, porous media, drainage system, design criteria

1 INTRODUCTION

Rivers are considered as one of the providers of water and energy for the nature and the human. The provision of water has been the most important economical role of the rivers and the suitable design of a river intake is one of the oldest issues in hydraulic engineering. However, due to complexity of river flows, designing an intake in a natural river has remained as an important topic in the river engineering.
The water diversion method depends on flow conditions, topology and morphology of river and economical considerations. The multitude of types of intake from rivers can be divided into lateral intakes, frontal intakes and bottom intakes (Raudkivi, 1993). In bottom intakes that are used mostly in mountainous rivers; the flow is diverted through a conduit installed underneath the river bed. Some parts or all of the length and width of the conduit in river bed are made as openings and water is unloaded into the conduit through these openings. Garot (1939) conducted experiments on the bottom intake with longitudinal bars as the horizontal grid. Other researches such as De Marchi (1947), Bouvard (1953), Kuntzmann and Bouvard (1954), Noseda (1956 a, b), Mostkow (1957), Brunella (2003), Righetti and Lanzoni (2008) and Maghrebi and Razaz (2009) have investigate different aspects of the bottom intakes with the reticular bottom.

Problems such as clogging, corrosion, freezing, storage and discharge of sediment to the system limit the applicability of this type of intake (Castillo and Lima, 2010). These disadvantages caused the replacing the meshed conduit with a porous media to be advised. Naqhavi et al. (2010) studied the properties of bottom intake with the porous material experimentally. The efficiency of the porous bottom intake is also reduced via the sedimentation and reduction of the media transmissivity (Koorosh Vahid et al., 2010). Furthermore, the subsurface flow that is crucial in seasonal rivers of the arid and semiarid regions cannot be extracted using this intake.

To diminish these problems a method (based on infiltration gallery idea) for diversion of surface and subsurface flow in the seasonal rivers has been implemented. In this type of intake a subsurface drainage system is buried in very porous media in the river bed. Although the subsurface drainage is an elder idea the hydraulic properties of this type of intake has been rarely investigated.

In this study, the effective parameters on subsurface intake efficiency are experimentally investigated. Moreover, based on the hydraulic parameters and dimensionless groups obtained by dimensional analysis,

some regression equations between effective parameters and diversion discharge of each drain are developed which facilitate the design procedure of this structure.

2 MATERIALS AND METHODS

2.1 *Experimental Setup*

A model (half of the prototype) of longitudinal axisymmetric subsurface river intake was constructed as a rectangular cube (1 m width × 2 m long × 1m height). To control the water level along the model, two reservoirs were considered on both sides of the model. The water was introduced to the porous media through two perforated plates on both sides of the model (Fig.1). The 11-mm internal diameter perforated drain pipes were installed along the width of the model on two levels. The 15 and 14 lateral pipes were installed on 50 and 30 cm height from the model bed in a zigzag mode. The distance between the lateral drain was 10 cm. the longitude slope of the model and lateral drains was considered as 1%. Based on FAO standard, the whole opening area on the pipe was 4% of pipe surface. To prevent entering fine particles into the drains, the drains were folded by a layer of glass fiber.

Figure 1. A view of the rectangular cube and installation of the perforated plates

A set of manometers were installed on the bottom of the cube to check the water level in the porous media. The space between two perforated plates was filled with graded sand (d_{50}=1.5 mm) up to height of 80 cm from the cube bed (Fig. 2). The hydraulic conductivity of the porous media was measured via leading different discharge under different hydraulic gradient as 60 m/day. The water circulation was conducted using a pump and a water collection tank. The distance between lateral was changed by clogging the valves of the drain pipes.

More than 276 set of experiments were designed to investigate the effect of different parameters such as installation depth (D = 30 and 50 cm), the distance between lateral drains (10, 20, 30, 40, 50, 60, 150 cm), the porous media length (50,100,150 cm), the arrangement of drains (mono level and bi-level drains). The upstream discharge was considered in four rates (i.e., 0.4, 0.8, 1.2 and 1.6 L/s). The constant inlet flow associated with extinction of cut-off wall. With the cu-off wall the constant head is set over the up and down reservoirs. For each set of experiment, the drain discharge was measured three times and the average values were stored. The water level was also measured in each test by the manometers.

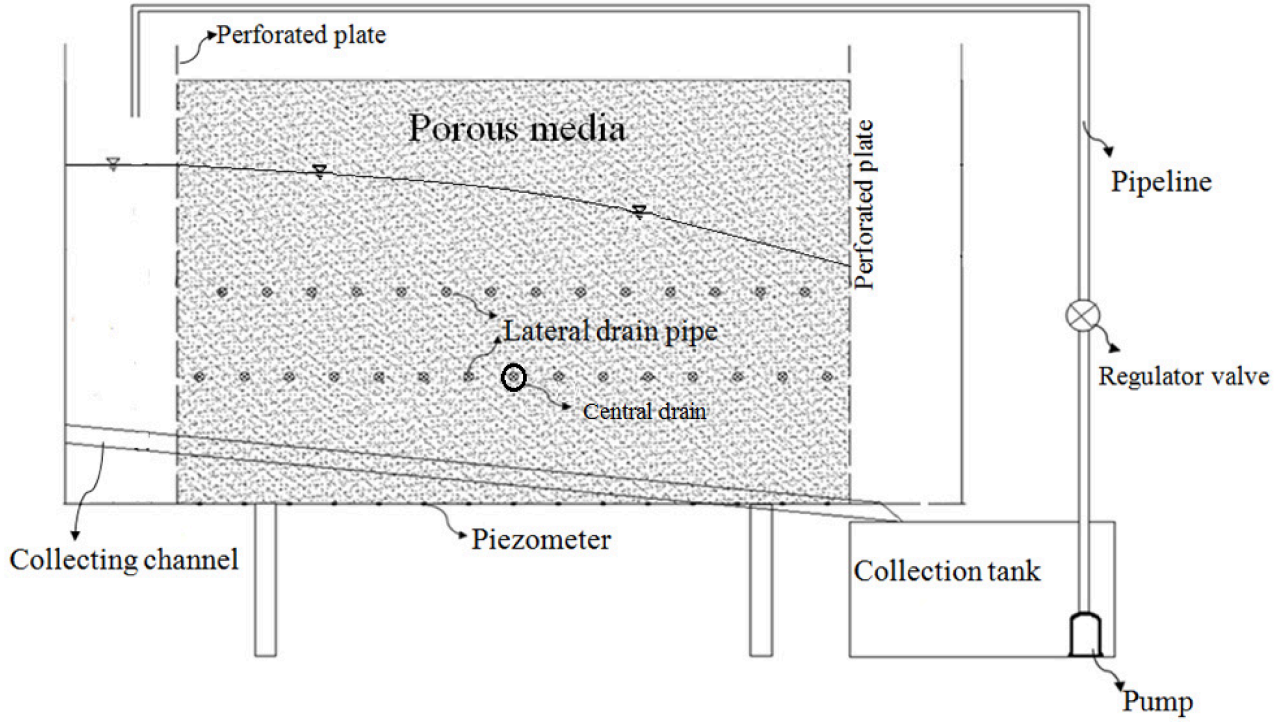

Figure 2. Schematic view of the longitudinal section of the model constructed in the laboratory in constant upstream flow rate conditions

2.2 *Dimensional analysis*

Dimensional analysis in this research can be accomplished based on known upstream water head or known upstream subsurface flow rate. These two are associated with existence and extinction of the cutoff wall. In the known upstream flow rate conditions, it is assumed that water is flowed through the stream with a constant upstream discharge. In this study the variables are divided in three groups; the flow variables, drainage system properties, and porous media parameters.
In case of extinction of the cut-off wall, all probable effective variables can be included as the following equation.

$$f\left(\rho, g, \mu, q, n, d_{50}, k, L, w, D, Q, x, d_p, S_0, S_l, A_d, n_f, form\right) = 0 \qquad (1)$$

Where ρ is water density, g gravity acceleration, μ water viscosity, q a drain flow rate, Q upstream discharge, n media porosity, d_{50} diameter 50% of material are less than, k hydraulic conductivity, L length of porous media, w lateral distance between drains, D installation depth, x distance from the media upstream, d_p drain diameter, S_0 the river bed slope, S_l drain lateral slope, A_d perforated drain opening area, n_f envelop resistance factor, and $form$ installation form parameter.
Having selected an identical envelop and drain pipe diameter for all experiments, constant river bed and drain slope, the parameters can be categorized through following dimensionless Π:

$$\emptyset\left(\frac{qw^2}{k^3}, \frac{Qw^2}{k^3}, \frac{\mu}{\rho kw}, \frac{wg}{k^2}, \frac{D}{w}, \frac{L}{w}, \frac{x}{w}\right) = 0 \qquad (2)$$

Where gw/k^2 and $\mu/\rho kw$ are representation of Froude and Reynolds numbers. Notice that the hydraulic conductivity is related to d_{50} and n. Thus, k is used as the porous media parameter and the other two parameters are omitted and the effective parameters are reduced to the following form (Eq. 3).

$$\emptyset\left(\frac{qw^2}{k^3}, \frac{Qw^2}{k^3}, Re, Fr, \frac{D}{w}, \frac{L}{w}, \frac{x}{w}\right) = 0 \qquad (3)$$

3 RESULTS AND DISCUSSION

3.1 *The effect of drain distance and upstream discharge*

As the first step, the diverted water from the drainage system was measured under different upstream discharges and drain intervals. It was observed that the drains flow rate changed along the model. The water head measured with the piezometers also varied along the model even where the uniform surface water depth existed. The flow rate from the central drains (drain No. 7 and No. 8 for two installation depth D= 30, and D= 50 cm, respectively) was evaluated in different upstream discharges and drain intervals that are depicted in Fig. 4. It is observed that increasing the drain intervals caused the drain flow rate to be increased. The greater drain interval in a constant model length led to the smaller number of drains and consequently the increased upstream discharge which introduced the greater flow rate. Note that the flow pattern was identical for the different upstream discharge and the significant difference between 60 cm and 150 cm drain interval was not observed in the all upstream discharges. The direct effect of upstream discharge on the drains discharge can be obviously observed in this figure.

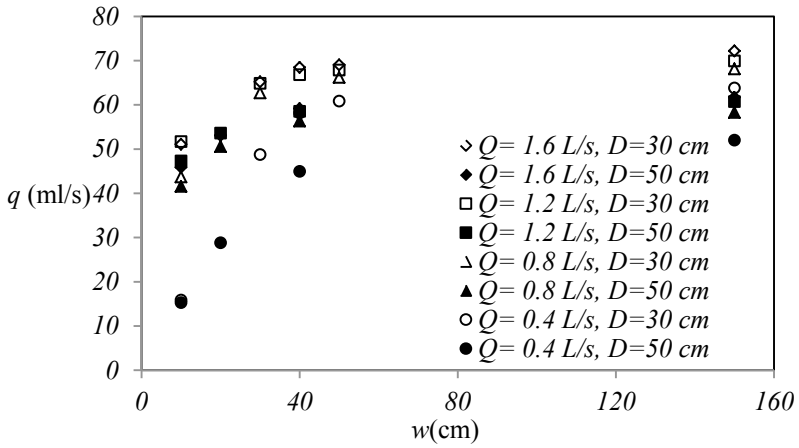

Figure 3. The central drain discharge in different drain intervals and upstream discharge

The discharge relation for the central drain (indicated in Fig.2) (Fig. 4) obeyed from a logarithmic function and the flow rate reached a constant value depending on the media hydraulic conductivity and the drain conductance capacity. The great difference between 10 cm interval and other intervals can be related the side effect of the radial flow of the very close drains.

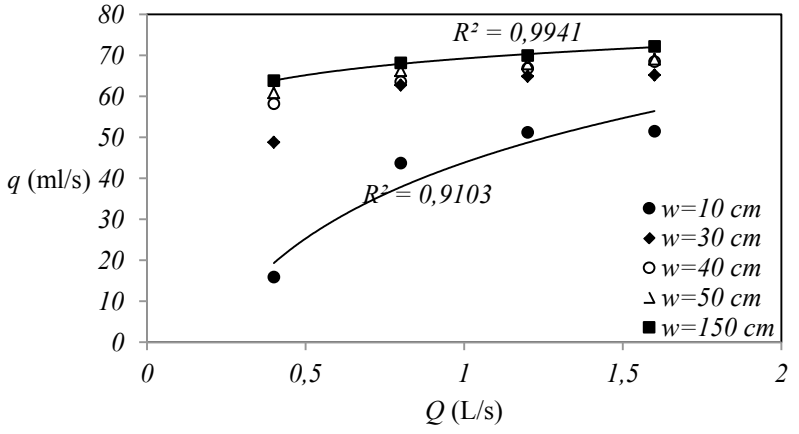

Figure 4. The central drain discharge – flow rate relation for the central drain in different drain intervals for *D*=50 cm

3.2 *The effect of distance from the upstream*

The flow rate of each drain along the model in different upstream discharge and installation depth was presented in Fig. 5. The drain flow rate always reduced with different slope in length of model.

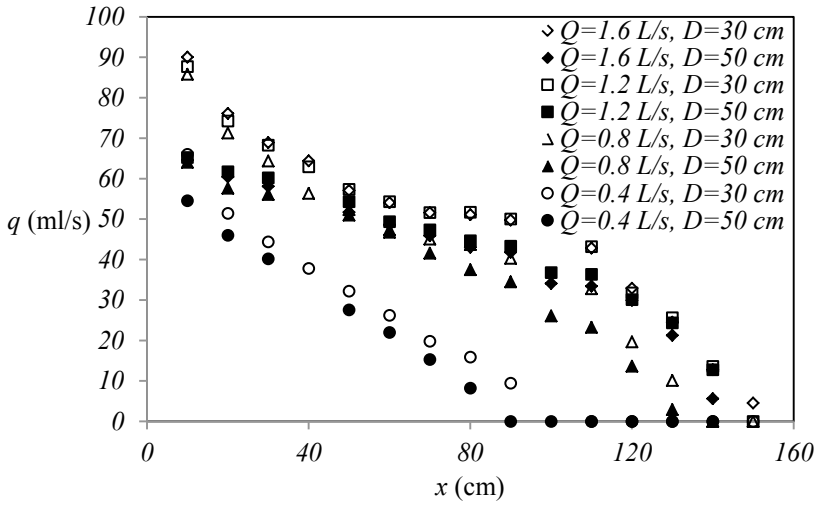

Figure 5. The drain discharge changes along the model in different flow rate and installation depth (w=10cm)

The variation of the drain flow rate in different intervals for Q=1.2 L/s and D= 30 was shown in Fig. 6. As the interval increased the q variation along the model has decreased. It means that the flow rate of each drain was less influenced by the neighbor drains when the intervals were increased. Furthermore, there is a decreased parabolic trend of drainages discharge along the porous media length.

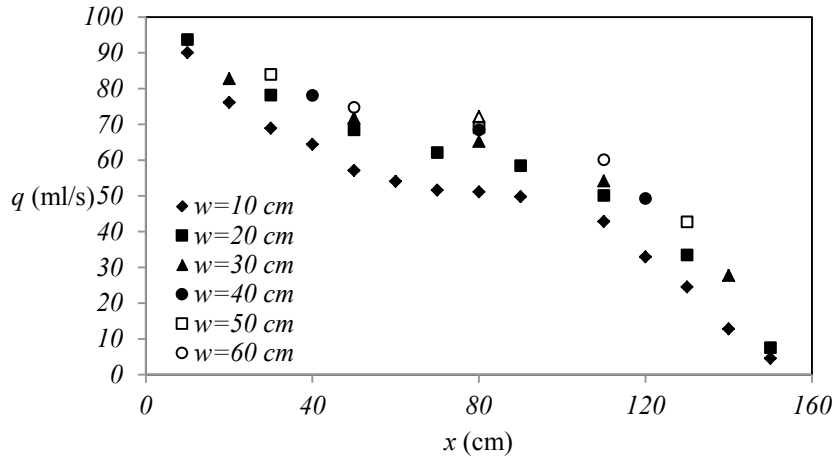

Figure 6. The drain discharge variations along the model length for Q= 1.2 L/s and D= 30 cm in different drain intervals

3.3 *The relationships between effective parameters*

Based on dimension analysis and Buckingham theory two effective dimensionless variables were selected and related to each other as follows:

$$\frac{qk^3\rho D}{Q\mu g x} = \emptyset\left(\frac{x}{L}\right) \qquad (4)$$

In this equation a dimensionless parameter involving the drain discharge, the hydraulic conductivity and upstream discharge is related to distance ratio. To obtain $\emptyset$ function in Eq. 4, a curve was fitted to the dimensionless variables (Fig. 7) based on least square analysis.

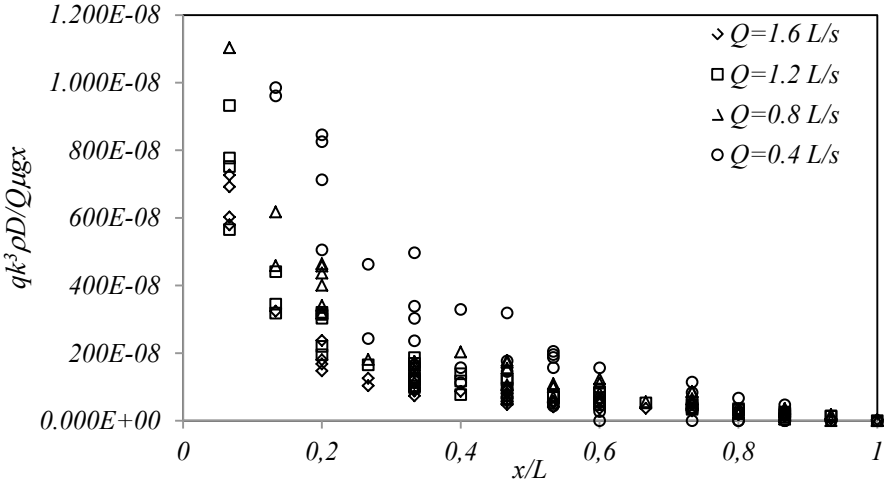

Figure 7. The variations of dimensionless drain discharge in different distance ratio

The 70 percent of the experimental data were randomly selected for curve fitting and the last 30 % adopted for evaluation of the obtained equations. The statistical measures of the fitted model were tabulated in Table 1. Figure 8 shows the curves fitted to the experimental data in different upstream discharge.

Table 1. Model Obtained from the fitted over 70% of the Experimental data

Model	Q	*Std. Error*	*Residual Sum*	*Residual Avg.*	*RSS*	R^2	Ra^2	Variable	Value
$Y=a+b/x+c/x^2$	1.6 L/s	2.39×10^{-7}	-9.37×10^{-21}	-1.91×10^{-22}	2.62×10^{-12}	0.982	0.981	***a***	-2.61×10^{-7}
								b	4.15×10^{-7}
								c	2.42×10^{-9}
	1.2 L/s	4.77×10^{-7}	-3.59×10^{-19}	-7.19×10^{-21}	1.07×10^{-11}	0.948	0.946	***a***	-4.15×10^{-7}
								b	6.24×10^{-7}
								c	-6.21×10^{-9}
	0.8 L/s	5.50×10^{-7}	0	0	1.30×10^{-11}	0.962	0.960	***a***	-6.90×10^{-7}
								b	8.73×10^{-7}
								c	4.26×10^{-10}
	0.4 L/s	9.61×10^{-7}	-1.36×10^{-20}	-2.82×10^{-22}	4.16×10^{-11}	0.960	0.958	***a***	-1.88×10^{-6}
								b	1.71×10^{-6}
								c	-1.12×10^{-8}

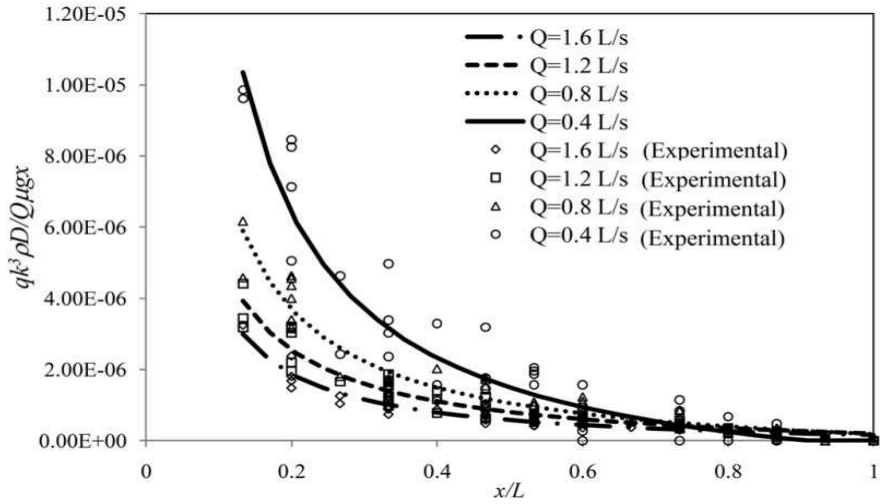

Figure 8. The curve fitted to 70% of the observed value in different upstream discharges

To evaluate the goodness of the fitted curve, the equation was used to estimate the drain discharge of the 30% of the experimental data (Fig. 9). It was revealed that the maximum discrepancy was less than 37%. This error was for the minimum upstream discharge (Q=0.4 L/s).

Finally, the achieved model can be expressed as Eq. 5. The equation constants (a, b and c) are shown in Table 1 for the different water heads.

$$(\mathrm{qk}^3\rho D)/(Q\mu gx) = a + b/(x/L) + c/(x/L)^2 \quad (5)$$

The estimated discharges using Eq. 5 have been compared with the 30% of the observed value and good agreement was observed (Table 2).

Table 2. Statistical measure for the comparison of the estimated drain discharges with 30% of the observed values

Upstream Discharge (Q)	d (Wilmot,1981)	RMSE	MAE	lative Error	an Relative Error
1.6 L/s	0.849	0.0136	0.0011	18.94%	
1.2 L/s	0.865	0.0127	0.0017	29.35%	
0.8 L/s	0.922	0.0123	0.0021	20.88%	27.85%
0.4 L/s	0.916	0.0148	0.0032	42.23%	

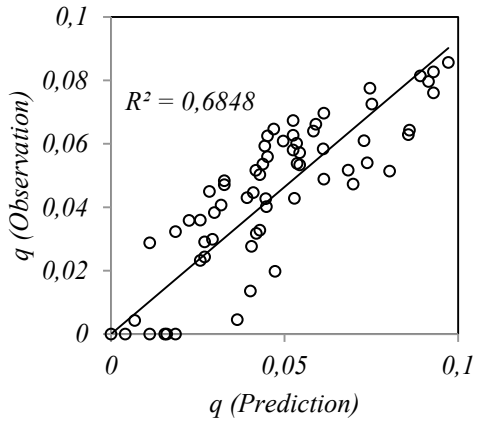

Figure 9. Comparison of the estimated drain discharges with the 30% of observed values

4 CONCLUSION

In this study a rather new method for surface and subsurface water diversion in the seasonal rivers of the arid and semi-arid regions was introduced. In this type of intake a subsurface drainage system is installed in a very porous media buried on the river bed. The effective parameters on water diversion efficiency of this type of intake were experimentally evaluated. It was shown that the water diversion mostly influenced by the upstream flow rate. The water head also varied along the porous media even when a constant upstream discharge existed. The very small drain interval caused the discharge of each drain to be reduced. It was also revealed that the total drained discharge in the very transmitting media was mostly controlled with the number of drain and drain interval did have a marginal effect. The regression equations were present to relate the effective parameters of the water diversion. This equation can be utilized to design the subsurface intake with a porous media.

NOTATION

ρ	fluid density
g	gravity acceleration
S_b	bed slope
ϕ	roughness geometry function
τ	total fluid stress
z	vertical coordinate
μ	water viscosity
q	a drain flow rate
Q	upstream discharge
n	media porosity
d_{50}	the median diameter of the fill material
k	hydraulic conductivity

L length of porous media
w lateral distance between drains
D installation depth
x distance from the media upstream
d_p drain diameter
S_0 the river bed slope
S_l drain lateral slope
A_d perforated drain opening area
n_f envelop resistance factor
form installation form parameter

REFERENCES

Bouvard, M. (1953). "Discharge passing through a bottom grid." Houille Blanche. Vol.3, pp. 290–291.

Bouvard, M. (1992). "Mobile Barrages and Intakes on Sediment Transporting Rivers." IAHR monograph series, Rotterdam, Balkema.

Brunella, S., Hager, W. H., and Minor, H. E. (2003). "Hydraulics of bottom rack intake" Journal of Hydraulic Engineering. Vol.129, No.1, pp. 2–10.

Castillo, L. and Guama, P. (2010). "Analisis Del Dimensionamiento de la langitud de reja en una captacion de fondo" Hydrualic Congress of Latin American(IAHR., Punta Del Est., Uruga, November 2010 (Espanish)

Drobir, H., Kienberger, V. and Krouzecky, N. (1999). "The wetted rack length of the Tyrolean weir". IAHR-28th Congress, Graz, Austria.

Kooroshvahid, F., Esmaili, K. and Naghavi, B. (2011). "Experimental study on hydraulic characteristics of bottom intake with granular porous media" Special Topics and Reviews in Porous Media. Vol.2, No.4, pp.301-311.

Li, B., and Garga, V.K. (1998). "Theoretical solution for seepage flow in overtopped rockfill" Journal of Hydraulic Engineering, ASCE. Vol.124, No.2, pp.213-217.

Li, B., Garga, V.K., and Davies, M.H. (1998). "Relationship for non Darcy flow in rockfill" Journal of Hydraulic Engineering. Vol.120, No.6, pp.451-467.

Mostkow, M. (1957). "Theoretical study of bottom type water intake" Houille Blanche. Vol.4, pp.570–580.

Noseda, G. (1955). "Operation and design of bottom intake racks" Proc, VI General Meeting IAHR. Vol.3, No.17, pp.1-11.

Ramamurthy, A.S., Qu, J., and Vo, D. (2007). "Simulation of flow past an open- channel floor slot" Journal of Hydraulic Engineering. Vol.133, No.1, pp.106-110.

Righetti, M., lanzoni, S. (2008). "Experimental study of the flow field over bottom intake racks" Journal of Hydraulic Engineering. Vol.134, pp.1-15.

Subramanya, K. and Shukla, S.K. (1988). "Discharge diversion characteristics of trench weirs" Inst. Engineering. Vol.69, No.11, pp.163–168.

Willmott, C. J. (1981). "On the validation of models". Phys. Geog., Vol.2, pp.184-194.

7 Small Hydropower

IWLHS, 20-22/02/2013, Aachen - Bung & Pagliara (eds) - © 2013 Bundesanstalt für Wasserbau ISBN 978-3-939230-04-5

Contributions and Solutions Using Small Hydro Power in Advanced Energy Recovery Strategies on WWTPs

V. Berger & A. Niemann
Institute of Hydraulic Engineering and Water Resources Management, University of Duisburg-Essen, Universitätsstrasse 15, 45 141 Essen, Germany

T. Frehmann
Emschergenossenschaft & Lippeverband, Kronprinzenstrasse 24, 45 134 Essen, Germany

ABSTRACT: Operation strategies of Wastewater Treatment plants (WWTPs) are changing at the moment. Because of the huge amount of energy needed for treatment more and more efforts are carried out to gain an overall energy recovery from the urban water cycle. Therefore additional renewable energy facilities are added in order to reduce the overall demand of energy supply taken from the power grid. As a consequence an additional goal in plant operation has been defined, complementing the main focus on water purification needs and matching all effluent standards in water quality. Today most often WWTPs are the facilities with the highest energy needed and which are owned by public (e.g. cities). Consequently also small hydropower plants are part of this strategy, thus using an again new identified site for small hydropower implementations. This paper gives an overview of suitable techniques and boundary conditions which have to be considered for an operation of small hydropower concepts on WWTP. Results show that bigger WWTPs at larger rivers with higher flood level offer the highest potential for an economic implementation. Finally a case study at the WWTP Bottrop is presented. Results of the case study show that an Archimedean screw is suited best at the case study site.

Keywords: small hydro power, wastewater treatment plants, sewer systems, advanced energy recovery

1 INTRODUCTION

The current requirements for more efficient pollutant removal on waste water treatment plants (WWTPs) tend towards the installation of additional treatment steps to eliminate micropollutants like pharmaceutical trace elements. These units are commonly high energy-consuming (cf. ozonization). Nevertheless, WWTP are even without these additional treatment steps the biggest energy-consumer within a municipality or, like not unusual in Germany, within a water board (cf. Figure 1).

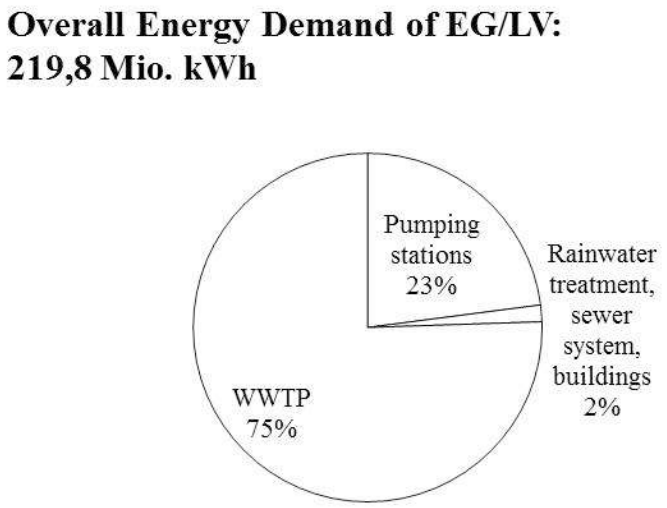

Figure 1. Distribution of energy consumption of Emschergenossenschaft & Lippeverband, 2011

In particular the nitrification processes are highly energy consuming due to aeration needs. Therefore many attempts have been made to reduce the energy demand of biological treatment (Dichtl, 2004, Siegrist, 2008), mainly focusing on aeration. In addition, due to the finiteness of fossil fuels as well as energy costs increase the aim of energy autarky gains even more importance.

As a result there is a change in energy management at WWTPs since approximately the last ten years (Schroeder, 2002). Whereas in former times biogas has been combusted as there was no need for cogeneration, nowadays WWTPs aim to recover as much energy as possible (Singh et al., 2012). Improvement of sewage sludge treatment (Schmelz et al., 2007), benchmarking of energy usage (Stemplewski et al., 2001, Möller et. al., 2012) as well as shifting of highly energy consuming processes to off-peak hours (Lawrence, 2004) are implemented steps towards an advanced energy recovery at WWTPs. Figure 2 shows the new overall strategy of plant operators.

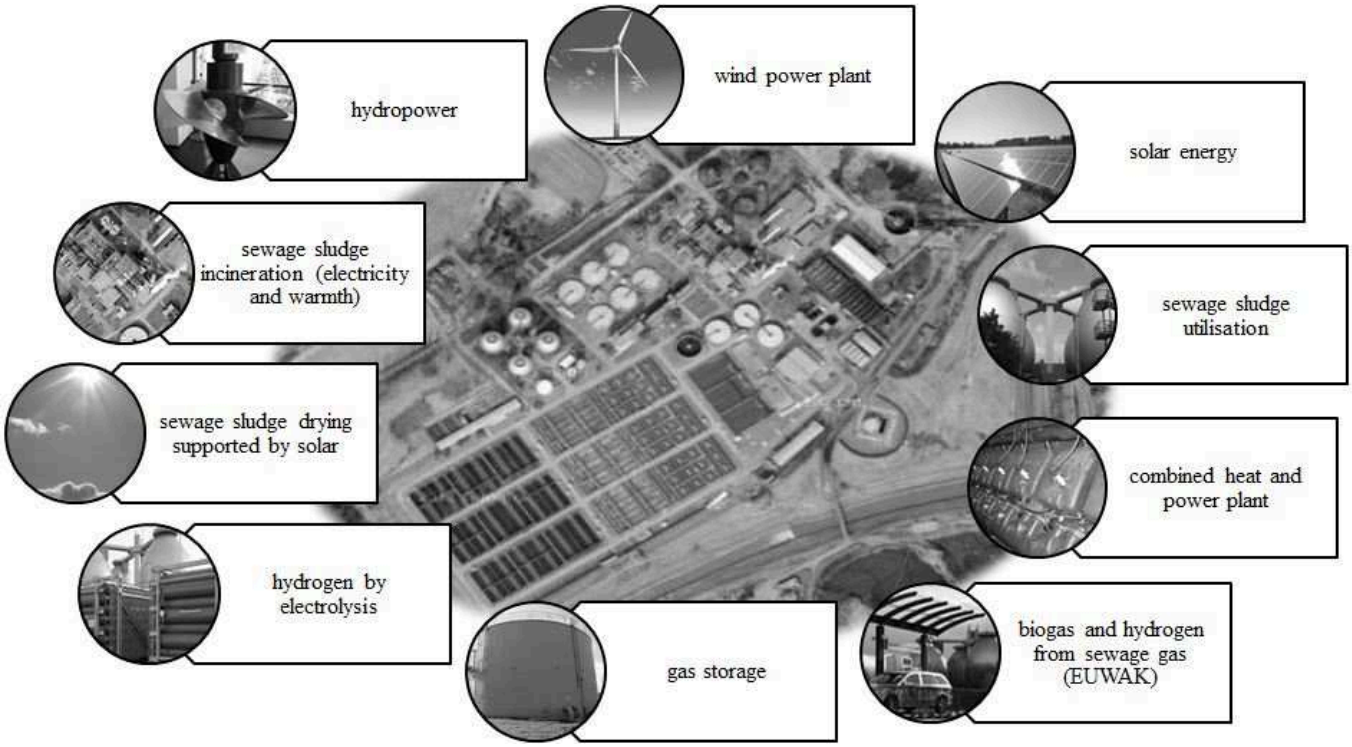

Figure 2. Elements of a hybrid power plant using renewable energies and advanced energy recovery at WWTPs (according to Stemplewski, 2012)

An effective utilization of sewage sludge starts with the digestion of excess sludge. This process aims to stabilize sludge conditions for further treatment steps – as a by-product, biogas is produced. A well adjusted process decomposes the biomass effectively, diminishes the sludge volume and produces a high amount of biogas (Gujer, 2007). The biogas is collected in storage tanks to compensate fluctuations in volume and quality, respectively. Subsequently, the biogas is combusted using cogeneration. The produced electricity and heat can be used within the plant, for example for aeration and heating digesters, respectively. The digested sludge is commonly transferred to chamber filter presses to reduce the volume of sludge by draining it mechanically. In former times the sludge was dried at the outside with only little efficiency, but current developments offer new opportunities to use solar light for drying processes in a new way. Nevertheless, the dried sludge is incinerated afterwards – once again producing a countable amount of energy and heat. The effectiveness may significantly be increased by using additional biomass (co-substrates, Schmelz et. al., 2007). Instead of using the produced biogas for cogeneration, it also may be purified and used as domestic gas or even fuel. The idea of using biogas as fuel is again not new, there are many examples for WWTP – gas stations in the 1950s and 60s but they were non-competitive to fossil fuels in that time (Schröder, 2007).

Energy storage is consequently becoming a more sincere problem as the production and consumption of energy is not necessarily parallel. This leads either to the elimination of excess biogas or the demand for peak load energy – which is both cost-intensive. Therefore the storage of biogas and the production of hydrogen via electrolysis is yet another way to store the energy. The hydrogen can be stored and used – on demand – in fuel cells to produce high-demand electricity.

After the improvement of sludge treatment and replacement of highly energy consuming utilities the next step is the integration of renewable energies, as it was already mentioned by Meliß et al. 1998. Solar cells are nowadays well established and can easily be applied at WWTPs as these provide large surface-areas of buildings and fallow areas, respectively (Stampolidis et al., 2006). Photovoltaic technology is fully developed. For example an area of 40,000 m² with a sun intensity of 1.000 kWh/(m²*year) may produce 4,500 MWh a year which means a saving of approximately 1,125,000 Euros (25 ct/kWh) if the energy is used on site. Even the applicability of wind power has been mentioned (Meliß et al. 2008) and is also analyzed (Stemplewski, 2012). Consequently, the applicability of hydro power for energy recovery has to also be investigated also. Small hydropower solutions are thus also becoming part of this strategy. They may also be applied at WWTPs as there is a stable and well defined discharge and, in dependency of the location, a certain available hydraulic head. As hydropower is originally designed for rivers there are some differences in the situation which are as follows:

- Outfall of the WWTP must be available all time
- Most often screens and trash racks are not needed
- Integration into energy-grid of the WWTP is very simple
- Staff for operation and maintenance is located nearby at the WWTP

2 APPLICABILITY OF HYDROPOWER ON WWTPS

Historically hydropower has been developed for small heads. Since over two thousand years hydropower in its simplest way, i.e. water wheels, has been used to irrigate fields or support industry by producing energy for example in mills or forging hammers. During the last two hundred years the technology has been improved and transferred into turbines which generate energy out of heads up to even more than 1,000 m. During industrialization the production of cheap energy using fossil fuels lead to the demolition of historical/small hydro power units (Denny, 2004). Nowadays, global warming, the scarcity of fossil fuels, the changes in energy policy and the increasing energy costs lead to changes in energy politics; this leads to a renaissance of very low head hydropower technologies (Müller et al., 2002).

As many enhanced hydropower technologies like highly efficient turbines cause a certain amount of constructional effort – the constructional costs often prevent the application as the expectable benefits do not legitimate these costs. Thereby modular based concepts as well as advanced technologies have been developed especially for small heads (Bozhinova et al., 2012). As there are numerous concepts available worldwide, this paper is categorizing the available technologies due to the mode of operation and their applicability at WWTPs. It is not intended to present all small hydropower concepts and techniques.

2.1 *Available Technologies*

The discharges at WWTPs are closely connected to the design of the urban drainage system. The diurnal flow can be recognized in the WWTP's discharge. This means, as the hydro power unit should use as much discharge as possible, every small hydropower concept has to be designed for a certain range of discharges to cover the night minima as well as the day's maximum during dry weather flows. Consequently only hydropower concepts providing a broad and high effectiveness are suitable. During the last years research and development led to an increasing amount of hydropower units for small heads. Some of them are using/improving historical concepts and some use/develop new aspects. Although there are theoretically lots of techniques available, only few offer long term experiences. Nevertheless, it is useful to categorize these technologies due to their mode of operation.

2.1.1 *Water wheels*

Water wheels are the most classical hydro power technique, which can be divided by the point of water loading into overshot, breast shot and undershot, respectively. Overshot water wheels (cf. Fig. 3) mainly use potential energy whereas undershot water wheels use the kinetic energy of the water. The blade configuration mainly depends on the water loading point. Overshot water wheels have a low capacity per blade, which leads to a larger width. Undershot water wheels have a higher capacity and are therefore capable of larger discharges. Nevertheless overshot water wheels have the highest efficiency (Denny, 2004). Fig. 4 shows the measured performance characteristics of three overshot water wheels of different characteristics depending on the load discharge given in the ratio of given discharge to optimal discharge

(Q/Q_{max}). It is obvious that water wheels provide a high efficiency (around 80 %) for discharges between 20 and 120 % of the optimal discharge. Thereby they are very suitable for varying discharges.

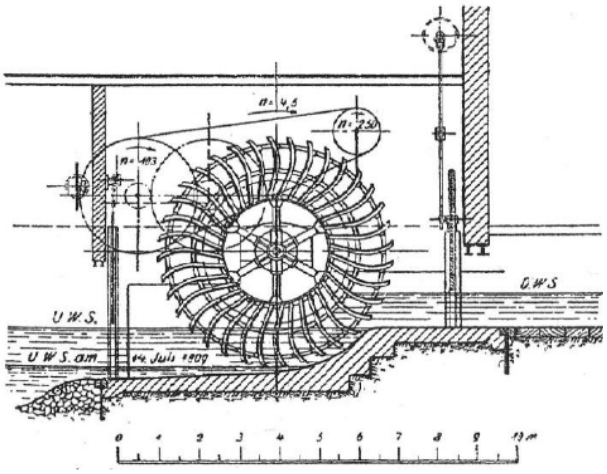

Figure 3. Example for a classical undershot (Zuppinger) water wheel (Müller, 1939)

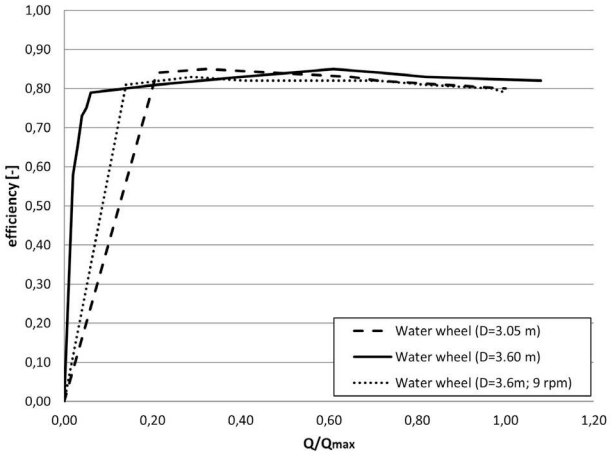

Figure 4. Measured performance characteristics of three overshot water wheels (according to Müller & Kauppert, 2003)

Water wheels are made of different materials like certain types of woods or metals depending on their location. Several companies produce water wheels, sometimes since generations. New developments often use an implementation of module-based concepts to decrease costs. As a result less cost intensive modular concepts as well as traditionally produced customized waterwheels are available; for every application site both alternatives have to be considered.

The advantages of water wheels are their low constructional costs and their wide range of high efficiency. This means that both small and high discharges can be used effectively and thus energy will be produced continuously.

2.1.2 *Archimedean Screw*

Since ancient times the Archimedean screw is used to lift water to higher levels. Further, they are state of the art at e.g. WWTPs to lift the inflow, pretreated sewage or sludge inside the WWTP. As result the staff members on WWTP are used to this concept resulting in a good acceptance for this technology, because of its high reliability even dealing with a complex media like raw sewage. Since several years they are also used vice versa to generate energy in very low-head situations (Hellmann, 2003). The falling water moves the helical blades wrapped around the axis which drives via a gear the generator; therefore it lies in a semi-circular trough. Hydro Power Screws are nowadays also state of the art and produced in different standardized versions (Cf. Fig. 5). Due to its construction the Archimedean screw has also a wide range of good efficiency (cf. Fig. 5 - right). Hereby, the usable discharge of max. 10 m³/s determines the diameter of the screw (up to 4 m) whereas the head determines the length of the screw (Lashofer, et al., 2011) in dependency of the angle. Thus, decreasing the angle increases the efficiency (Müller & Senior, 2009). Disadvantageous can be the required huge dimensions due to the flat angle (< 30 °) as well as the high load due to a massive steel construction.

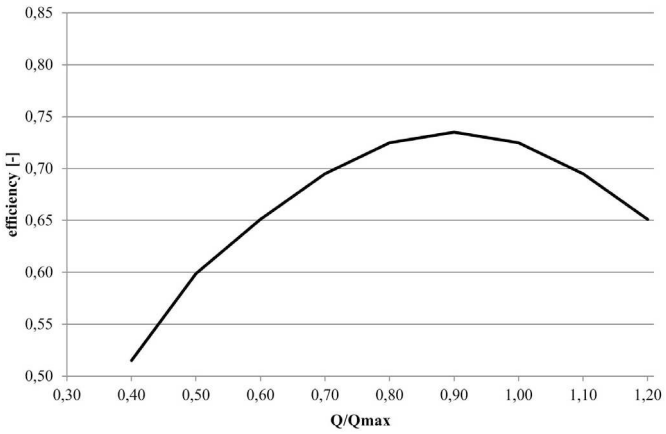

Figure 5. Archimedean Screw: left: example (Andritz Atro, 2012); right: range of efficiency of an Archimedean Screw with frequency converter (Lashofer et al., 2011)

2.1.3 *Turbines and turbine-based concepts*

Turbines are the classic hydro power units. Nevertheless, they are most suitable for heads bigger than two meters. Of the three classical turbines, Pelton, Francis and Kaplan, only the latter one is suitable for small heads, i.e. low-pressure applications. Moreover, further developments of the Kaplan turbine like the horizontal mounted Straflo-turbine as well as the tube turbine focus on very low heads. Thus, they still need a penstock for the inflow and a draft tube as outlet to decelerate the water. This causes a certain amount of constructional work which most of the times makes the implementation of a classical turbine at low heads not economic (Giesecke & Mosonyi, 2009).

Different hydro power units based on the Kaplan turbine concept have therefore been developed (Bozhinova et. al., 2012). These concepts are generally thought for the application in rivers, therefore they focus on little constructional effort and fish friendliness. Nevertheless, all concepts keep the penstock as well as the draft tube as necessary parts. Still they are more suitable for sites of at least 50 kW. A common disadvantage is that hydro power technologies based on propeller concepts are still more sensible to discharge variations and atmospheric influences. Due to the diurnal variations in discharge a turbine, implemented at the outflow of the WWTP is on a higher risk of cavitation. On WWTPs turbines should already be planned at the building/construction phase of the plant (Bolle & Billmaier, 2012); if a continuous discharge can be guaranteed they are low in maintenance and contribute constant energy.

2.1.4 *Chain conveyer concepts*

The field of chain conveyer is the less established of the mentioned technologies although it is quite promising for application at WWTP. The idea of chain conveyer is again not new; moreover chain pumps, i.e. rectangular-trough pallet-chain pumps were used in acient China for drainage and irrigation, respectively (Needham, 2004). Consequently, this technique can also be used to generate energy from water. To the authors there is only one concept known; the "Katamax"-concept. It consists of troughs mounted on a vertical chain. If the troughs are filled with water they move the chain and thereby drive the generator. One Prototype has been implemented (Kastner, 2006); there is no official report of the prototype available, but it is known that it has not been implemented successfully due to several constructional/material difficulties.

Nevertheless, the idea of the vertical chain conveyer seems to be quite useful. Big advantages are the insensitivity towards contraries and the applicability if a certain head is available but no broadness to implement a large energy conveyer such as waterwheels or Archimedean screws.

2.2 *Procedure to determine application sites at domestic WWTPs*

At WWTPs there are two different treatment paths – the one is the treatment of sewage water, the other one is the treatment of/energy recovery from the sewage sludge. Both paths have in a first step to be taken into account as both provide possible application sites for small hydropower applications.

2.2.1 *Sludge treatment*

Beginning with sludge treatment, it simplified consists of three steps. First, fermentation whereby biogas is produced, second, drying of the digested sludge, which produces filtrate and finally, the energy recovery using incineration (cf. Fig. 6).

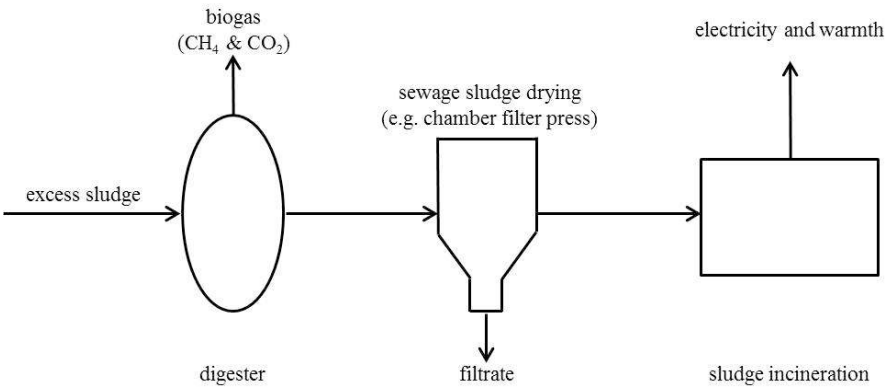

Figure 6. Simplified schematic longitudinal section of sludge treatment line

Concerning hydropower, the digesters offer a continuous discharge for hypothetical energy recovery. Thus, the discharge is rather small, i.e. although there are higher heads (~30 m), the discharge is so little (p.e. 20 L/s), that the expected energy potential ranges about 4 kW. Thus, even after the fermentation process, the sludge is still tough-flowing and contains fibres which may still cause a high risk of blocking. By blocking the outflow of the fermentation towers, the whole sludge treatment might be affected. As a result digesters are not suitable for the application of hydropower applications.

Another treatment step that can be focused on is the effluent of the filtration, p.e. chamber filter presses. The effluent is suitable for energy recovery using hydropower as it does not contain any contraries. Furthermore the filters are usually mounted on a higher level to ease the treatment of filter cake and effluent, respectively. The study sight, a WWTP of 1.3 Mio. PE, provides filter effluent of 46 L/s. In combination with the head of 3 m there is an expectable potential of 1 kW. As the filters are working one after the other in order to ease maintenance the real discharge is even less. Further, the hydro power unit should be positioned within the main pipe. At the moment there is no technique available to use small discharges within pipes. If development and research create a suitable technique there is small potential that can be used to produce/ re-win energy from filtration processes. The effluent of chamber filter presses is hardly economical realizable.

2.2.2 *Wastewater treatment*

The main focus has to be put onto the waste water treatment itself. Generally, WWTPs are constructed with a higher positioned even pumped inflow and a gravity flow towards the river. Due to constructional reasons there might be some heads left within the WWTP, too. Good points to have a look on are the discharge of the mechanical treatment, higher mounted basins for biological treatment and the overall outflow of the WWTP.

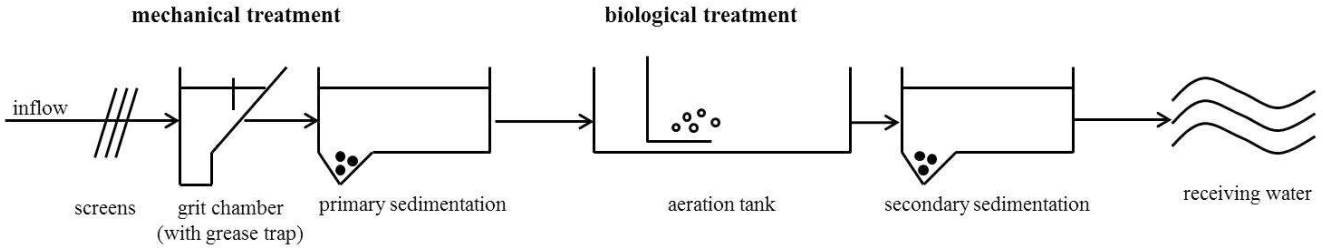

Figure 7. Simplified longitudinal cut of wastewater treatment

The implementation of a hydropower unit within the WWTP is difficult due to the properties of the wastewater, i.e. chemical composition, pH-value and contraries, respectively. This leads to advanced material requirements, especially in corrosion resistance.

The discharge of the primary sedimentation has the advantage that the water is already mechanically treated and does not yet contain activated sludge. If there is a head available a hydro power unit can be implemented. Disadvantageous might be the design of the basins, as the outflow of the mechanical treatment usually is constructed as a wide overflow whereas hydro power requires the discharge concentrated in a compact way. New developments like several small waterwheels driving the same axis may be a solution.

Generally, the biological treatment offers only poor possibilities for hydro power facilities. If activated sludge is applied, the water usually flows by gravity flow through the biological treatment tank directly into the secondary sedimentation. Usually there is no hydraulic head available. Further, the activated sludge makes the water a poor media due to high density which makes the application in sludge containing treatment difficult.

The most suitable site is the effluent discharge of the WWTP. To avoid pumping the effluent is situated on a certain level above the river level to guarantee a gravity flow even during smaller floods. This often leads to a certain useable head. Thus, the complete treated discharge of the WWTP can be used. Implementing small hydropower at a WWTP is advantageous as there are no biological restrictions to be concerned and the connection to the power grid is already available. Instead of biological restrictions the design of the discharge and structural matters are the limiting factors. Generally, the discharge controls the diameter of the hydropower unit. Depending on the operation mode the head influences the length of the hydro power unit. Therefore the spatial conditions determine the applicable technique.

2.3 *Small hydropower concepts at WWTP – Overall Economics*

Mainly Hydropower units at WWTPs are established by operators to enhance self-energy production. Thus the savings (i.e. expected energy delivery costs) have to be calculated rather than the gratification due to individual energy Laws (e.g. EEG in Germany). There are numerous scenarios concerning the development of the energy costs in the near future. In any case, the price for energy will not decrease. Therefore it is suitable to implement a hydropower unit as soon as possible to decrease the plants overall energy costs. At the moment the energy delivery costs range around 20 ct/kWh in the German Federal State of North Rhine-Westphalia.

The capital costs for the implementation of a small hydropower plant in general depend on the constructional cost for the unit. The costs for operation depend on maintenance needs. The constructional costs of new developed small hydropower units are usually smaller than those of classic turbine applications. This leads to short amortization times of less than ten years, whereas the units are expected to be working for longer time.

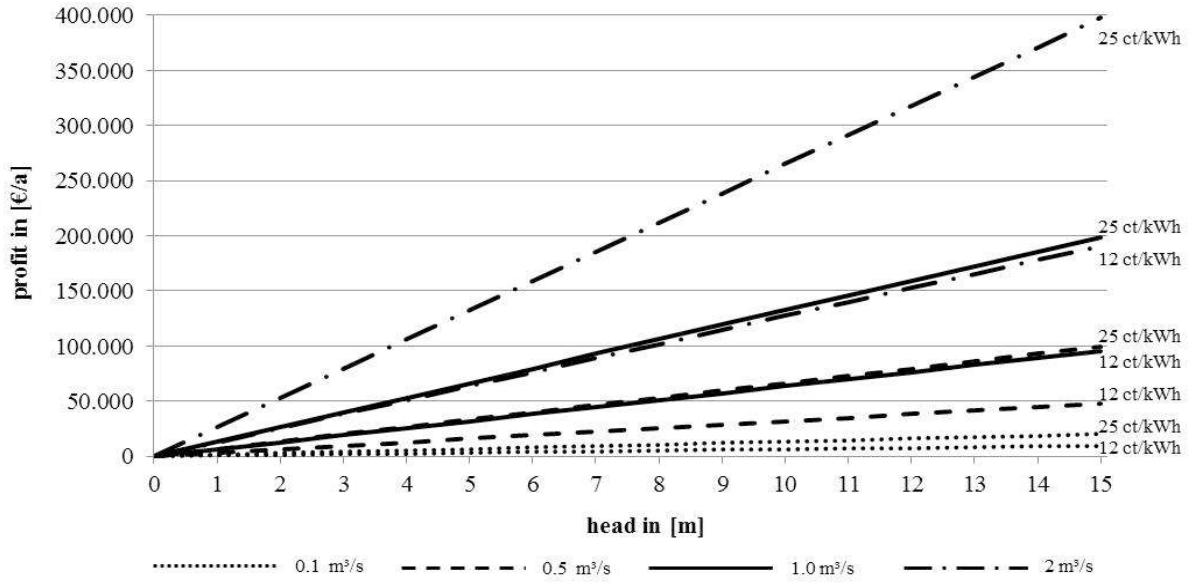

Figure 8. Achievable profits depending on energy costs showing the profit of energy procurement costs

Figure 8 shows the correlations between discharge, head and earned profit for a range of conventional energy costs. Whereas discharge and head influence the power and therefore the profits equally, the energy costs have the biggest effect onto the profits. The profits depend on the achievable work per year and therefore on local conditions. The profits may actively be influenced by the chosen gratification. As the energy procurement costs are twice as high as the feed-in tariff of e.g. the German EEG, the margin between both rises proportionally to achieved power/work. Even this small detail of the dependencies shows the high effect of saving energy costs by enhancing self-production. As it is expected that the energy costs will increase in future the margin and the savings, respectively, are also expected to increase.

3 WWTP BOTTROP – A CASE STUDY

The WWTP in Bottrop treats 1.3 Mio. PE and belongs to the German water board Emschergenossenschaft/Lippeverband. It was systematically investigated to distinguish possible hydropower sites. Concerning a first estimation, four possible sites have been investigated in further detail:

- Digesters
- Outflow of chamber filter presses
- Outflow of primary sedimentation
- General outflow

Hereby it was investigated that the sludge treatment, as already mentioned in chapter 2.2.1, is not suitable for hydro power application due to the characteristics of the sludge. Despite the big heads of the digesters

of about 30 m the fluid characteristics of the sludge would block any mechanical energy conveyer and therefore disrupt sludge treatment. The discharges of the chamber filter presses are so little that no economic realization could be found. The mechanical treatment is hydraulically decoupled from the biological treatment; therefore a head of approx. 1 m was detected. The mechanically pretreated sewage is suitable for hydropower units but the design of the basins prevents the installation of a hydropower unit.

Only the general effluent can be used for hydropower application. Depending on the water level in the river there is a net head of 1.40 up to 1.80 m. The average discharge is 4 m³/s; within a margin of 40 %. After determining the hydrological suitable hydropower technologies the constructional restrictions have to be taken into account. Finally an Archimedean screw was considered the best solution. It fits the existing hydraulic and constructional conditions and is applicable at fluctuating discharges.

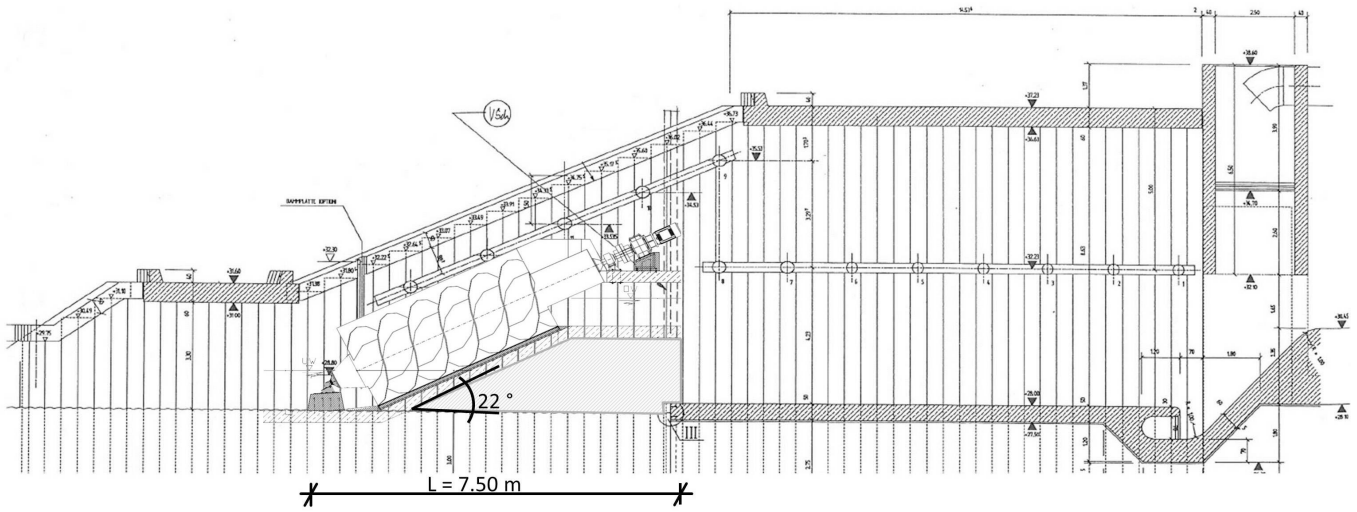

Figure 9. Most probable implementation of the Archimedean Screw in the outfall of the WWTP Bottrop; L is the length of the hydropower unit, the diameter is 3 m, the ankle 22 °

Figure 9 shows a possible implementation of an Archimedean screw of 3 m diameter for a given head of 1.4 to 1.8 m and a medium discharge of 4 m³/s in the outfall of the WWTP.

While constructing an Archimedean screw within the outlet of a WWTP several restrictions have to be taken into account. To secure the undisturbed treatment of the WWTP the outfall has to be dissipated all the time, even at heavy rain events and if the hydropower unit is damaged, respectively. To guarantee the outfall in this case it is suggested to mount the Archimedean screw in the middle of the channel in combination with a weir of the given head. In operating conditions the weir will damp the water and lead it to the screw; if the screw is not able to use all the water available or is damaged, two bulkheads in the weir on the left and right can be opened to guarantee the rated discharge.

The costs are dominated by construction costs. The hydropower unit accounts hereby only for 1/3 of the total construction costs. The constructional effort, i.e. the alteration of the effluent structure building securing both the flood discharge as well as the stability generates the lion's share.

The expected average power is 40 kW, which leads, depending on hydrologic conditions to an annual work of 340,000 kWh. Considering energy costs of 25 ct/kWh, the profit totals 85,000 €/a. As the WWTP in Bottrop has an annual energy demand of approx. 40,000 MWh, whereof 29,000 MWh are already produced at the WWTP itself (which equals a self-energy production of 72.5 %) the additional self-produced energy by hydropower would enhance the self-energy rate to 73.4 %.

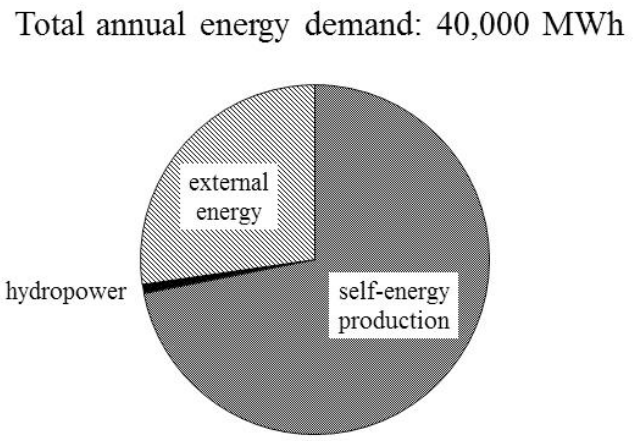

Figure 10. Total annual energy demand of the WWTP in Bottrop and supply distribution; basis 2010

4 CONCLUSION AND OUTLOOK

Since several years the increasing energy costs are forcing operators of WWTP to intensively enhance self-energy production. Many steps like improved sludge treatment have already been realized; consequently, the application of hydropower solutions has to be taken into account. Particularly small hydro power units provide suitable requirements for WWTPs.

Conducting this study, both possible hydropower sites at WWTPs as well as suitable technologies have been considered. Suitable sites are the intersection between mechanical and biological treatment as well as the effluent structure of the WWTP. As gravity flow is mostly used within every plant, it is expected that the most promising site is the effluent of the plant. For guaranteeing the effluent even at flood conditions, a certain head to the receiving water is usually given. Constructional restrictions determine the applicable technology. Recapitulating different studies it was realized that only few so-called small hydropower techniques are suitable for WWTP. Economic viability is not necessarily achieved yet. Considering increasing energy costs and the lifetime of hydropower plants on a long-term scale the implementation of hydropower is a foresighted investment. Nevertheless, the research and development of small hydropower has to be observed within the next years as there are many promising technologies being established.

If suitable discharges and heads are available hydro power is a simple and effective way to enhance self-energy production and thereby save energy costs as well as diminish CO_2-emissions and thereby improve the operator's carbon footprint.

REFERENCES

Andritz Atro (2012): Hydrodynamic screws, Information brochure, www.andritz.com

Bolle, F.-W.; Billmaier, K. (2012): Einsatz eines Wasserrades zur Stromerzeugung in der Kanalisation, [Application of a water wheel to generate energy in the sewer system] Wasser und Abfall, No. 5, pp. 20-25. [in German]

Bozhinova, S., Hecht, V., Kisliakov, D; Schneider, S., Müller, G. (2012): Hydropower Converters with Head Differences below 2.5 m, Proceedings of the ICE – Energy, Vol.: 165.

Denny, M. (2004): The efficiency of overshot and undershot waterwheels, European Journal of Physics, Vol. 25(2): pp. 193-202.

Dichtl, N. (2004): Die Eigenenergieversorgung von Kläranlagen – Rückblick und Ausblick, [Self-energy supply of Wastewater Treatment Plants – retrospect and forecast] KA Abwasser, Abfall, Vol. 51, No. 6, pp. 614-618. [in German]

Giesecke, J., Mosonyi, E. (2009): Wasserkraftanlagen, [Hydropower plants] 5. revised edition, Springer: Heidelberg. [in German]

Gujer, W. (2007): Siedlungswasserwirtschaft [Urban Water Management], 3. Revised edition, Springer: Berlin [in German]

Hellmann, H.D. (2003). Gutachten zur Wirkungsgradbestimmung einer Wasserkraftschnecke Fabrikat Ritz-Atro [Report on determination of hydraulic screw efficiency manufactured by Ritz-Atro Ltd.] Fachbereich Maschinenbau und Verfahrenstechnik, Technical University, Kaiserslautern, Germany.

Kastner, H.-J. (2006): KataMax – Wasserkraftanlage. Eine Chance zu mehr Ertrag aus der Wasserkraft. [KataMax - Hydeopower plant. A chance for more benefit from Hydropower] In: Workshop: Lebendige Flüsse und kleine Wasserkraft, [Workshop: Living rivers and small hydro power] Büro am Fluss: Plochingen, April 2006. [in German]

Lashofer, A., Kaltenberger, F., Pelikan, B. (2011): Does the Archimedean Screw Turbine Stand the Test?, Wasserwirtschaft, Vol. 101, Issue: 7-8, pp. 76-81.
Meliß, M., A. Neskakis, J. Plettner-Marliani, C. Lange, A. Hövelmann and J. Schumacher (1998): Waste water recycling supplied by renewable energies - basic conditions and possible treatment technologies, Renewable Energy Vol. 14(1–4), pp. 325-331.
Möller, K., Bertzbach, F., Nothhaft, S., Waidelich, P., Schulz, A. (2012): Benchmarking in der Abwasserbeseitigung – eine Bestandsaufnahme. Teil1: Ziele und Ergebnisse des Benchmarkings [Benchmarking in sewage disposal – Baseline Study part 1: aims ands results of Benchmarking], Korrespondenz Abwasser, Abfall, Vol. 2012(59), No. 8:.pp. 730-737.
Müller, G., Kauppert, K. (2002): Old watermills – Britain's new source of energy? Proceedings of the ICE – Civil Engineering, Volume 150, Issue 4, pp. 178-186.
Müller, G., Kauppert, K. (2003): Die Wasserräder als hydraulische Kraftmaschinen [The water wheels as hydraulic engines] in: Bautechnik Vol. 80, No. 3, pp. 181-189. [in German]
Müller, G., Senior, J. (2009): Simplified theory of Archimedean screws, Journal of Hydraulic Research, Vol. 47No. 5, pp. 666-669.
Müller, W. (1939). Die Wasserräder [The water wheels], unchanged reprint, Moritz Schäfer Verlag, Detmold [in German]
Needham, J., Robinson, K., Huang, R., Elvin, M. (2004): Science and Civilisation in China. Vol. 7, the social Background, Part 2, Conclusions and Reflections: Cambridge University Press.
Schmelz, K.G., Reipa, A., Rossol, D. (2007): Reduction of the quantity of sewage sludge and increase in the digester gas production, Jounral of residuals science & Technology, 4(4), pp. 191-202.
Schröder, M. (2002): Produktionsunternehmen Kläranlage [producer Wastewater Treatment Plant], KA Korrespondenz Abwasser, Abfall, Vol. 49 (2002), No. 10, pp. 1380-1387. [in German]
Schröder, M. (2007): Klärschlamm als Energieträger [Sewage sludge as energy carrier], KA Korrespondenz Abwasser, Abfall, Vol. 2007 (54), No. 10, pp. 1035-1040. [in German]
Siegrist, H., Salzgeber, d., Eugster, J., Joss, A. (2008): Annamox brings WWTP closer to energy autarky due to increased biogas production and reduced aeration energy for N-removal, Water Science & Technology – WST, Vol. 57, No. 3, pp. 383-388.
Singh, P.; Carlill-Marquet, C., Kansal, A. (2012): Energy pattern analysis of a wasterwater treatment plant, Applied Water Science, No. 2, pp. 221-226.
Stampolidis, V., Y. Katsigiannis and P. Georgilakis (2006): A methodology for the economic evaluation of photovoltaic systems, Operational Research Vol. 6 No. 1, pp. 37-54.
Stemplewski, J., A. Schulz and J. Schon (2001): Benchmarking - an approach to efficiency enhancement in planning, construction and operation of wastewater treatment plants, Water Science and Technology Vol. 44, No. 2-3, pp. 111-117.
Stemplewski, J. (2012): Das Hybridkraftwerk Emscher in Bottrop. Energiepotentiale der Wasserwirtschaft nutzen! [The hybrid power plant Emscher in Bottrop – Use energy potentials of water resource management!], KA Korrespondenz Abwasser, Abfall, Vol. 2012 (59), No. 4, pp. 325-329.

IWLHS, 20-22/02/2013, Aachen - Bung & Pagliara (eds) - © 2013 Bundesanstalt für Wasserbau ISBN 978-3-939230-04-5

The Application of Environmental Flow Regulations to Small Hydropower Plants in Alpine Areas

L. Milanesi, M. Pilotti & G. Valerio
Department of Civil Engineering, Architecture, Land, Environment and Mathematics (DICATAM), Università degli Studi di Brescia – Via Branze, 43, Brescia, Italy

ABSTRACT: within a framework of conflicting needs and under water scarcity scenarios, environmental issues are assuming more and more relevance in water cycle management. An important role in this context is played by the minimum discharge release downstream of diversion structures, the so-called "environmental flow", aiming at assuring acceptable ecological conditions along natural watercourses. In this paper the regulation criteria adopted in several European alpine countries will be briefly discussed. The implementation of environmental flow regulations to small hydropower plants in the province of Brescia (Northern Italy), which is one of the most relevant Italian district in terms of number of hydropower plants, installed capacity and energy production, will be presented. In particular, the prevailing environmental flow release devices and their main technical characteristics, operating features and design criteria are briefly discussed. The introduction of environmental flow legislation entails both benefits and disadvantages which are often difficult to quantify. This paper gives a contribution to this costs-benefits analysis, by estimating the loss of energy producibility for a small alpine hydropower plant, related to the enforcement of environmental flow regulations and to the design criteria of the release devices.

Keywords: Alpine hydropower plants, Energy production, Environmental flow, Loss of producibility.

1 INTRODUCTION

According to the Water Framework Directive 2000/60/CE (European Parliament, 2000), the water cycle has to be managed with a catchment-wise approach. In this context, the Directive remarks the importance of the release of environmental flow, also identified as "minimum" or "ecological" flow, defined as *"the water regime provided within a river, wetland or coastal zone to maintain ecosystems and their benefits where there are competing water uses and where flows are regulated"* (Dyson et al, 2003). Accordingly, environmental flow prescriptions do not necessarily aim to bring stream ecosystems back to their original condition; rather, they aim to a re-regulation of the existing water uses in order to match with ecological goals. Adequate quantity, quality and timing of flow are the founding elements of such rules, which prove really effective only when included into a wider catchment governance background. The compliance with such criteria introduces both detriments and benefits, the latter being hardly quantifiable, since they are related to recreational opportunities, economical activities, increased water quality (e.g., pollutant dilution) or cultural aspects. On the contrary, detriments are often well measurable, because direct and opportunity costs are a consequence of needed structural adaptation and of reduced earnings from water use (e.g., Ranzi et al., 2009). In particular, in the case of hydropower, the additional environmental cost of increased request of fossil fuel due to the reduced hydroelectric production should not be disregarded. In order to find a match point between these conflicting aspects, a costs-benefits analysis may be a starting point that accounts for both stream quality objectives and water uses (Dyson et al., 2003; Richter & Thomas, 2007).

Environmental flow quantity and timing definition are related to the hydrologic, physical and biotic characteristics of the stream. Accordingly, the discharge value in itself may not be adequate to protect the ecosystem if other hydraulic parameters (e.g., wetted perimeter and velocity) are not considered (e.g.,

Kumar et al., 2007); moreover, all these variables are constrained by the biotic species to be preserved. Accordingly, there is a progression from low to high level assessment methods: hydrological, hydraulic, microhabitat and holistic (Rebillard, 2006). In general, the most efficient way to handle this issue is case by case testing based on local hydrological, morphological and ecological status (e.g., APER, 2006, Gollessi & Valerio, 2007).

Although Small Hydropower Plants (in the following, SHP) have a lower impact on the hydrologic variability of a watercourse than reservoirs (APER, 2006; Richter & Thomas, 2007), nevertheless they have to be built, or adapted, and managed in order to release downstream the suitable environmental flow discharge and to preserve the continuity of the stream (e.g., through fish passages). The operation of these devices is usually based on the respect of a minimum design depth, computed using energy balance principle, that guarantees the release of environmental flow before any water diversion. A proper design of the release devices makes possible to cope with seasonal variability and future adjustments of regulations (e.g., Ferri et al., 2004), reducing at the same time obstructions by sediments and floating debris. A relevant issue in SHP is related to the natural flow variability of the stream, that induces level fluctuations upstream of the barrage, leading in turn to an increase of the released ecological flow. Accordingly, where it is not possible to apply electronic or mechanic self-regulating devices, incremental production losses can be expected and frequent human maintenance is needed.

Moving from these considerations, in this paper environmental flow application in province of Brescia will be considered; the province of Brescia is a wide area (4.784 km^2) located in the northern part of Italy, that, with its 2181 MW of installed hydroelectric power (12.2% of the national total) and 2863 GWh of energy production (5.6% of the national total), ranks second in terms of national installed power and fifth in terms of production (GSE, 2009 and 2010). In particular we shall focus our contribution on existing SHP with an installed power lower than 3 MW and low head barrages (<15 m), with specific attention to the devices used for the discharge release and the related hydraulic design criteria. As a specific case, an alpine SHP has been studied in order to assess the energy production loss due to the introduction of environmental flow rules, comparing the increase of production obtainable with an ideal device that releases no more than established outflow, with respect to the production achievable with ordinary devices whose release varies as a function of water level fluctuations.

2 ENVIRONMENTAL FLOW REGULATIONS IN THE ALPINE REGION

In the following, a review of regulations of European alpine States regarding environmental flow release from barrages will be presented, in order to identify a common methodology based on simple hydrological criteria with further hydraulic and ecological assessments.

2.1 Austria

According to the Federal Austrian regulation, the *ecologically-required minimum discharge level* ($NQ_{Residual\ flow}$) is defined on the basis of hydrological criteria to be coupled with hydraulic and ecological elements. Three conditions may satisfy the requisites for a good hydromorphological status of a stream:

- the permanent minimum flow is greater than the *natural lowest daily minimum flow* ($NQ_{t\ natural}$);
- the permanent minimum flow is equal at least to one third of the *natural mean annual minimum flow* ($MJNQ_{t\ natural}$, which for the Austrian territory is closely correlated to the discharge exceeded 95% of time – e.g., Laaha & Blöschl, 2007) in streams where $NQ_{t\ natural}$<1/3 $MJNQ_{t\ natural}$;
- the permanent minimum flow is equal at least to one half of the *natural mean annual minimum flow* ($MJNQ_{t\ natural}$) in streams where $NQ_{t\ natural}$<1/2 $MJNQ_{t\ natural}$ and a mean discharge lower than 1 m^3/s.

The parameters involved in this procedure has to be calculated from datasets that ideally cover at least the last ten years. Beside this hydrological requirement, water depth, flow velocity, thermal condition and oxygen disposability constraints have to be fulfilled; in particular, a minimum velocity of 0.3 m/s and a minimum water depth ranging from 0.1 m to 0.3 m are suggested (Republic of Austria, 2010).

2.2 France

Minimum flow releases are regulated by the Ministre of Ecology, Sustainable Development and Energy through the Environmental Code (art. 214-18) (Gouverne de France, 2012); this duty is compulsory for each new structure and has to be fulfilled by existing barrages or dams by January 2014. The minimum

flow to be released by diversion structures in each watercourse is a function of the mean annual discharge, calculated as the average value of at least five years data. The release must be equal or greater than 10% of the mean annual flow; for rivers with an average annual discharge of 80 m^3/s or greater, this contribution can be reduced to 5%. This exception can be applied also to reservoirs assigned to supply the high power request peaks. A variable distribution in time of minimum flow is possible unless the mean value obeys the general principle and the minimum value is at least 1/2 of the uniform minimum flow.

2.3 Italy

The Italian regulation of environmental flow is based on the Ministerial Decree 28 July 2004 that states general definitions and guidelines, while the specific procedures for the definition of environmental flow values have to be given by regional or local water authorities. Since several different approaches characterize the Italian territory, in the following only some of the most representative ones in the alpine area will be briefly described.

2.3.1 *Po river Water Authority*

The Po river Water Authority (Autorità di Bacino del Fiume Po, 2002) suggests a parametric relation to calculate the environmental flow discharge *DMV* [l/s]:

$$DMV = k \cdot q_{mean\_y} \cdot S \cdot M \cdot Z \cdot A \cdot T \qquad (1)$$

where k [-] is an experimental parameter to be defined for each hydrographic area as a function of the watershed surface, q_{mean_y} [l/s/km^2] the mean annual specific discharge, S [km^2] the catchment area, M [-]a morphological parameter (from 0.7 to 1.3), A [-] a coefficient between 0.5 and 1.5 that represents the interaction between surface water and groundwater, T [-] the environmental flow timing, Z [-] the maximum value assumed by the naturalistic, fruition and quality parameters, which are all dimensionless and equal or greater than 1. The product of the first three parameters gives the "*hydrological factor"* to be released by the end of 2008, while the "*corrective"* parameters have to be applied by 2016 for existing structures. The regional Authorities within the Po river basin have to define both the hydrological and the corrective parameters. In particular Regione Lombardia (2008), which enjoins a minimum release of 50 l/s for new withdrawals in mountain watersheds, suggests k=0.10 and provides two methodologies for the determination of q_{mean_y} through regionalization procedures or stream gauging measures; the corrective parameters are not defined yet. Regione Piemonte (2007) provides similar approaches for the definition of q_{mean_y} while allows different values of k factor (from 0.07 to 0.15); moreover, the assessment of M and A parameters is already available. Finally, Regione Valle d'Aosta (2006) provides k values as function of the basin area; here the definition of the corrective parameter has been completed except for the factor A.

2.3.2 *Autonomous Province of Bolzano*

The autonomous Province of Bolzano demands a minimum specific discharge from 2 l/s/km^2 to 4 l/s/km^2, to be increased in case of specific environmental needs. An additional variable percent (from 3% to 25%) has to be applied depending on the natural flow values and the basin area, as to guarantee the natural discharge variability (Provincia Autonoma di Bolzano, 2010).

2.3.3 *Autonomous Province of Trento*

The autonomous Province of Trento provides, for each basin, the value of specific environmental flow to be released downstream each new diversion structure and its seasonal variability; the demanded release for existing withdrawals is 50% of the provided value, but not lower than 2 l/s/km^2 (Provincia Autonoma di Trento, 2005).

2.3.4 *Regione Veneto*

For the regional areas into the Po river catchment the mean specific discharge q_{mean_y} is 30 l/s/km^2, the experimental parameter k is 0.14 and no corrective coefficients have to be applied. For the Piave river basin, specific environmental flow values have been identified by the Alto Adriatico Water Authority (Autorità di Bacino dei Fiumi dell'Alto Adriatico, 2007). For all the remaining streams in the Regione Veneto (2012) a specific discharge of 4 l/s/km^2 or 3 l/s/km^2, depending on the basin area, must be applied.

2.4 Switzerland

The Swiss Confederation (1991) defined the environmental flow release criteria into the Water Protection Act (art. 30-32), where minor and major withdrawals are distinguished. With regard to the former, the maximum amount of total withdrawn discharge has to be less than 20% of Q_{347} and 1000 l/s. For the major diversions the hydrological criterion described in Table 1 has to be followed. In case water quality cannot be complied with existing wastewater discharges or water depth does not allow free fish migration (e.g., lower than 20 cm), the minimum flow has to be increased. On the contrary, ecological flow can be reduced for water bodies with low ecological potential or in case of emergency situations.

Table 1. Swiss minimum flow criterion

Q_{347} classes	minimum flow	additional release to the minimum flow values
Q_{347} up to 60 l/s	50 l/s	for each additional 10 l/s of Q_{347} add 8 l/s
Q_{347} up to 160 l/s	130 l/s	for each additional 10 l/s of Q_{347} add 4.4 l/s
Q_{347} up to 500 l/s	280 l/s	for each additional 100 l/s of Q_{347} add 31 l/s
Q_{347} up to 2500 l/s	900 l/s	for each additional 100 l/s of Q_{347} add 21.3 l/s
Q_{347} up to 10000 l/s	2500 l/s	for each additional 1000 l/s of Q_{347} add 150 l/s
Q_{347} greater than 60000 l/s	10000 l/s	----------

An approach similar to the Swiss one has been followed by the Friuli Venezia Giulia Regional Water Authority (Italy), where the suggested values in Table 1 are multiplied by the factor *CL* [-] which is a function of the distance *D* [km] along the water course between the withdrawal and the tailrace: $CL=1+0.075 \cdot D$ (Autorità di Bacino Regionale della Regione Friuli Venezia Giulia, 2007).

Finally, according to several regulations, the established value of the ecological flow release from barrages has to be clearly displayed in correspondence of each diversion structure and the minimum water level in compliance with the environmental flow release should be shown on a staff gauge properly located upstream of the barrage in order to ease the control.

3 THE RELEASE OF ENVIRONMENTAL FLOW FROM LOW HEAD STRUCTURES: THE SITUATION IN PROVINCE OF BRESCIA

The province of Brescia is one of the most important Italian areas in terms of installed hydropower capacity and production. Because of the morphological complexity and economic relevance of the territory, both low and high head power plants and diversion structures are present; in the following, due to space constraints, only SHP will be considered.

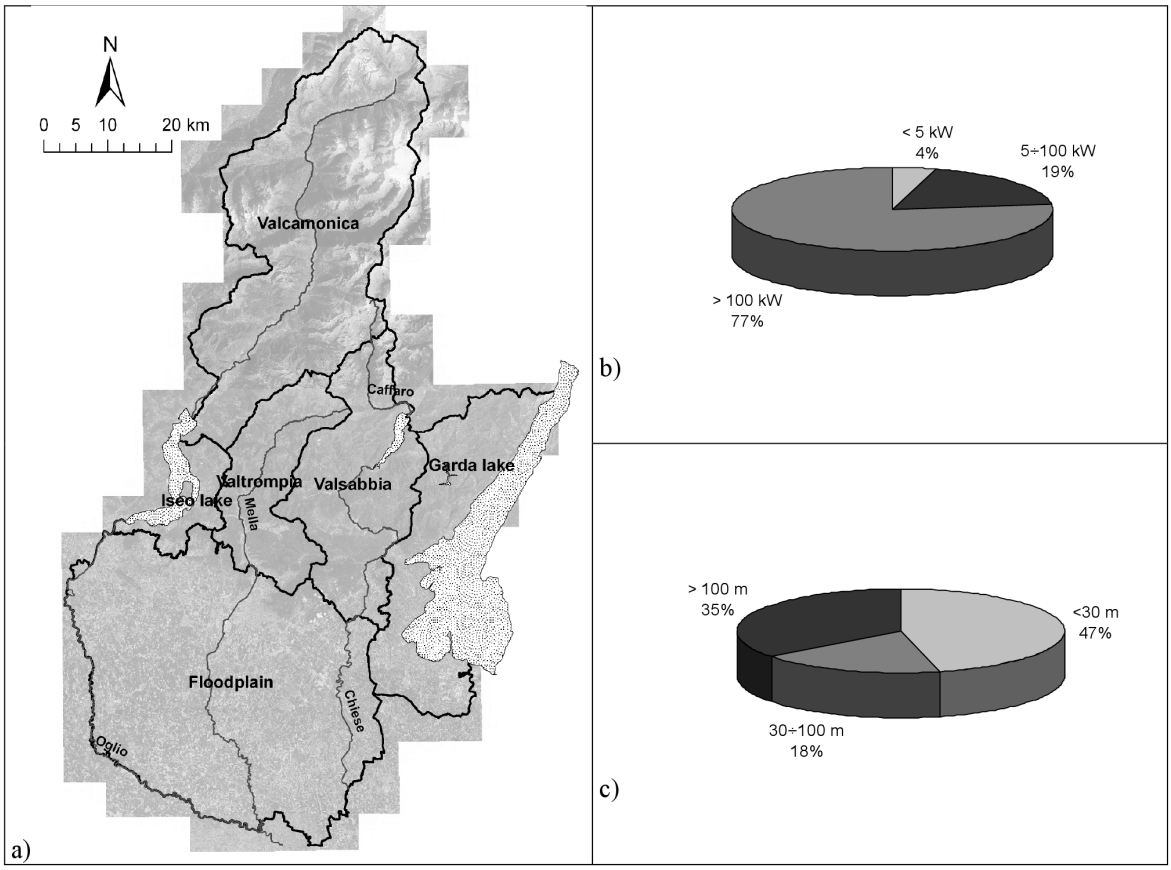

Figure 1. The province of Brescia (a) and distribution of SHP according to their capacity (b) and gross head (c) classes.

In the province of Brescia 6 homogenous zones can be identified (Figure 1a): the alpine valley along the Oglio river (Valcamonica, 34% of SHP present in the whole Province), the alpine valley along the Mella river (Valtrompia, 16% of SHP), the alpine valley along the Caffaro and Chiese rivers (Valsabbia, 19% of SHP), the area directly drained by Iseo lake (4% of SHP), the area directly drained by Garda lake (13% of SHP) and the floodplain area in the southern part of the province (13% of SHP). In the whole district, about 90 low head weir SHP can be found; among them, 70 have an installed capacity between 100 kW and 3 MW while 4 are enclosed into the pico-hydro class (<5 kW) (Figure 1b). According to the gross head classification (ESHA, 2004), the distribution appears equilibrated, with low and high head SHP numerically quite equivalent and only few medium head SHP (Figure 1c). According to the morphology of the territory, Valcamonica is characterized by the maximum value of the mean geodetic head (Figure 2a). On the contrary, in the floodplain, in Valsabbia and in Valtrompia, the higher values of withdrawn discharge are registered (Figure 2b). Finally, the peak value of the percent distribution of mean annual potential energy production (37%) is concentrated in Valcamonica, because of the elevated number of high head plants, whilst the lowest percentage is located in Valtrompia and in the areas surrounding the lakes (each one contributing with 7%). An intermediate situation characterizes Valsabbia (27%), where many low head plants with considerable discharges are located, and the floodplain (15%), with few low head plants with large discharges.

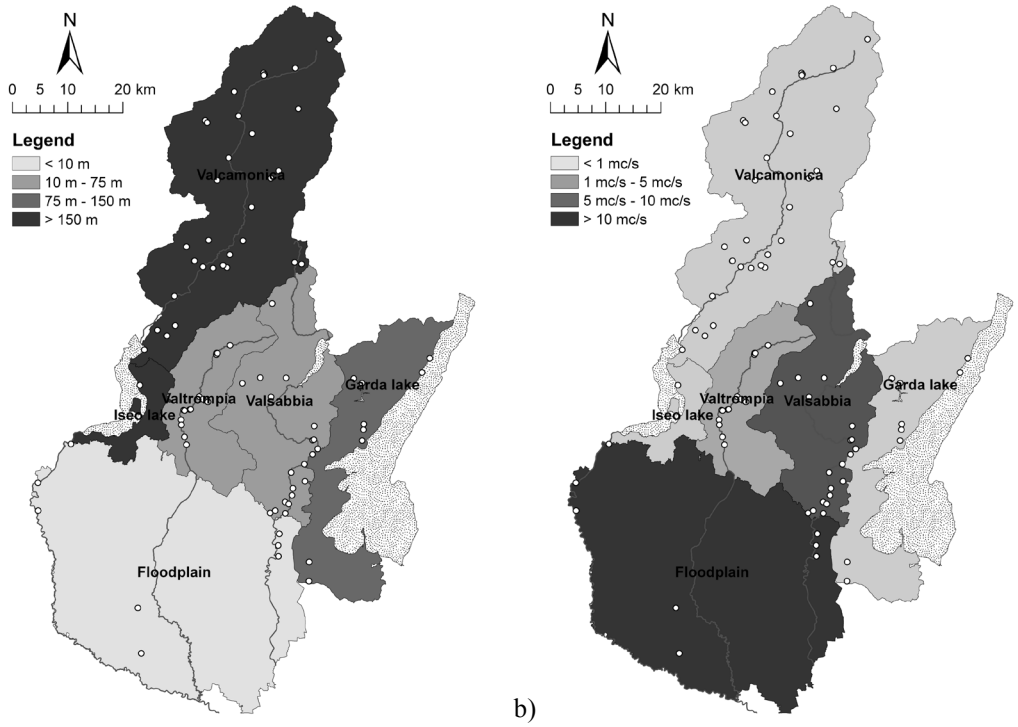

a) b)

Figure 2. Mean values per homogeneous area of gross head (a) and withdrawn discharge (b).

The most widespread barrage typologies, among SHP in this district, are low head gates and gravity weirs with lateral intakes or drop (especially tyrolean) intake. The first category is peculiar of the floodplain areas and of the lower part of Valsabbia and Valtrompia, while gravity weirs are common devices in high head plants of Valcamonica. According to national and local regulations, each new or existing barrage needs equipments for the release of environmental flow. Generally three main outflow solutions may be identified: gates, weirs and orifices. The first type of release can occur under gates opened in the barrage and sediment flushing gates in gravel or sand desilting basins; while the first group is peculiar of SHP with large diverted discharge and related ecological flow values, the second class is indifferently widespread. Weirs, often in thin plate, are usual outflow devices especially where fish passages are present; in particular, these solutions can be coupled with gate releases in order to reduce fish ladder dimensions. In many plants, especially in alpine basins where a small ecological flow discharge is required, this is often released from orifices opened within existing gates. Figure 3 shows the percentage distribution of release devices for SHP in Brescia district.

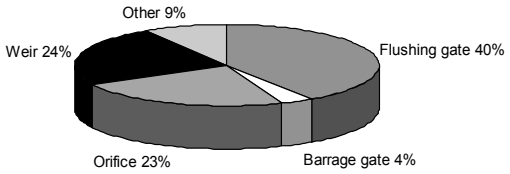

Figure 3. Percent distribution of environmental flow release devices in province of Brescia SHP.

4 CONSIDERATIONS ON THE DESIGN OF ENVIRONMENTAL FLOW RELEASE DEVICES

Due to its simplicity, the most widespread solution is the release of ecological flow under gates, because it does not require additional intervention in existing structures. This approach is often favored by the plant manager because it guarantees high flexibility with respect to the annual release trend and to possible adjustments by the Authorities, also contributing to a gradual self cleaning effect of the area upstream of the barrage where sediment clogging could be a problem. On the other hand and for the same reason, these structures are extremely prone to obstructions, especially if the transport of coarse sediment is relevant. For this reasons, release under gate is in our opinion seldom acceptable because it is difficult to guarantee a total cleaning of the gate opening. Moreover, in many situations the theoretical clearance under the gate would be only few centimeters high or even less: in these cases it is doubtful whether ordinary gates mechanics allow this level of precision, especially if no electronic controls are installed. In any case the installation of mechanical blocking systems to guarantee the minimum required opening and an appropriate maintenance program to ensure the respect of ecological flow release are needed. Free

surface outlets (e.g., weirs, sector gates, etc.) can be considered very effective devices to be designed on the basis of weirs efflux law or free surface flow theory; the risk of obstruction is usually limited to floating debris and it can be reduced through an appropriate upkeep program. The main criticalities of traditional weirs with fixed height are linked to their low flexibility and to the high variability of flow due to water level fluctuations. When such facilities are communicating with fish passages, the knowledge of the ichthyologic aspects of the stream and specific fish species requirements are basic information needed for their rational design (Grishin, 1982). Then, when an existing fish ladder is used for the adaptation to ecological flow release, attention must be paid because the modification of the flow parameters from design conditions may reduce its effectiveness. Finally, as far as obstruction risk is concerned, the best release solution is possibly provided by orifices opened within sluice gates, when their axis is located at a sufficient distance from the bottom and from the water surface; in such a case only partly floating advected debris may reduce the opening so that an appropriate upkeep program would be anyway advisable. The drawbacks of this solution are its poor flexibility if no partialization is possible and the possible weakening if the gate structure; for this reason, orifices require a case-by-case evaluation.

All of the presented solutions are designed using the energy balance equation, usually under the assumption of still water behind the barrage so that the whole specific energy available is equal to the water depth. Accordingly, a drought condition depth must be selected as reference for their design and it must be guaranteed by some geometrical constraint (e.g., desilting basin or diversion channel threshold height) or by a hydraulic machinery set point. Whilst in the first case (Figure 4) an incoming discharge less than the ecological flow cannot enter into the diversion channel, in the second one the constancy of an upstream water level (e.g., in the forebay) is controlled by pre-set hydraulic machinery regulations. Both these design conditions imply that if in operational conditions the discharge in the stream is greater than the environmental one, the water level behind the barrage may rise and a greater discharge than the design one will flow out from the release devices to the detriment of the production. For this reason, in order to minimize the loss of production, practitioners often design release devices with respect to a mean water depth upstream of the barrage, identified through recorded time series or experience. Clearly, this is not an acceptable criterion because, in case of low flows, the release prescribed by law is not guaranteed.

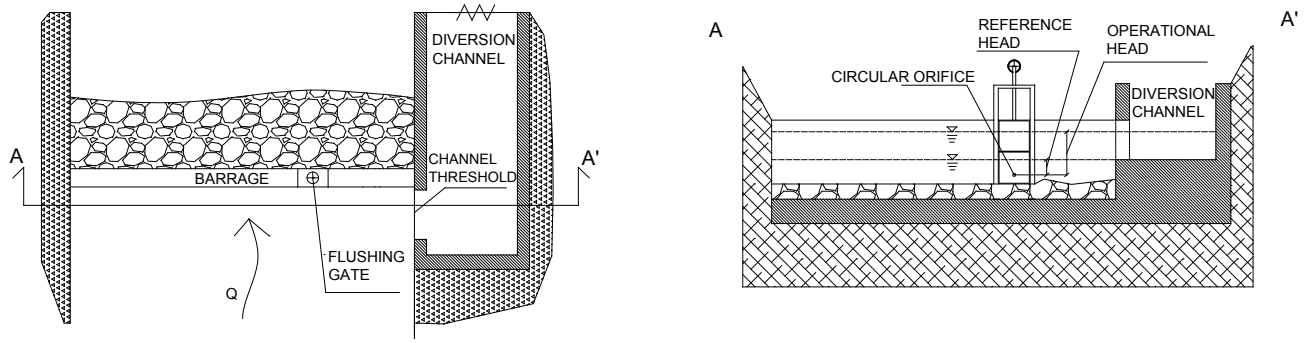

Figure 4. Example of intake, plan and cross sectional views.

The best solution to cope with this problem would be the installation of self-regulating mechanisms adapting the device geometry on the base of the upstream water level. In the considered district, both oleodynamic small plane gates and buoyant systems, that partialize orifices on the base of the upstream water level, are installed. Anyway these approaches are hardly applicable in absence of power supply or in case of severe freezing problems. In such cases orifices are preferable to free surface weirs because their stage-discharge relation is a function of the water level at the power 0.5 and so less sensitive to depth variations. Other approaches to reduce outflow variability are weirs with narrow vertical slot (e.g., Regione Piemonte, 2006), which however appears to be obstruction-prone, or proportional weirs, that assure more self-cleaning capacity. For these reasons, in case of refurbishment of SHP with already present fish passage, a combination of free surface and low pressure devices might be preferable.

5 EVALUATION ON THE LOSS OF HYDROPOWER PRODUCIBILITY FOR AN ALPINE SHP DUE TO THE ENFORCEMENT OF ENVIRONMENTAL FLOW REGULATIONS

The run-of-river SHP case study is located into an alpine sub-basin of the Po river watershed. It has a drained catchment of 11.6 km^2, mean altitude of 2250 m a.s.l. and an average slope gradient of 0.50 m/m. The basin is characterized by a mean annual precipitation of about 1000 mm; taking into account a snow

equivalent of 280 mm of rainfall, through regionalization procedures (Regione Lombardia, 2008), a mean annual discharge of 0.38 m^3/s can be estimated. An aerial image of the watershed is shown in Figure 5a while Figures 5b and 5c respectively present geological units and land use from Corine 2000.

Since no gauged data are available for this basin, the flow duration and the characteristic hydrological curves (Figure 6) have been estimated moving from the dataset of 34 years daily measured discharge data from the Sarca of Nambrone stream watershed (Northern Italy) (Bacchi et al., 2000; Bavera & Ranzi, 2006; Bavera et al., 2007) because of the geological and hydrological similarity between the two basins.

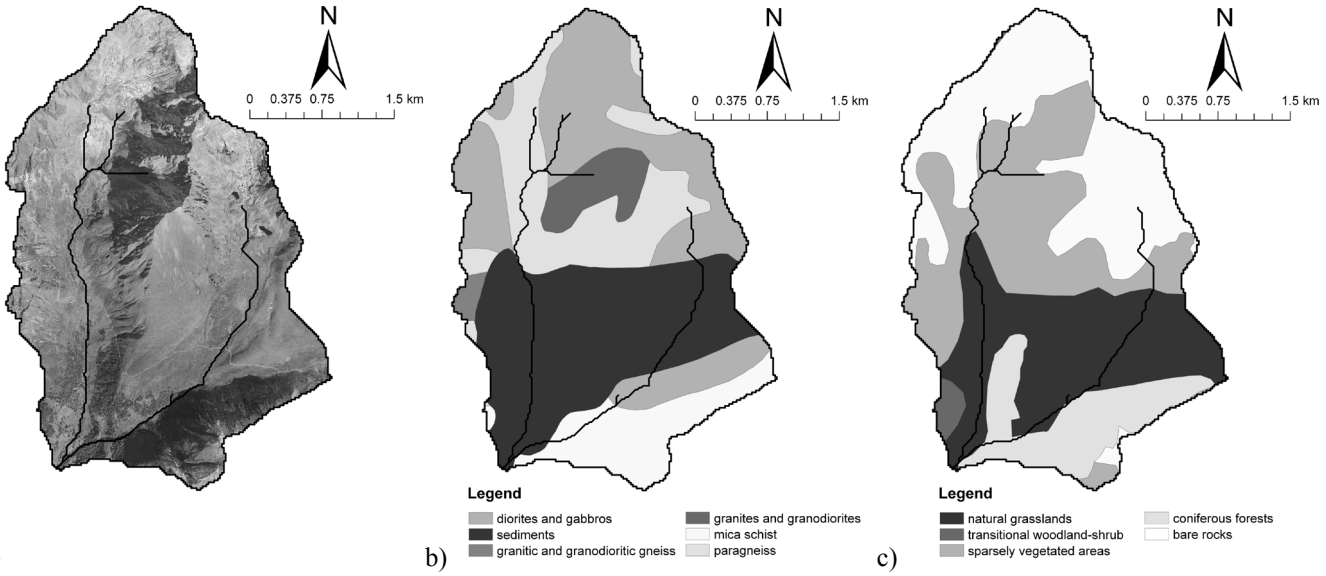

a) b) c)

Figure 5. Case study catchment aerial image (a), geological units (b), Corine 2000 land use (c).

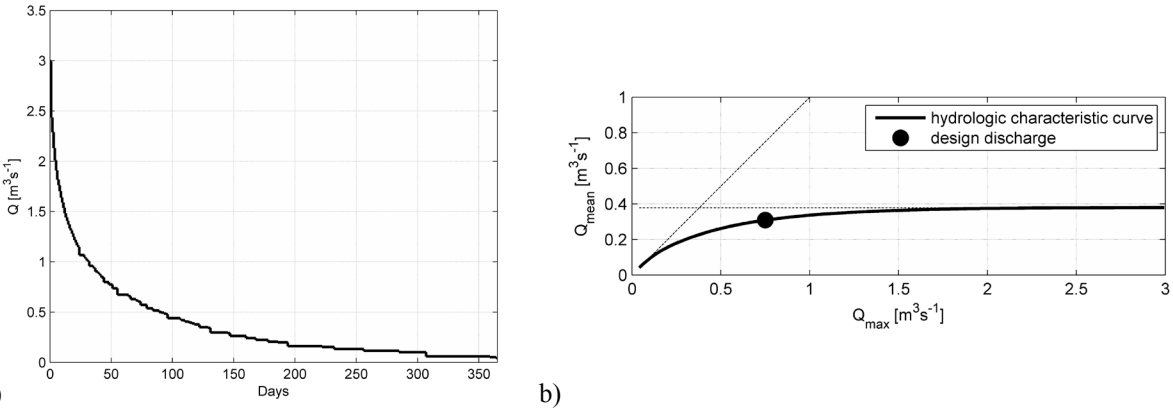

a) b)

Figure 6. Flow duration curve (a) and characteristic hydrological curve (b) without ecological flow abstraction.

The case study barrage (Figure 7) is a 2 m high gravity broad crested weir with a lateral intake which is followed by a chamber containing the desilting basin and the forebay, separated by a sill; the steel penstock is 3800 m long and with a diameter of 0.6 m. Two Pelton turbines are present for greater flexibility, operating with a discharge ranging from 0.030 m^3/s to 0.750 m^3/s and a gross head of 564 m; the operational scheme of the hydraulic machinery, in terms of sequence and number of running turbines, is set to keep its efficiency from 0.78 to 0.93, depending on the flowing discharge. At the barrage, the flow repartition is controlled by a frontal broad crested weir for high flows and a lateral Belanger intake weir; the environmental flow is released through a thin plate triangular weir for fish passage and a low pressure circular orifice into the flushing gate at 0.3 m from the bottom. From the operational viewpoint, considerations related to minimum submergence on the inlet of the penstock suggest to keep constant the water depth at the forebay. This is done by controlling the depth with an ultrasonic water level gauge and regulating the discharge in the penstock through the conical needle inside each nozzle ahead of the runner. Accordingly, the design of the release devices is based on the set point water depth.

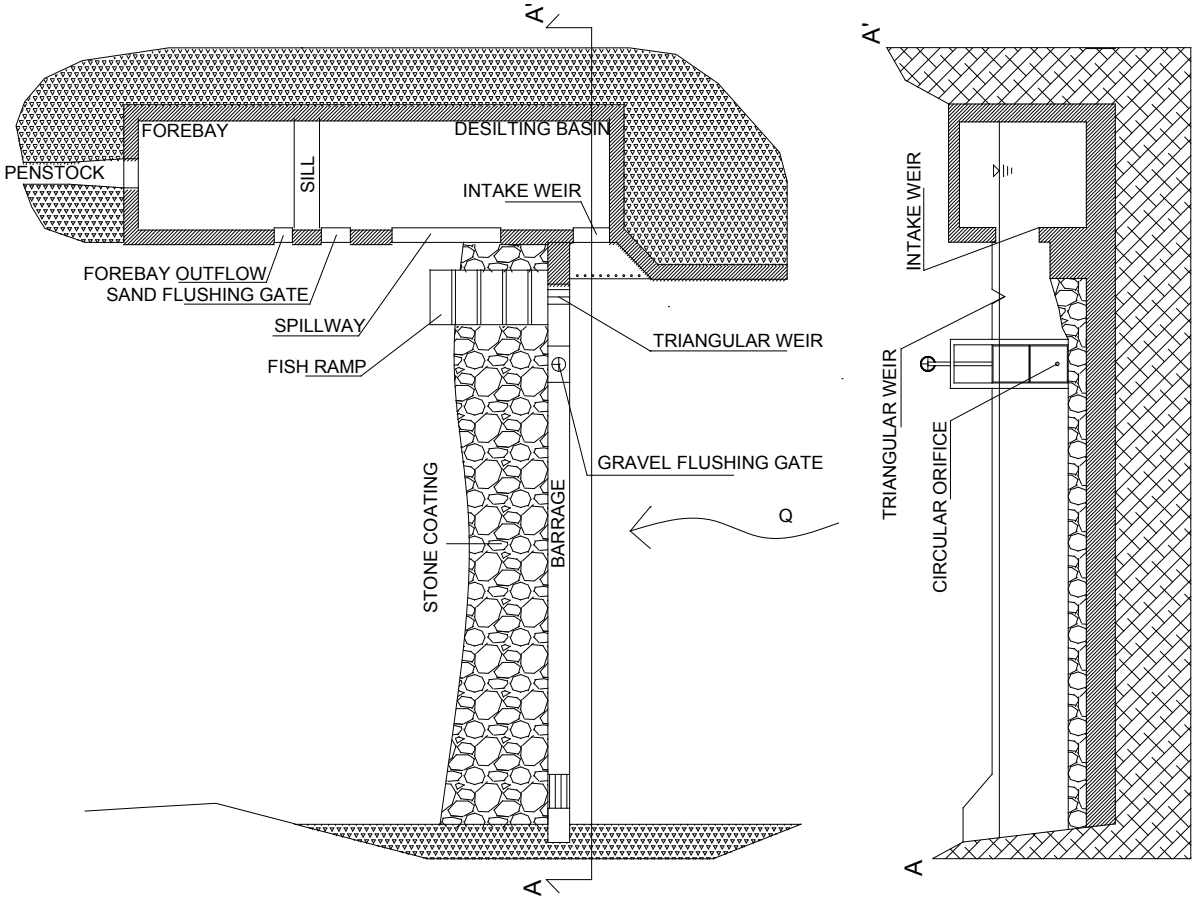

Figure 7. Plan view and transversal section of the barrage and the intake.

In order to assess the loss of production for this SHP due to the enforcement of ecological flow, the incoming discharge Q at the barrage must be partitioned between the elements that characterize the intake (i.e., broad crested weir of the barrage, triangular weir, circular orifice and drowned broad crested weir at the intake). The unknown discharges flowing through the listed devices are functions of the unknown water depth h at the barrage; on the other hand Q, from the flow duration curve, and the fixed water level of the forebay are known values. To this purpose, a simple numerical code has been written to solve the continuity equation (2) providing, for each Q, the upstream water depth and the related discharge sharing:

$$Q = \sum_{i=1}^{4} f_i(h) \qquad (2)$$

where $f_i(h)$ is the stage-discharge relation of the i-th device. Initially, an ideal device that releases constantly the ecological flow discharge that could be provided by each national regulation (Table 2) has been supposed, so that these discharges substituted the $f_i(h)$ functions related to the triangular weir and to the orifice in Equation (2). Afterward, the real release devices have been considered and the additional production loss due to the increased flowing environmental discharge has been computed.

Table 2. Environmental flow values

Country	Environmental flow discharge [m^3/s]
Austria	0.042
France	0.038
Italy – Regione Lombardia	0.038
Switzerland	0.050

Finally, the net head has been estimated through an energy balance along the penstock and the annual energy producibility in the two scenarios has been computed; the results are shown in Table 3, where reductions are calculated with respect to the potential production, in absence of any ecological release, of 10691 MWh.

Table 3. Results

Country	Energy production [MWh]		Reduction [%]		Variation ideal/real [%]
	Ideal	Real	Ideal	Real	
Austria	9940	9842	-7.0	-7.9	-1.0
France	10020	9938	-6.3	-7.0	-0.8
Italy – Regione Lombardia	10020	9938	-6.3	-7.0	-0.8
Switzerland	9786	9696	-8.5	-9.3	-0.9

As one can see, the application of ecological regulations under ideal conditions implies a producibility reduction ranging from 6.3% to 8.5%. Since the actual release varies with the water depth at the barrage, that increases with the discharge Q in the stream, in real operating conditions a further energy reduction of about 1% is expected so that the overall loss of producibility ranges from 7.0% to 9.3%.

6 CONCLUSIONS

The assessment of environmental flow discharge implies hydrological and ecological aspects; all the European alpine states considered in this paper deal with this topic on the basis of an hydrologic approach, often supported by hydraulic and ecological evaluations. Moving from the analysis of the application of such regulation in province of Brescia, pros and cons of different devices used for environmental flow release are briefly discussed. Although bottom opened flushing gate are the most widely used solutions, they are inevitably prone to obstructions with consequent potential reduction of released discharge; in particular this solution may be considered acceptable only if accompanied by an appropriate management program and if the self-cleaning effect under the gate is guaranteed. Weirs are suitable approaches especially if fish ladders are required. In case of streams with small ecological flow release and relevant sediment transport, the most suitable solution might be low-pressure orifices, opened sufficiently far from the bottom in order to prevent obstructions. A key point for the verification of the correct operation of such devices is the identification of a reference level, chosen on the basis of geometrical or hydraulic constraints, that guarantees the absence of water diversion before the complete release of the environmental flow. Moving from these considerations, the influence of different ecological flow rules and structure design criteria on the potential loss of producibility for an alpine high head SHP has been assessed. To this purpose, the annual producibility obtainable with an ideal adaptive device, that releases constantly the design environmental discharge, and with a real outflow configuration, characterized by a circular orifice and a triangular weir for fish passage, have been compared. Accordingly, in the real situation the actual released discharge may increase, with respect to the design one, as a function of the water depth behind the barrage. Then, an ideal loss of production ranging from 6.3% to 8.5% has been estimated while a further 1% reduction is caused by water level variability. Although this additional loss is small in relative terms, from an economic point of view it might justify technical improvements aiming at keeping environmental flow release as constant as possible.

ACKNOWLEDGEMENTS

We gratefully acknowledge the support of *Provincia di Brescia*, *Ufficio Usi Acque*, that prompted the research on the issue of ecological flow and supported the monitoring activities which provided the basis for this publication. We also acknowledge Prof. Roberto Ranzi for his support in hydrological analysis.

NOTATION

A	parameter of interaction between surface water and groundwater in Eq. 1 [-]
CL	amplification factor [-]
D	distance between the intake and the tailrace [km]
DMV	environmental flow discharge in Eq.1 [l/s]
h	water depth at the barrage [m]
k	experimental parameter in Eq. 1 [-]
M	morphological parameter in Eq. 1 [-]
$MJNQ_{t\ natural}$	natural mean annual minimum flow according to Austrian regulation

$NQ_{Residual\ flow}$	ecologically required minimum discharge according to Austrian regulation
$NQ_{t\ natural}$	natural lowest daily minimum flow according to Austrian regulation
Q	discharge [m^3/s]
Q_{347}	discharge equaled or exceeded for 347 days each year [m^3/s]
Q_{max}	design discharge for the SHP in Figure 6 [m^3/s]
Q_{mean}	mean discharge usable in the SHP in Figure 6 [m^3/s]
q_{mean_y}	mean annual specific discharge in Eq. 1[$l/s/km^2$]
S	catchment surface in Eq. 1 [km^2]
T	parameter of environmental flow timing in Eq. 1 [-]
Z	parameter accounting naturalistic, fruition and water quality aspects in Eq. 1 [-]

REFERENCES

Autorità di Bacino dei Fiumi dell'Alto Adriatico (2007). Piano di Bacino del Fiume Piave. Piano Stralcio per la Gestione delle Risorse Idriche.

APER (2006). Hydropower and Environment. APER. Milano, Italy. [online] www.aper.it/public/sitoaper/AperNelMondo /ProgettiEuropei/reportsh.pdf

Autorità di Bacino del Fiume Po (2002). Criteri per la regolazione delle portate in alveo. ALLEGATO B alla deliberazione n. 7 del 13 Marzo 2002. Parma.

Autorità di Bacino Regionale della Regione Friuli Venezia Giulia (2007). Determinazione del minimo deflusso vitale per sorgenti, corsi d'acqua con bacino idrografico collinare e montano e corsi d'acqua di risorgiva. Delibera n. 4/2007.

Bacchi, B., Falappi, L., Grossi, G., Ranzi, R. (2000). Measurements and simulations of low flows in Alpine rivers. New trends in water and environmental engineering for safety and life. Maione, Majone Letho & Monti (eds), Balkema, Rotterdam.

Bavera, D., Ranzi, R. (2006). Regionalizzazione delle portate di magra e morbida nei bacini alpini. XXX Italian Workhsop on Hydraulics and Hydraulic Engineering. Proceedings of the 2006 Conference, Rome.

Bavera, D., Barontini, S., Maran, S., Ranzi, R. (2007). Low flows as an index of droughts in mountain areas. Water resources assessment under water scarcity scenarios. La Loggia, Aronica and Circolo (eds), Centro Studi Idraulica Urbana, Milano.

Dyson, M., Bergkamp, G., Scanlon, J. (eds). (2003). Flow. The Essentials of Environmental Flows. IUCN, Gland, Switzerland and Cambridge, UK. 118 pages.

European Parliament (2000). Directive 2000/60/EC of the European Parliament and of the Council of 23 October 2000 establishing a framework for Community action in the field of water policy.

European Small Hydropower Association (ESHA). (2004) Guide on how to develop a small hydropower plant. ESHA. Brussels, Belgium. [online] www.esha.be/publications/publications.html

Ferri, M., Artusato, C., Baruffi, F., Rusconi, A. (2004). Sulle opere di derivazione nel rispetto del deflusso minimo vitale. XXIX Italian Workhsop on Hydraulics and Hydraulic Engineering. Proceedings of the 2004 Conference, Trento.

GSE (2009). Idroelettrico – Rapporto statistico. Gestore Servizi Energetici (GSE). Roma, Italy.

GSE (2010). Rapporto Statistico 2010 Impianti a fonti rinnovabili. Gestore Servizi Energetici (GSE). Roma, Italy.

Gollessi, S., Valerio, G. (2007) Implementation of WFD in Italy and experimental studies on reserved flow. Hydro 2007: New Approaches for a New Era, Granada, 15 - 17 October 2007.

Gouverne de France (2012). Code de l'environnement. [online] www.legifrance.gouv.fr/

Grishin, M.M. (1982). Hydraulic Structures. Vol 1. Mir Publishers, Moscow, 468 pages.

Kumar, P., Chaube, U.C., Kumar Mishra, S. (2007). Environmental flows for hydropower projects – A case study. International Conference on small Hydropower – Hydro Sri Lanka. Proceedings of the 2007 Conference.

Laaha, G., Blöschl, G. (2007). A national low flow estimation procedure for Austria. Hydrological Sciences Journal, 52 (4), pp. 625-644.

Provincia Autonoma di Bolzano (2010). Piano Generale di Utilizzazione delle Acque Pubbliche. Parte 2. Obiettivi e criteri di Gestione. Progetto di Piano.

Provincia Autonoma di Trento (2005). Piano di Tutela della Qualità delle Acque. Relazione di Sintesi.

Ranzi, R., Barontini, S., Grossi, G., Faggian, P., Kouwen, N. & Maran, S. (2009). Impact of climate change scenarios on water resources management in the Italian Alps. Proc. IAHR Congress, Vancouver, August 9-14, ISBN 978-90-78046-08-0.

Rebillard, V. (2006). Determination et mise en place de regimes reserves pou les cours d'eau. Synthese technique, ENGREF, Montpellier.

Regione Lombardia (2008). Direttive per l'adeguamento delle derivazioni al rilascio del Deflusso Minimo Vitale. Bollettino Ufficiale Regione Lombardia n. 9 Edizione Speciale del 25 Febbraio 2008. Milano

Regione Piemonte (2006). Proposta di linee guida per l'adeguamento delle opere di presa esistenti al rilascio del deflusso minimo vitale. [online] www.regione.piemonte.it/acqua/dwd/Linee%20guida%20DMV%2016%20maggio%202006.pdf

Regione Piemonte (2007). Regolamento Regionale recante: "Disposizioni per la prima attuazione delle norme in materia di deflusso minimo vitale (Legge Regionale 29 Dicembre 2000, n. 61). Regolamento Regionale 17 Luglio 2007, n. 8/r.

Regione Valle d'Aosta (2006). Piano di Tutela delle Acque. Allegato G.

Regione Veneto (2012). Allegato D alla Delibera di Giunta Regionale n. 842 del 15/5/2012.

Republic of Austria (2010). 99th Ordinance. Quality Target Ordinance – Ecological Status of Surface Waters. Federal Law Gazette for the Republic of Austria. Volume 2012, Part II.

Richter, B.D., Thomas, G.A. (2007). Restoring environmental flows by modifying dam operations. Ecology and Society. Vol. 12, No. 1. [online] www.ecologyandsociety.org\vol12\iss1\art12\

Swiss Confederation (1991). Water Protection Act. [online] http://www.admin.ch/ch/e/rs/c814_20.html

Author Index

IWLHS 2013

CD included

Nowadays, hydraulic engineers face different challenges, resulting mainly from the benefits of the rapid development of new materials and construction techniques, and from the added requirements of ecological and economic considerations, resulting in the adaptation of hydraulic structures. On the other hand, climate change becomes apparent in many regions of the world. More variable rainfall and resulting runoff challenge hydraulic engineers to review discharge capacity, refurbish and upgrade existing structures.

The investigation of water-structure interaction thus still demands our attention to fulfill future needs. Particularly, multiphase flow problems, such as air-water flows and sediment-water flows, are still not fully understood. Research can be based on different approaches, experimental and numerical modeling as well as field studies. Each of these approaches may provide useful results, but most notably the combination of all approaches may still be the most appropriate means.

The International Workshop on Hydraulic-Design of Low-Head Structures, held on 20 - 22 February 2013 in Aachen / Germany, aimed to contribute to the advance and spread of knowledge by bringing together experts working in the specialized field of low-head structure design from both research and practice communities.

The following themes were regarded:

- *Weirs and gates,*
- *Spillways,*
- *Ramps and fishways,*
- *Drop structures,*
- *Hydraulic jumps,*
- *Experimental studies and*
- *Small hydropower.*

The IWLHS 2013 was yet another event in a series of successful workshops and symposia organized by the IAHR Hydraulic Structures Technical Committee during the last decade.

ISBN 978-3-939230-04-5
Printed in Germany

BAW Bundesanstalt für Wasserbau
Kompetenz für die Wasserstraßen